



BRNO UNIVERSITY OF TECHNOLOGY

VYSOKÉ UČENÍ TECHNICKÉ V BRNĚ

FACULTY OF CIVIL ENGINEERING

FAKULTA STAVEBNÍ

DEPARTMENT OF CONCRETE AND MASONRY STRUCTURES

ÚSTAV BETONOVÝCH A ZDĚNÝCH KONSTRUKCÍ

STRENGTHENING OF CIRCULAR COLUMN SUBJECTED TO LATERAL CYCLIC LOADING

ZESÍLENÍ KRUHOVÉHO SLOUPU NAMÁHÁNÉHO LATERÁLNÍM CYKlickým
ZATÍŽENÍM

DOCTORAL THESIS SUMMARY

TEZE DISERTAČNÍ PRÁCE

AUTHOR

AUTOR PRÁCE

Ing. Mohamad MANSOUR

SUPERVISOR

VEDOUCÍ PRÁCE

prof. RNDr. Ing. Petr ŠTĚPÁNEK, CSc.

BRNO 2019

DISSERTATION
DISERTAČNÍ PRÁCE

© Copyright by Mohamad Mansour 2019
All right reserved

Brno University of Technology
Faculty of Civil Engineering
Institute of Concrete and Masonry Structures

CONTENTS

ABSTRACT	7
KEYWORDS	7
DECLARATION	9
ACKNOWLEDGMENTS	10
NOTATIONS	11
CHAPTER 1-INTRODUCTION	14
1.1 INTRODUCTION.....	14
1.2 PROBLEM	15
1.3 RESEARCH OBJECTIVES.....	15
1.4 DISSERTATION OUTLINE	16
CHAPTER 2- LITERATURE REVIEW	18
2.1 INTRODUCTION.....	18
2.2 COMPOSITE MATERIALS.....	18
2.3 METHODS OF RETROFITTING OR JACKETING.....	21
2.3.1 REINFORCED CONCRETE JACKETING	21
2.3.2 STEEL JACKETING	22
2.3.3 FRP JACKETING.....	23
2.4 CONFINEMENT ACTION.....	24
2.4.1 PASSIVE CONFINEMENT	25
2.4.2 ACTIVE CONFINEMENT	26
2.5 FACTORS INFLUENCING THE CONFINEMENT PERFORMANCES	27
2.5.1 EFFECT OF THICKNESS OF FRP WRAPS – NUMBER OF LAYERS.....	27
2.5.2 EFFECT OF FRP TYPE (MATERIAL CHARACTERISTICS).....	28
2.5.3 EFFECT OF SIZE OF THE STRUCTURAL ELEMENTS	28
2.5.4 EFFECT OF BOND CAPACITY (FRP-CONCRETE INTERFACE)	29
2.5.5 EFFECT OF COLUMN SHAPE (SQUARE-CIRCULAR) & WRAPPING)	29
2.6 PROPOSED MODELS FOR CONFINEMENT.....	31
2.6.1 FARDIS AND KHALILI (1981, 1982).....	32
2.6.2 SAMAAAN, SHAHAWY AND MIRMIRAN (1998)	33
2.6.3 TOUTANJI (1999).....	34
2.6.4 SPOELSTRA AND MONTI (1999)	35
2.6.5 LAM AND TENG (2003)	37

2.6.6 STRENGTHENING AND CONFINEMENT RATIO	40
2.7 CODE PROVISIONS	41
2.7.1 CONFINEMENT OF CONCRETE - EN 1992-1-1	41
2.7.2 CONFINEMENT OF CONCRETE - ACI 440.2R.....	42
2.8 REINFORCED CONCRETE COLUMNS IN SEISMIC ZONES	44
2.8.1 FAILURE MODES.....	44
2.8.2 DUCTILITY OF STRUCTURES.....	47
2.8.3 DUCTILITY AMENDMENT	49
2.8.4 DESIGN METHODOLOGY	50
2.8.5 DEFORMATION CAPACITY OF RC COLUMNS	53
2.8.6 SEISMIC TESTS ON FRP-CONFINED CONCRETE COLUMNS.....	56
2.8.6.1 SHEIKH SHAMIM A. AND YAU GRACE (2002)	56
2.8.6.2 OZBAKKALOGLU T. AND SAATCIOGLU M. (2006, 2007).....	59
2.8.6.3 OKAN OZCAN, BARIS BINICI, GUNEY OZCEBE (2008)	62
2.8.7 CONCLUSION OF EXPERIMENTAL WORK.....	65
CHAPTER 3-RESEARCH STUDY	66
3.1 INTRODUCTION.....	66
3.2 THEORETICAL PART	66
3.2.1 ANALYTICAL PART.....	66
3.2.1.1 CROSS-SECTION ANALYSIS OF CIRCULAR COLUMNS	66
3.2.1.2 ANALYTICAL SOLUTION-EXAMPLE.....	73
3.2.1.3 CANTILEVER COLUMNS.....	75
3.2.1.4 ASSESSMENT OF CONCRETE SUBJECTED TO CYLCIC LOADING /FATIGUE	76
3.2.1.5 MOMENT CURVATURE ANALYSIS OF TEST SPECIMENS	77
3.2.1.6 INTERACTION BETWEEN DUCTILITY DISPLACEMENT AND CURVATURE	
FACTORS	85
3.3 EXPERIMENTAL PART.....	87
3.3.1 TEST SPECIMENS PARAMETERS	87
3.3.2 MANUFACTURING AND GEOMETRY OF TEST SPECIMENS	87
3.3.3 GEOMETRY OF THE TEST SPECIMENS.....	87
3.3.4 CONCRETE MIX DESIGN	88
3.3.5 STEEL REINFORCEMENT	90

3.3.6	SPECIMENS PREPARATION – CFRP APPLICATION	90
3.3.7	STEEL FOOTING	92
3.3.8	TEST SPECIMENS SET-UP AND PROCEDURES	94
3.3.9	INSTRUMENTATIONS	100
3.3.10	STATIC SCHEME DIAGRAM OF COLUMNS TEST	103
3.4.	TEST RESULTS AND DISCUSSION	106
3.4.1	UNCONFINED SPECIMEN – COLUMN TYPE C1 (CONTROL SPECIMEN)	106
3.4.1.1	HIGH-CYCLE LOADING TEST-COLUMN TYPE C1	106
3.4.1.2	LOW-CYCLE LOADING TEST-COLUMN TYPE C1	112
3.4.2	CONFINED SPECIMEN – COLUMN TYPE C2 AND C3 (6x CFRP)	115
3.4.2.1	HIGH-CYCLE LOADING TEST-COLUMN TYPE C2 AND C3	115
3.4.2.2	LOW-CYCLE LOADING TEST-COLUMN TYPE C2 AND C3	122
3.4.3	UNCONFINED SPECIMEN – COLUMN TYPE C4	126
3.5	NUMERICAL ANALYSIS	129
3.5.1	FINITE ELEMENT METHOD	129
3.5.2	NUMERICAL ANALYSIS BY ATENA 3D	131
3.5.3	ANALYSIS PROCEDURE OF TESTED SPECIMENS	132
3.5.3.1	ELEMENT FORMULATION OF THE SPECIMENS	132
3.5.3.2	GEOMETRY AND MATERIALS OF SPECIMENS	132
3.5.3.3	LOADING, SUPPORTING, AND MONITORING	132
3.5.3.4	BOUNDARY CONDITIONS	133
CHAPTER 4-	EVALUATION AND COMPARISON OF EXPERIMENTAL AND NUMERICAL RESULTS	135
4.1	INTRODUCTION	135
4.2	FORCE -DISPLACEMENT ENVELOPE DIAGRAMS	135
4.3	ENERGY DISSIPATION -DISPLACEMENT ENVELOPE DIAGRAMS	137
4.4	LATERAL FORCE-DRIFT DIAGRAMS	141
4.5	EMPERICAL MODEL FOR FRP CONFINED CONCRETE SUBJECTED TO CYCLIC LOADING	142
4.6	NUMERICAL RESULTS OF COLUMNS TYPE C1, C3 AND C4-ATENA	146
4.7	COMPARISON OF THE EXPERIMENTL AND NUMERICAL RESULTS	148
4.8	DESIGN PROCEDURE	154
4.9	SUMMARY AND CONCLUSION OF THE INVESTIGATION	159

4.10 FUTURE RESEARCH AND RECOMMENDATIONS	164
APPENDIX.....	166
GRAPHICAL USER INTERFACE	184
CODE	188
FLOW CHARTS	196
REFERENCES	199
LIST OF FIGURES.....	203
LIST OF TABLES	206
BIBLIOGRAPHY.....	208
LIST OF PUBLICATIONS	208
CURRICULUM VITAE	209

ABSTRACT

Fibre Reinforced Polymer (FRP) composite materials have been widely used in the form of jacketing to enhance shear and flexural strengths as well as ductility. This research study focuses on examining the use of fibre reinforced polymers (FRP) for retrofitting, improving the performance of circular reinforced concrete columns and developing a design algorithm for circular column strengthening by FRP composite materials. Experimental tests are conducted on unconfined and confined circular column specimens. Two unconfined circular columns and two confined columns with carbon fibre reinforced polymers (CFRP) composites are wrapped in hoop direction. The specimens are subjected to axial load and lateral cyclic load. The lateral cyclic load is provided in two different ways; first, it was applied under force control - test (i.e. same lateral cyclic force pulling in one direction for certain number of cycle's~1 million cycles), second, it was applied under displacement control - reversed cyclic loading test based on a pattern of progressively increasing displacements. Three of the specimens (one unconfined and two confined) are subjected to first and second loading test, and one unconfined specimen is subjected only to second loading test.

Several research programs launched to study the effects of strengthening and retrofitting methods using composite materials (fibre reinforced polymers) on the strength and ductility of normal strength concrete, considering the low-cycle (reversed cyclic loading test), are reported in the literature. In the present study, an attempt is made to expand the test database with larger range by considering both cycle; low and high.

KEYWORDS

Fibre Reinforced Polymer composite materials, strengthening of circular column subjected to cyclic load.

BIBLIOGRAPHIC CITATION OF UNIVERSITY QUALIFICATION WORK (VŠKP)

Ing. Mohamad Mansour Strengthening of circular column subjected to lateral cyclic loading. Brno, 2019. 209 p. Doctoral thesis. Brno University of Technology, Faculty of Civil Engineering, Institute of Concrete and Masonry Structures. Supervisor prof. RNDr. Ing. Petr Štěpánek, CSc.

DECLARATION

I declare that I have prepared my dissertation work independently using the specialized literatures and under the supervision of prof. RNDr. Ing. Petr Štěpánek, CSc.

Brno 26.02.2019

.....

Ing. Mohamad Mansour

ACKNOWLEDGMENTS

I would like to express my sincere gratitude to my major prof. RNDr. Ing. Petr Štěpánek, CSc. and my technical advisor Ing. František Girgle, Ph.D. for their support and guidance throughout the course of this work.

I also express my gratitude to all laboratory 's staff specially Ing. Jiří Veselý and his team from the “Institute of Metal and Timber Structures”, and Ing. Petr Daněk, PhD. from the “Institute of Building Testing”, and colleagues at Brno University of Technology for their help.

Finally, I would like to thank my family, who has been a constant source of inspiration, encouragement and support throughout my academic pursuit.

This work was obtained with the financial support of the Grant Agency of the Czech Republic within the project 103/09/H085 - "Modern Composite Structures." Knowledge gained from the project of the Ministry of Industry and Trade FR TI 4/159 "Light Structures - progressive construction of advanced composite materials" was also used. This work was supported by the Ministry of Education, Youth and Sport by the project CZ.1.07/2.3.00/30.0005 – “Support for the creation of excellent interdisciplinary research teams at Brno University of Technology”. The experimental work has been carried out with the support of the company SIKa CZ, s. r. o. and PREFa-Brno a.s.

NOTATIONS

Latina upper case letters

A_c	Cross sectional area of concrete
A_f	Cross sectional area of FRP wrap
A_s	Cross sectional area of longitudinal steel reinforcement
A_{sp}	Cross sectional area of transverse steel reinforcement
E_c	Modulus of elasticity of concrete
E_{cm}	Secant modulus of elasticity of concrete
E_{fk}	Characteristic modulus of elasticity of FRP in hoop direction
E_j	Design modulus of elasticity of FRP in hoop direction = $0.9 E_f$
E_s	Modulus of elasticity of steel reinforcement
EI	Bending stiffness of cross section
I_c	Second moment of area of concrete cross section
L	Length
M_c	Moment resistance of concrete
M_s	Moment of steel reinforcement
M_f	Moment resistance of FRP wrap
N_c	Axial load resistance of concrete
N_s	Axial load resistance of steel reinforcement
N_f	Axial load resistance of FRP wrap

Latina lower case letters

b	Width of cross section
c	Concrete cover
d	Diameter of concrete cross section
d	Effective depth of concrete cross section
d_s	Diameter of steel reinforcement section
d_f	Diameter of FRP wrap
e_0	Minimum eccentricity $e_0 = h/30$ but not less than 20 mm
e_1	Eccentricity due to geometrical imperfections
e_2	Eccentricity due to second order effects

f_{ck}	Characteristic compressive cylinder strength of concrete at 28 days
f_{cd}	Design value of concrete compressive strength
f_{cm}	Mean value of concrete cylinder compressive strength
$f_{ck,c}$	Characteristic compressive strength of confined concrete
f_{co}	Peak strength of unconfined concrete or (f'_{co})
f_{cc}	Peak strength of confined concrete or (f'_{cc})
f_{FRP}	Tensile strength of FRP in hoop direction
f_{yk}	Characteristic yield strength of steel reinforcement
f_{yd}	Design yield strength of steel reinforcement
h	Height
h	Overall depth of cross section
K_1	Confinement effectiveness coefficient
K_2	Strain coefficient of the effective lateral confinement pressure
K_{eff}	Coefficient of efficiency
K_H	Coefficient of horizontal efficiency
K_V	Coefficient of vertical efficiency
K_α	Coefficient of efficiency, regardless of the section shape
n	Number of plies or layers of FRP wrap
n_i	Number of longitudinal steel reinforcement
t_f	Thickness of FRP wrap
z	Lever arm of internal forces
x	Neutral axis depth
y	Distance of the compressive force to the center of cross section

Greek lower case letters

α_{cc}	Coefficient taking account of sustained compression
γ_c	Partial safety factor for concrete
γ_s	Partial safety factor for steel reinforcement
γ_f	Partial safety factor for FRP wrap
γ_m	Partial safety factor for material property
δ	Increment/redistribution ratio
ζ	Reduction factor/distribution coefficient
ϵ_{cu}	Ultimate compressive strain in the concrete
ϵ_{cc}	Compressive strain in the concrete at the peak stress f_{cc} or f'_{cc}
ϵ_{co}	Compressive strain in the concrete at the peak stress f_{co} or f'_{co}
ϵ_{yd}	Ultimate tensile strain of steel reinforcement
ϵ_{si}	Tensile strain in the reinforcement layer of area A_{si}
ϵ_f	Tensile strain of FRP wrap
ϵ_{fk}	Characteristic rupture strain of FRP wrap
σ_c	Compressive stress provided by concrete
σ_{si}	Tensile stress provided by reinforcement layer of area A_{si}
σ_l	Lateral confining pressure provided by FRP
$\sigma_{l,eff}$	Effective lateral confining pressure provide by FRP
λ	Slenderness ratio
λ	Reduction factor for the depth of the stress block
η	Strength factor for the stress block
θ	One half of the angle subtended at the center of the cross – section by the concrete compressive stress block
ϕ_u	Ultimate curvature
ϕ_y	Yielding curvature
Δ_y	Yielding deformation
Δ_u	Ultimate deformation

CHAPTER 1-INTRODUCTION

1.1 INTRODUCTION

Columns/piers are ones of the most important structural elements in buildings and bridges. A significant number of structural failures are attributed to column failure, especially those constructed under-designed according to load demands or seismic design provisions. Improving ductility, compressive strength and durability of concrete structures, which are affected by the environmental degradation, corrosion of steel and which are required for upgrading of structures to current seismic codes, can be achieved by lateral confinement. The conventional methods of confinement (concrete, steel) may not always be adequate or suitable to provide the desired levels of ductility. Fiber Reinforced Polymer (FRP) composites have been used as longitudinal reinforcement, admixtures, and fiber wraps to improve flexure, shear, ductility and compressive strengths of reinforced concrete elements. FRP confinement can provide significantly higher confining pressure than conventional methods and it can enhance its performance potential in seismic design of existing and new structures.

In past years, the use of FRP composites was limited due to the high cost and lack of product knowledge. Recent cost reductions have allowed FRP composites to become a feasible option for structural applications, which results in an increase in research on this topic. FRPs have been widely applied in construction and structural rehabilitation due to their high strength, stiffness-to-weight ratio, high-corrosion resistance, minimal thickness, ease and speed of application, and ability to fit to any structural shape.

1.2 PROBLEM

In recent decades, the analysis and application of FRP confinement has been subject of interest in both the construction of concrete-filled FRP tubes as earthquake-resistant columns in new construction and in the retrofit of existing reinforced concrete columns.

Many models and standards are proposed for estimating the compressive strength and strain enhancement provided by the FRP wraps, but there is still lacking to identify adequately accurate model to use for design purposes. Most of these models were calibrated by limited data. Additionally, most research studies regarding FRP-confined concrete has been focused on normal strength concrete (NSC) and low-cycle loading. Because of lack of reliable test database for high performance concrete (HPC), existing design equations are all restricted to normal strength concrete (NSC). In particular, limited experiments have been conducted on large-scale circular concrete columns confined by FRP wraps and subjected to cycle loading (high and low). Therefore more experimental investigations and theoretical analysis shall be conducted.

1.3 RESEARCH OBJECTIVES

This present study is part of a comprehensive research program, which has been carried out at Brno University of Technology in the Institute of Concrete and Masonry Structures.

The research objectives are:

1. To investigate the behavior of cantilever circular concrete columns transversally confined by CFRP wrap
2. To propose design algorithm to strengthen circular concrete columns with CFRP wraps subjected to axial load and cyclic lateral load
3. To propose an empirical model for FRP confined concrete subjected to cyclic loading.

The procedures carried out in this research are as follows:

1. **Experimental test:** Four specimens of cantilever circular concrete columns have been selected to provide experimental test; one specimen as control specimen subjected to high and low cycle loading and two specimens confined with six layers of CFRP wrap at plastic hinge length subjected to the same load configuration as control specimen and one unconfined specimen subjected to low cycle loading only. Columns were subjected to axial force and lateral cyclic load in two different ways. Firstly under force control; i.e. same lateral cyclic force pulling in one direction for certain number of cycles (approximately 1 million cycles), secondly under displacement control; i.e. reversed cyclic lateral load based on a pattern of progressively increasing displacements.
2. **Analysis:** Numerical study consists of mathematical model based on finite element method, was created by ATENA 3D software to simulate the behavior of unconfined and confined circular columns subjected to axial load and cyclic lateral load under displacement control.
3. **Design:** Design Algorithm introduces the considerations of the design of circular column confined with FRP subjected to cyclic loading (Empirical Model), and the procedures to improve flexural hinge ductility, and lap splice clamp developed by C# programming language.

1.4 DISSERTATION OUTLINE

The dissertation work consists of the following chapters:

Chapter 1 presents an introduction, the problem, the research objectives and the dissertation outline.

Chapter 2 presents a literature review of some previous research studies on the FRP confined concrete. It presents an overview of the composite materials, methods of retrofitting,

confinement action, factors influencing the confinement performances, proposed models for confinement by composite materials, code provisions, reinforced concrete columns in seismic zones, and conclusion of experimental works.

Chapter 3 presents the research study, which consists of three parts:

First part presents a theoretical part that introduces an analytical analysis of the circular concrete column cross-section.

Second part presents an experimental work at Brno University of Technology's laboratory that was carried out on a number of FRP-confined circular concrete columns and the test results evaluations. An experimental study is provided to evaluate the efficiency of the confinement of externally bonded FRP when cyclic loading is applied.

Third part presents numerical analysis that introduces a mathematical model prepared by ATENA 3D software based on finite element method to simulate the behavior of unconfined and confined circular columns subjected to axial load and cyclic lateral load.

Chapter 4 presents experimental evaluations, comparison of the experimental and numerical results, empirical model for FRP confined concrete subjected to cyclic loading, summary of investigation, design algorithm developed by C# programming language, conclusions and recommendations for future research.

CHAPTER 2- LITERATURE REVIEW

2.1 INTRODUCTION

This chapter presents an overview of the composite materials, the common methods of jacketing, both types of confinement active and passive, the factors influencing the confinement performances, a review of available models for FRP-confined columns to predict the strength and strain enhancement, code provisions, reinforced concrete columns in seismic zones.

2.2 COMPOSITE MATERIALS

Composite materials are materials formed from two or more materials with significantly different physical or chemical properties, that when combined, produce a material with characteristics different from the individual components. The individual components remain separate and distinct within the finished structure. Composite materials have the advantages of being stronger and lighter or less expensive when compared to traditional materials. For example Fiber-reinforced polymer tensile strength and Young's modulus of elasticity can be increased four and two times more than that of traditional materials, respectively. This means that a composite material structure may weigh nearly half of a traditional material structure of equal stiffness.

Fiber Reinforced Polymer (FRP) is a composite material consisting of polymer matrix reinforced with fibers. The fibers are stronger than the matrix. There are many types of fiber, usually are glass (G), carbon (C) and aramid (A). The polymer matrix is usually an epoxy, vinyl ester or polyester thermosetting plastic, and phenol formaldehyde resins are still in use. FRP is commonly used in the aerospace, automotive, marine, construction industries and ballistic armor. FRP involves two distinct processes, the first is the process whereby the fibrous material is manufactured and formed, and the second is the process whereby fibrous materials are bonded with the matrix during molding. The mechanical properties of FRP depend on many factors; fiber quality, form, direction, volumetric ratio, adhesion to the matrix, and the manufacturing process.

The stress-strain relationships for fibers, matrix, and the resulting FRP material are illustrated in *Figure 1*.

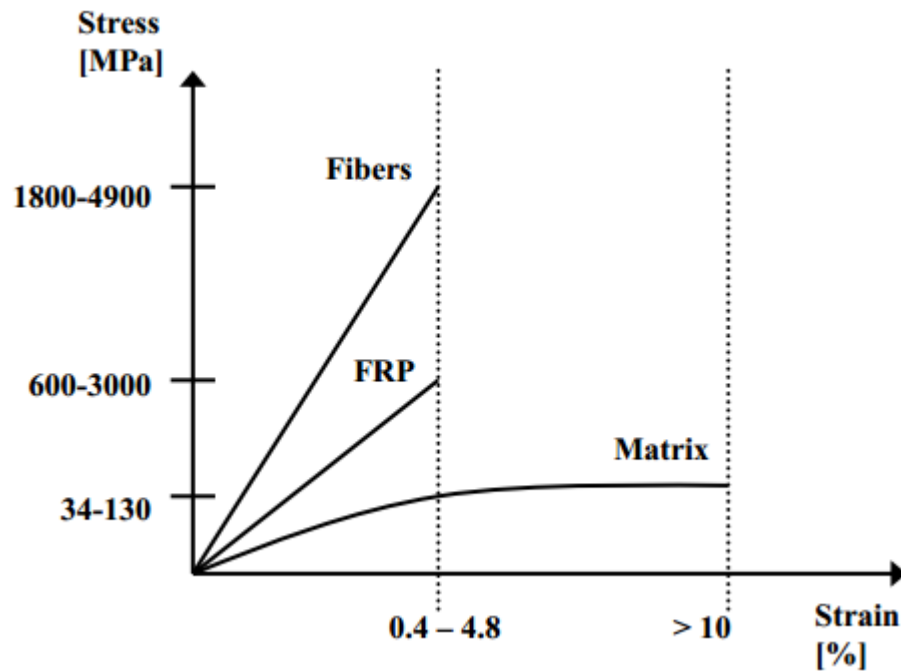


Figure 1 - Stress-strain relationship of fiber, matrix and FRP [26]

Glass fibers are common in the naval and industrial fields to produce composites of medium high performance. They are characterized by high strength. Glass is mainly made of silicon with tetrahedral structure. Glass fibers are classified into three types: E-glass fibers, S-glass and alkali resistant AR-glass fibers. E-glass fibers contain high amounts of boric and acid aluminate, and are disadvantageous in having low alkali resistance. S-glass fibers are stronger and stiffer than E-glass, but still not resistant to alkali. AR-glass fibers contain a considerable amount of zircon to prevent erosion by cement-alkali. Glass fibers are susceptible to creep and have low fatigue strength.

Aramid fibers are organic fibers, made of aromatic polyamides in an extremely oriented form. The structure of aramid is anisotropic and gives high strength and modulus in the fiber in longitudinal direction. Aramid fibers exhibit high toughness, damage tolerance and fatigue characteristics. They are sensitive to moisture, and may degrade after extensive exposure to sunlight. Their creep behavior is similar to that of glass fibers, even though their failure strength and fatigue behavior is higher than that of glass fibers.

Carbon fibers are based on pitch or PAN, as raw material. PAN fibers are made of polyacrylonitrile that is carbonized through burning. Carbon fibers are used for their high performance and are characterized by high strength. Carbon fibers exhibit higher values of Young's modulus of elasticity than that of typical construction materials. Therefore, they are more

effective from a structural point of view. They have a brittle failure with relatively low energy absorption. Their failure strength are larger compared to glass and aramid fibers. Carbon fibers are less sensitive to creep rupture and fatigue and they may show a slight reduction of the long-term tensile strength.

Typical properties of various types of fiber materials (Feldman 1989, Kim 1995) [4] are provided in *Table 1*.

Table 1 - Typical properties of fibers [4]

Fiber Type		Tensile Strength [MPa]	Elastic Modulus [GPa]	Ultimate Tensile Strain [%]
Carbon	High Strength	3500-4800	215-235	1.4-2.0
	Ultra High Strength	3500-6000	215-235	1.5-2.3
	High Modulus	2500-3100	350-500	0.5-0.9
	Ultra High Modulus	2100-2400	500-700	0.2-0.4
Glass	E-Glass	1900-3000	70	3.0-4.5
	S-Glass	3500-4800	85-90	4.5-5.5
Aramid	Low Modulus	3500-4100	70-80	4.3-5.0
	High Modulus	3500-4000	115-130	2.5-3.5

To illustrate the variation in confining material properties, *Figure 2* shows typical stress-strain diagrams for common materials. FRP has elastic behavior up to failure contrary than steel, which applies a constant confining pressure after yield. Therefore, FRP exhibits its confining action on concrete under axial load in a different way than steel.

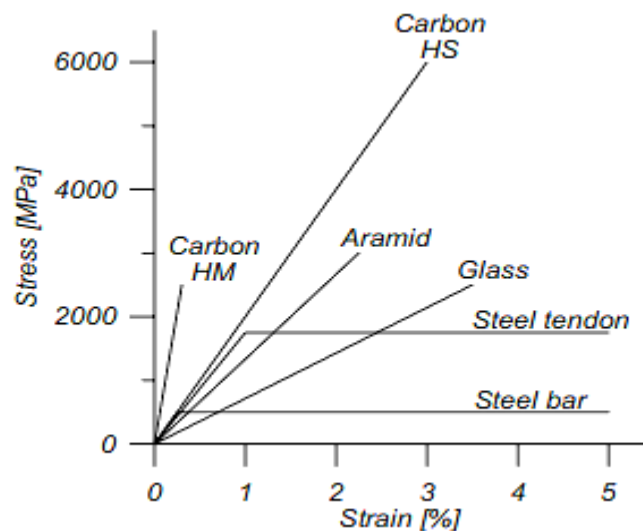


Figure 2 - Stress-strain diagram for fibers & reinforcement steel [2]

The matrix must also meet certain requirements in order to be convenient for FRPs and maintain a successful reinforcement of it. The matrix must be able to properly saturate, and bond with the fibers within a suitable curing period. The matrix should preferably bond chemically with the fiber reinforcement for maximum adhesion. The matrix must also completely envelope the fibers to protect them from cuts and notches that would reduce their strength, and to transfer forces to the fibers. The fibers must be maintained separately from each other to avoid global failure as much as possible and if failure occurs the matrix must be deboned from the fiber for similar reasons. In civil engineering, thermosetting resins are almost used. The thermosets vinyl ester and epoxy are the most common matrices. Epoxy is mostly favored above vinyl ester but it is more costly. Epoxy has a pot life around 30 minutes at 20°C but it can be changed with different formulations. The curing process goes faster with increased temperature. Epoxies have good strength, bond, creep properties, and chemical resistance. Material properties of epoxy and polyester are shown in *Table 2*.

Table 2 - Properties of matrix materials [52]

Materials	Tensile strength [MPa]	Tensile modulus [GPa]	Failure strain [%]	Density [kg/m ³]
Epoxy	55-130	2,5-4,1	1,5-9,0	1100-1300
Polyester	20-100	2,1-4,1	1,0-6,5	1000-1450

2.3 METHODS OF RETROFITTING OR JACKETING

Retrofitting method is the modification of existing structures to make them more resistant to seismic excitation, increasing in load demands, and failure due to environmental degradation. Three common methods of jacketing are available for retrofitting and strengthening existing reinforced concrete columns; reinforced concrete jackets, steel jackets and composite materials FRP jackets.

2.3.1 REINFORCED CONCRETE JACKETING

Reinforced Concrete jacketing as shown in *Figure 3* is conducted by enlarging the existing cross-section with a new layer of reinforced concrete (longitudinal, transversal or ties reinforcement, and concrete). This method is a traditional method used to strengthen existing reinforced concrete columns (for seismic upgrading of damaged or poorly detailed reinforced concrete construction). In applying this technique, the objective is to inhibit premature modes of failure that would otherwise obtain in the structural members under reversed cyclic loading, thereby promoting flexural yielding of primary reinforcement [25].



Figure 3 - Concrete jacketing of circular & square columns [46]

Through reinforced concrete jacketing the axial strength, the bending strength and the stiffness of the existing structures are increased, whereas dependable deformation quantities may or may not be enhanced, depending on the aspect ratio of the upgraded element and the factors limiting deformation capacity in the initial state of the element. The concrete jacketed columns have similar requirements of construction of formwork, reinforcement detailing and concrete casting.

2.3.2 STEEL JACKETING

Steel jacketing as shown in *Figure 4* has been used as a method to enhance the shear strength and the ductility of existing reinforced concrete columns. Previous research (Chai, Priestley and Seible, 1991) [23], [24] has shown that steel jacketing is an effective column retrofit method for deficient reinforced concrete columns to improve earthquake resistant capacity. Steel jackets provide deficient columns with the necessary confinement and are approximately equivalent to external, closely spaced spiral reinforcement. Steel jacket retrofitting was originally developed for retrofitting circular columns using two semi-circular shells of steel rolled. After the two shells are welded together around the column, the gap between the jacket and the column is filled with non-shrink grout. A clearance of approximately 50 mm between the ends of the jacket and footing or cap beam is typically specified in order to prevent the jacket from bearing against the member at large drift angles. Steel jacket does not require any formwork, which results in considerable economy of time. This method of jacketing requires a surface treatment against corrosion of steel.



Figure 4 - Steel jacketing of circular & square columns [46]

2.3.3 FRP JACKETING

Recent development in the manufacturing of FRP makes these materials (used as confinement materials) available for a wide range of applications in retrofitting and strengthening of existing reinforced concrete structures including seismic upgrading of columns. Compared to concrete and steel jacketing, FRP wrapping has several advantages (high-corrosion resistance, minimal thickness, ease and fast application, ability to fit to any structural shape, etc.). For columns as shown in *Figure 5*, the same idea applies for steel and concrete jackets. Composite jacket reinforcement acts in most cases in passive way to increase confinement, which leads to significant increase in strength and ductility [4], [6]. A great number of researches and tests on composite column retrofit systems have shown to be effective. These systems are mainly divided into three types [4]:

- 1) Wet lay-up systems
- 2) Pre-fabricated systems and
- 3) Special systems e.g. automated wrapping, pre-stressing etc.

Surface preparation of existing column is very important. FRP wrapping is vulnerable to stress concentration. The prepared column surface should be roughened to ensure proper bonding of FRP wrap with the existing column. FRP jacketing of columns also does not require any formwork which economizes time.



Figure 5 - FRP jacketing of columns [45]

2.4 CONFINEMENT ACTION

The main purpose of confinement is to provide lateral support to the vertical reinforcement, to improve the compressive strain and the deformation capacity of the concrete columns. In recent years, the strengthening of existing reinforced concrete (RC) columns using external Fiber Reinforced Polymers (FRP) jackets is the most common method for repair and retrofit of RC columns. The increase in strength is attributed to the lateral confinement of FRP materials. The benefits of using FRP jackets and the differences of the behavior of the concrete confined with FRP, compared to steel, attract the attention of civil and construction industry to work on developing more accurate models for FRP-confined concrete especially in seismic zones. The differences originate from the elastic behavior of FRP jackets that supply increasing pressure on the concrete with lateral expansion. On the contrary, a steel jacket applies constant pressure after yielding.

In last decades, a large number of experimental and analytical studies have been published on FRP-confined concrete specimens. Two different types of confinement can be recognized: passive and active confinement. *Figure 6* shows the schematic of passively and actively confined circular concrete columns.

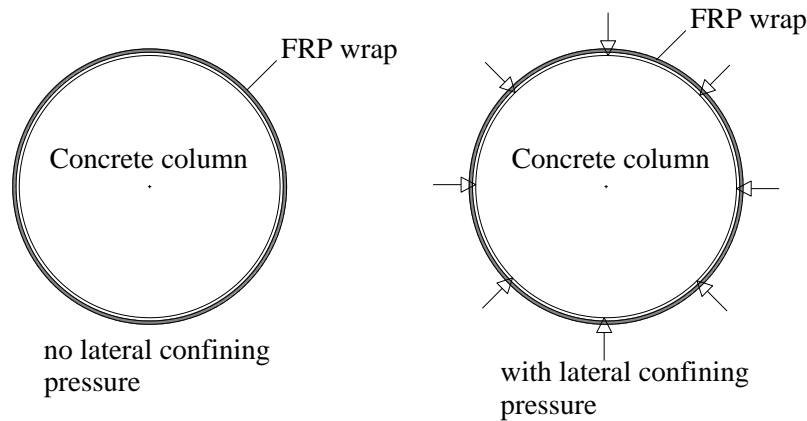


Figure 6 - Passive and active confinement of column cross-section

2.4.1 PASSIVE CONFINEMENT

Passive confinement controls the lateral expansion of concrete, and it is achieved by wrapping the concrete with FRP wrap. When the concrete is loaded axially, a lateral expansion of the concrete occurred, which is restrained by the confining device, which produces a lateral pressure at the interface. As the axial load increases, the tendency for lateral expansion increases and therefore the confining pressure increases. The amount of confining pressure is the function of deformation characteristics of concrete, which in turn, depend on the lateral stiffness of the confining material.

As fiber-reinforced polymers are composite materials that have been widely used in constructions for retrofitting and repairing of RC structures due to their characteristics as presented before, these characteristics encouraged many practitioners to use FRP wraps for concrete passive confinement instead of steel and concrete jackets. Many studies attempted to use FRP to encase concrete cylinders and many analytical models were developed to predict the behavior and the stress-strain relationship of confined concrete with FRPs. The authors observed that the strength and the ductility of the confined concrete were improved. Mander et al. (1988) [15] model was formulated using the tri-axial test data which is characterized by a constant confining pressure unlike the constantly increasing confining pressure applied by the FRP wraps. In addition, the Mander et al. model [15] adopted the stress-strain curve proposed by Popovics (1973), which was inappropriate for describing the bilinear behavior of concrete confined by FRPs. The bilinear behavior of the confined concrete was exhibited and confirmed experimentally by many studies. The lateral confining pressure can be derived using the stress equilibrium and

radial displacement compatibility considerations between the concrete core and the jacket as shown in *Figure 7*.

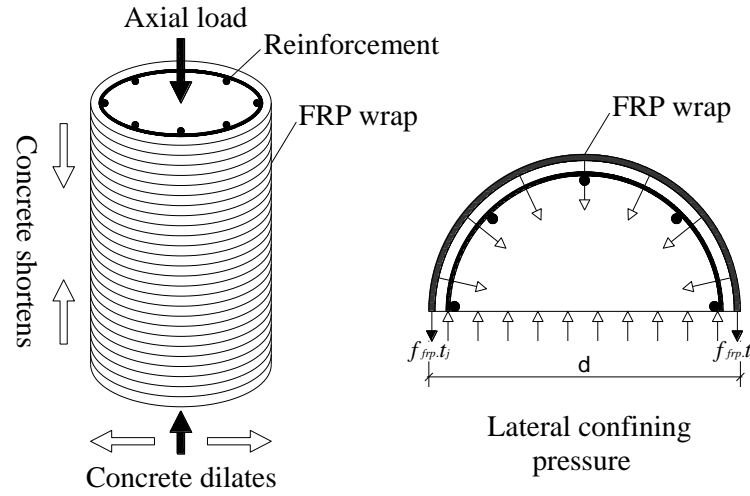


Figure 7 - Confining action of FRP

The lateral pressure can be computed [26]

$$\sigma_l = \frac{2f_{frp}t_j}{d} = \frac{2E_{frp}\varepsilon_{frp}t_j}{d}, \quad (1)$$

where $f_{frp} = E_{frp}\varepsilon_{frp}$; the tensile strength of FRP in the hoop direction, t_j = total thickness of the FRP jacket, d = diameter of the confined concrete core. The effectiveness of FRP confined members only depends on a fraction of the confinement lateral pressure exerted by the system, namely effective confinement lateral pressure $\sigma_{l,eff}$. The effective confinement lateral pressure is a function of member cross-section and FRP configuration as indicated in the following equations

$$\sigma_{l,eff} = k_{eff}\sigma_l, \quad (2)$$

where k_{eff} is the coefficient of efficiency ($k_{eff} = 1$ for circular cross section), which will be discussed in details in the next paragraph (Factors influencing the confinement performances).

2.4.2 ACTIVE CONFINEMENT

Active confinement, which can be achieved by pre-stressing the confinement material before applying axial load to the concrete, is independent on the lateral expansion of concrete and the lateral stiffness of confining material.

Richart et al. (1928) [27] was one of the pioneers who worked in the field of concrete confinement, especially under tri-axial stress state. The authors used a tri-axial pressure vessel to exert active confining pressure on concrete cylinders. Lateral confining pressure was widely varied from 7% to 57% of the compressive strength of unconfined concrete.

The superiority of active confinement compared to passive confinement encouraged some researchers to investigate the feasibility of applying active confinement in the field of seismic retrofit. The methodology of applying active confinement pressure varied in each study. A few studies focused on exploring experimentally the effect of active confinement on the material level. Other studies attempted to describe analytically the constitutive behavior of concrete when subjected to active confinement.

2.5 FACTORS INFLUENCING THE CONFINEMENT PERFORMANCES

FRP jacketing is a feasible and efficient method for retrofitting and strengthening of existing concrete columns. Performance of FRP jacketing is evaluated by examination of different parameters. Parameters that affect the strength and ductility of FRP-confined concrete columns are as follows:

- Effect of thickness of FRP wraps (number of layers),
- Effect of FRP type (material characteristics, i.e., tensile strength, modulus of elasticity),
- Effect of size of the structural elements (columns, beams, etc.),
- Effect of bond capacity (FRP-concrete interface),
- Effect of column shape (circular and square shape), and wrapping.

There are other parameters that affect the strength and ductility of confined columns like original material properties of unconfined concrete (compressive strength, modulus of elasticity, etc.).

2.5.1 EFFECT OF THICKNESS OF FRP WRAPS – NUMBER OF LAYERS

The increasing in the thickness of FRP can remarkably enhance the strength and ductility of confined concrete. The second slope of stress-strain response as shown in *Figure 8* is mainly depending on the number of FRP layers as observed by Shahawy et al. (2000) [28]. Cui Ciyan (2009) [29] came to the same results except for high strength concrete specimen where the increasing in number of FRP leads to a decrease in confinement efficiency.

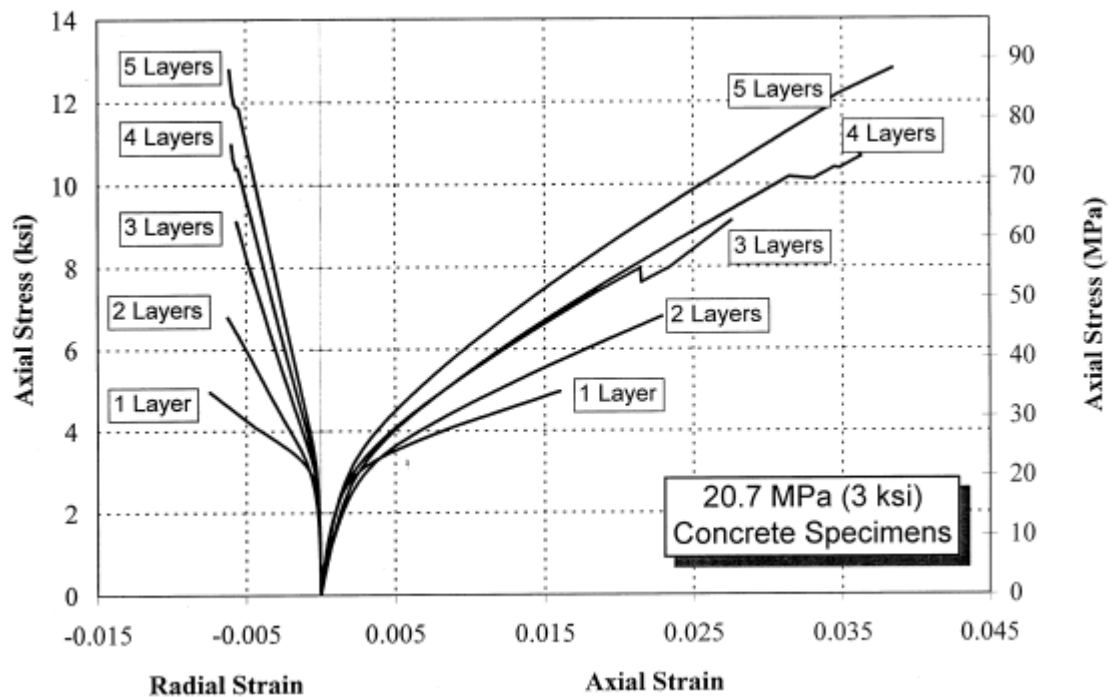


Figure 8 - Stress-strain response [28]

2.5.2 EFFECT OF FRP TYPE (MATERIAL CHARACTERISTICS)

Based on the material properties of fibers mentioned in paragraph 2.1, glass fibers have low modulus of elasticity, better fatigue resistance and higher fiber self-abrasion characteristics compared to other structural fibers. Carbon fibers have a larger energy absorbing capacity that results in an increase in ultimate axial load and ductility. Xiao et al. (2003) [30] studied the stress-strain behavior of concrete columns confined by different types of FRP jackets. The jacket types consisted of CFRP, GFRP, and machine wound CFRP. CFRP jacketed specimen attained higher strength than GFRP.

2.5.3 EFFECT OF SIZE OF THE STRUCTURAL ELEMENTS

Size effect was investigated by many researchers; Miyauchi et al. (1999) [33] studied the size effect by comparing FRP-confined specimens with sizes of 100x200 mm and 150x300 mm. Strength enhancements from FRP confinement were reported to be independent of specimen size. Thériault et al. (2004) [34] studied the effect of specimen size and slenderness ratio on axially loaded FRP-confined concrete by testing specimens with diameters of 150 mm and 300 mm and slenderness ratios of 2 and 6. The experimental work conducted on one type of CFRP and one type of GFRP specimens indicated that the slenderness and size studied had very little influence on confined concrete strength. It was suggested that laboratory investigations using small-scale

150x300 mm specimens could be effectively utilized to evaluate the strength of FRP-confined large-scale columns. A numerical study conducted by T.Jiang and J.G.Teng (2012) [35] on slender FRP-confined column confirmed that the experimental observation of the effectiveness of FRP confinement in enhancing the load bearing capacity of a column decreases as the column becomes more slender.

2.5.4 EFFECT OF BOND CAPACITY (FRP-CONCRETE INTERFACE)

Bond between the FRP jacket and the concrete can be developed using an adhesive such as epoxy. The de-bonding of FRP-concrete interface is one of the main failure modes of the strengthened structures. The interfacial bond plays an important role in the load carrying capacity of FRP reinforced RC members mainly subjected to bending moment. Factors affecting the interfacial bond strength include FRP bond length, FRP stiffness, the adhesive properties, concrete strength, and surface preparation (Antonopoulos & Triantafillou 2002, Cao et al. 2005, Dai et al. 2005, Niu & Wu 2006, Toutanji & Ortiz 2001, Ueda & Dai 2005, Yao et al. 2005)

Diab H., Wu Z. (2007) [36] studied the time-dependent behavior of FRP-concrete interface. The study presents a viscoelastic model for studying the time-dependent behavior and creep failure of the FRP-concrete interface. The proposed model shows its ability to predict the de-bonding and crack propagation along the FRP-concrete interface due to the creep of adhesive not only under low-sustained loadings but also under high-sustained loadings. The effect of bond capacity has no significant influence in columns under axial compressive loads.

2.5.5 EFFECT OF COLUMN SHAPE (SQUARE-CIRCULAR) & WRAPPING)

The main difference between the circular and rectangular shape in terms of confinement is that the lateral pressure is uniformly distributed over the surface of concrete core while in the latter does not. The confinement will be effective at the column corner only, the flat sides of square and rectangular columns remain unconfined as shown in *Figure 9*.

Usually, the sharp corners of the square and rectangular columns are generally rounded off to reduce the stress concentrations at the corners. Al Salloum YA. (2007) [37] examined the influence of edge sharpness on the compressive strength of FRP-Confined square concrete column. Results show that smoothing the edges of square cross-section plays significant roles in delaying the rupture of the FRP at the edges, and the confining stress influenced by the edge sharpness (r), as a result compressive strength of the column decreases.

Additionally, it has been found experimentally and theoretically that with higher corner radius the effective confined concrete area increases for externally confined columns, which help to increase the ultimate confined compressive strength of concrete.

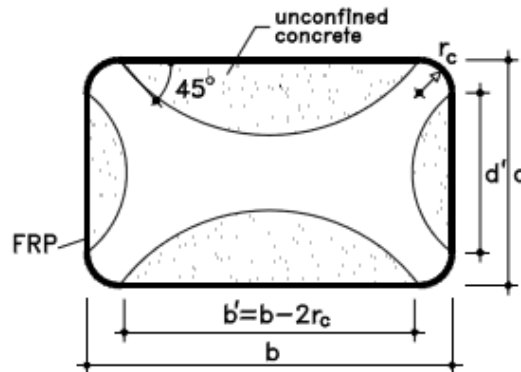


Figure 9 - Effectively confined core of non-circular section [26]

If the concrete is partially wrapped, less efficiency is obtained as both confined and unconfined zones exist, such FRP strips installed with a center to center spacing of p_f and clear spacing of p_f' . Reduction in the confinement effectiveness due to the diffusion of stresses (approx. 45°) between two subsequent wrappings shall be considered as shown in *Figure 10*.

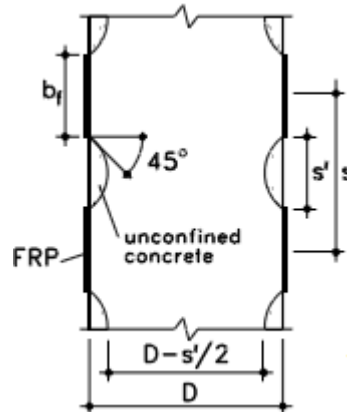


Figure 10 - Concrete confined with FRP strips [26]

As mentioned in the previous paragraph 2.4.1, the effective confinement lateral pressure, is a function of strengthened member cross-section and FRP configurations, the coefficient of efficiency [26], k_{eff} , shall be expressed as

$$k_{eff} = k_H \cdot k_V \cdot k_\alpha \quad (3)$$

The horizontal coefficient of efficiency, k_H depends on cross-section shape. For circular cross-sections $k_H = 1$, and for square and rectangular cross-sections $k_H = 1 - \frac{b'^2 + d'^2}{3 \cdot A_g}$, b' and d' are the dimensions indicated in *Figure 9*, and A_g is the cross-section area.

The vertical coefficient of efficiency, k_v depends on FRP configurations. For RC confined members with continuous FRP wrapping $k_v = 1$, for discontinuous FRP wrapping

$$k_v = \left(1 - \frac{p'_f}{2.d_{\min}}\right)^2, \text{ } d_{\min} \text{ is the minimum dimension of the cross-sections.}$$

Regardless of the section shape, the efficiency coefficient, k_α to be used when fibers are spirally installed with an angle of α with respect to the member cross-section $k_\alpha = \frac{1}{1 + (\tan \alpha)^2}$.

2.6 PROPOSED MODELS FOR CONFINEMENT

The existing models are classified into two categories Lam & Teng (2003) [9]:

- 1) Numerical or analysis-oriented models and
- 2) Empirical or design-oriented models.

For the first category, constitutive models were improved using incremental procedure to plot the entire stress-strain response. Such models need special computer programs, for example; non-linear finite element analysis, therefore, they are not suitable for direct use in design applications. For the second category, the models are mainly based on test results with regression analysis methods in order to calibrate those results. Although, there are several empirical models to predict strength, they are not satisfactory accurate to use in design applications for estimating the overall strengthening effects of columns retrofitted by FRP. This lack is attributed to the three main issues:

(1) Early models were proposed based on steel-confined concrete, although many empirical results have revealed that steel has different response from FRP material in terms of stress –strain response;

(2) The complexity in the interaction phase between FRP jacket and concrete causes difficulty to determine the ultimate hoop rupture strain throughout the variety of FRP forms;

(3) Limited test database is used to assess the existing models, leading to predict unreliable model, so these models need a comprehensive comparative assessment in view of a large database.

The typical form of design-oriented expressions for the prediction of axial strength is as follows:

$$\frac{f_{cc}}{f_{co}} = k_1 + \frac{k_2 \sigma_l^{k_3}}{f_{co}}, \quad (4)$$

where k_1, k_2, k_3 are constants, the value of k_1 is usually 1, the values of k_2 and k_3 are different for each model.

The analysis-oriented models are based on the tri-axial concrete material models with strain and stress compatibility between the concrete and the FRP. Several models are based on non-linear elastic material law. In this case there is a direct relationship between stresses and strains

$$\sigma = [D] \varepsilon, \quad (5)$$

where the stress σ and the strain ε are represented by vectors of six components for a three dimensional approximation and $[D]$ is the elasticity matrix is defined in terms of the material properties. The elements $[D]$ depend on the current level of stresses. In uniaxial loading with monotonic axial strain the elastic modulus of concrete decreases, meanwhile the Poisson's ratio increases. After reaching the peak stress, elements of $[D]$ become negative. In these models the actual confining pressure, $\sigma_{l,a}$ is used. However f_{frp} is usually lower than the tensile strength of composite, and it is calculated as $f_{frp} = E_{frp} \varepsilon_{frp}$, where ε_{frp} , is the experimentally measured hoop strain at rupture.

2.6.1 FARDIS AND KHALILI (1981, 1982)

The authors [38], [39] tested 46 cylindrical short specimens loaded concentrically with size of 75x150 mm for 34.5 MPa concrete and 100x200 mm concrete cylinders that had strength of 31 MPa, four types of glass fiber were used as confinement materials with the number of layers varying from 1 to 5. It was observed that failure of specimens occurred while the lateral strain of confined concrete reaches the failure strain of the FRP in hoop direction. It was stated that the failure of the FRP and concrete occurred simultaneously. Fardis and Khalili implemented Richart et al. model (1929) on FRP-confined concrete and a more accurate criterion suggested by Newman and Newman. (1971) as per *equation (6)*, both can provide satisfactory estimates for the ultimate compressive strength of FRP-confined concrete. The ultimate strain was based on the experimental observations as shown in *equation (7)*

$$\frac{f_{cc}}{f_{co}} = 1 + 3.7 \left(\frac{\sigma_l}{f_{co}} \right)^{0.86}, \quad (6)$$

$$\varepsilon_{cc} = \varepsilon_{co} + 0.0001 \left(\frac{E_f t_f}{D f_{co}''} \right). \quad (7)$$

2.6.2 SAMAAN, SHAHAWY AND MIRMIRAN (1998)

The authors [40] tested cylindrical specimens with size of 152.5 x 305 mm. Concrete cylinders had strength of 30 MPa, and the fiber was unidirectional E-glass at $\pm 75^\circ$ winding angle and the thickness from 1.44 mm to 2.97 mm. The model they developed was one of the first to recognize the principal difference between steel spiral and FRP confined concrete, while the confining stress provided by a steel spiral is constant once the spiral yields, the confining stress provided by FRP increases linearly based on the stiffness of the FRP, until it ruptures

$$\frac{f_{cc}}{f_{co}} = 1 + 6 \frac{\sigma_l^{0.7}}{f_{co}}. \quad (8)$$

In terms of stress-strain, the slope of the second branch model is obtained from the geometry of stress-strain curve as shown in *Figure 11*. The proposed equation by Samaan et al. (1998), [40] to estimate the slope of the second branch of the stress-strain curve reflects the influence of both unconfined concrete strength and the confinement modulus of FRP composites

$$\varepsilon_{cc} = \frac{f_{cc} - f_0}{E_2}, \quad (9)$$

$$f_0 = 0.872 f_{co}' + 0.371 \sigma_l + 6.258, \quad (10)$$

$$E_2 = 245.61 (f_{co}')^{0.20} + 1.3456 \frac{E_f t_f}{D}. \quad (11)$$

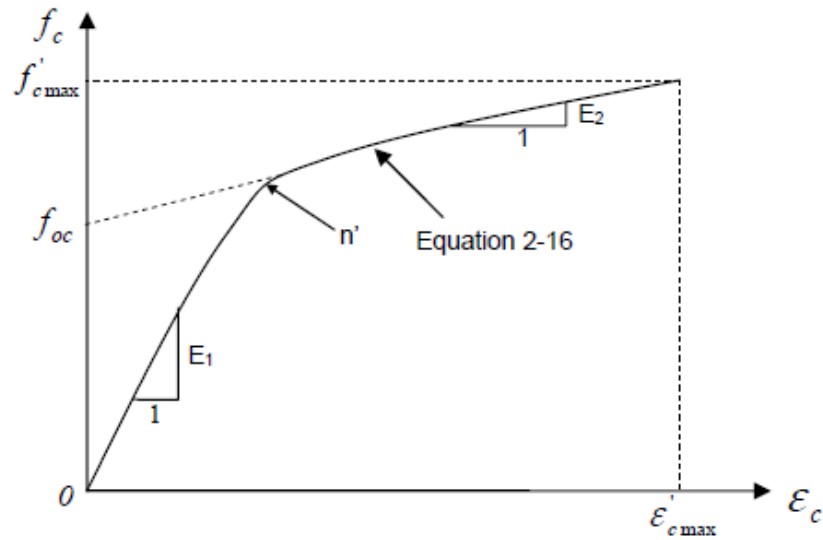


Figure 11 - Stress-strain response of FRP confined concrete [40]

2.6.3 TOUTANJI (1999)

The model was based on analytical and experimental studies [41]; the tests were carried out on 12 cylinder specimens with size of 76 x 305 mm. Two layers of CFRP and one layer of GFRP were used in the tests. The core concrete strength was 31 MPa for all specimens. The model was based on Richart et al. model (1929)

$$\frac{f_{cc}}{f_{co}} = 1 + 3.5 \left(\frac{\sigma_l}{f_{co}} \right)^{0.85} . \quad (12)$$

In terms of strain, the slope of the second branch was based on the assumption that $\varepsilon_0 = 0.002$ as shown in *Figure 12*

$$\varepsilon_{cc} = \varepsilon_{co} \left[1 + (1.90 + 310.57 \varepsilon_f) \left(\frac{f_{cc}}{f_{co}} - 1 \right) \right] . \quad (13)$$

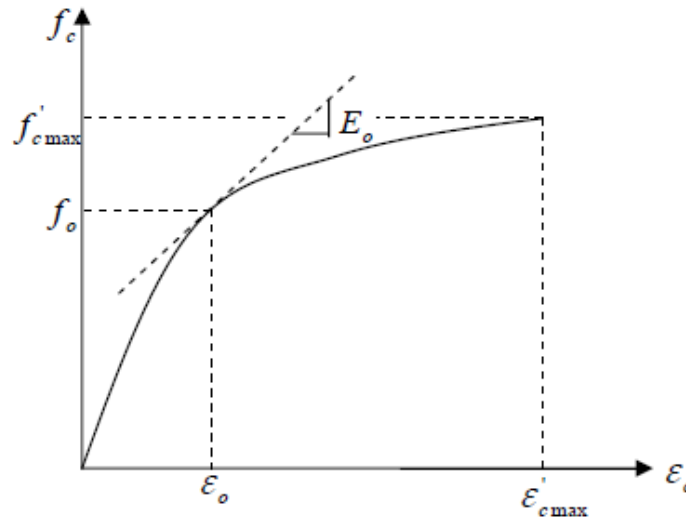


Figure 12 - Stress-strain response of FRP confined concrete [41]

2.6.4 SPOELSTRA AND MONTI (1999)

Spolestra and Monti (1999) [14] developed an analytic, iterative model suitable for either steel or FRP confined concrete and intended for use in a fiber type finite element model. The model is suitable for either type of confinement because it was recognized that FRP, properly applied, provides an ever-increasing confining pressure while a steel spiral provides a constant confining pressure upon yield. The process constructs a stress-strain curve that crosses a series of Mander, Priestly, and Park curves that are each of them calculated for a constant confining stress that is based on a corresponding lateral strain. The iterative process requires seven equations and the following sequence:

Impose ε_c .

1. Set confining stress $\sigma_l = \sigma_{lp}$ from previous iteration;
2. Calculate $f_{cc}(\sigma_l)$ using *equation (14)*;
3. Calculate current stress $f_c(f_{cc})$ from *equation (15)* with *equation (16)*;
4. Update radial strain $\varepsilon_r(f_c)$ from *equation (17)*;
5. Update confining stress σ_l from *equation (18)*;
6. Is $\sigma_l = \sigma_{lp}$? If yes, go to 1 and impose next step. If no, go to 2;

$$\frac{f_{cc}}{f_{co}} = 2.254 \sqrt{1 + \frac{7.94\sigma_l}{f_{co}}} - 2 \frac{\sigma_l}{f_{co}} - 1.254, \quad (14)$$

$$f_c = \frac{f_{cc} x r}{r - 1 + x^r}, \quad (15)$$

$$x = \frac{\varepsilon_c}{\varepsilon_{cc}}; r = \frac{E_c}{E_c - E_{sec}}; \varepsilon_{cc} = \varepsilon_{co} \left[1 + 5 \left(\frac{f_{cc}}{f_{co}} - 1 \right) \right], \quad (16)$$

$$\varepsilon_r(\varepsilon_c, \sigma_l) = \frac{E_c \varepsilon_c - f_c(\varepsilon_c, \sigma_l)}{2\beta f_f(\varepsilon_c, \sigma_l)}, \quad (17)$$

$$\sigma_l = \frac{2E_{frp} \varepsilon_r t_j}{d}. \quad (18)$$

Evaluations performed by Spolestra and Monti indicate that the procedure converges rapidly on an acceptably accurate solution. Based on this model, Spolestra and Monti also developed exact and approximate expressions for the ultimate FRP stress and strain confined specimens. Determination of the exact expression for the ultimate compressive stress and strain begins by calculating the ultimate confining pressure by *equation (18)*.

Next, the Mander stress-strain curve parameters corresponding to the ultimate confining pressure are calculated by *equations (14) and (16)*. Then the secant modulus of elasticity is determined by *equation (19)* which allows the finding of the ultimate compressive stress and strain by *equations (20) and (21)*

$$E_{secu} = \frac{E_{co}}{1 + \frac{2\beta f_{frp}}{E_{frp}}} \quad \text{with} \quad \beta = \frac{E_c}{|f_{co}|} - \frac{1}{|\varepsilon_{co}|}, \quad (19)$$

$$\varepsilon_{cu} = \varepsilon_{cc} \left[\frac{E_{sec}(E_c - E_{secu})}{E_{secu}(E_c - E_{secu})} \right]^{\frac{1-E_{sec}}{E_c}}, \quad (20)$$

$$f_{cu} = E_{secu} \varepsilon_{cu} \quad \text{where} \quad E_{secu} = \frac{f_{cc}}{\varepsilon_{cc}}. \quad (21)$$

2.6.5 LAM AND TENG (2003)

Lam and Teng (2003) [9], using a database of 76 specimens from a variety of researchers, developed a design type model which addresses behavioral aspects that were not included in most previous models. First, they confirmed Spolestra and Monti's (1999) [14] requirement for sufficient confinement. Second, they advanced the understanding of the first branch of the bi-linear stress-strain curve. Many previous models based on the equation for this curve, on one of the expressions for plain concrete, stated that the presence of FRP did not affect behavior in this region. Lam and Teng demonstrated that the FRP confinement becomes effective once the concrete behavior becomes non-linear and that the first branch model must include the contribution of the FRP. Third, many previous researchers reported that models failed to predict the ultimate strain accurately and that the FRP jackets are ruptured at a lower strain than expected. Lam and Teng indicated that the rupture strain of the FRP jacket, when employed on a circular column, should be taken as 58.6% of the tensile coupon rupture strain.

Lam and Teng's model uses two closed form equations to generate the stress-strain curve. First, the actual maximum confining stress is calculated by *equation (22)* which includes a correction for the aforementioned FRP rupture strain

$$\sigma_{l,a} = \frac{2E_{frp}\varepsilon_{h,rupt}}{d} \quad \text{with} \quad \varepsilon_{h,rupt} = 0.586\varepsilon_{frp}. \quad (22)$$

The ultimate stress and strain can be calculated from the following equations:

$$\frac{f_{cc}}{f_{co}} = 1 + 3.3 \frac{\sigma_{l,a}}{f_{co}}, \quad (23)$$

$$\frac{\varepsilon_{cc}}{\varepsilon_{co}} = 1.75 + 12 \left(\frac{\sigma_{l,a}}{f_{co}} \right) \left(\frac{\varepsilon_{h,rupt}}{\varepsilon_{co}} \right)^{0.45}. \quad (24)$$

A constitutive model was proposed for FRP-confined concrete based on bilinear shape as shown in *Figure 13*. Two portions (parabolic and straight) were used to describe the complete response.

$$f_c = E_c \varepsilon_c - \frac{(E_c - E_2)^2}{4f_{co}} \varepsilon_c^2 \quad \text{for} \quad 0 \leq \varepsilon_c \leq \varepsilon_0 \quad (25)$$

$$f_c = f_{co} + E_{c2} \varepsilon_c \quad \text{for} \quad \varepsilon_0 \leq \varepsilon_c \leq \varepsilon_{\max} \quad (26)$$

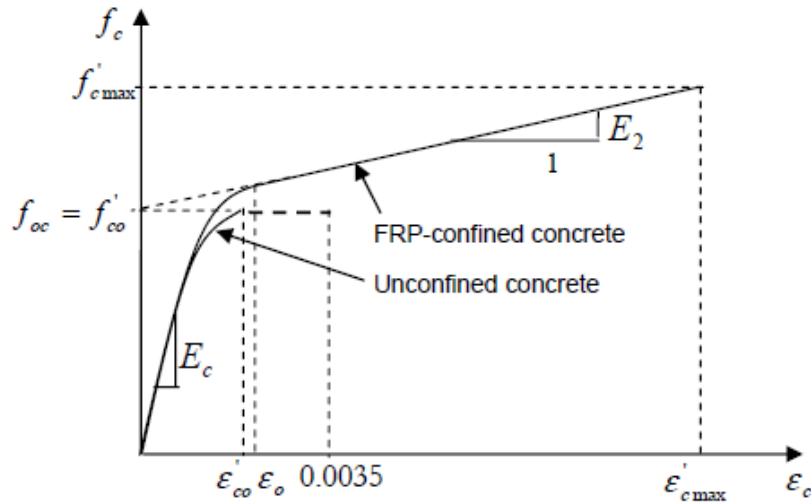


Figure 13 - Stress-strain response for FRP confined concrete [9]

When these parameters are known, the transition strain ε_0 can be found by *equation (28)*

$$E_2 = \frac{f_{cc} - f_{co}}{\varepsilon_{c \max}}, \quad (27)$$

$$\varepsilon_0 = \frac{2f_{co}}{(E_c - E_2)}. \quad (28)$$

Lam and Teng's model represents the current state of the art in designing oriented models. Based on a wide variety of tests from various researchers, it accurately models the FRP confined concrete behavior. Its closed form equations and its use of readily available material parameters make it very user-friendly and applicable to programming in a spreadsheet. Its principal drawback is that the reference database only includes specimens that failed in FRP rupture. Other failure modes are excluded from the database and the results comparison. In addition, *Table 4* and *Table 4* illustrate the summary of some existing design and analysis-oriented models to predict the ultimate axial compressive strength and strain of confined concrete.

Table 3 - Design-oriented models for confined concrete

Models	Ultimate compressive strength	Ultimate strain
Fardis & Khalili 1982	$\frac{f_{cc}}{f_{co}} = 1 + 3,7 \left(\frac{\sigma_l}{f_{co}} \right)^{0,86}$ by Richart et al. $\frac{f_{cc}}{f_{co}} = 1 + 4,1 \left(\frac{\sigma_l}{f_{co}} \right)$ by Newman et al.	$\varepsilon_{cc} = \varepsilon_{co} + 0,001 \left(\frac{E_f t_f}{D f_{co}} \right)$
Spoelstra & Monti 1999	$\frac{f_{cc}}{f_{co}} = 0,2 + 3,0 \sqrt{\frac{\sigma_l}{f_{co}}}$	$\varepsilon_{cc} = \varepsilon_{co} \left[2 + 1,25 \frac{E_c}{f_{co}} \varepsilon_f \left(\frac{\sigma_l}{f_{co}} \right)^{0,5} \right]$ where $\varepsilon_{co} = 0,002$
Ilki et al. 2002	$\frac{f_{cc}}{f_{co}} = 1 + 2,227 \left(\frac{\sigma_l}{f_{co}} \right)$ for CFRP wraps	$\varepsilon_{cc} = \varepsilon_{co} \left[1 + 15,156 \left(\frac{\sigma_l}{f_{co}} \right)^{0,735} \right]$
Lam and Teng 2003	$\frac{f_{cc}}{f_{co}} = 1 + 3,5 \frac{\sigma_l}{f_{co}}$	$\varepsilon_{cc} = \varepsilon_{co} \left(1,75 + 12 \left(\frac{\sigma_l}{f_{co}} \right) \left(\frac{\varepsilon_{h,rupt}}{\varepsilon_{co}} \right)^{0,45} \right)$
Bisby et al. 2005	$\frac{f_{cc}}{f_{co}} = 1 + 2,217 \left(\frac{\sigma_l}{f_{co}} \right)^{0,911}$ $\frac{f_{cc}}{f_{co}} = 1 + 3,587 \frac{\sigma_l^{0,84}}{f_{co}}$	$K_2 = 0,0240$ for CFRP-confined concrete $K_2 = 0,0137$ for GFRP-confined concrete $K_2 = 0,0536$ for AFRP-confined concrete
Youssef et al. 2007	$\frac{f_{cc}}{f_{co}} = 1 + 2,25 \left(\frac{\sigma_l}{f_{co}} \right)^{\frac{5}{4}}$	$\varepsilon_{cc} = 0,003368 + 0,259 \left(\frac{\sigma_l}{f_{co}} \right) \left(\frac{f_{frp}}{E_{frp}} \right)^{0,5}$
Wu et al. 2009	$\frac{f_{cc}}{f_{co}} = 1 + 3,2 \frac{\sigma_l}{f_{co}}$	$\varepsilon_{cc} = \varepsilon_{co} \left[1 + 9,5 \left(\frac{\sigma_l}{f_{co}} \right) \right]$
Benzaid et al. 2010	$\frac{f_{cc}}{f_{co}} = 1 + 2,2 \frac{\sigma_l}{f_{co}}$	$\varepsilon_{cc} = \varepsilon_{co} \left[2 + 7,6 \left(\frac{\sigma_l}{f_{co}} \right) \right]$

Table 4 - Analysis-oriented models for confined concrete

Models	Ultimate compressive strength	Ultimate strain
Mander et al. 1988	$\frac{f_{cc}}{f_{co}} = 2,254 \sqrt{1 + \frac{7,94\sigma_l}{f_{co}}} - 2\frac{\sigma_l}{f_{co}} - 1,254$	$\varepsilon_{cc} = \varepsilon_{co} \left[1 + 5 \left(\frac{f_{cc}}{f_{co}} - 1 \right) \right]$
Marques et al. 2004	$\frac{f_{cc}}{f_{co}} = 1 + 6,7 \frac{\sigma_l^{0,83}}{f_{co}}$	$\varepsilon_{cc} = \varepsilon_{co} \left(1 + 33,5k_3 \frac{\sigma_l^{0,83}}{f_{co}} \right)$ $k_3 = \frac{40}{f_{co}} \leq 1$
Binici et al. 2005	$\frac{f_{cc}}{f_{co}} = \sqrt{1 + \frac{9,9\sigma_l}{f_{co}}} + \frac{\sigma_l}{f_{co}}$	$\varepsilon_{cc} = 5\varepsilon_{co} \left(\frac{f_{cc}}{f_{co}} - 0,8 \right)$
Albanesi et al. 2007	$\frac{f_{cc}}{f_{co}} = 1 + 3,609 \left(\frac{\sigma_l}{f_{co}} \right)$	$\varepsilon_{cc} = \varepsilon_{co} \left[1 + 18,045 \left(\frac{\sigma_l}{f_{co}} \right) \right]$
Teng et al. 2007	$\frac{f_{cc}}{f_{co}} = 1 + 3,5 \frac{\sigma_l}{f_{co}}$	$\varepsilon_{cc} = 5\varepsilon_{co} \left(\frac{f_{cc}}{f_{co}} - 0,8 \right)$
Xiao et al. 2010	$\frac{f_{cc}}{f_{co}} = 1 + 3,24 \left(\frac{\sigma_l}{f_{co}} \right)^{0,80}$	$\varepsilon_{cc} = \varepsilon_{co} \left[1 + 17,4 \left(\frac{\sigma_l}{f_{co}} \right)^{1,06} \right]$

2.6.6 STRENGTHENING AND CONFINEMENT RATIO

There are different recommended equations to predict the strength enhancement of confinement as mentioned before. *Figure 14* displays the comparison of the predicted confined compressive strength enhancement of different models as function of the confinement ratio with considering the effect of layers number. Low confining lateral pressure leads to small increase in strength, which cannot be reliably predicted and therefore it should be avoided. To reach sufficient confinement, a minimum value for the confinement ratio σ_l/f_{co} is recommended. Mirmiran et al. suggested confinement ratio $\sigma_l/f_{co} > 0.15$, while Spoelstra and Monti gave a lower value $\sigma_l/f_{co} > 0.07$ according to their experimental results.

The diameter of circular column adopted to plot the comparison of the predicted confined compressive strength shown in the figure below is 200 mm and the compressive strength of concrete is 73 MPa and the number of CFRP layers is 6. The strengthening ratio is ranged between 1.70 and 2.1 % for maximum confinement ratio of 0.25%.

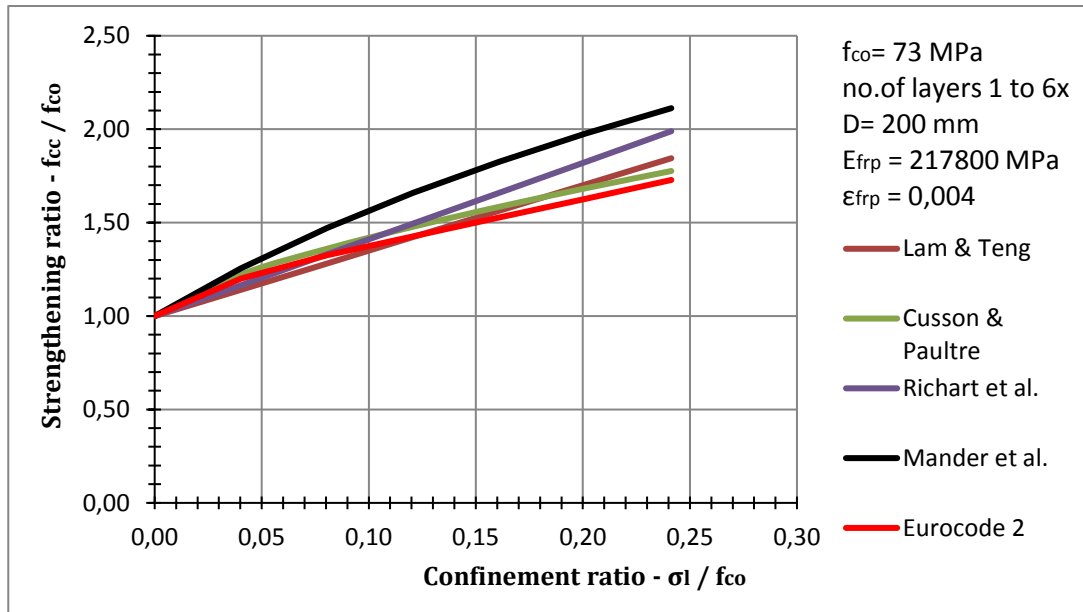


Figure 14 - Strengthening and confinement ratio

2.7 CODE PROVISIONS

2.7.1 CONFINEMENT OF CONCRETE - EN 1992-1-1

Confinement of concrete results in a modification of the effective stress-strain relationship: higher strength and higher critical strains are achieved. The other basic material characteristics may be considered as unaffected for design.

In the absence of more precise data, the stress-strain relation [1] shown in *Figure 15* (Compressive strain shown positive) may be used, with increased characteristic strength and strains according to

$$f_{ck,c} = f_{ck} \left(1 + 5 \frac{\sigma_l}{f_{ck}} \right) \quad \text{for } \sigma_l < 0.05 f_{ck}, \quad (29)$$

$$f_{ck,c} = f_{ck} \left(1.125 + 2.5 \frac{\sigma_l}{f_{ck}} \right) \quad \text{for } \sigma_l > 0.05 f_{ck}, \quad (30)$$

$$\varepsilon_{c2,c} = \varepsilon_{c2} \left(\frac{f_{ck,c}}{f_{ck}} \right)^2, \quad (31)$$

$$\varepsilon_{cu2,c} = \varepsilon_{cu2} + 0.2 \frac{\sigma_l}{f_{ck}}, \quad (32)$$

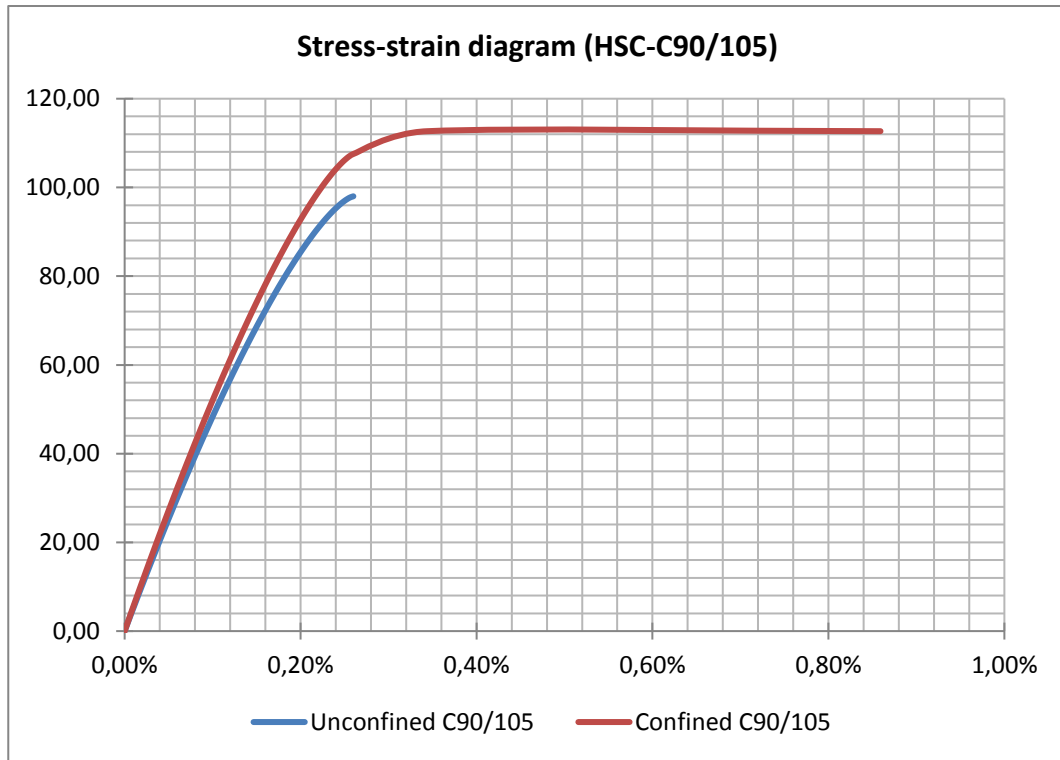


Figure 15 - Stress-strain diagram HPC 90/105 [1]

where

f_{ck} = characteristic compressive cylinder strength of concrete at 28 days;

$f_{ck,c}$ = characteristic compressive cylinder strength of confined concrete at 28 days;

σ_l = effective lateral confining pressure;

$\varepsilon_{cu2,c}$ = ultimate compressive strain of confined concrete;

$\varepsilon_{c2,c}$ = compressive strain of confined concrete;

ε_{cu2} = ultimate Compressive strain of unconfined concrete;

ε_{c2} = compressive strain of unconfined concrete.

2.7.2 CONFINEMENT OF CONCRETE - ACI 440.2R

ACI 440 committee adopted the stress-strain model for FRP-confined concrete by Lam and Teng (2003a, b) based on reasonable predictions including for real size columns. The stress-strain model [2] is illustrated in *Figure 13* and computed using the following expressions:

$$f_c = \begin{cases} E_c \varepsilon_c - \frac{(E_c - E_2)^2 \varepsilon^2}{4f_c} & \text{for } 0 \leq \varepsilon_c \leq \varepsilon_t \\ f_c + E_2 \varepsilon_c & \varepsilon_t \leq \varepsilon_c \leq \varepsilon_{ccu} \end{cases} \quad (33)$$

$$\varepsilon_t = \frac{2f_c}{E_c - E_2}, \quad (34)$$

$$E_2 = \frac{f_{cc} - f_c}{\varepsilon_{ccu}}. \quad (35)$$

The maximum confined concrete compressive strength, f_{cc} and the maximum confinement pressure, σ_l shall be calculated using the following equations with the inclusion of an additional reduction factor $\psi_f = 0.95$.

$$f_{cc} = f_c + 3.3\psi_f\kappa_a\sigma_l, \quad (36)$$

$$\sigma_l = \frac{2nE_f\varepsilon_{fe}t_f}{D}; \text{ for circular cross-section} \quad (37)$$

$$\sigma_l = \frac{2nE_f\varepsilon_{fe}t_f}{\sqrt{b^2 + h^2}}; \text{ for non-circular cross-section} \quad (38)$$

The effective strain level in the FRP at failure ε_{fe} shall be given by

$$\varepsilon_{fe} = 0.55\varepsilon_{fu}. \quad (39)$$

The minimum confinement ratio $\frac{\sigma_l}{f_c}$ shall not be less than 0.08.

The maximum compressive strain in the FRP-confined concrete ε_{ccu} shall not be exceeding 0.01 to prevent excessive cracking and the resulting loss of concrete integrity. The corresponding maximum value of f_{cc} shall be calculated using the following stress-strain relationship

$$\varepsilon_{ccu} = \varepsilon_c \left[1.5 + 12\kappa_b \frac{\sigma_l}{f_c} \left(\frac{\varepsilon_{fe}}{\varepsilon_c} \right)^{0.45} \right] \leq 0.01. \quad (40)$$

For circular cross-section, the shape factors κ_a and κ_b shall be taken as 1.0

For rectangular cross-section, the shape factors are calculated as follows

$$\kappa_a = \frac{A_e}{A_c} \left(\frac{b}{h} \right)^2; \kappa_b = \frac{A_e}{A_c} \left(\frac{h}{b} \right)^{0.5}, \quad (41)$$

$$\frac{A_e}{A_c} = \frac{1 - \left[\left(\frac{b}{h} \right) (h - 2r)^2 + \left(\frac{h}{b} \right) (b - 2r)^2 \right]}{3A_g} \cdot \frac{1}{1 - \rho_g} \quad (42)$$

2.8 REINFORCED CONCRETE COLUMNS IN SEISMIC ZONES

Most of the reinforced concrete columns are designed to support gravity loads without consideration of the lateral forces from seismic loading. Due to the seismic loading, lateral force components causing generation of shear and flexural forces. In order to have structures safe against seismic these must be made ductile enough to withstand the lateral forces while some damage may be allowed. Ductile structures dissipate more energy and thereby may be designed for lower lateral forces than brittle structures. The deformation capacity of existing structures can be enhanced by confinement.

2.8.1 FAILURE MODES

Three different types of failure modes [12] as shown in *Figure 16* (shear, flexural plastic hinge, and lap splice) can be observed in the existing reinforced concrete columns under seismic excitation.



Figure 16 - Shear, plastic hinge, and lap splice failure modes of column [7]

First, shear failure is the most common failure mode; it may lead to the development of inclined cracking, cover concrete spalling, and rupture or opening of the transverse reinforcement,

which leads to brittle column failures. Shear strength of existing inconvenient columns can be enhanced by providing external shear reinforcement or strength to the column through the application of composites with fibres oriented predominantly in the hoop direction. The shear capacity of columns has to be checked, both in the column end regions and in potential plastic hinge regions where the concrete shear capacity can degrade with increasing ductility demands, and in the column centre portion between flexural plastic and /or existing built-in column hinges.

Second, the potential confinement failure of the flexural plastic hinge region, where subsequent to flexural cracking, cover concrete crushing and spalling, buckling of the longitudinal reinforcement or compression failure of the core concrete, initiates plastic hinge deterioration. Plastic hinge failures typically occur with some displacement ductility and are limited to shorter regions in the column. These failures are less destructive and, because of their large inelastic flexural deformations, are more desirable than the brittle column shear failures of the entire column. This desired ductile flexural plastic hinging at the column ends can be achieved by providing confinement in the form of hoop or transverse reinforcement, and using external jacketing in existing columns. The objective of confinement is to prevent cover concrete spalling, provide lateral support of the longitudinal reinforcement, and to enhance concrete strength and deformation capacity.

Third, starter bars for the column reinforcement are placed during the footing construction and lapped with the longitudinal column reinforcement in this region of maximum column moment demand, i.e. the potential plastic hinge region. While the confinement concepts discussed above for plastic hinge regions also apply to lap spliced column ends, the flexural strength of the column can only be developed and maintained when de-bonding of the reinforcement lap splice is prevented. Lap splice de-bonding occurs once vertical cracks develop in the cover concrete and de-bonding progress with increased dilation and cover concrete spalling. The associated flexural capacity degradation can occur rapidly at low flexural ductility in cases where short lap splices are present and little confinement is provided but can also occur more gradual with increased lap length and confinement.

Six design regions [12] defined are based on the different failure mechanisms discussed above. Different column regions require different jacket designs as shown in *Figure 17*, they are as follows:

1. L_s = the lap splice length;
2. L_{cl} = the primary confinement region for plastic hinge;

3. L_{c2} = the secondary confinement region adjacent to the plastic hinge;
4. L_v = the shear strengthening region;
5. L_{vi} = the shear retrofit inside the plastic hinge zone;
6. L_{vo} = the shear retrofit outside the plastic hinge zone.

Strength confinement is required for the entire length of the columns, except for the small gaps at the footing and the cap-beam to allow for the hinge rotation without adding strength or stiffness.

The secondary confinement region is necessary to prevent flexural plastic hinging above the primary plastic hinge zone when confinement allows for significant over strength development in the primary plastic hinge. Plastic hinge confinement lengths L_{c1} and L_{c2} are linked actually to the column geometry based on the expected plastic hinge length both in terms of column depth or diameter in the loading direction, and to the shear span or distance from the column hinge to the point of contra-flexure.

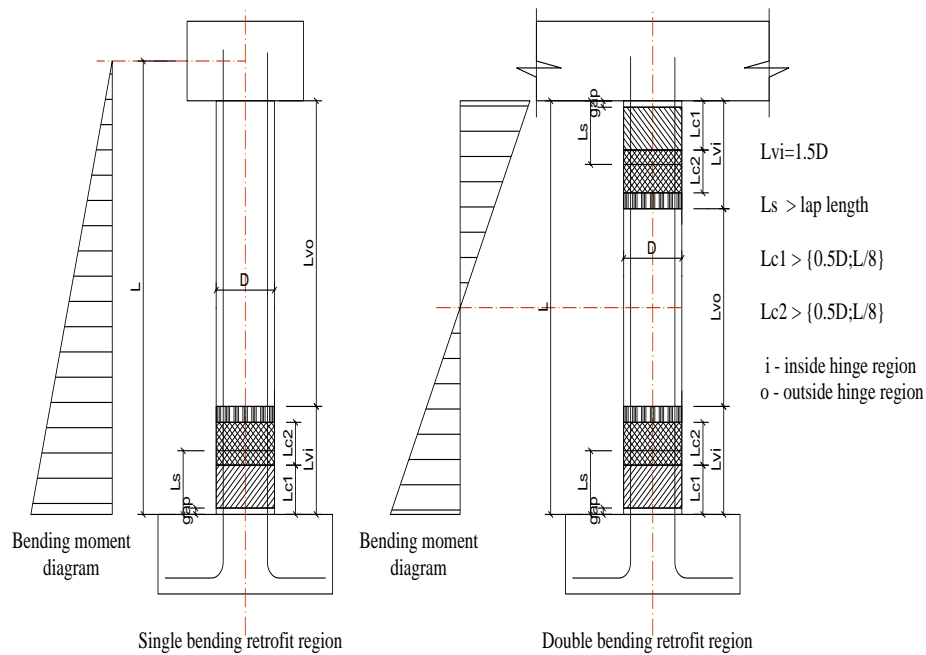


Figure 17 - Single and double bending retrofit region [12]

The lap splice length L_s is defined by the lap length of the starter and column bars and the shear length L_v is the remaining region between the previously defined end zones. In order to avoid direct contact between thick column end jackets and the adjacent bridge footing or cap-beam, a gap is designed to allow plastic hinge rotation without adding strength or stiffness from longitudinal jacket action. For thin jackets wound directly onto the original column geometry this

gap can be very small, i.e. less than 25 mm, whereas in cases where concrete bolsters are added to convert column cross-sections to circular or oval shapes, gaps of 50 mm or more may be required to prevent contact between the retrofit and the adjacent bent portions.

2.8.2 DUCTILITY OF STRUCTURES

Ductility is defined as the ability of a structure to undergo large amplitude cyclic/static deformations in the inelastic range without reduction in strength. It is a very important parameter in seismic design. Generally, ductility relates to energy dissipation and its transformation to heat. When cracks occur, they must close during motion reversal; the absorbed energy is reduced (pinching). In high performance concrete without confinement, ductility is limited. The increased energy dissipation ability offered by ductility will protect the structures from damage and collapse. It should be emphasized that current understanding of seismic resistant design of structures is the assurance of the ductile behaviour of the system through the definition of appropriate positions where inelastic deformations will occur. This method is called capacity design and comprises the basis of many modern seismic resistant design Codes (e.g. EC8, [3]). Confinement enhances both strength and ductility of structures. Confinement of structural columns can be provided by transverse reinforcement placed at close intervals or by confining the columns by composite materials (FRP). The required ductility of a structure can be estimated analytically by nonlinear time history dynamic analysis or more approximately by the consideration of static mechanisms of inelastic deformation. Alternatively, it can be estimated experimentally by shaking table tests or pseudo-dynamic tests. In the nonlinear time-history dynamic analysis of structures, responding to a severe earthquake goes in the inelastic range. It is usual to express the maximum deformations in terms of ductility factor defined as the maximum/ultimate deformation Δ_u divided by corresponding deformation when yielding deformation, Δ_y , occurs. Ductility factors have been commonly expressed in terms of the various response parameters related to deformations, namely the displacements, rotations and curvatures. The displacement ductility ratio in cyclic loading is based on the envelope curve of the hysteretic loops that show the relationship between the strength and displacement of a structural element. A typical envelope of the structure response is shown in *Figure 18a*, which idealizing the actual structural response curve by the linear elastic-perfectly plastic curve. In a similar manner, the displacement, rotational, and curvature ductility factors are expressed respectively by

$$\mu_{\Delta} = \frac{\Delta_u}{\Delta_y}, \quad (43)$$

$$\mu_{\theta} = \frac{\theta_u}{\theta_y}, \quad (44)$$

$$\mu_{\phi} = \frac{\phi_u}{\phi_y}, \quad (45)$$

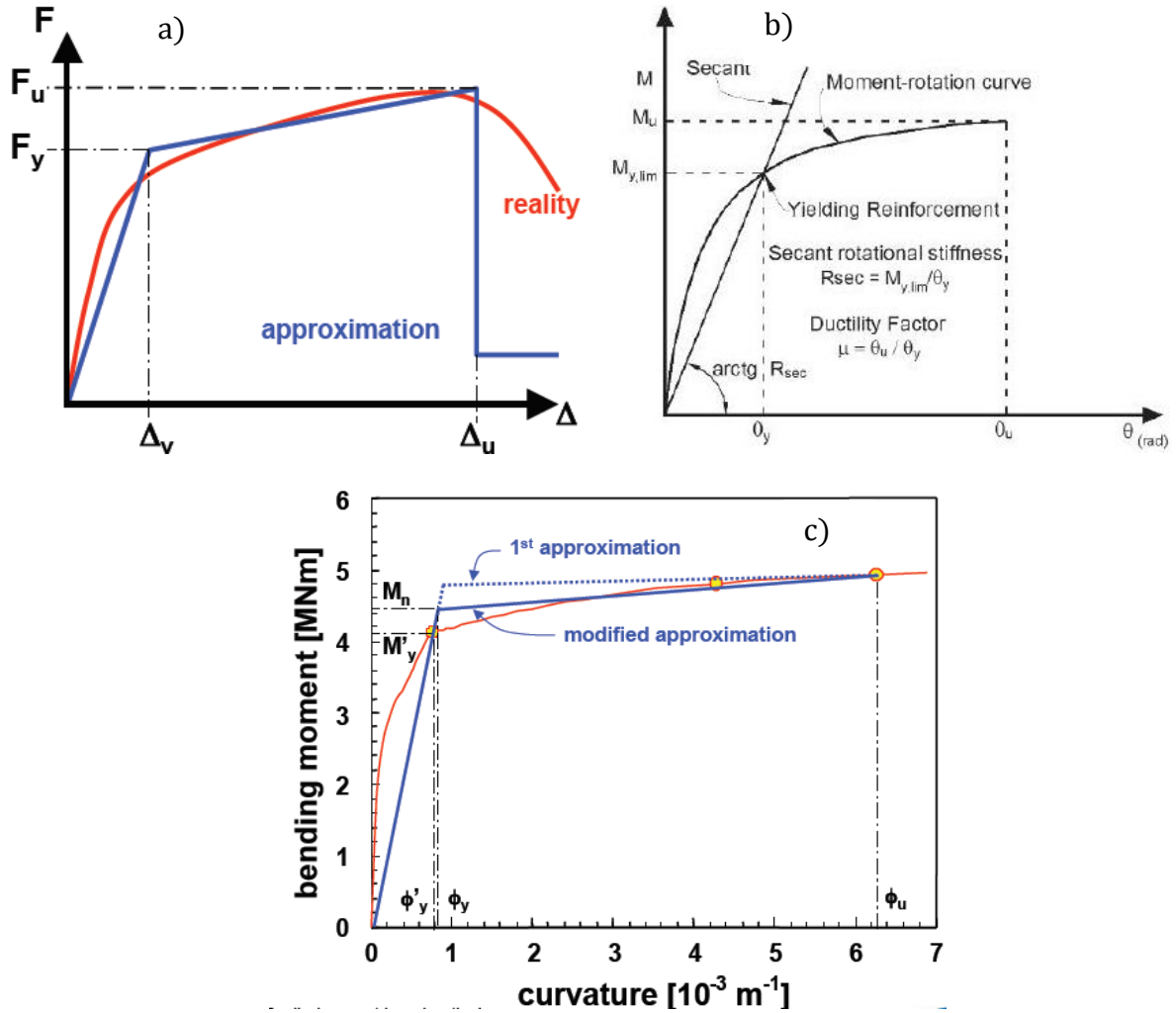


Figure 18 – a) Envelope of actual and idealized structural response, b) Moment rotation curve, c) Moment curvature curve [44]

where

θ_u = ultimate rotation of the structure;

θ_y = yield rotation of the structure;

ϕ_u = ultimate curvature;

ϕ_y = yield curvature;

Δ_u = ultimate deformation;

Δ_y = yield deformation;

μ_A = displacement factor;

μ_θ = rotational factor;

μ_ϕ = curvature factor.

2.8.3 DUCTILITY AMENDMENT

Wrapping of the critical zones of reinforced concrete members/columns with FRP sheets where the plastic hinges are developed might enhance the ductility. These sheets, in the form of hoops, are arranged perpendicularly to the axis of the members. This approach of strengthening increases the strain capacity of the concrete members due to confinement. Eurocode EC8-part3 demonstrates a ratio between target or requested curvature ductility and the available curvature ductility to define the necessary amount of confinement pressure

$$I_x = \frac{\mu_{\phi, tar}}{\mu_{\phi, avail}}, \quad (46)$$

$$f_l = 0.4 I_x^2 \frac{f_{cd} \varepsilon_{cu}^2}{\varepsilon_{ju}^{1.5}}, \quad (47)$$

where

f_l = confinement pressure;

f_{cd} = concrete compressive strength;

ε_{cu} = concrete ultimate strain;

ε_{ju} = adopted FRP jacket strain.

In the case of circular cross-sections, the confinement pressure is computed by equation (1), and in the case of rectangular cross-sections in which the corners have been rounded to allow wrapping, the confinement pressure is computed after been multiplied by $K=2R/D$, where D is larger section width.

Based on the relationship between the confinement pressure and the ratio of the target to available ductility curvature ratio, *Figure 19* shows that the ductility of the structure increases with the increasing of the amount of confinement pressure.

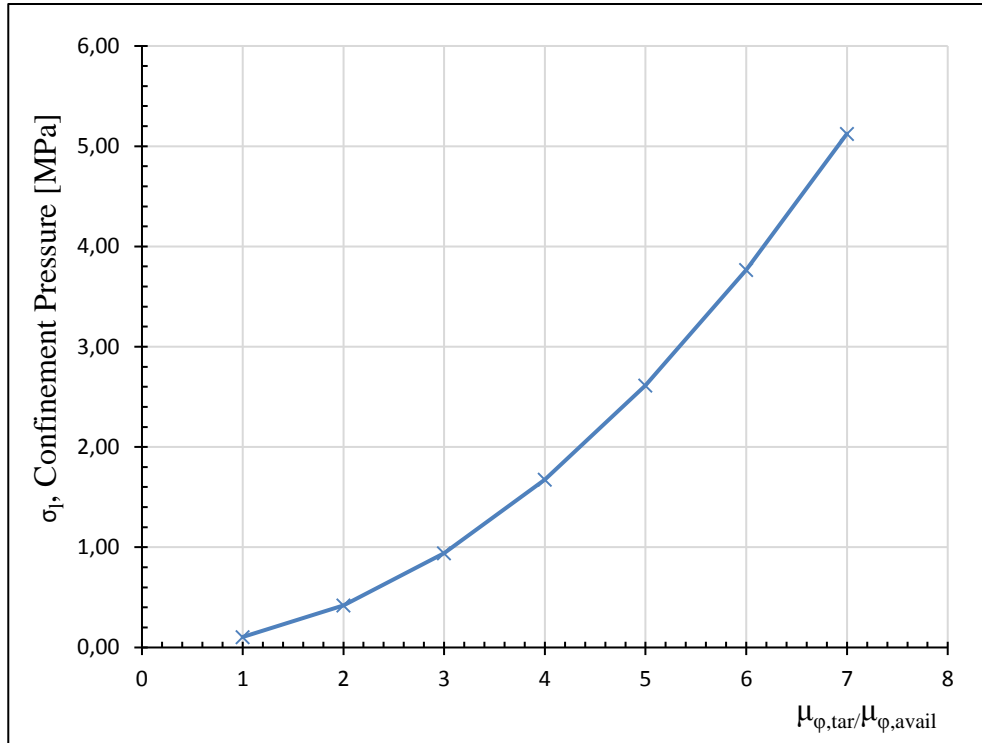


Figure 19 - Ductility and Confinement Pressure Diagram

2.8.4 DESIGN METHODOLOGY

Based on the column failure modes, design guidelines to determine the thickness of composite jacket for the different column regions as shown *Figure 17* are discussed. The approach presented herein by Seible et al. (1995) [12] is one of a number of approaches for the design of jackets for the seismic retrofit of columns.

Confinement to improve shear resistance [7]

The jacket thickness to prevent shear failure of concrete columns can be determined based on equation

$$t_j = \frac{\frac{V_0}{\phi_v} - (V_c + V_s + V_p)}{0.004 \left(\frac{\pi}{2} \right) E_f D}, \quad (48)$$

where

$$V_0 = \frac{1.5M_{yi}}{H}; V_c = kA_e \sqrt{f_{co}''}; V_s = \frac{\pi A_h f_y D'' \cot \theta}{2S}; V_p = \frac{P(D-c)}{H} \text{ for double bending,}$$

V_0 = shear stress in the zone of plastic articulation of the column obtained from an analysis by side bending;

M_{yi} = bending moment;

H = height of the column;

ϕ_v = resistance reduction factor by shear stress = 0.85;

V_c = resistance shear stress taken by the concrete;

V_s = shear stress capacity taken by the transverse reinforcement;

V_p = contribution of the shear stress force by the axial load;

$k = 0.50$; in the zone of plastic articulation, and $k = 0.30$ outside of it;

A_e = effective area = 0.8x area of the column;

A_h = area of the transverse reinforcement;

θ = angle of the crack by shear stress;

S = spacing of the transverse reinforcement;

D' = effective diameter = $D - 2cc - \phi_{trans}$;

P = applied axial load;

c = depth of the neutral axis.

Confinement to improve flexural hinge ductility [7]

Inelastic deformation capacity of flexural plastic hinge regions can be increased by confinement of the column concrete with hoop reinforcement from an advanced composite jacket system. For circular columns, the required jacket thickness can be expressed as

$$t_{frp} = 0.09 \frac{D(\varepsilon_{cu} - 0.004)f'_{cc}}{f_{frp}\varepsilon_{frp}\phi_f}, \quad (49)$$

where $\Phi_f=0.9$ is the flexural capacity reduction factor.

The ultimate concrete strain which depends on the level of confinement provided by the jacket

$$\varepsilon_{cu} = 0.004 + \frac{2.8\rho_{frp}f_{frp}\varepsilon_{frp}}{f'_{cc}}, \quad (50)$$

where ρ_{frp} is the volumetric jacket reinforcement ratio. In turn, ε_{cu} can be obtained from

$$\varepsilon_{cu} = \Phi_u c_u. \quad (51)$$

Based on the ultimate section curvature Φ_u and the corresponding neutral axis depth c_u which both can be determined from a sectional moment-curvature analysis. They are directly related to a structural member ductility factor

$$\mu_{\Delta} = 1 + 3 \left(\frac{\Phi_u}{\Phi_y} - 1 \right) \frac{L_p}{L} \left(1 - 0.5 \frac{L_p}{L} \right), \quad (52)$$

and a semi-empirical plastic hinge length assumption of

$$L_p = 0.08L + 0.022f_{sy}d_b, \quad (53)$$

where L_p represents the shear span to the plastic hinge, Φ_u is the section yield curvature, and f_{sy} , d_b are the yield strength and bar diameter of the main column reinforcement.

Confinement to improve lap splice clamping [7]

The load transfer from the steel reinforcement into the concrete leads to the formation of micro-cracks in the concrete that will reduce the bond between steel and concrete. Retrofitting with FRP jackets and with pre-stressed FRP systems in particular, enhances this bond.

$$t_{frp} = 500 \frac{D(f_l - f_h)}{E_{frp}}. \quad (54)$$

The horizontal stress f_h provided by the existing hoop reinforcement at strain of 10% is calculated as follows:

$$f_h = \frac{0.002A_hE_s}{SD}. \quad (55)$$

The lateral clamping pressure f_l is calculated as follows

$$f_l = \frac{A_s f_y}{\left[\frac{P}{2n} + 2(d_b + cc) \right] L_s}, \quad (56)$$

where

P = perimeter line in the column cross section along the lap spliced bar locations;

n = number of spliced bars along P;

A_s = area of the main column reinforcement bar;

cc = concrete cover to the main column reinforcement;

d_b = diameter of the main column reinforcement bars;

L_s = lap splices reinforcement length.

2.8.5 DEFORMATION CAPACITY OF RC COLUMNS

The deformation capacity of reinforced concrete columns is very important for the determination of their response and the response of the structure under cyclic or seismic loading. The simplest procedure for the calculation of the effective stiffness and the deformation capacity of RC members includes an assumption for the bending behaviour by a moment-curvature relation, which is integrated along the member length. The actual curvature distribution can be modelled in a simplified manner by elastic and inelastic regions. The contribution of the elastic region can be considered by the equation of beam theory

$$\phi = \frac{M}{EI}, \quad (57)$$

where (EI) is the elastic stiffness before yielding, ϕ is the flexural/moment curvature.

The contribution of the plastic region can be considered by assuming that the inelastic deformation is caused by the total plastic rotation θ_p , which is developed in the plastic hinge region. The plastic rotation at failure [47] is equal to

$$\theta_{p,u} = (\phi_u - \phi_y)L_{pl}, \quad (58)$$

where

ϕ_u = the ultimate curvature at the end section;

ϕ_y = the yield curvature at the end section;

L_{pl} = the length of the plastic hinge.

For a simple cantilever member, the chord rotation capacity at failure as [EC8 - Eq. (A.4)] is given

$$\theta_u = \frac{1}{\gamma_{el}} \left[\theta_y + (\phi_u - \phi_y) L_{pl} \left(1 - 0.5 \frac{L_{pl}}{L_v} \right) \right], \quad (59)$$

where

$\theta_y = \phi_y \frac{L_v}{3}$ - The chord rotation at yield;

$L_v = \frac{M}{V}$ - The ratio moment/shear at the end section;

$\gamma_{el} = 1.5$ for primary seismic elements and 1.0 for secondary seismic elements.

The plastic hinge length for as built columns proposed by Priestly et al. is defined as

$$L_{pl} = 0.08L_v + 0.022d_{bl}f_y. \quad (60)$$

For FRP jacket columns based on the formulas proposed by Priestly et al.

$$L_{pl} = gap + 0.044d_{bl}f_y. \quad (61)$$

If the concrete confinement model given in 3.1.9 in Eurocode 2 is assumed, the plastic hinge length is equal to [EC8 - Eq. (A.5)]

$$L_{pl} = 0.1L_v + 0.17h + 0.24 \frac{d_{bl}f_y [MPa]}{\sqrt{f_c [MPa]}}. \quad (62)$$

If the confinement model proposed by Eurocode 8 – part 3 is adopted, to better represent the effects of confinement under cyclic loading, the plastic hinge length is given by

$$L_{pl} = \frac{L_v}{30} + 0.2h + 0.11 \frac{d_{bl}f_y [MPa]}{\sqrt{f_c [MPa]}}. \quad (63)$$

A proposed expression for the ultimate displacement Δ_u , at the tip of a cantilever column

$$\Delta_u = \Delta_y + \Delta_p, \quad (64)$$

where Δ_y is the yield displacement, Δ_p is the plastic displacement. The expression of the yield and plastic displacement are given as follows:

$$\Delta_y = \frac{\phi_y L_v^2}{3}, \quad (65)$$

$$\Delta_p = (\phi_u - \phi_p) L_p (L - 0.5L_p). \quad (66)$$

Priestley et al. (2003) proposed that the yield curvature can be approximated as a function of the column depth and the yield strain of the tension reinforcement

$$\phi_y = \lambda \frac{\varepsilon_y}{D}, \quad (67)$$

where $\lambda = 2.25$ for spiral-reinforced concrete columns and $\lambda = 2.10$ for rectangular columns, D is the diameter of the column, and ε_y is the yield strain of the longitudinal reinforcement.

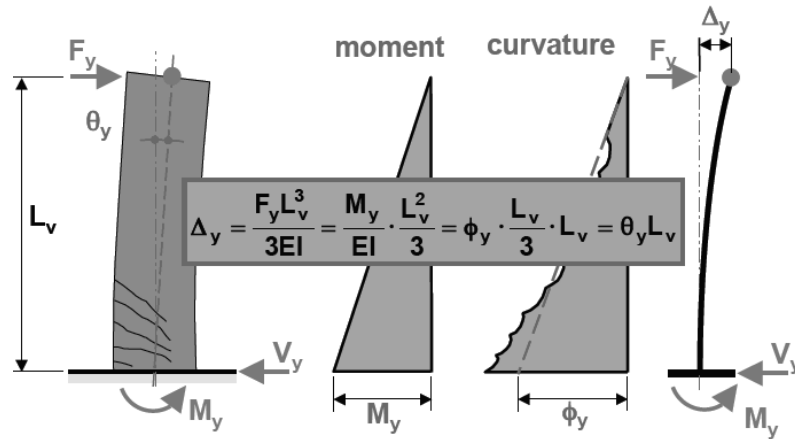


Figure 20 - Yielding chord rotation [44]

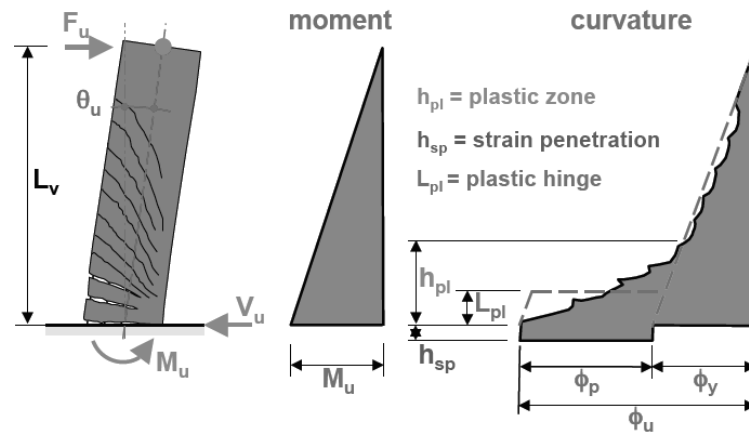


Figure 21 - Plastic hinge length [44]

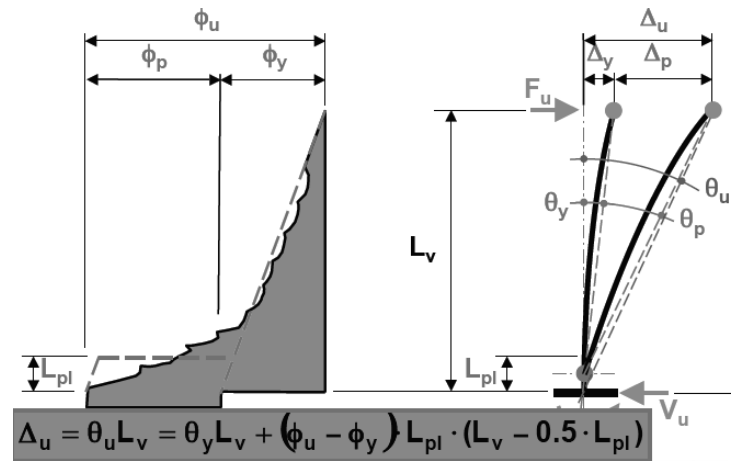


Figure 22 - Ultimate chord rotation [44]

2.8.6 SEISMIC TESTS ON FRP-CONFINED CONCRETE COLUMNS

In the last decades, FRP wrap has become an alternative seismic retrofit technique due to many advantages mentioned in the previous paragraphs. Available experimental results are still limited for large-scale FRP-confined columns tested under seismic loading. In the following sections, some experiments are reported by Sheikh S.A. and Yau G. (2002) [32], Ozbakkaloglu and Saatcioglu (2006, 2007) [21], [22], and O. Ozcan, B. Binici and G. Ozcebe (2008) [31], in which the confined concrete columns were tested under simulated seismic effects and which were consisted of constant axial load and lateral reversed cyclic displacements applied simultaneously.

2.8.6.1 SHEIKH SHAMIM A. AND YAU GRACE (2002)

A total of 12 specimens were tested. Each specimen consisted of a 356 mm diameter and 1470 mm long column cast integrally with a 510x760x810 mm stub. All columns were tested under lateral cyclic loading while simultaneously being subjected to constant axial load throughout the test. The column represented the part of a bridge column or a building column between the section of maximum moment and the point of contra flexure. The stub represented a discontinuity, such as a beam column joint or a footing. In all specimens, the ratio of the core area measured to the centreline of spiral to the gross area of the column section was kept constant at 74%, which is similar to that used in previous tests. All columns contained six 25M (500 mm²) longitudinal steel bars, and the spirals were made of U.S. No. 3 (71 mm²) bars. The reinforcement for the stub consisted of 10M (100 mm²) horizontal and vertical stirrups at 64 mm spacing. In addition, 10M bars with 135 degree hooks were placed at the top and bottom of the stub at the same spacing. The longitudinal bars in the columns were completely extended into the stub, whereas the spiral reinforcement was extended into the stub for 100 mm.

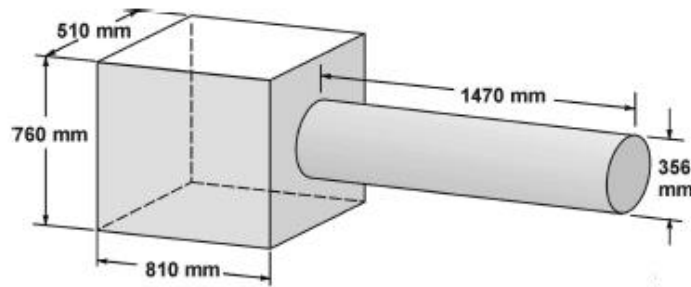


Figure 23 - Geometry of test specimens [32]

The design of the specimens aimed at forcing the failure in the potential plastic hinge region of the column, that is, within a length of 800 mm from the face of the stub. All specimens were cast together in vertical positions. The test specimens are divided into three groups. The first group, Series S, consisted of columns S-1NT, S-2NT, S-3NT, and S-4NT. Only steel spirals were used as lateral reinforcement in these columns. Specimens S-1NT and S-2NT contained the amount of spiral reinforcement that satisfied the 1999 ACI Code provisions for seismic resistance, whereas Specimens S-3NT and S-4NT contained much less spiral reinforcement. These four columns were tested to failure to establish the standard behavior against which columns retrofitted with FRP could be compared. The second group, Series ST, consisted of six columns that contained the same amount of spiral reinforcement as Specimens S-3NT and S-4NT; however, they were strengthened with GFRP or CFRP before testing. Specimens ST-1NT to ST-6NT falls in this group. The third group, Series R, included Specimens R-1NT and R-2NT that contained 50% less spiral reinforcement compared with Specimens S-1NT and S-2NT. These two columns were damaged to a certain extent under axial and lateral loads, repaired under axial load with FRP, and then tested to failure. For Specimens ST-1NT and ST-2NT, the FRP composite was wrapped within the potential plastic hinge zones of the columns, that is, for a length of approximately 800 mm starting from the stub face and the failure occurred in the test zone. During the testing of Specimen ST-3NT, however, crushing of concrete was observed outside the test region; therefore, to ensure that the failure took place within the plastic hinge zone, it was decided to wrap the whole column for the rest of the specimens. Column ST-6NT was strengthened with four 100 mm wide CFRP bands at a clear spacing of 100 mm. The first band was applied at a distance of 50 mm from the stub face. The glass fabric was 1.25 mm thick, whereas the carbon fabric was either 0.5 or 1.0 mm thick. The type of fabric and the number of layers used were designed to study a range of parameters for their effects on column behavior. Four columns were reinforced conventionally with longitudinal and spiral steel. Of the remaining eight columns, six were strengthened with

carbon or GFRP before testing, and two columns were tested to a certain damage level, repaired with FRP under axial load, and retested to failure. FRP was used only in the transverse direction of the column section to confine concrete.

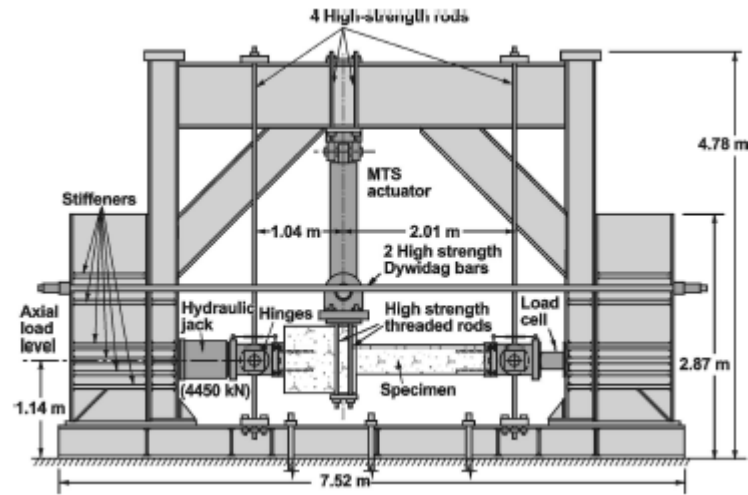


Figure 24 - Test setup [32]

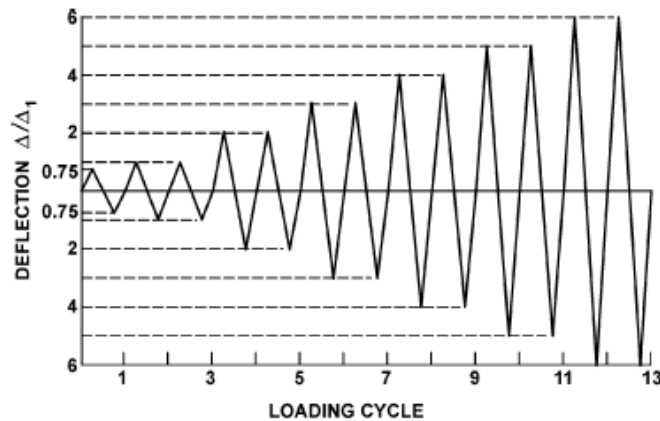


Figure 25 - Specified displacement history [32]

The following conclusions can be drawn from this study.

- Use of carbon and GFRP resulted in remarkable improvement in the performance of columns, resulting in large increases in ductility, energy dissipation capacity, and strength. For a column subjected to an axial load equal to $0.27P_o$, which is approximately equal to a balanced load, one layer of carbon or GFRP increased the energy dissipation capacity by a factor of more than 100;
- Unlike the internal spiral reinforcement that only confines the core concrete; the FRP wraps effectively confine the entire column section. The behavior of FRP retrofitted columns

under simulated earthquake loads matched or exceeded the performance of slab-reinforced columns designed according to the seismic provisions of the ACI Code;

- In steel reinforced columns, section and member ductility decreased significantly with an increased spiral pitch and reduced amount of spiral reinforcement. The adverse effects of a reduced amount of spiral reinforcement and larger spacing can be compensated for by the confinement provided by FRP;
- Column ductility deteriorates as the level of axial load increases. The amount of FRP reinforcement needed to improve column behavior depends on the level of axial load. It was observed that the amount of FRP reinforcement required under an axial load of $0.54P_o$ is slightly more than twice that needed for an axial load of $0.27P_o$ for similar performance enhancement;
- Columns retrofitted with FRP showed little strength degradation with increased displacement excursions until failure;
- FRP composites are very effective for the rehabilitation of damaged columns. The amount of FRP needed and the performance achieved is influenced by the extent of damage.

2.8.6.2 OZBAKKALOGLU T. AND SAATCIOGLU M. (2006, 2007)

Ozbakkaloglu and Saatcioglu conducted experimental tests on HSC columns with circular and square geometry, cast in FRP stay-in-place formwork, were tested under constant axial compression and slowly applied lateral deformation reversals. The columns were designed with due considerations given to the parameters that affect the efficiency and level of confinement reinforcement. It has been established that circular spirals are more effective in confining concrete than rectilinear ties. Similarly, it has been reported that the effectiveness of externally applied FRP jackets is higher in circular columns than square columns (Rochette and Labossiere 2000; Mirmiran et al. 1998; Pessiki et al. 2001). The pressure due to FRP stay-in-place formwork is generated by the membrane action at the corners, whereas it depends on the flexural rigidity of FRP casing between the corners. Increased corner radius (R) promotes hoop tension, thereby improving the effectiveness of confinement. Furthermore, the cross-sectional size (D) influences the flexural rigidity of FRP casing between the corners, affecting confinement efficiency. These two parameters can be expressed in the form of R/D ratio. Circular and square columns were constructed with a 270 mm cross-section and 1720 mm cantilever height. The shear span for each column was 2000 mm since the point of application of lateral force was located on a steel loading beam 280 mm above the column. The specimens represented the lower half of a first-story building column with an inter-story height of 4.00 m between fully fixed ends.

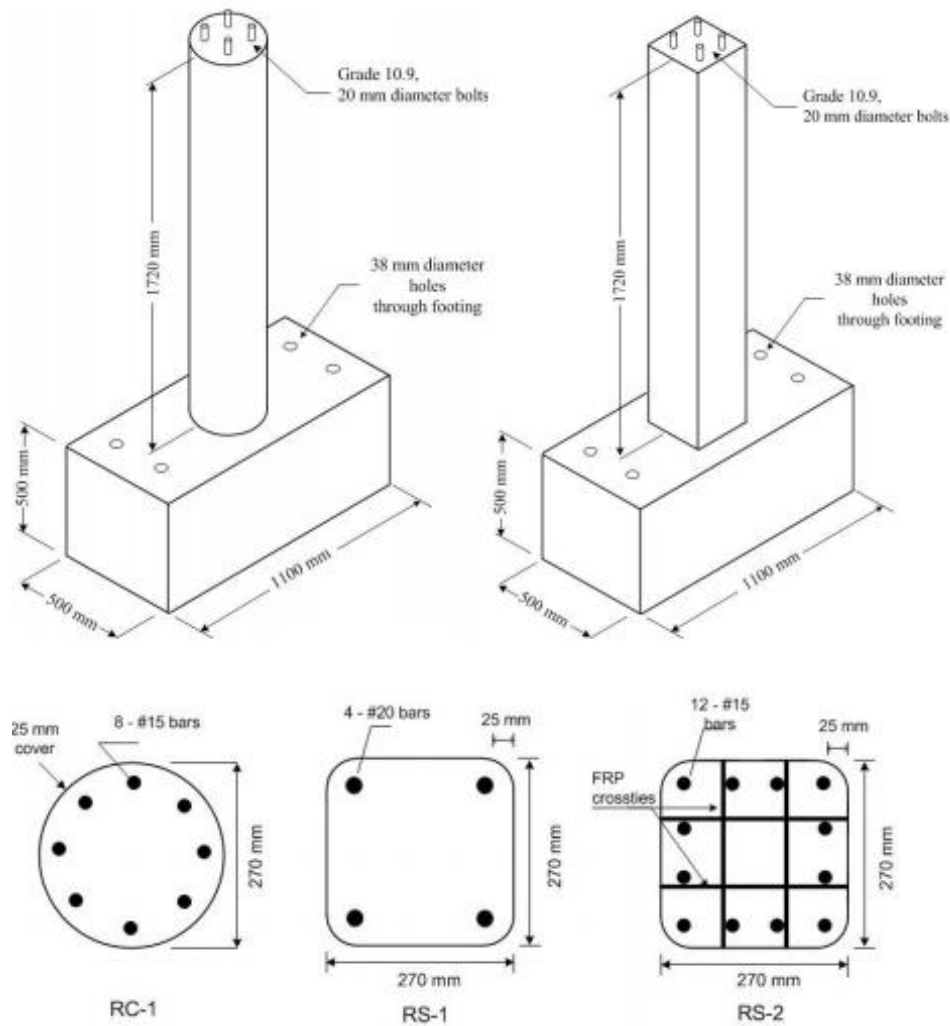


Figure 26 - Geometry of columns [21]

HSC, with cylinder strengths (f_c) of 75 MPa and 90 MPa, were used to cast the columns. A clear concrete cover of 25 mm was provided as measured to the outside of longitudinal reinforcement. No.15 (16 mm diameter) deformed steel bars, with yield strength (f_y) of 500 MPa, were used as longitudinal reinforcement. The specimens were tested in two groups. Circular (RC-1) and square (RS-3) columns tested in the first group had four and five plies of FRP in their casings, respectively. Circular (RC-2) and square (RS-4 and RS-6) columns of second group had two and three plies of FRP, respectively. The number of FRP plies was established based on the behavior of FRP confined (Miyauchi et al. 1997; Samaan et al. 1998; Spoelstra and Monti 1999; Saafi et al. 1999; Moran and Pantelides 2002; Lam and Teng 2002) and steel confined (Sheikh and Uzumeri 1980; Mander et al. 1988; Saatcioglu and Razvi 1992) concrete columns, while also considering current FRP design guidelines (Buckle and Friedland 1994; ACI 440 2002; CSA S806 2002). Because of the linear elastic behavior of FRP, the determination of design transverse strain is critical in establishing the required number of FRP plies. Column corners of square columns

were provided with a corner radius of 45 mm, resulting in an R/D ratio of 1/6, except for column RS-6, which had a corner radius of 8 mm, resulting in an R/D ratio of 1/34.

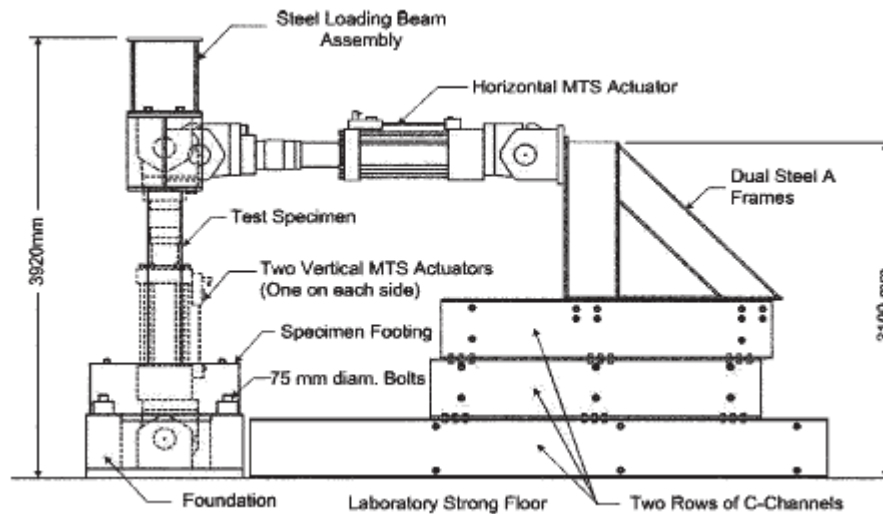


Figure 27 - Test setup [21]

From the experimental study reported here, the following conclusions can be drawn:

- High-strength concrete columns confined by carbon FRP stay-in-place formwork can develop ductile behavior under simulated seismic loading. The use of FRP formwork as confinement reinforcement substantially increases deformability of circular and square columns. Column tests reported indicate that inelastic deformability of 90 MPa concrete columns can be increased up to 12% lateral drift ratio with FRP stay-in-place formwork.
- The increased confinement requirements for HSC columns can be met by using FRP stay-in-place formwork. Unlike conventional steel reinforcement that only confines the core concrete, FRP stay-in-place formwork confines the entire column. Furthermore, unlike the discrete nature of conventional steel reinforcement, FRP formwork provides continuous confinement, covering the entire column face, resulting in higher confinement efficiency.
- The strain data recorded during column tests indicate that the strain limit of 0.4%, often used in current design practice for jacketing bridge columns under low levels of axial compression, can be relaxed for columns under high axial compression.
- The ratio of corner radius to column dimension (R/D) has significant impact on the effectiveness of square FRP stay-in-place formwork. Increased corner radius promotes effectiveness of FRP, while preventing premature material failure associated with sharp corners. Columns with three plies of FRP, tested in the experimental program, were able to develop 6% drift ratio prior to significant strength decay when the R/D ratio was 1/6, whereas the column with sharper corners (R/D = 1.34) was able to develop a limited drift ratio of approximately 2%.

The test specimens had dimensions of 350×350×2000 mm and they were connected to a column stub of 1350 × 500 ×400 mm. The column and the stub of the specimens were cast vertically at the same time in order to simulate the actual casting conditions. The longitudinal reinforcement consisted of eight 18-mm-diameter plain bars and the lateral reinforcement consisted of 10-mm-diameter plain bars with a spacing of 200 mm with 90-degree hooks. The names and details of test specimens are presented in *Table 5*.

Table 5 - Detail of test specimens [31]

Specimen	Specimen properties				Longitudinal steel ratio (%)	Axial load level, N/N_0 (%) ^c	CFRP Implementation	
	f'_c (MPa)	f_y (MPa)	Reinforcement				Ply no.	Strengthening
			Longitudinal	Transverse				
S-NL-0-34	14.0	287	8 × 18 mm (plain bars)	10-mm-diameter bars at 200 mm	1.66	34	0	Reference
S-NL-1-27	19.4					27	1	NL ^a
S-UL-1-34	14.0					34	1	UL ^b
S-NL-2-39	11.4					39	2	NL
S-UL-2-32	15.6					32	2	UL

^a NL indicates strengthening intervention was made under no load.

^b UL indicates strengthening intervention was made under axial load.

^c $N_0 = 0.85f'_cA_g + A_s f_y$.

All specimens were tested with no pre-damage prior to CFRP wrapping, hence the focus of the study reported herein is strengthening rather than repair. Specimen S-NL-0-34 had no strengthening and served as the control specimen. Specimens S-NL-1-27 and S-UL-1-34 had one layer of CFRP strengthening in the plastic hinge region, whereas specimens S-NL-2-39 and S-UL-2-32 had two layers of CFRP strengthening. During the strengthening of all specimens, except S-UL-1-34 and S-UL-2-32, no axial load was present and the axial load was applied and held constant only during the tests. Pre-compression load was applied and held constant on specimens S-UL-2-32 (34% and 32% of axial load carrying capacities, respectively) during CFRP application and kept constant until the end of the tests. Results from an experimental study, in which five column specimens were tested under constant axial load and cyclic lateral displacement excursions that simulated seismic forces, are presented in this study. Each specimen consisted of a 350×350 × 2000 mm column cast vertically together with a 1350 ×500×400 mm stub. Besides the reference specimen simulating a typical deficient building column with insufficient transverse reinforcement and low concrete compressive strength, there were two sets of companion specimens that were strengthened with 1 and 2 layers of CFRP. The effect of CFRP confinement, presence of axial load during retrofit and plain bars were studied. The following conclusions can be drawn from this study:

- The number of CFRP sheets used to confine plastic hinge regions of columns significantly improved the seismic behavior of the deficient columns although negligible lateral load carrying

capacity enhancement was observed (10%–15%). Increasing number of CFRP layers wrapped around the column improved drift capacities but that was not in proportion with the CFRP confinement.

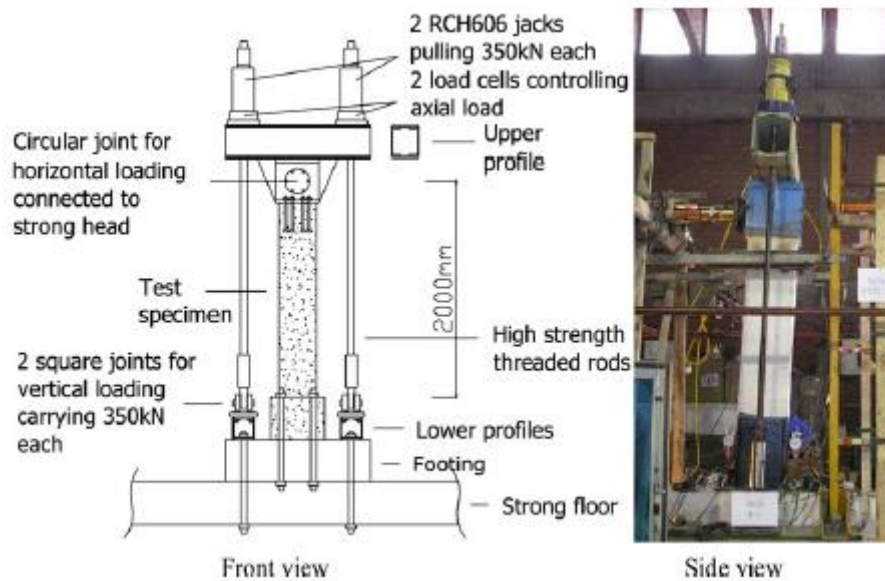


Figure 29 - Test setup [31]

- Wrapping the column critical region under an axial load level of about 35% of capacity did not have a considerable influence on the behavior of the columns as the experimental results revealed that axial strain and column lateral expansion due to existing axial load on the column had no significant effect. Additional studies, however, are needed to support this result at higher axial load levels further.
- Use of plain bars can result in a higher contribution of fixed end rotation component. While strengthening columns with CFRP increased the fixed end rotations up to 2 times of the reference, the plain bars should be considered carefully in the assessment and retrofit design of deficient RC columns.
- A simple analytical model that takes into account FRP confinement, longitudinal rebar buckling and deformations due to slip of plain bar is employed. A good agreement between analytical and experimental results was observed.

2.8.7 CONCLUSION OF EXPERIMENTAL WORK

Experimental studies introduced here presents concrete columns transversally confined by FRP wraps and subjected to lateral reversed cyclic load and constant axial compressive load. Most of the experimental results are based in the form of hysteresis loops of moment- curvature and lateral shear-tip deflection curves under seismic load. Following common conclusions are drawn here below:

- Ductility, deformability, energy dissipation capacity and flexural strength of the concrete columns are enhanced by providing of FRP wraps and with the increase of confinement level.
- The level of confinement should increase with the increase of axial compressive load to achieve similar curvature ductility level.
- Seismic resistance of concrete columns can be improved by providing FRP confinement.
- The efficiency of confinement is higher in circular concrete columns than in square or rectangular concrete columns.
- FRP wraps lead to significant enhancement of flexural strength in columns under higher axial compressive loading.
- Confined specimens with FRP jackets exhibited an increase in both lateral strength and deformation capacity compared to unconfined specimens.
- The failure mode is changed from the brittle response (diagonal shear) to a ductile response.

CHAPTER 3-RESEARCH STUDY

3.1 INTRODUCTION

This chapter introduces three main parts; theoretical, experimental, and numerical.

Firstly, the theoretical part introduces an analytical analysis of the circular concrete column cross-section.

Secondly, the experimental part focuses on examining experimentally the effectiveness of the FRP-confinement on the circular reinforced concrete single columns with fixed-free ends. The cyclic loading behavior of retrofitted columns using passive confinement applied with CFRP wraps is studied and discussed in this chapter. The behavior is compared to unconfined column. This research work was carried out in the laboratory of the Faculty of Civil Engineering of Brno University of Technology (Czech Republic). In this part, the test results and discussion of the experiments are introduced.

Thirdly, the numerical analysis presents a mathematical model prepared by ATENA 3D software based on finite element method to simulate the behavior of unconfined and confined circular columns subjected to axial load and cyclic lateral load.

3.2 THEORETICAL PART

3.2.1 ANALYTICAL PART

3.2.1.1 CROSS-SECTION ANALYSIS OF CIRCULAR COLUMNS

An interaction diagram can express the axial and flexural resistance of reinforced concrete column sections. The behavior of an axially loaded column depends on the magnitude of the load eccentricity. *Figure 30a* shows a typical interaction diagram, the vertical axis on the diagram presents the axial load resistance, whereas the horizontal axis presents the moment resistance. The regions of a column interaction diagram are associated with different types of column behavior, as follows:

Point “A” on *Figure 30a* presents a concentrically loaded column. This point corresponds to the zero-eccentricity condition ($e=0$) and bending moment ($M=0$), failure of the column occurs by the crushing of the concrete and yielding of the compressed steel reinforcement.

Region “A-C” on *Figure 30a* presents an eccentrically loaded column with small eccentricity. This region is characterized by concrete failure initiated by the concrete crushing.

This failure mode is brittle, as the column fails as soon as the concrete compressive strain reaches 0.0035 without large deformations or sufficient warning, and the tension steel does not yield.

Region “C-E” on *Figure 30a* presents an eccentrically loaded column with large eccentricity. This region is characterized by steel failure caused by the steel yielding before the concrete crushes. This failure mode is ductile, since the section will crack and develop large deformations before failure, thus giving sufficient signs of warning before the complete collapse.

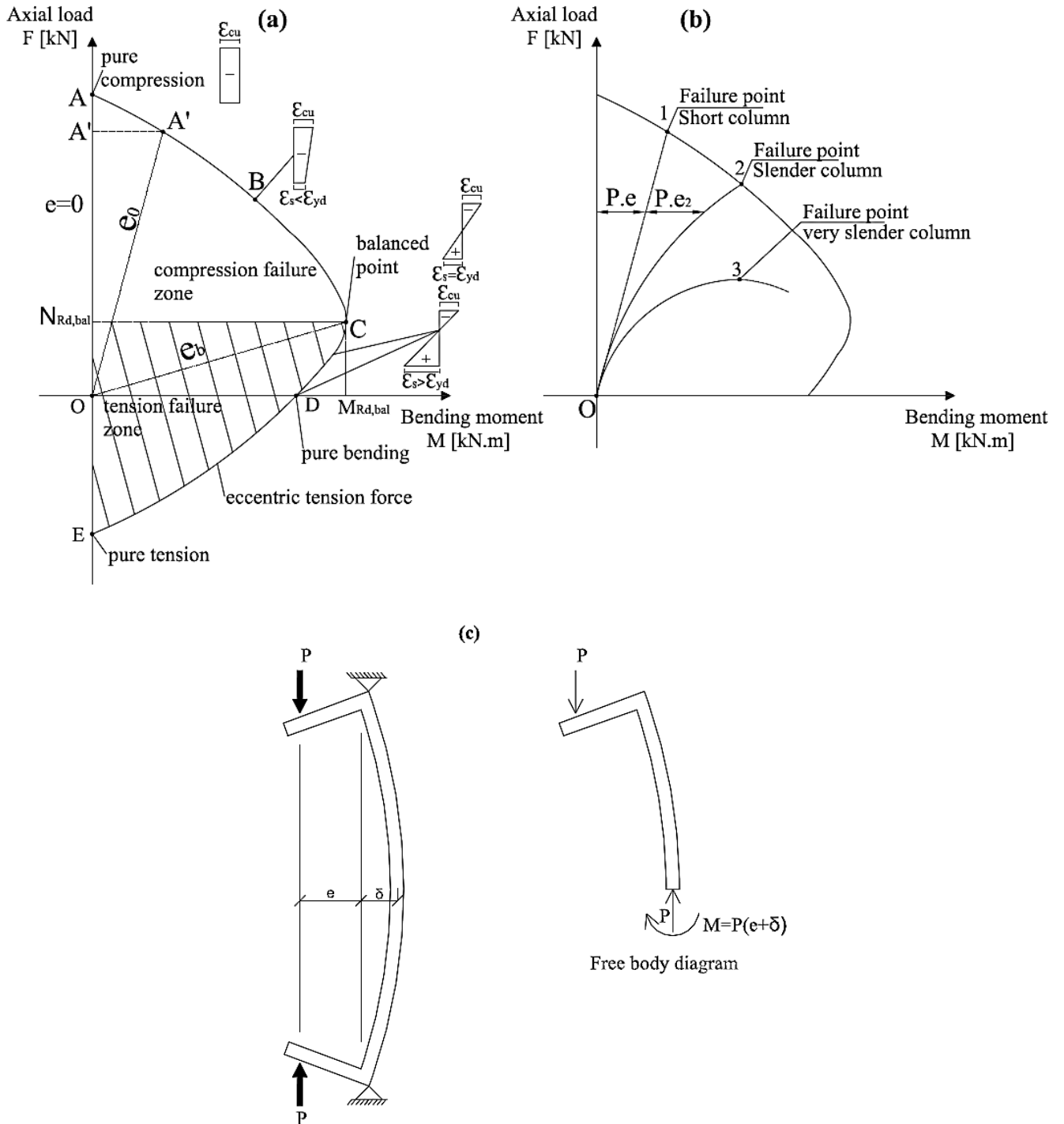


Figure 30 - Interaction diagram of columns [42]

Line “O-C” on the diagram on *Figure 30a* presents the threshold between these types of behavior introduced by the balanced condition. This region is characterized by the balanced eccentricity (e_b). At this point, the failure occurs with yielding of the tension steel and crushing of the concrete at the same instant (i.e. compression strain in the concrete reaches 0.0035 and the strain in the tensile reinforcement reaches $\epsilon_y = f_y/E_s$ simultaneously). The maximum bending moment capacity for the section occurs at this point. Loadings larger than the balanced load N_{bal} cause compression failure and loadings smaller than the balanced load cause tension failure.

Depending upon the slenderness ratio (ratio of effective length to least lateral dimension of the columns), the columns are classified as short columns or slender/long columns. A short column fails by crushing (pure compression failure) and a slender/long column fails by buckling or bending. A column is considered slender/long if its cross-sectional dimension is small in comparison to its length. Slender/long columns have smaller axial load capacity than short columns, this reduction in its axial load capacity due to buckling and second-order effects might lead to failure. Buckling is an instability that leads to failure mode. Buckling is characterized by excessive bowing of columns between the supports due to axial load. Buckling might also be caused by imperfections due to variations in material properties, construction tolerances, and load characteristics. Euler originally developed the basic concept of the buckling failure in 1759. Second-order effects can be developed when a slender column is subjected to axial force and bending moments. The influence of deformation of the structures on the internal forces should be considered. Second-order effects are these additional effects, bending moments or eccentricities.

The **line “0-1”** on *Figure 30b* is referred to as load-moment curve for the end moment ($M_e = P \cdot e$), while the **line “0-2”** is the load-moment curve for the total column moment ($M = P \cdot (e + \delta)$). If the column is slender, failure occurs when the load-moment curve “0-2” behind point “2”. Because of the increase in maximum moment due to the secondary moments, the axial load capacity is reduced from “1” to “2”. This reduction in axial load capacity results, from what are referred to as *slenderness effect*. For very slender columns, failure occurs well within the cross-section interaction diagram because of the pronounced second-order effect. This failure is called stability failure. In this type of failure, the collapse load of the column “3” is less than the actual material given by the interaction diagram.

The main steps in the general computational procedure used to determine a certain point on the column interaction diagram for unconfined column cross-sections with more than two layers of reinforcement are as follows:

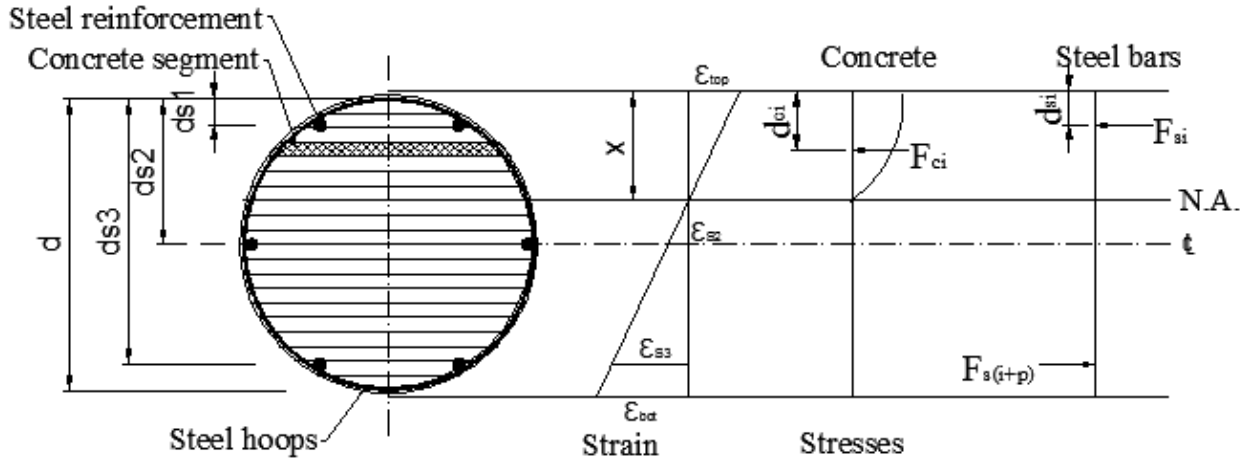


Figure 31 - Cross section of unconfined circular columns

1. Calculate the neutral axis depth corresponding to the balanced condition (point C) in *Figure 30*

$x = x_{bal}$;

$$x_{bal} = \frac{\epsilon_{cu}}{\epsilon_{cu} + \epsilon_y} d_{s3}, \quad (68)$$

where

$$\epsilon_{cu} = 0.0035; \epsilon_y = \frac{f_{yd}}{E_s}; d_{s3} = \text{effective depth of cross-section}.$$

2. Determine at least two points (A, B) between the zero eccentricity condition and the balanced condition (corresponding to condition $x > x_{bal}$) and another two points (D, E) corresponding to a large eccentricity and a small neutral axis depth ($x < x_{bal}$);
3. Compute the strain in all reinforcement layers (at d_{si} , where $i=1$ to $n=3$) using the equation;

$$\text{For } d_{si} \leq x \rightarrow \epsilon_{si} = \epsilon_{cu} \left(1 - \frac{d_{si}}{x} \right), \quad (69)$$

$$\text{For } d_{si} > x \rightarrow \epsilon_{si} = \epsilon_{cu} \left(\frac{d_{si}}{x} - 1 \right), \quad (70)$$

4. Compute the stresses in all reinforcement layers ($i=1$ to n);

$$\text{If } \epsilon_{si} \geq \epsilon_y \rightarrow \sigma_{si} = f_{yd} \text{ (Reinforcement has yield)}, \quad (71)$$

$$\text{If } \epsilon_{si} \leq \epsilon_y \rightarrow \sigma_{si} = E_s \epsilon_{si} < f_{yd} \text{ (Reinforcement has not yield)}, \quad (72)$$

5. Calculate the stress resultants in unconfined concrete and steel;

$$\text{Stress resultant in concrete: } F_c = \eta A_c f_{cd}, \quad (73)$$

$$\text{Stress resultant in } i\text{-th steel layer: } F_{si} = A_{si} \sigma_{si}, \quad (74)$$

6. Calculate the force N based on the force equilibrium equation;

$$N = F_c + \sum_{i=1}^n F_{si}, \quad (75)$$

7. Calculate the moment resistance M from the moment equilibrium equation around the center of gravity; assume that the center of gravity of the columns cross-section is located at a distance $d/2$ from the column face;

$$M = M_c + \sum_{i=1}^n M_{si}, \quad (76)$$

where

$M_c = F_c Y$; Y is the distance of the center of gravity of the circular cross section to the center of the compressive stress block in equation(78), and $M_{si} = F_{si} \left(\frac{d}{2} - d_{si} \right)$.

The following equations are used to calculate the area of the compressive stress block and the distance from the centric of the circular cross section to the center of this block area;

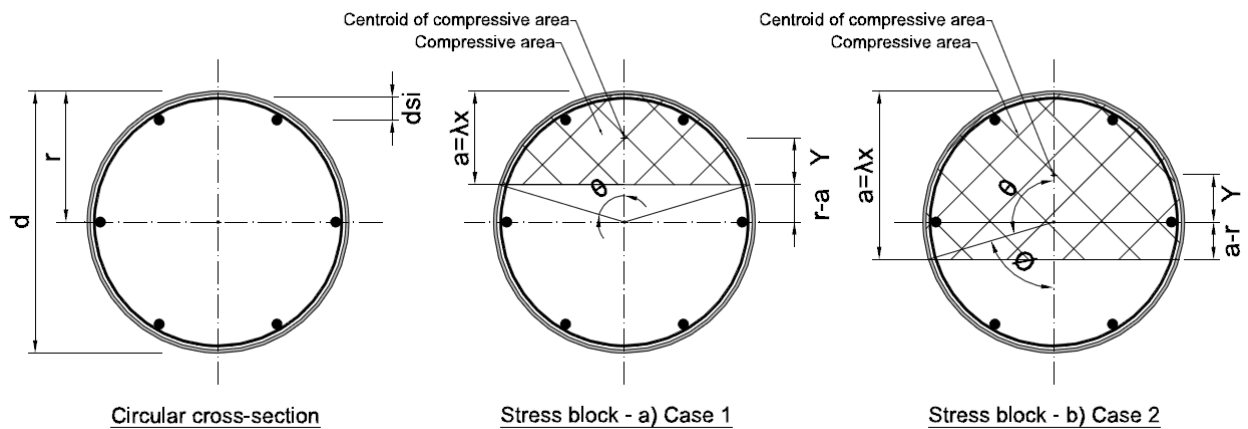


Figure 32 - Circular column cross-section

$$A_c = d^2 \left(\frac{\theta - \sin \theta \cdot \cos \theta}{4} \right), \quad (77)$$

$$Y = \frac{2}{3} \left(\frac{\sin^3 \theta}{2\theta - \sin 2\theta} \right) d. \quad (78)$$

The cross section, strain and stress distribution is shown in *Figure 31*. The angle θ as shown in *Figure 32* can be expressed as follows;

Case 1: for $a = \lambda x \leq r$, $\theta < \frac{\pi}{2}$; $\theta = \cos^{-1} \left(\frac{r - \lambda x}{r} \right)$, (79)

Case 2: for $a = \lambda x > r$; $\theta > \frac{\pi}{2}$; $\theta = \pi - \varphi$; $\varphi = \cos^{-1} \left(\frac{\lambda x - r}{r} \right)$. (80)

Similar procedures are used to plot the interaction diagram of the confined concrete columns with FRP in transversal/hoop direction.

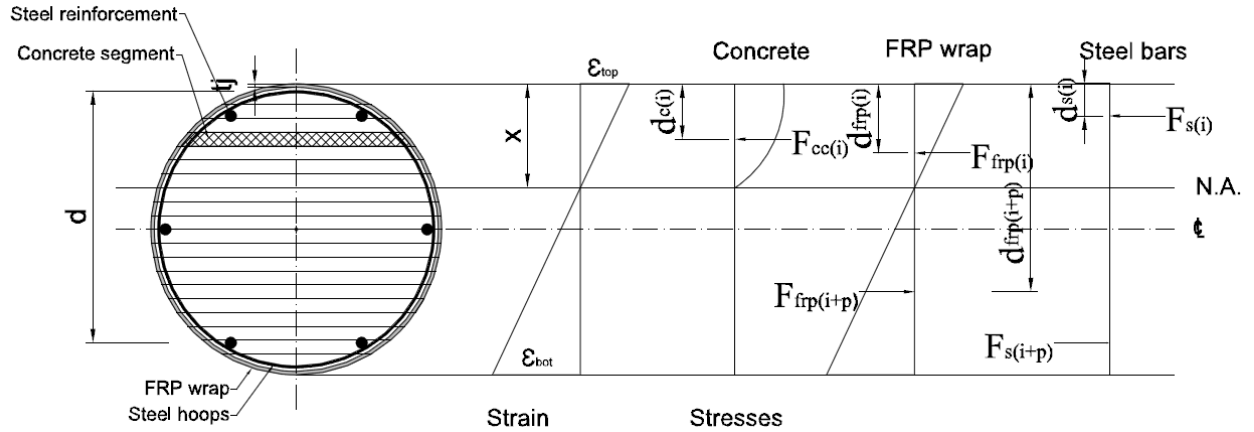


Figure 33 - Cross sections of confined circular columns with FRP

1. Calculate the force N including the contribution of FRP wraps based on the force equilibrium equation;

$$N = F'_c + \sum_{i=1}^n F_{si}, \quad (81)$$

where $F'_c = \eta A_c f'_{cd}$ is the stress resultant in confined concrete, and $F_{si} = A_{si} \sigma_{si}$ is the stress resultant of i -th steel layer.

2. Calculate the moment resistance M including the contribution of FRP wraps from the moment equilibrium equation around the center of gravity; assume that the center of gravity of the columns cross-section is located at a distance $d/2$ from the column face;

$$M = M'_c + \sum_{i=1}^n M_{si} , \quad (82)$$

where

$M'_c = F'_c Y$; Y is the distance of the center of gravity of the circular cross section to the center of the compressive stress block in *equation (78)*, and $M_{si} = F_{si} \left(\frac{d}{2} - d_{si} \right)$.

The summary of formulas considered plotting the interaction diagram of the unconfined and confined reinforced concrete circular columns with transversal contribution of FRP are illustrated in the following table:

Table 6 - Summary of formulas for confined and unconfined RCC columns

	Unconfined RC Columns	Confined RC Column with transversal contribution of FRP	$F_c = A_c \cdot f_{cd}$ and $F_{si} = A_{si} \cdot f_{yd}$ $M_c = F_c \cdot Y$ and $M_{si} = F_{si} \cdot (R - d_i)$
Force Resistance	$N = F_c + \sum_{i=1}^n F_{si}$	$N = F'_c + \sum_{i=1}^n F_{si}$	$F'_c = A_c \cdot f'_{cd}$ $M'_c = F'_c \cdot Y$
Moment Resistance	$M = M_c + \sum_{i=1}^n M_{si}$	$M = M'_c + \sum_{i=1}^n M_{si}$	

Notations and symbols used in the table:

F_c = stress resultant of unconfined concrete;

F'_c = stress resultant of confined concrete;

F_{si} = stress resultants of i -th steel layer;

M_c = moment resultant of unconfined concrete;

M'_c = moment resultant of confined concrete;

M_{si} = moment resultants of i -th steel layer;

A_c = area of the compressive stress block;

A_{si} = area of the i -th steel layer;

f_{cd} = compressive strength of the concrete;

f_y = yielding strength of the steel bar;

f'_{cd} = compressive strength of the confined concrete;

R = radius of the concrete column;

Y = distance of the center of gravity of the circular cross section to the center of the compressive stress block.

3.2.1.2 ANALYTICAL SOLUTION-EXAMPLE

The analytical example is provided on the specimen presented in the experiment to show the influence of confinement action of unidirectional (transverse direction) and multi-layers of carbon fibre reinforced polymers (CFRP) wrap on the interaction diagram of circular reinforced concrete columns. The axial and flexural resistance of unconfined and confined reinforced concrete column are expressed by a column interaction diagrams as shown in *Figure 34* and *Figure 35* respectively. The theory adopted was based on the Eurocode provisions and design-oriented models for confinement concrete predicted by some authors as mentioned in *Table 4* (Richard et al., Cuson and Paultre, Kono et al., Mander et al., Lam and Teng). In addition, the effect of numbers of FRP layers on the interaction diagram using the confinement action in Eurocode provisions was provided. Mean value of concrete compressive strength of 73.0 MPa was obtained from compressive test on a specimen of 200 mm of diameter and 400 mm of height. The material properties of the circular reinforced concrete columns considered in the experiment are illustrated in *Table 7*.

Table 7 - Properties of materials – RC columns

Properties of RC columns					
Concrete		Steel reinforcement			
d (mm)	$f_{ck,m}$ (MPa)	f_{yk} (MPa)	d_s (mm)	No of bars, n_i	A_{si} (mm ²)
200,00	73,00	500,00	8,00	6	301,59
Properties of FRP-SikaWrap® 600 C/120					
Number of layers	t_f (mm)	E_f (MPa)	f_f (MPa)	ε_f [%]	ρ_j
1	0,3370	242000	3800	1,55	0,00674

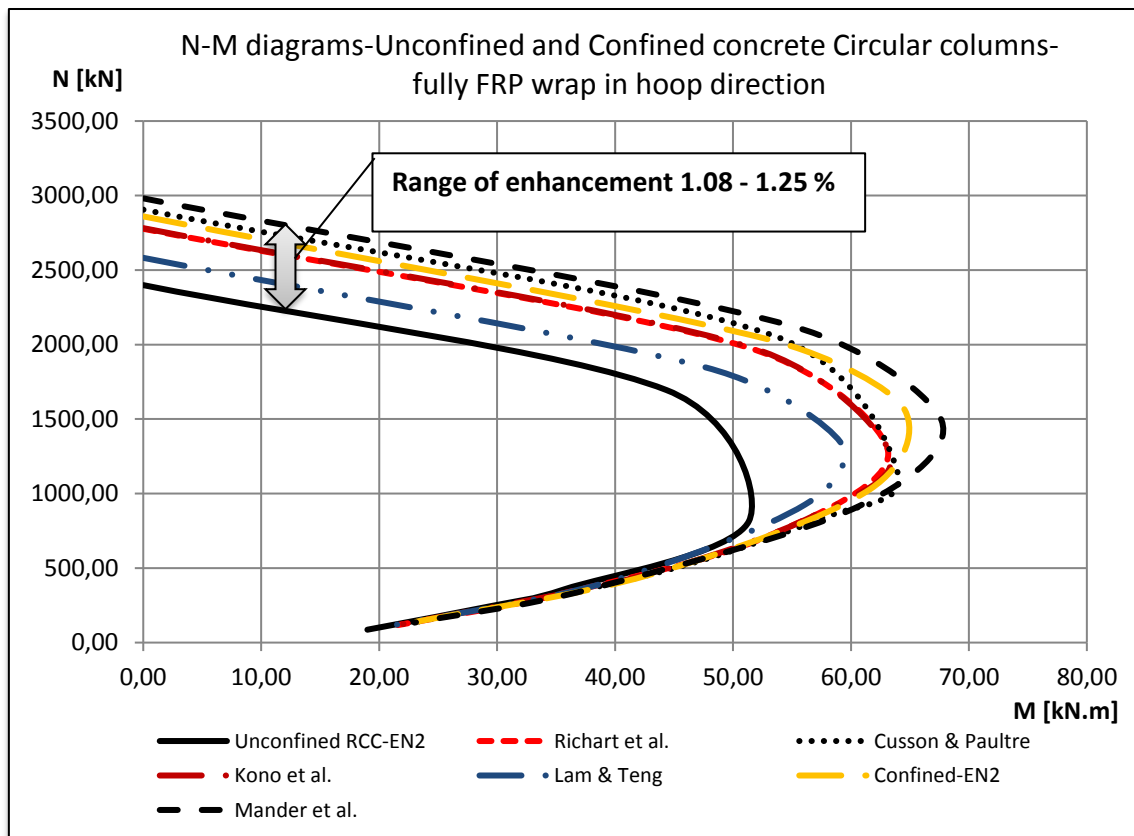


Figure 34 - N-M diagram of RC circular column wrapped with FRP in hoop direction

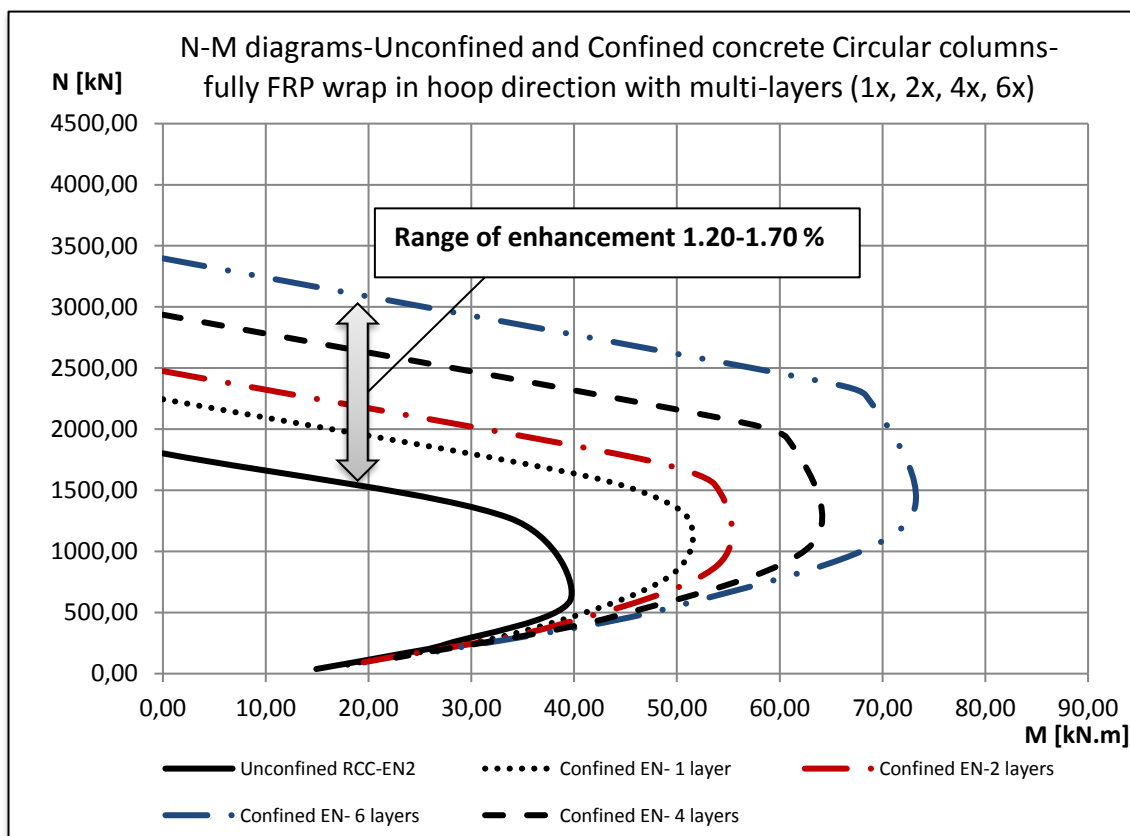


Figure 35- N-M diagram of RC column wrapped with multi-layers of FRP based on Eurocode

Figure 34 shows the comparison of interaction diagrams between unconfined and CFRP-confined circular reinforced concrete of selected models adopted by Richart et al., Kono et al., Cusson and Paultre, Lam and Teng, Mander et al., and Eurocode. The axial capacity of the selected unconfined concrete column is 2398 kN, and the range of the enhancement on the axial capacity provided by CFRP wrap in hoop direction as per selected design-oriented models is 2600 to 2981 kN which present 1.08 % to 1.25 %.

Figure 35 shows the influence of multi-layers CFRP wrap (1x, 2x, 4x and 6x) on the interaction diagram of reinforced concrete columns adopting the Eurocode provisions for confinement, a substantial gain in both axial compression and flexural capacity can be expected. The axial capacity of the circular concrete column is 1.20, 1.29, 1.50, and 1.70 % for the 1x layer, 2x layers, 4x layers and 6x layers respectively.

3.2.1.3 CANTILEVER COLUMNS

Cantilever reinforced concrete columns are usually considered for seismic assessment. Top end of a column is subjected to axial (P) and lateral force (V). The shear force (V_v) and bending moment (M_v) will occur at the same time of a column. The load scheme of cantilever RC column is shown in *Figure 36*.

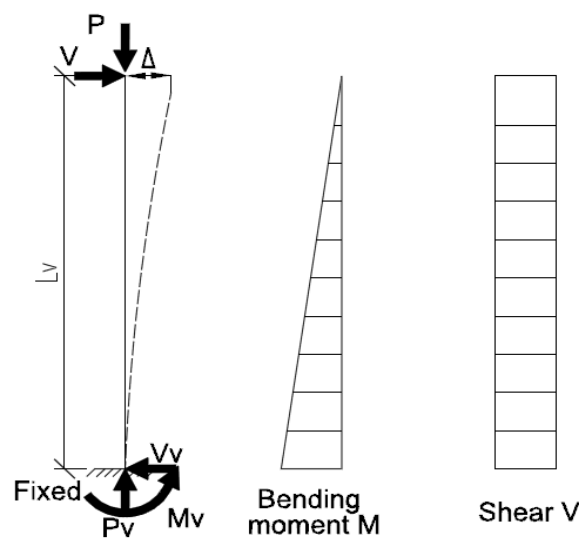


Figure 36 - Shear and moment diagrams of cantilever columns

When lateral displacement is small, the equilibrium is not influenced by its displacements. The shear force V_v , for a corresponding moment M_v in the first-order is calculated as follows:

$$V = \frac{M_v}{L_v}, \quad (83)$$

where L_v is the clear column height.

Considering the additional moment caused by an eccentric axial load P , (i.e. P - Δ effect or second-order effect), the shear force may be found as

$$V = \frac{M_v - P\Delta}{L_v}, \quad (84)$$

where Δ is the lateral displacement.

3.2.1.4 ASSESSMENT OF CONCRETE SUBJECTED TO CYLCIC LOADING /FATIGUE

Cyclic loading is defined as the continuous and repeated application of a load on a material or structural element that causes degradation of the strength of the materials and leads to fatigue. When a structure is subjected to a cyclic load, failure may occur before the static loading strength of the material is reached. This type of failure is known as a fatigue failure. The fatigue capacity of the material is influenced by several different parameters such as load frequency, maximal load level, stress amplitude and material composition.

Cyclic load or fatigue loading is divided into three different categories: low-cycle, high-cycle, and super high-cycle fatigue. The number of load cycles determines the type of fatigue. When performing a fatigue life assessment of structural elements, there are two basic approaches that can be used. The first approach considers an analysis of crack propagation at the point under consideration, and it is based on linear elastic fracture mechanics. The second approach, which is more commonly applied, uses a curve that shows the relation between cycle stress range and number of cycles to fatigue failure in logarithmic scales. This is known as a Wohler or S-N curve, where S is the stress range and N is the number of cycles. Fatigue failure is divided into three stages: crack initiation, crack propagation, and failure. *Table 8* illustrates the comparison of test specimen types used in the experimental study while the specimens are unconfined and confined considering the influence of fatigue. The design fatigue resistance of concrete was computed according to EN1992-1-1. As shown below, lateral pressure contributed by six layers of CFRP wraps improves the compressive strength of concrete subjected to fatigue.

Table 8 - Unconfined and confined compressive strength of concrete with fatigue [EN1992]

Column Type	Unconfined Compressive Strength	Lateral Pressure	Confined compressive strength	Unconfined compressive strength with fatigue	Confined compressive strength with fatigue
	f_{cm} (MPa)	$\sigma_{l,eff}$ (MPa)	$f_{cm,c}$ (MPa)	$f_{cm,fat}$ (MPa)	$f_{cm,c,fat}$ (MPa)
C1	60,00	17,62	111,54	38,76	87,64
C2	52,00	17,62	102,54	35,01	83,42
C3	58,00	17,62	109,29	37,86	86,63
C4	76,00	17,62	129,54	44,96	94,62

3.2.1.5 MOMENT CURVATURE ANALYSIS OF TEST SPECIMENS

Moment curvature diagram is a graphical representative of variation of moment of resistance at a section with respect to curvature. Calculating moment for an assumed curvature required that we assume the strain dependent on depth is distributed linearly across the depth of the column section, compute the stressed based on the stressed strain relation for materials and then determine the location of the neutral axis to satisfy equilibrium. Curvature is the angle in radians made by the final position of the cross section based on the assumed extreme fibre strain and the vertical direction. These steps are repeated for different values of extreme fibre strain. As the extreme fibre strain increases beyond yield strain, some fibres reach yield. Moment curvature relation shown in the paragraph 2.8.5 *equation (57)* is helpful to understand the ductility of reinforced concrete elements. Analysis of moment curvature diagram including the effect of the fatigue due to cyclic loading shall be considered into account.

Section analysis conducted by Sap2000 software is performed in moment curvature response using a fibre section decomposition approach, which shows that the diagrams for test specimen C1 with various configurations; unconfined, confined with spiral reinforcement, and confined with spiral and wraps. Additionally, compressive strength of concrete and reinforcement at fatigue were studied after getting 10^6 cycles. Figures below illustrate the comparison between all various configurations. The values of the initial yield moment correspond to the yield curvature of the reinforcement, and the ultimate moment corresponding to ultimate curvature in concrete and steel are illustrated in the *Table 15*.

Table 9 - Moment curvature Analysis-Column type C1-unconfined

Concrete Strain	Neutral Axis	Steel Strain	Curvature	Moment
	[mm]		[1/mm]	[kN.m]
0	0	0	0	0
-6,12E-05	51,2192	1,47E-04	1,26E-06	0,466714
-1,53E-04	51,2897	3,67E-04	3,14E-06	1,162361
-2,75E-04	51,3414	6,61E-04	5,65E-06	2,086405
-4,27E-04	51,344	1,03E-03	8,78E-06	3,24507
-6,11E-04	51,3291	1,47E-03	1,26E-05	4,639534
-8,24E-04	51,3269	1,98E-03	1,69E-05	6,264142
-1,04E-03	52,7439	2,60E-03	2,20E-05	6,700222
-1,28E-03	53,7756	3,30E-03	2,76E-05	7,134797
-1,54E-03	54,5072	4,08E-03	3,39E-05	7,625805
-1,82E-03	55,3954	4,94E-03	4,08E-05	7,867279
-2,11E-03	56,2737	5,90E-03	4,83E-05	7,924896
-2,40E-03	57,5665	6,97E-03	5,65E-05	7,929845
-2,70E-03	58,658	8,12E-03	6,52E-05	7,922735
-3,02E-03	59,5308	9,36E-03	7,47E-05	7,925082
-3,37E-03	60,208	0,0107	8,47E-05	8,00607
-3,74E-03	60,7353	0,0121	9,54E-05	8,171818
-4,14E-03	61,1871	0,0135	0,0001066	8,336984
-4,56E-03	61,5581	0,0151	0,0001186	8,528282
-5,00E-03	61,8786	0,0167	0,0001311	8,725302

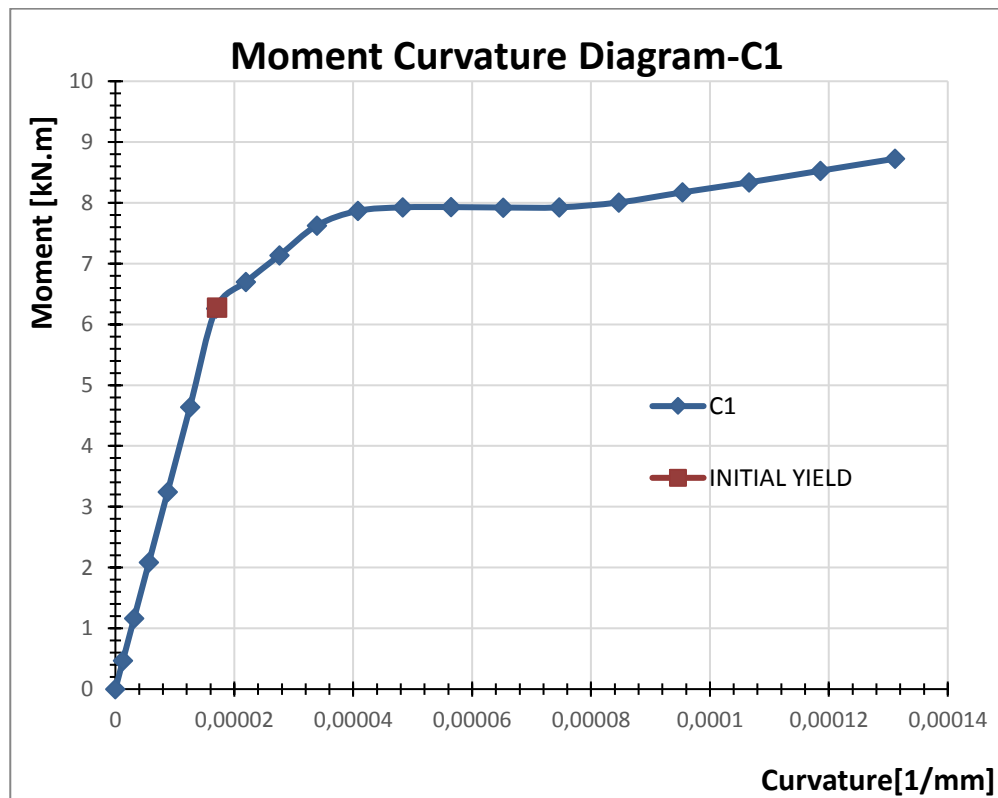
**Figure 37 - Moment Curvature Diagram- Column type C1- Unconfined**

Table 10 - Moment curvature Analysis-Column type C1-Confined by Spiral

Concrete Strain	Neutral Axis	Steel Strain	Curvature	Moment
	[mm]		[1/mm]	[kN.m]
0	0	0	0	0
-1,37E-04	52,0325	3,21E-04	2,85E-06	1,098488
-3,41E-04	52,1082	8,02E-04	7,11E-06	2,737259
-6,13E-04	52,1001	1,44E-03	1,28E-05	4,928782
-9,39E-04	52,8558	2,26E-03	1,99E-05	7,064152
-1,29E-03	54,6966	3,28E-03	2,85E-05	7,996857
-1,67E-03	56,6197	4,50E-03	3,84E-05	8,828577
-2,04E-03	59,0615	5,96E-03	4,98E-05	9,028178
-2,46E-03	60,649	7,59E-03	6,26E-05	9,242031
-2,95E-03	61,6647	9,39E-03	7,68E-05	9,419072
-3,51E-03	62,0679	0,0113	9,25E-05	9,70427
-4,15E-03	62,0857	0,0134	0,0001095	10,00458
-4,88E-03	61,9196	0,0157	0,000128	10,23044
-5,68E-03	61,5906	0,0181	0,0001479	10,40352
-6,57E-03	61,2132	0,0206	0,0001693	10,54498
-7,52E-03	60,8459	0,0233	0,000192	10,71779
-8,53E-03	60,5455	0,0262	0,0002162	10,9184
-9,58E-03	60,3839	0,0293	0,0002418	10,96075
-0,0107	60,2693	0,0325	0,0002689	11,04754
-0,0118	60,2024	0,0359	0,0002973	11,16058

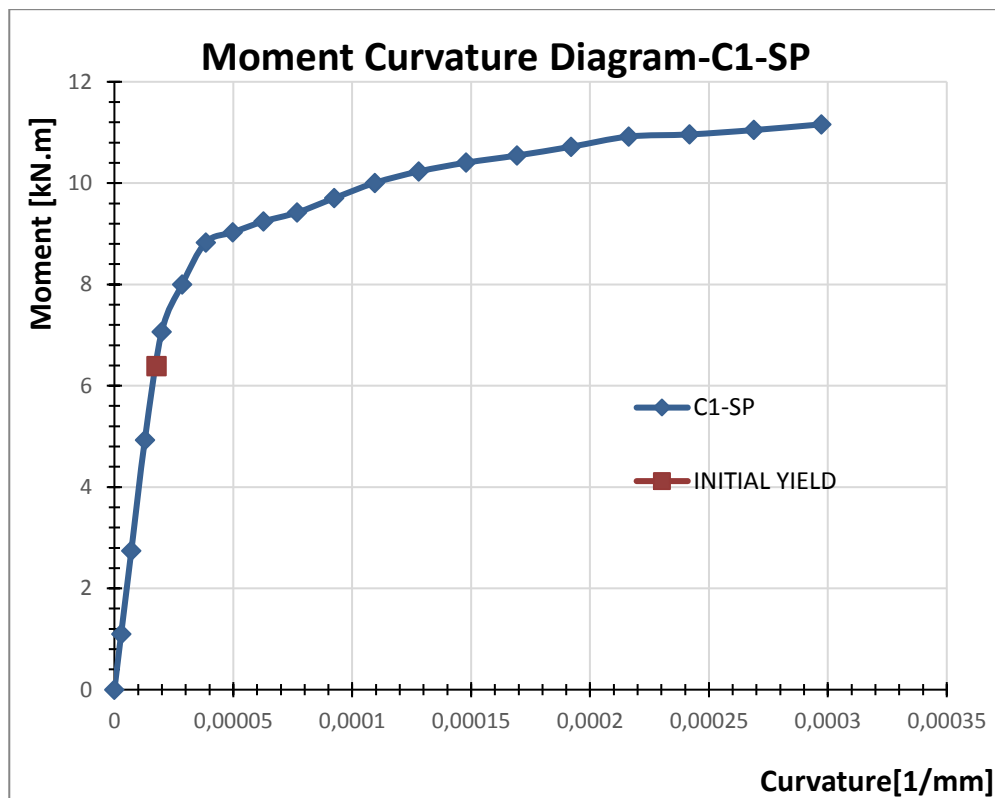
**Figure 38 - Moment Curvature Diagram- Column type C1- Confined by spiral**

Table 11 - Moment curvature Analysis-Column type C1-Confined by Spiral & wrap

Concrete Strain	Neutral Axis	Steel Strain	Curvature	Moment
	[mm]		[1/mm]	[kN.m]
0	0	0	0	0
-1,81E-04	50,7	6,86E-04	6,16E-06	2,31335
-4,50E-04	50,8014	1,72E-03	1,54E-05	5,760598
-7,28E-04	53,7466	3,17E-03	2,77E-05	7,753004
-1,01E-03	56,5719	5,05E-03	4,31E-05	8,851129
-1,20E-03	60,4622	7,46E-03	6,16E-05	9,221123
-1,39E-03	63,313	0,0103	8,31E-05	9,615697
-1,47E-03	66,3871	0,0137	0,0001078	10,27812
-1,56E-03	68,5052	0,0175	0,0001355	11,02607
-1,78E-03	69,3107	0,0216	0,0001663	11,89144
-2,08E-03	69,6315	0,0261	0,0002002	12,85305
-2,16E-03	70,905	0,0312	0,0002371	13,47039
-2,08E-03	72,5113	0,0369	0,0002771	14,04244
-1,99E-03	73,7748	0,043	0,0003203	14,66465
-1,85E-03	74,9625	0,0497	0,0003665	15,17538
-1,63E-03	76,079	0,0568	0,0004157	15,59644
-1,40E-03	77,0059	0,0644	0,0004681	16,02815
-1,15E-03	77,8034	0,0725	0,0005235	16,46176
-8,78E-04	78,4921	0,081	0,000582	16,87098
-6,38E-04	79,008	0,0899	0,0006436	17,33176

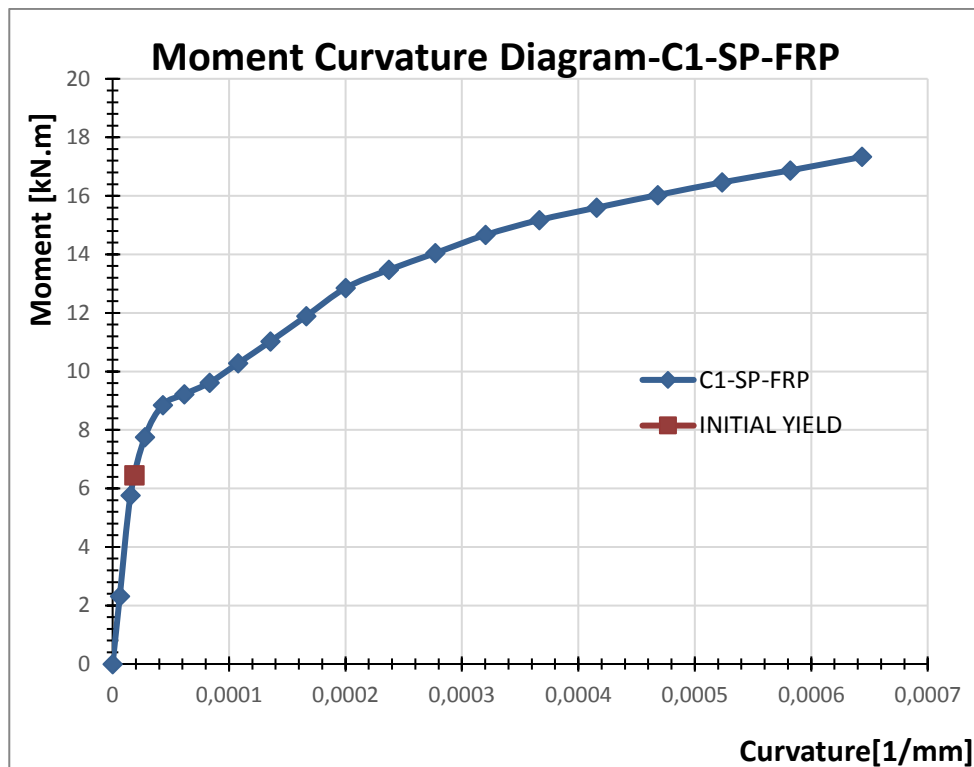
**Figure 39 - Moment Curvature Diagram- Column type C1- Confined by spiral & wrap**

Table 12 - Moment curvature Analysis-Column type C1-Unconfined -Fatigue

Concrete Strain	Neutral Axis [mm]	Steel Strain	Curvature [1/mm]	Moment [kN.m]
0	0	0	0	0
-6,12E-05	51,2192	1,47E-04	1,26E-06	0,4200426
-1,53E-04	51,2897	3,67E-04	3,14E-06	1,0461249
-2,75E-04	51,3414	6,61E-04	5,65E-06	1,8777645
-4,27E-04	51,344	1,03E-03	8,78E-06	2,920563
-6,11E-04	51,3291	1,47E-03	1,26E-05	4,1755806
-8,24E-04	51,3269	1,98E-03	1,69E-05	5,6377278
-1,04E-03	52,7615	2,60E-03	2,20E-05	6,0228081
-1,28E-03	53,7762	3,30E-03	2,76E-05	6,4209546
-1,54E-03	54,5072	4,08E-03	3,39E-05	6,8632146
-1,82E-03	55,3954	4,94E-03	4,08E-05	7,0805475
-2,11E-03	56,2737	5,90E-03	4,83E-05	7,1323983
-2,40E-03	57,5665	6,97E-03	5,65E-05	7,1368596
-2,70E-03	58,658	8,12E-03	6,52E-05	7,1304615
-3,02E-03	59,5308	9,36E-03	7,47E-05	7,1325738
-3,37E-03	60,208	0,0107	8,47E-05	7,205463
-3,74E-03	60,7353	0,0121	9,54E-05	7,3546362
-4,14E-03	61,1789	0,0135	0,0001066	7,5122667
-4,56E-03	61,5579	0,0151	0,0001186	7,6756752
-5,00E-03	61,8786	0,0167	0,0001311	7,85277

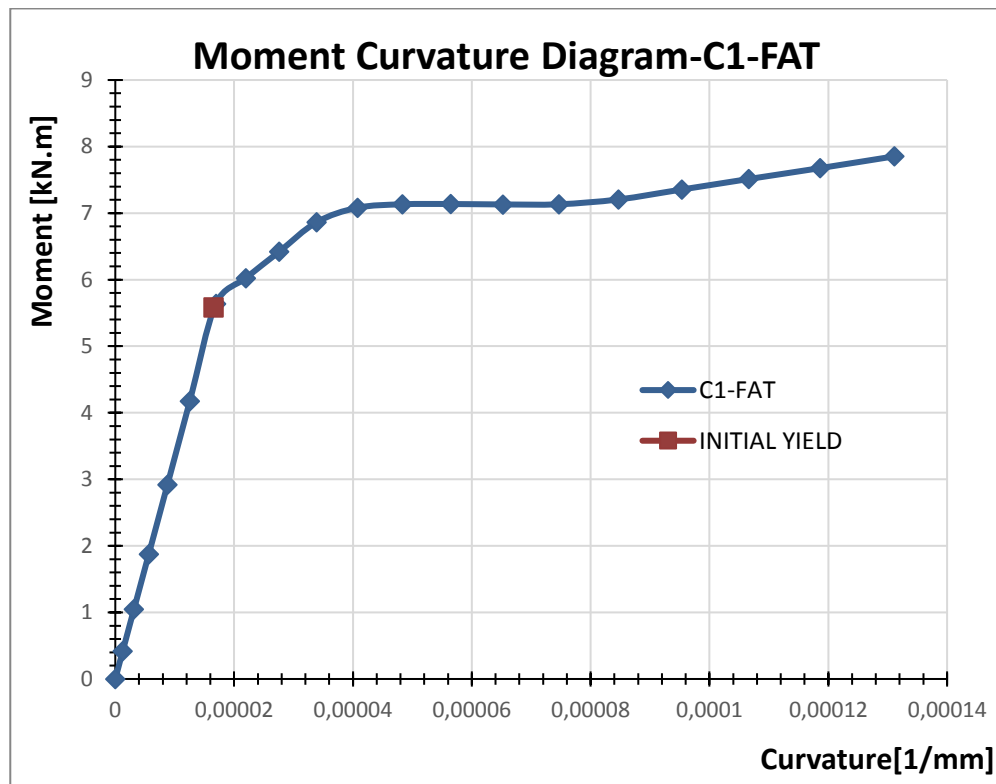
**Figure 40 - Moment Curvature Diagram- Column type C1- Unconfined-Fatigue**

Table 13 - Moment curvature Analysis-Column type C1-Confined by spiral-Fatigue

Concrete Strain	Neutral Axis [mm]	Steel Strain	Curvature [1/mm]	Moment [kN.m]
0	0	0	0	0
-1,37E-04	52,0325	3,21E-04	2,85E-06	0,9889713
-3,41E-04	52,1082	8,02E-04	7,12E-06	2,4643611
-6,13E-04	52,1001	1,44E-03	1,28E-05	4,437396
-9,39E-04	52,8579	2,26E-03	1,99E-05	6,358392
-1,29E-03	54,7208	3,28E-03	2,85E-05	7,1880408
-1,67E-03	56,6188	4,50E-03	3,84E-05	7,9479099
-2,04E-03	59,0638	5,96E-03	4,98E-05	8,1257517
-2,46E-03	60,6669	7,59E-03	6,26E-05	8,3089098
-2,95E-03	61,6645	9,40E-03	7,68E-05	8,478081
-3,51E-03	62,0684	0,0113	9,25E-05	8,7345846
-4,15E-03	62,0858	0,0134	0,0001096	9,0043452
-4,88E-03	61,9187	0,0157	0,0001281	9,2078145
-5,68E-03	61,5896	0,0181	0,000148	9,3634551
-6,57E-03	61,2122	0,0206	0,0001693	9,4908888
-7,52E-03	60,8374	0,0233	0,0001921	9,655371
-8,53E-03	60,5452	0,0262	0,0002163	9,8262909
-9,58E-03	60,3835	0,0293	0,0002419	9,8648406
-0,0107	60,269	0,0325	0,0002689	9,9430632
-0,0118	60,2023	0,0359	0,0002974	10,044943

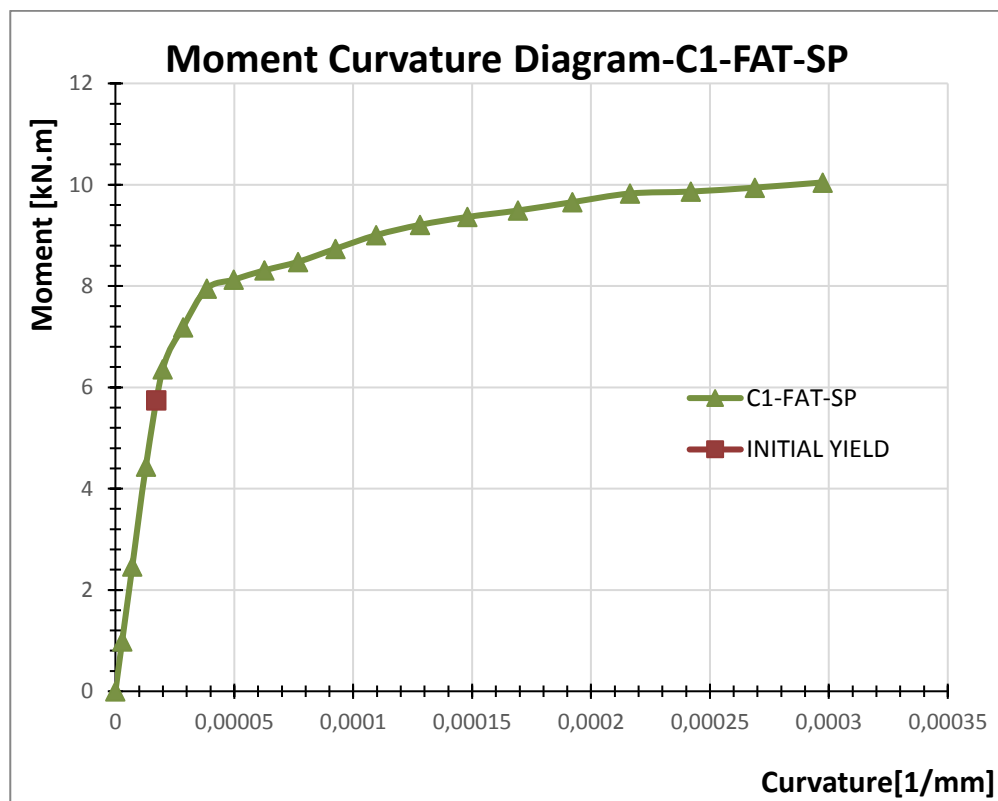
**Figure 41 - Moment Curvature Diagram- Column type C1- Confined by spiral-Fatigue**

Table 14 - Moment curvature Analysis-Column type C1-Confined by spiral & wrap-Fatigue

Concrete Strain	Neutral Axis [mm]	Steel Strain	Curvature [1/mm]	Moment [kN.m]
0	0	0	0	0
-1,80E-04	50,7782	6,86E-04	6,16E-06	2,0756916
-4,50E-04	50,8022	1,72E-03	1,54E-05	5,1843789
-7,28E-04	53,7473	3,17E-03	2,77E-05	6,977421
-1,01E-03	56,5473	5,05E-03	4,31E-05	7,9754661
-1,20E-03	60,4752	7,46E-03	6,16E-05	8,2918089
-1,39E-03	63,3132	0,0103	8,31E-05	8,6540643
-1,47E-03	66,3865	0,0137	0,0001078	9,2505762
-1,56E-03	68,5052	0,0175	0,0001355	9,9234639
-1,78E-03	69,3107	0,0216	0,0001663	10,702295
-2,08E-03	69,6315	0,0261	0,0002002	11,567746
-2,16E-03	70,905	0,0312	0,0002371	12,123347
-2,08E-03	72,5113	0,0369	0,0002771	12,638193
-1,99E-03	73,7939	0,043	0,0003203	13,186547
-1,84E-03	74,9755	0,0497	0,0003665	13,648793
-1,64E-03	76,0605	0,0568	0,0004157	14,051472
-1,40E-03	77,0081	0,0644	0,0004681	14,423356
-1,15E-03	77,8046	0,0725	0,0005235	14,814303
-8,78E-04	78,4921	0,081	0,000582	15,183872
-6,38E-04	79,008	0,0899	0,0006436	15,598579

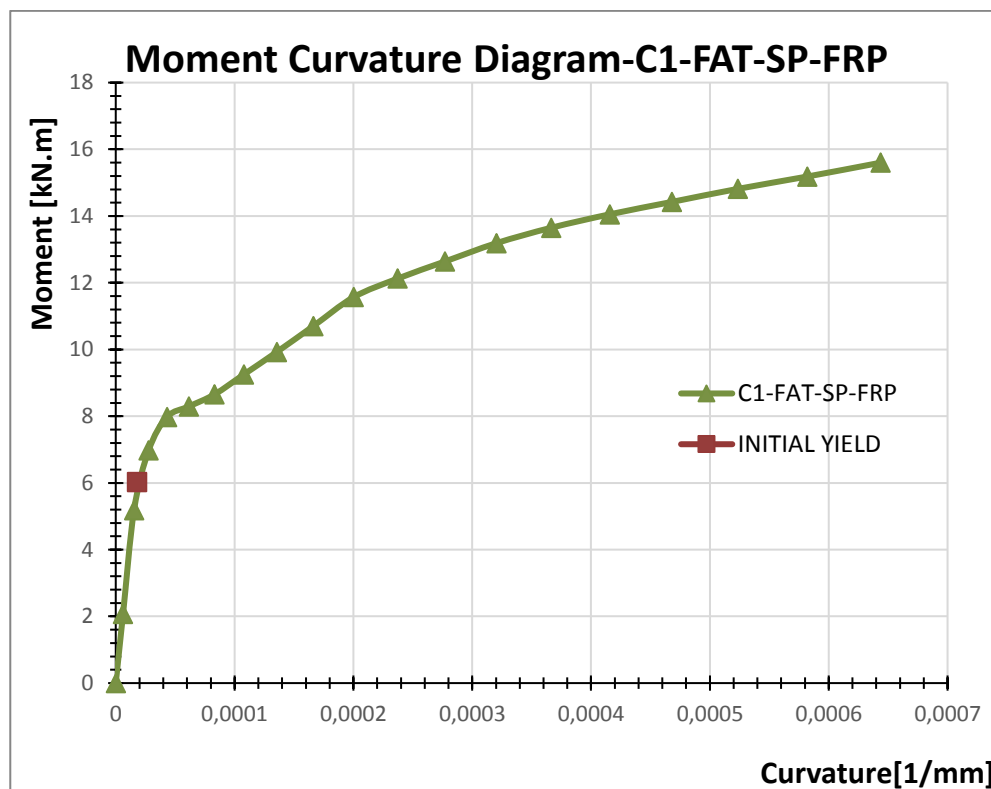


Figure 42 - Moment Curvature Diagram-Column type C1-Confined by spiral & wrap-Fatigue

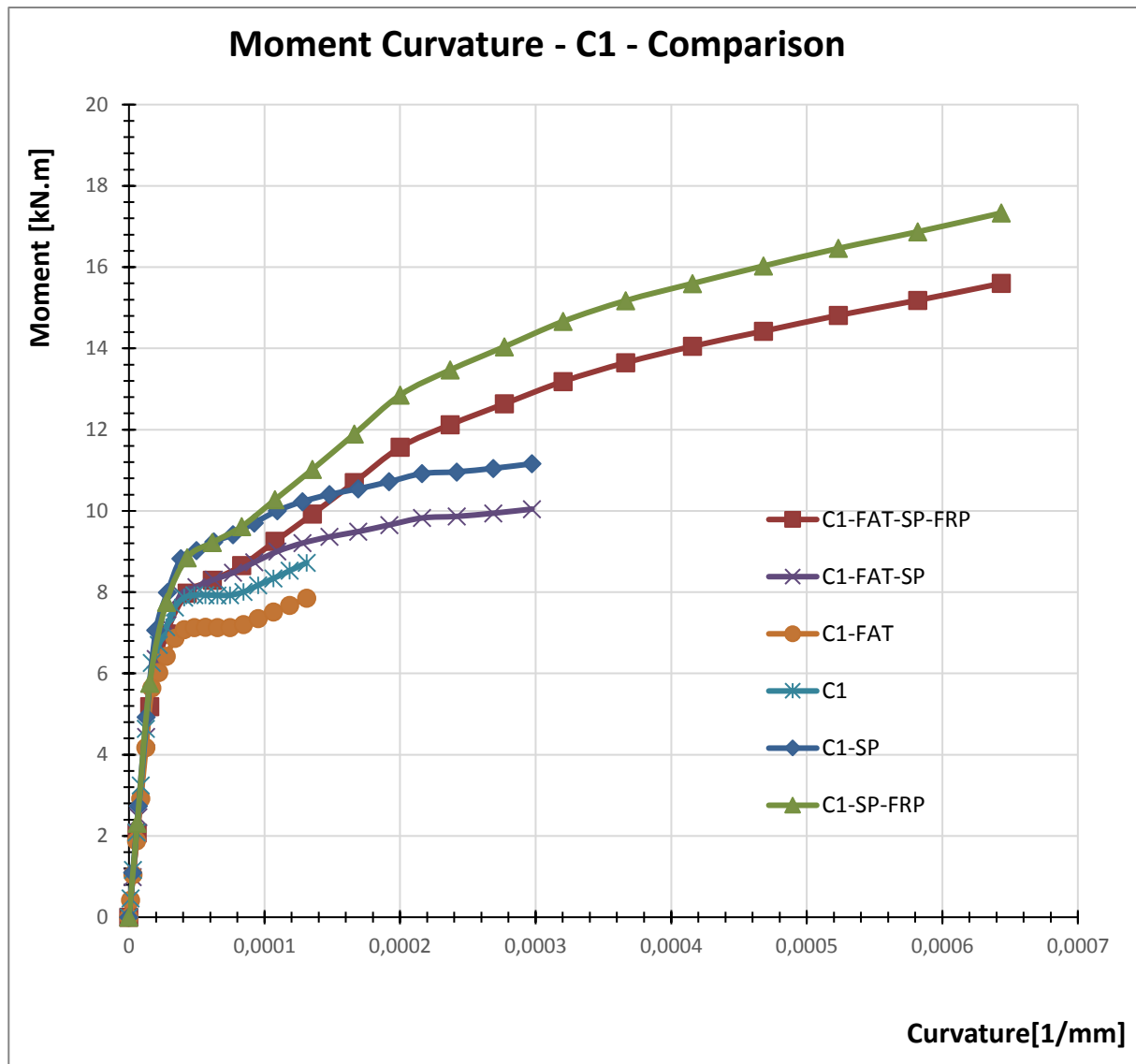


Figure 43 - Comparison of Moment vs. Curvature diagrams for test specimen C1

The fatigue of the material can affect the behavior of the moment curvature diagram, the performance of the initial yield curvature and moment are reduced approximately by 3 and 11% respectively. Confinement of the concrete column by wrap including the effect of spiral enhances the behavior of the moment curvature diagram. *Table 15* summarizes the results of the initial yield, the ultimate moment and curvature of the concrete and steel reinforcements. Curvature ductility of the circular concrete column increases by the confinement due to spiral and wrap.

Table 15 - Summary of Initial yield, ultimate curvature and moment in concrete of column type C1

	INITIAL YIELD OF STEEL		CONCRETE	
	CURVATURE	MOMENT	CURVATURE	MOMENT
	[1/mm]	[kN.m]	[1/mm]	[kN.m]
C1-UNCONFINED	1,71E-05	6,275776	1,31E-04	8,725302
C1-SP	1,77E-05	6,386066	2,97E-04	11,160578
C1-SP-WRAP	1,86E-05	6,450998	NA	NA
C1-FAT	1,66E-05	5,5854406	1,22E-04	8,114529
C1-FAT-SP	1,71E-05	5,7467331	2,68E-04	10,0445202
C1-FAT-SP-WRAP	1,85E-05	6,0277605	NA	NA

Notation of symbols in the graphs and tables:

- C1-Unconfined: represents the unconfined concrete circular column type C1;
- C1-SP: represents the column type C1 confined by spiral;
- C1-SP-WRAP: represents the column type C1 confined by spiral and wrap;
- C1-FAT: represents the unconfined column type C1 considering the degradation of strength of concrete and steel due to fatigue;
- C1-FAT-SP: represents the column type C1 confined by spiral and considering the degradation of strength of concrete and steel due to fatigue;
- C1-FAT-SP-WRAP: represents the column type C1 confined by spiral and wraps considering the degradation of strength of concrete and steel due to fatigue.

3.2.1.6 INTERACTION BETWEEN DUCTILITY DISPLACEMENT AND CURVATURE FACTORS

Displacement, rotation, and curvature ductility factors described in sections 2.8.2 and 2.8.4 are interrelated. For a simple cantilever column subjected to axial and lateral load, the relationships between three ductility factors can be investigated. There are some common factors, which will be appearing in each relationship. The plastic hinge length is one of the most significant factors. Besides, the plastic hinge length depends on various parameters. Some of the parameters that affect the plastic hinge length are the level of axial load, the moment gradient, the level of shear stresses in the hinging region, the mechanical properties of the reinforcements, the compressive strength of concrete, and the level of confinement. The relationship between displacement and curvature ductility factors for test specimens is shown in the *Figure 44* (refer to equation (52)). It can be noticed that for the defined displacement ductility, the corresponding

curvature ductility is significantly influenced by the shear span to depth ratio and the length of the plastic hinge length.

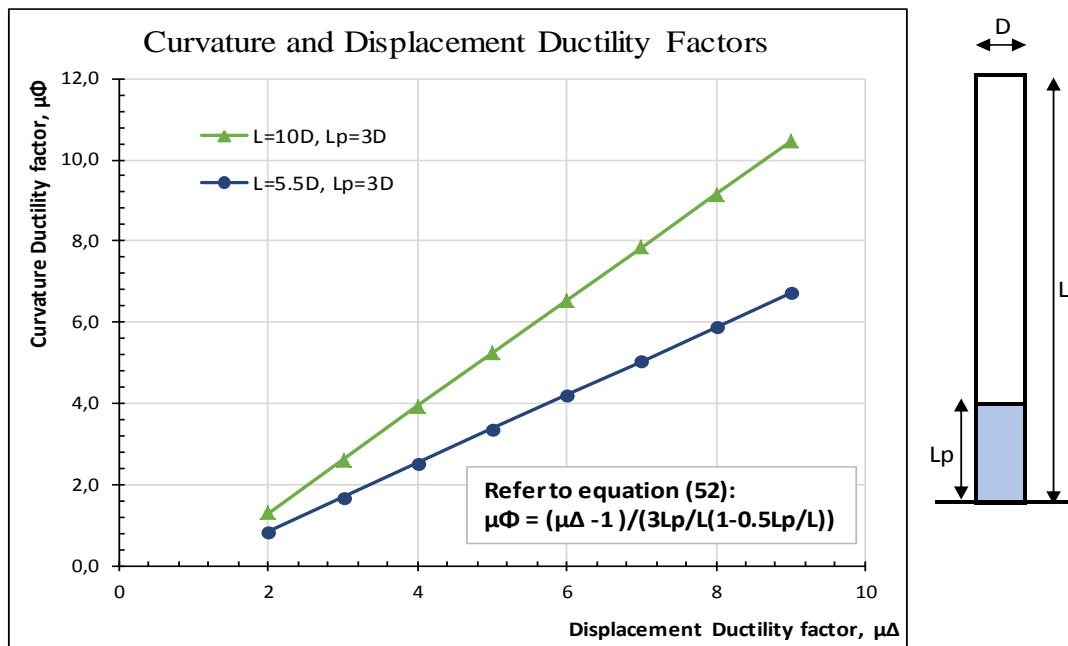


Figure 44 - Interaction between displacement and curvature ductility factors based on equation [52]

3.3 EXPERIMENTAL PART

3.3.1 TEST SPECIMENS PARAMETERS

Four specimens of circular reinforced concrete single columns were tested under axial compressive and lateral cyclic load applied at the top free-end of the columns. Two columns were confined by CFRP in hoop direction with six layers and two columns were unconfined (one considered as control specimen, and another has different load configuration, refer to paragraph 1.3- Experimental test). Circular cross-section for test specimens was selected for many reasons; in loaded circular cross-section the entire section is uniformly confined, while in rectangular or squared cross-sections the confinement is higher at the corners and lower at the middle sides (arch effect). Also, circular shape is preferable for seismic zones. The use of 6 layers of CFRP wraps was selected to show the manner performance of CFRP as shown in the interaction diagrams previously.

3.3.2 MANUFACTURING AND GEOMETRY OF TEST SPECIMENS

Manufacturing of the columns was carried out in a local company Prefa-Brno and the confinement process was provided at BUT's laboratory. Tubbox column formers from "Max. Frank GmbH" company was used to build the circular columns to defined diameter and height as presented in *Figure 45*.

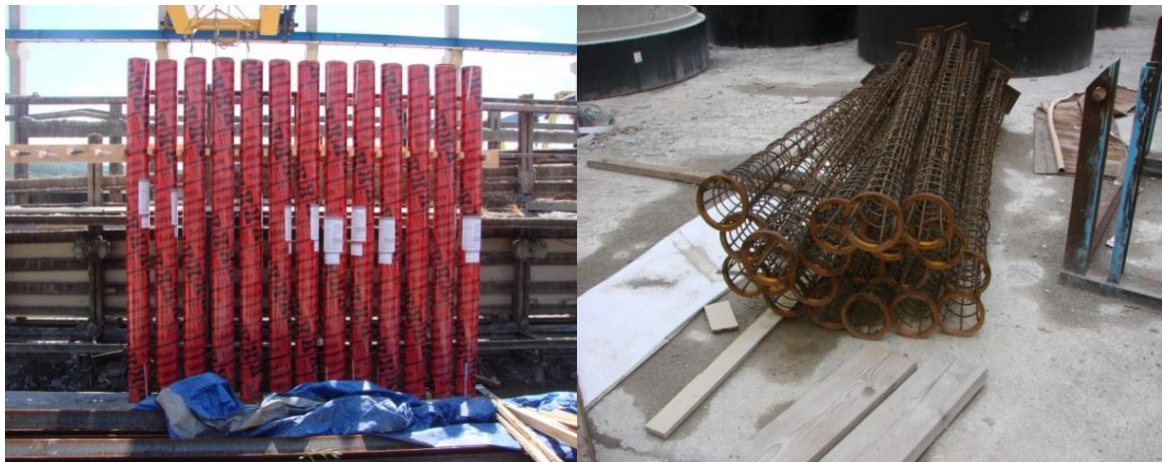


Figure 45 - The manufacturing of the circular columns

3.3.3 GEOMETRY OF THE TEST SPECIMENS

Geometry of the columns is illustrated in *Figure 46*; the diameter of all columns is 200 mm; the total height is 2440 mm, the effective height is 2090 mm measured from the column base to

the position of lateral load application and the part of column embedded in steel footing is 350 mm.

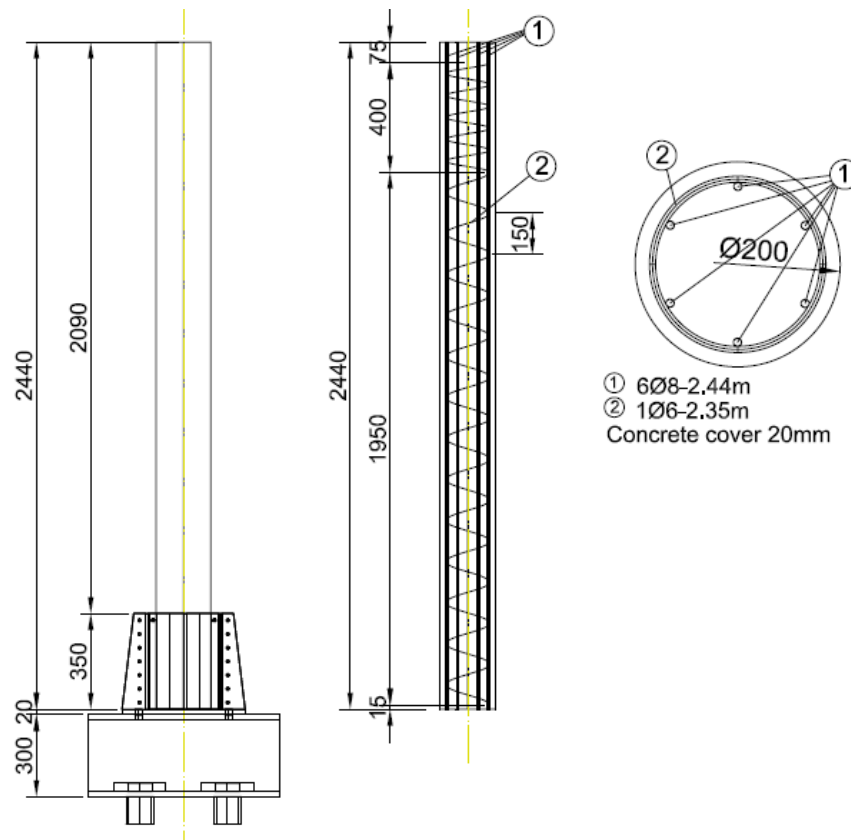


Figure 46 - The geometry of circular columns

A summary of test specimen's configuration is given in *Table 16*.

Table 16 - Configuration of test specimens

Column type	Diameter [mm]	Total height- H [mm]	Effective height H_e [mm]	Test Parameter
C1 & C4	200	2440	2090	Unconfined
C2 & C3	200	2440	2090	Confined

3.3.4 CONCRETE MIX DESIGN

All four specimens were cast vertically. The concrete mix design proportions per 1000 litre considered for the test specimens is shown in *Table 17*. It consisted mainly from cement CEM I 42.5, water, aggregates, sand, and additives.

Table 17 - Mix design proportions

Mix design for Concrete / 1000 litr			
Cement CEM I 42,5	430 kg	Stabilizer (Stabilan KP)	0,5 kg
Water	100 kg	Sand wet (0 - 4 mm)	1130 kg
Superplasticizers (Stachement 2180)	7,7 kg	Aggreagate (4 - 8 mm)	415 kg
Retardant additives (Retardal 540)	1,4 kg	Aggreagate (8 - 11 mm)	415 kg

The core testing was carried out in the Institute of Building testing (Ústav stavenbního zkušebnictví-SZK) at BUT to determine the material parameters (strengths and modulus of elasticity) of the concrete columns. Cores were cut using a drill with a hollow barrel tipped with industrial diamonds.

**Figure 47- Core Test Specimens of Circular Columns**

For compressive cubic strength testing, the length to diameter ratio of cores was 1.0, i.e. diameter and length of 74 mm. For compressive cylinder strength and modulus of elasticity testing, the length to diameter ratio of cores was 2.0, i.e. diameter and length of 74 and 149.5 mm respectively. The total number of cores used to determine the mean values of compressive cubic strength was 24 pieces, and it was 12 pieces for mean values of compressive cylinder strength and modulus of elasticity of concrete.

The properties of concrete (mean values) for test specimens are summarized in *Table 18*.

Table 18 - Properties of Concrete for test specimens (mean values)

Column types	Compressive Cubic Strength(mean values) $f_{cm,cubic}$ [MPa]	Compressive Cylinder Strength(mean values) $f_{cm,cyl}$ [MPa]	Modulus of Elasticity E_m [MPa]
Type C1	73,89	60,06	37333,33
Type C2	58,91	52,23	33800,00
Type C3	62,51	58,46	34500,00
Type C4	80,36	76,32	34766,67

3.3.5 STEEL REINFORCEMENT

Steel bars with different diameters were used in the test specimens for longitudinal and transverse reinforcement. The columns were reinforced with six longitudinal reinforcement bars of 8 mm diameter, and transverse reinforcement of 6 mm diameter. The concrete cover is 20 mm, and the characteristic yielding strength of steel reinforcement is 500 MPa (class of reinforcement B500B).

Table 19 - Summary of steel reinforcement

Column type	Column diameter [mm]	No. & size of long.bars [mm]	Steel - A_s [mm ²]	$\rho = A_s/A_c$ [%]
Type C1, C2, C3 & C4	200	6 \varnothing 8	301.59	0.96

3.3.6 SPECIMENS PREPARATION – CFRP APPLICATION

Two specimens were prepared for confinement by CFRP wraps using the following procedures. The surface of the concrete columns was sandblasted and cleaned. A structural adhesive mortar Sikadur®30 composed of two components A and B with convenient mix ratio A:B = 3:1 was used for improving the surface and closing the pores as shown in *Figure 48*. After repairing the surface, a layer of saturated resin Sikadur ®-300 is suitable for the wet lay-up process which is composed of two components A and B with convenient mix ratio A:B = 100:34.5 by weight. The first layer was applied as impregnation resin and followed by a saturated layer of carbon sheet of Sikawrap®-600C/120. Six number of CFRP layers were applied. The saturated fabrics with epoxy on both sides using roller brushes were wrapped manually on the surface of columns with respect to the hoop direction and with height of 600 mm. Each layer was wrapped around the columns with an overlap of 120 mm to avoid sliding or de-bonding of fibers during the loading tests.



Figure 48 - Preparation of RC columns surface

For additional layers of CFRP, another layer of resin was applied for at least 12 hours after the application of the first layer. All layers were tightly wrapped to ensure the absence of air bubbles between the layers.

Table 20 - Properties of Sikawrap and Sikadur [48] & [49]

Sikawrap® -600C/120		
Density of Sikawrap-600C/120	1,81	g/cm ³
Tensile strength	3800	N/mm ²
Tensile modulus of elasticity of wrap	242000	N/mm ²
Strain at rupture	1,55	%
Thickness of wrap	0,337	mm
Thickness of laminate(impregnated Sikadur 300)	1,3	mm
Tensile modulus of elasticity of laminate	50000	N/mm ²
Sikadur® -300		
Density of Sikadur-300 (component A+B)	1,16	kg/l
Tensile strength	45	N/mm ²
Tensile modulus of elasticity of Sikadur-300	3500	N/mm ²
Strain at rupture	1,5	%

Table 20 shows the properties of Sikawrap®-600C/120 and Sikadur ®-300. A gap of 5 mm was maintained between the footing top and CFRP wrap to avoid the strength contribution in the longitudinal direction.



Figure 49 - Preparation of CFRP confined column

The confinement configurations of each column type are in *Table 21*.

Table 21 - Confinement configurations

Column type	Column height H [mm]	no.of CFRP layers	Confinement height [mm]
Type C1& C4	2090	0	0
Type C2 & C3	2090	6	600

3.3.7 STEEL FOOTING

The bottom of columns was supported by circular steel footing with height of 350 mm encasing the circular concrete columns which are connected to stiffened steel profiles (2x HEB 300) and anchored to the laboratory floor by two bolts of 80 mm diameter to ensure the fixed-end support of the columns. The steel footing and members as presented in *Figure 50* were manufactured in an external local company. Steel class of S235JR was considered for all steel members.

For connections subject to fatigue friction grip, high strength bolts with different diameter of 8.8 and 10.9 grades were used due to their high fatigue strength and limited deformation characteristics. The spacing between circular steel footing and concrete columns was filled with

high strength precision non-shrinking cement-based grouting with compressive strength of 90-105 MPa [50] as shown in *Figure 51*.

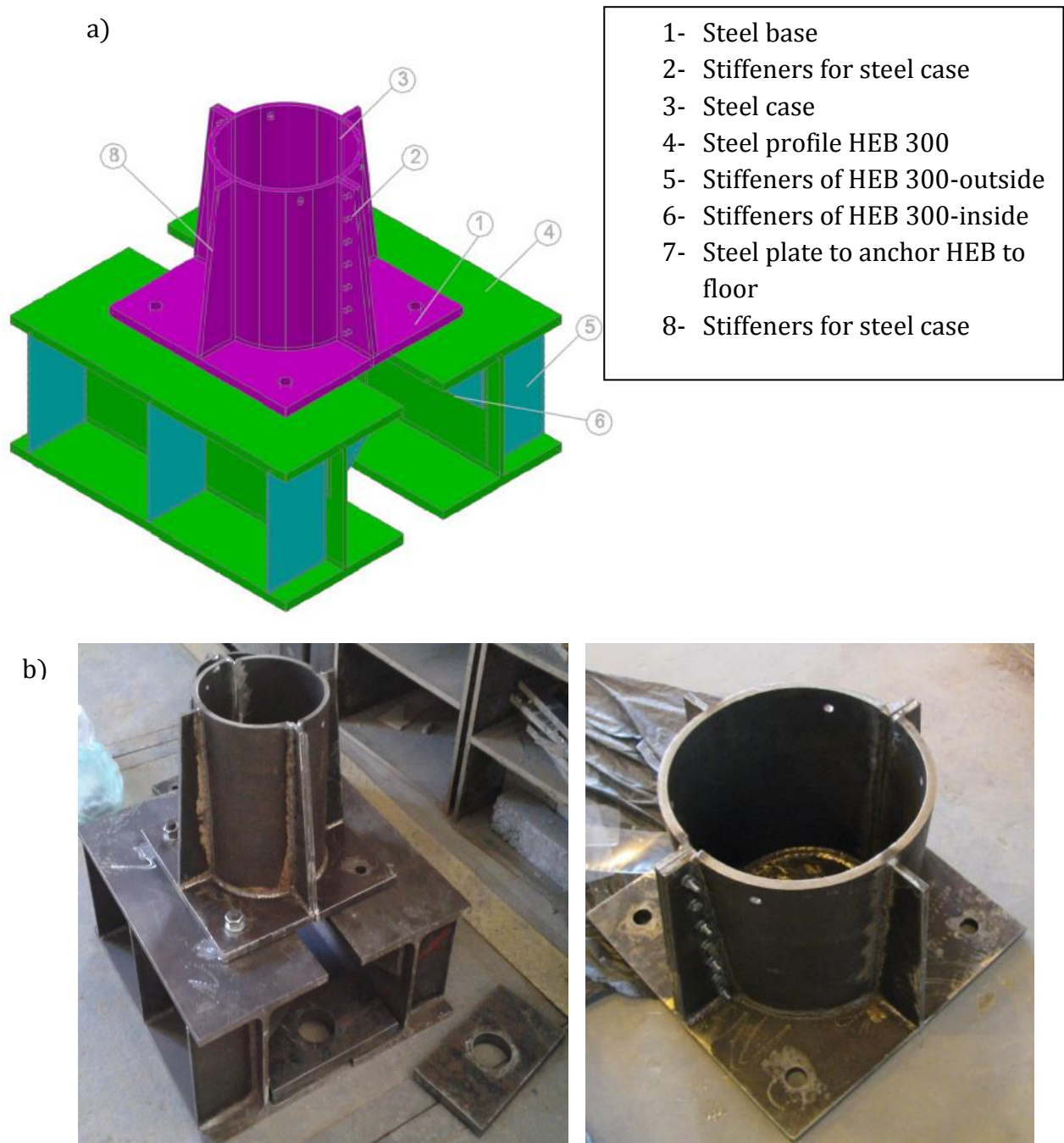


Figure 50 - Steel pocket footing a) computer model, b) realization



Figure 51 - RC column encased by steel footing

3.3.8 TEST SPECIMENS SET-UP AND PROCEDURES

The test set-up was designed to impose lateral cyclic load to a column, while the axial load was hold constant. The vertical load on the columns was maintained during testing at a value of 450 KN by using check valve mounted to hydraulic jack that permits flow only in one direction and that is measured by load cell, which represents approximately 21.50 % of the column cross-section compressive strength (the axial load level in reinforced concrete column; $n = P / (0.85f_c A_c + f_y A_y)$). On the top of columns, a steel plate was welded to transfer the axial load from the hydraulic jack to the columns as shown in *Figure 52*. Hydraulic jack was connected with the top of the columns by transverse steel beam (profile 2x I200) and two threaded rods of 27 mm diameter (tensile strength is 264 kN/rod) were connected by special steel shoes to the steel footing to insure the hinge connection in case of columns displacement as shown in *Figure 53*.

The lateral cyclic load was applied by using electrical hydraulic actuator with capacity of 100 KN and maximum stroke capacity of ± 50 mm. The hydraulic actuator was anchored to steel frame. The lateral cyclic loading was applied in a quasi-static manner. Lateral cyclic loading was applied on the columns in two different sequential manners:

First, high-cycle loading was applied under force control, i.e. constant lateral cyclic force pulling in one direction for certain number of cycle's~ 1 million cycles, the experimental cyclic

response was obtained by the loading history of 5 seconds interval described in *Figure 54* where the minimum and maximum forces applied are 2.0 and 8.0 kN respectively, this type of loading was applied to know the performing of column fatigue assessment.

Second, low-cycle loading was applied under displacement control (reversed cyclic load) based on a pattern of progressively increasing displacements. The loading pattern for the specimens consisted of three cycles at displacement levels of ± 2.5 , ± 5.0 , ± 7.5 , ± 1.0 , ± 12.5 , ± 15.0 , ± 20 , ± 25 , ± 30 , ± 35 , ± 40 mm. The lateral loading program is shown in *Figure 55*. The overall test set-up is shown in *Figure 56* and *Figure 57*.



Figure 52 - Arrangement of transverse beam, load cell and hydraulic jack

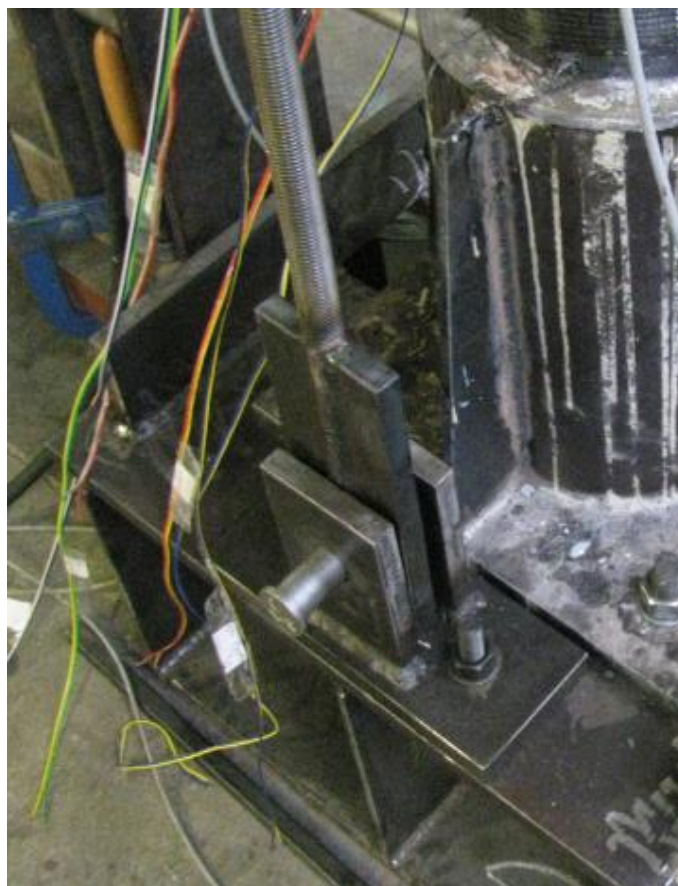


Figure 53 - Connection of tie rod to steel footing

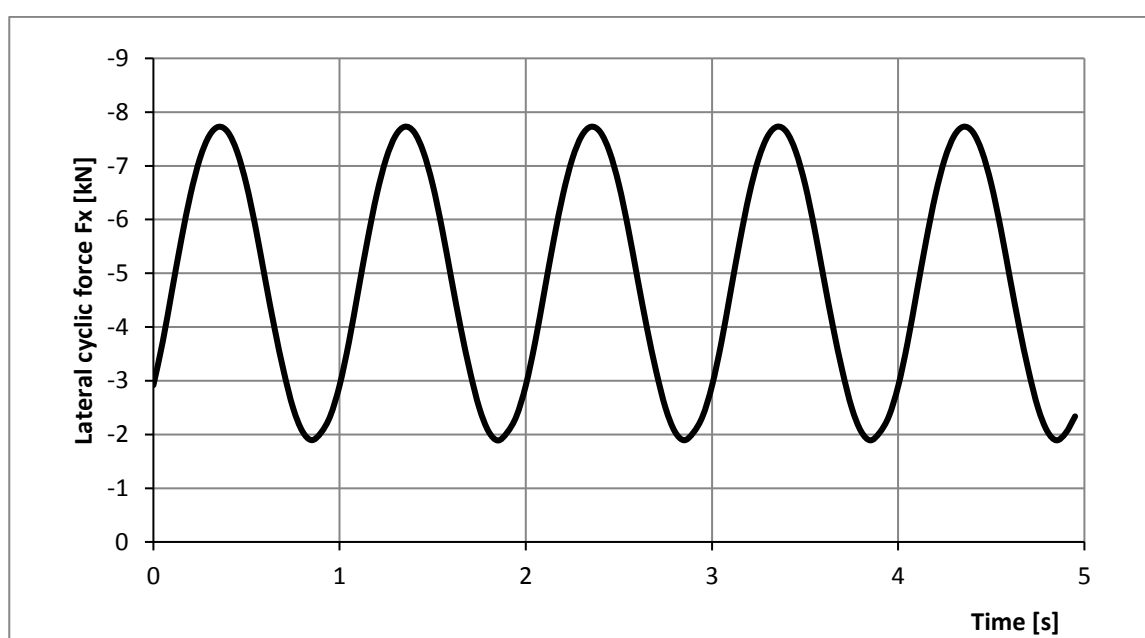


Figure 54 - 1st phase: loading history program of high-cycle test, 10^6 cycles

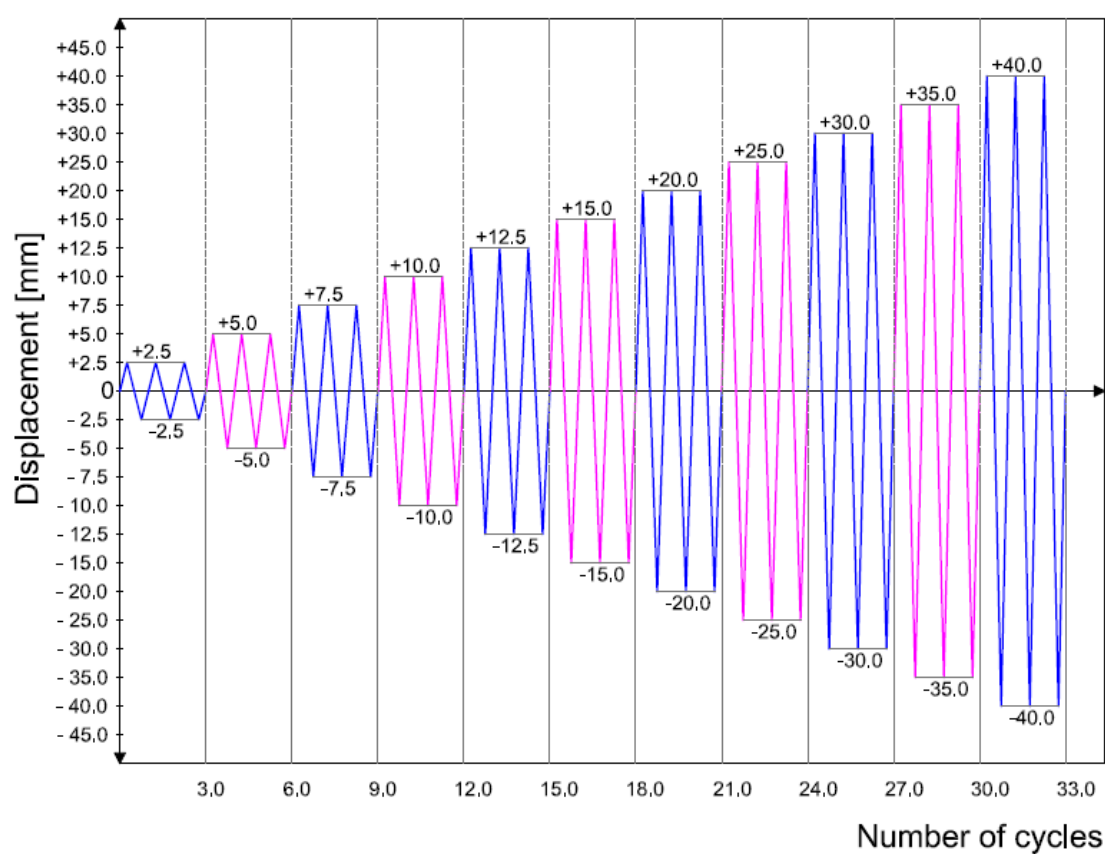


Figure 55 - 2nd phase: loading history program of low-cycle test (Displacement vs number of cycles)

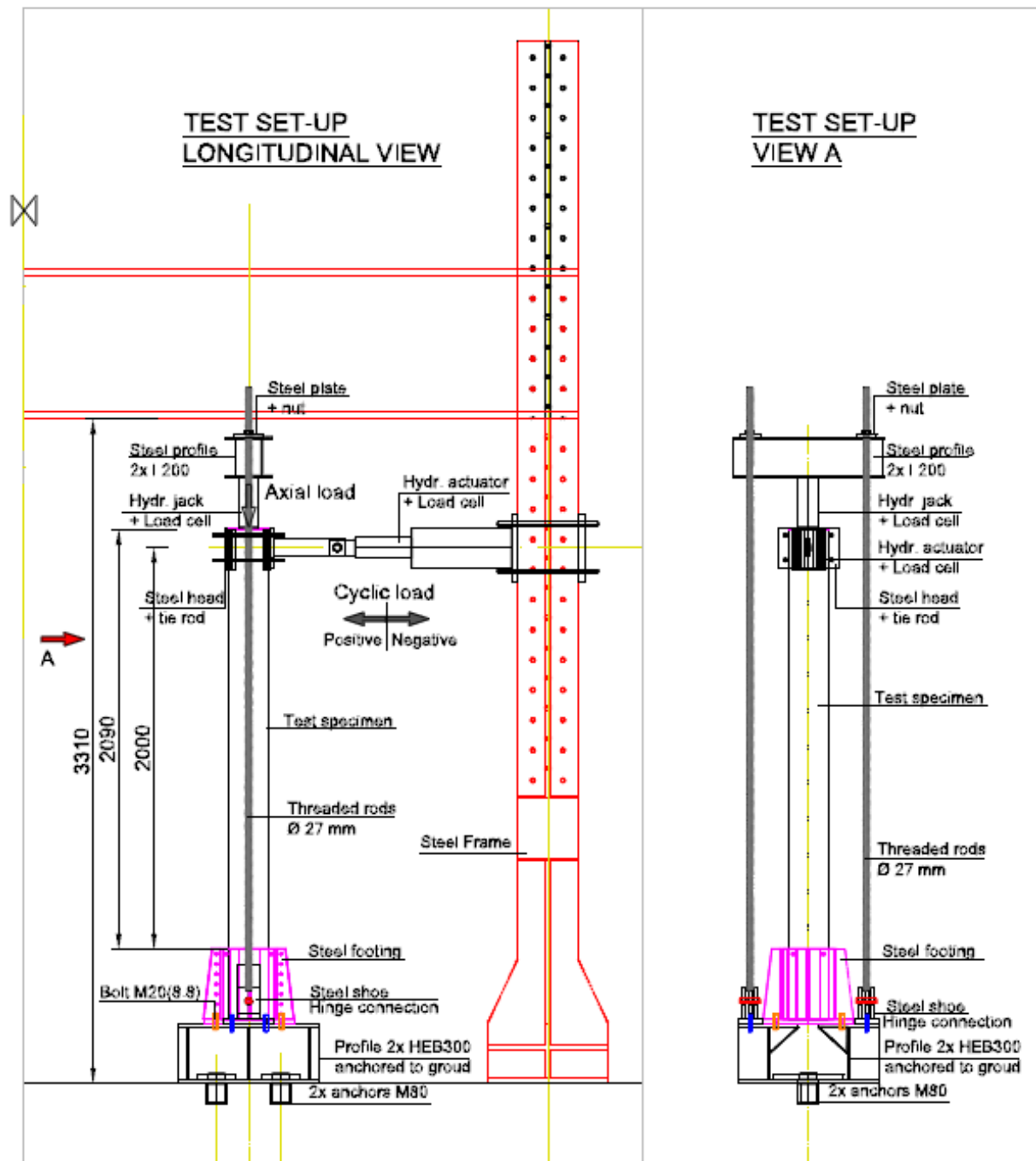


Figure 56 - Test set up 2D view

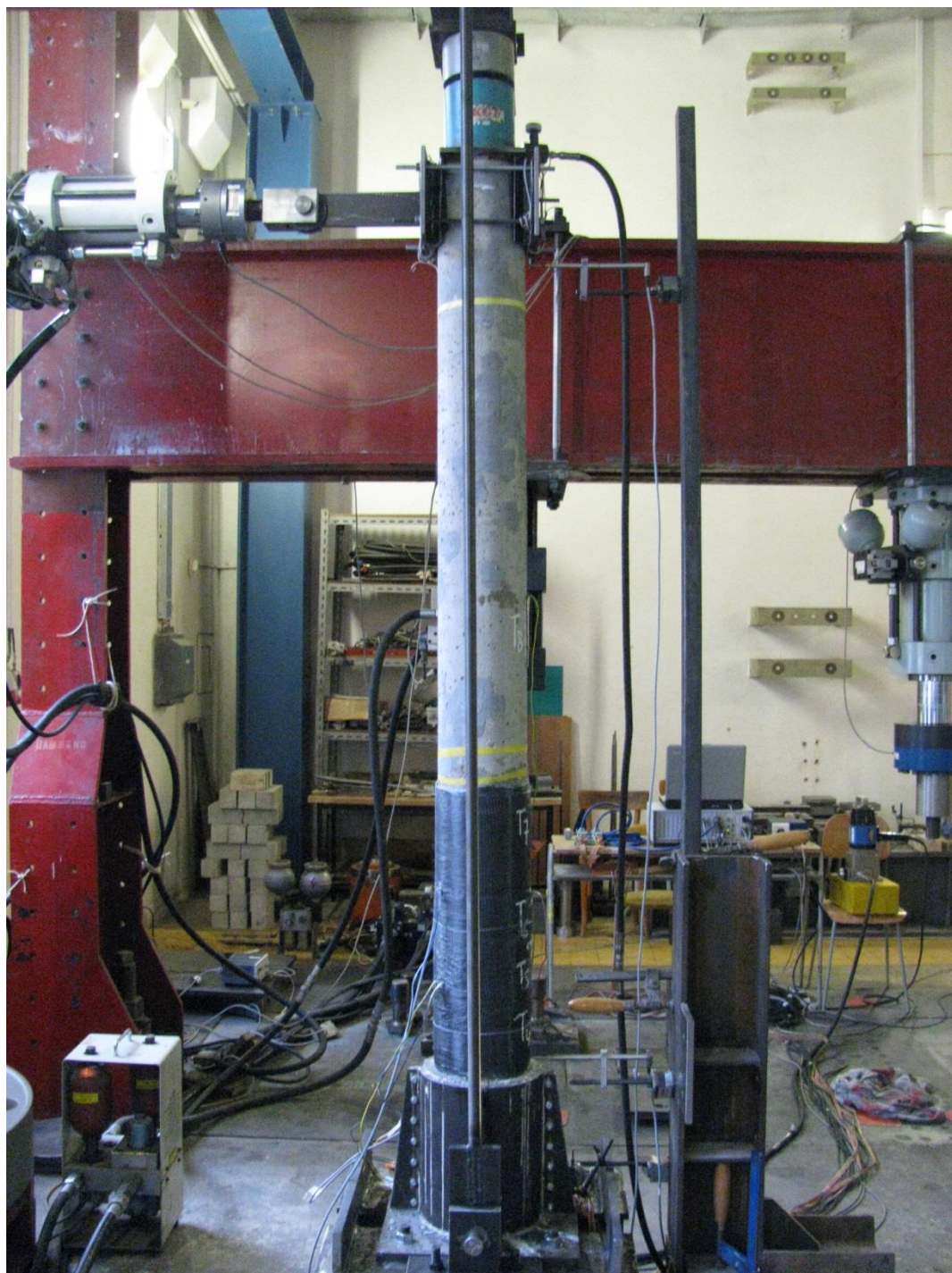


Figure 57 - Test set-up

3.3.9 INSTRUMENTATIONS

The applied loads were recorded and monitored with a computer based data acquisition system. Axial and lateral strains of concrete and FRP were measured by using strain gauges in vertical and horizontal position. The strain gauges were installed on the surface of the concrete and CFRP by using strain gauges adhesive after grinding the target surface and they were protected by Aluminum foil with kneading compound as shown in *Figure 58*. First series of vertical strain gauges (T1 and T4) were placed at 100 mm from the column base followed by second (T2 and T5) and third (T3 and T6) series of horizontal and vertical gauges respectively with distance of 100 mm center to center. Another two vertical strains (T7 and T8) were installed at 500 mm and 1000 mm from the column base. Columns confined by CFRP wraps, and a strain gauge (T9) were installed on the CFRP wraps perpendicular to lateral cyclic load at 300 mm from the column base. Strain gauges T1, T2 and T3 were in compression, and T4, T5, T6, T7 and T8 were in tension. All strain gauges were mounted parallel to column axis.

Lateral displacements were at different level measured using linear variable differential transducer (LVDTs) which was placed on the opposite side of hydraulic actuator at 2 cm, 40 cm and 185 cm from the column base and another two LVDTs were mounted on the steel footing as illustrated in *Figure 59*. All strain gauges and LVDTs were connected to data acquisition system to monitor and record the data. Load and displacement data were collected at 5-seconds interval from the hydraulic actuator cell, load cell of axial load, displacements potentiometers and strain gauges.

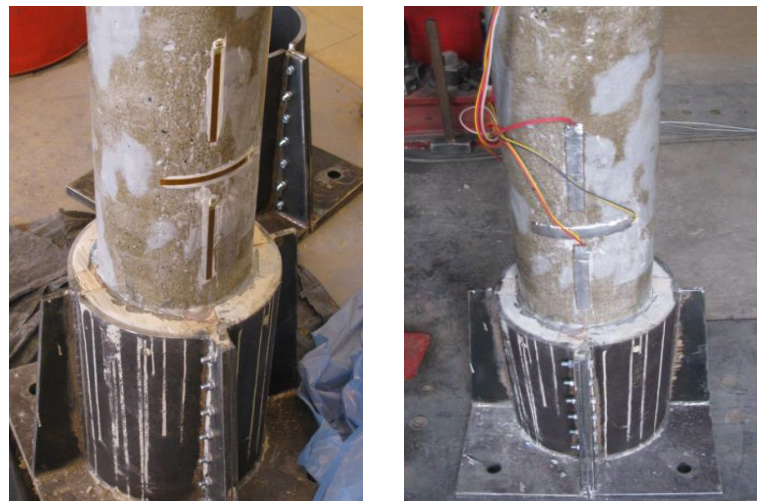
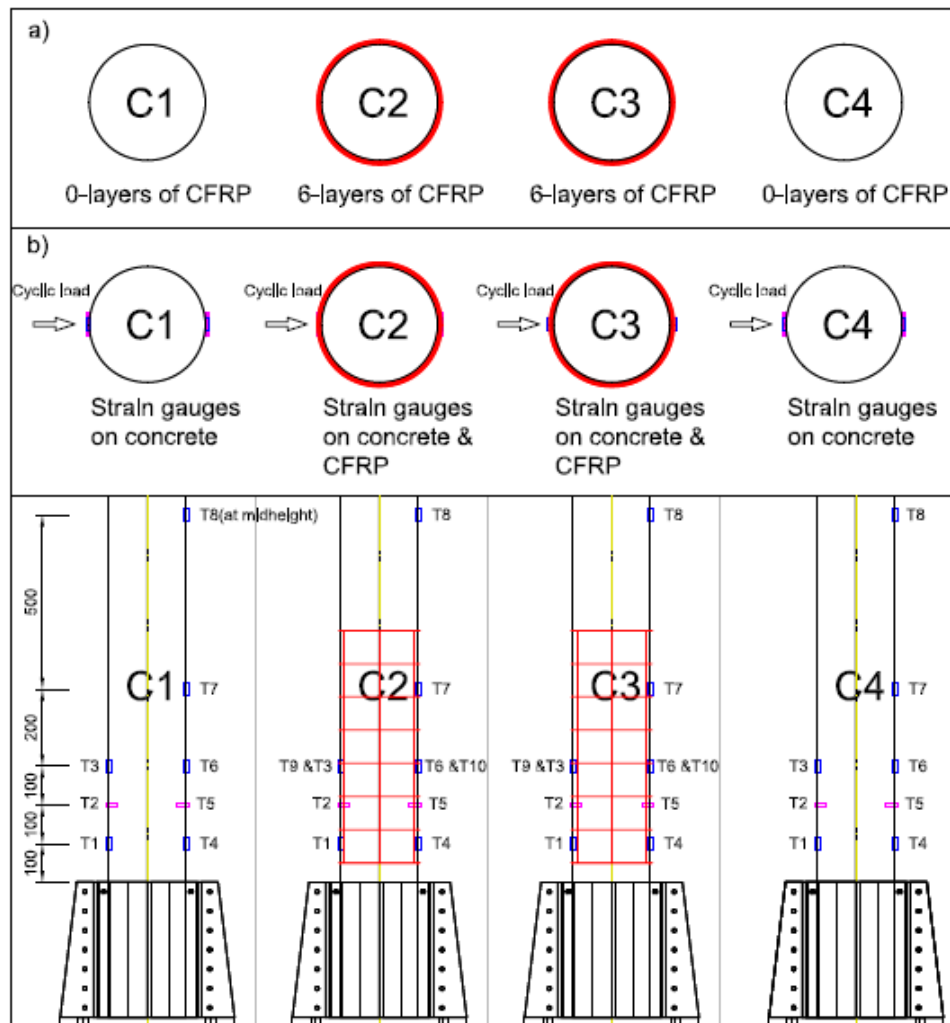


Figure 58 - Columns Surface a) Number of FRP layers, b) Strain gauges location

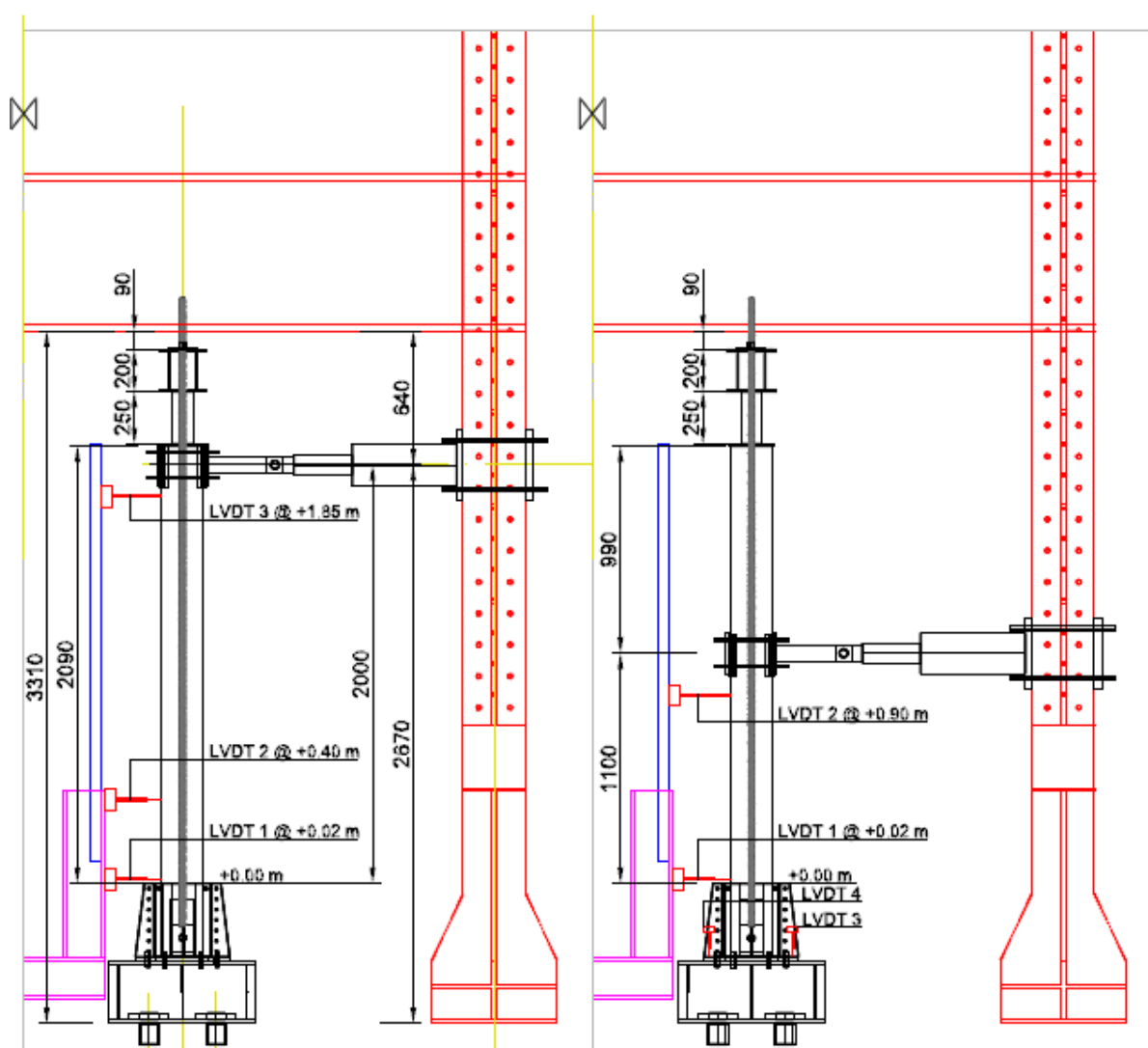


Figure 59 - LVDTs locations, a) high-cycle loading test, b) low-cycle loading test

3.3.10 STATIC SCHEME DIAGRAM OF COLUMNS TEST

Single cantilever columns with fixed base subjected to axial and lateral loads can behave in different ways depending on the boundary conditions. *Figure 60* is reflecting the status of the single cantilever column with fixed base. Fixed static vertical force (F_z) is applied downward (compressive load) and it is presumed that the vertical displacement is small according to the dimension of the member. This precondition allows writing equilibrium conditions for the initial shape of the structures.

First-order analysis is a method of structural analysis that does not consider the deformed shape of the structure to arrive at the internal actions of the structures, i.e. in the first order analysis, the effect of the deformation on the internal forces in the members is neglected. When a column is loaded, initially it will remain stable, when the load is larger than the buckling load (Euler's load), the column becomes unstable.

Opposite to the first-order, in the second order analysis the deformed shape of the structures (θ_2) is considered in the equation of equilibrium. An accurate estimate of the stability effects may be obtained by P-delta method or second-order analysis. Second order analysis is recommended in many codes by using equations to compute the additional moments.

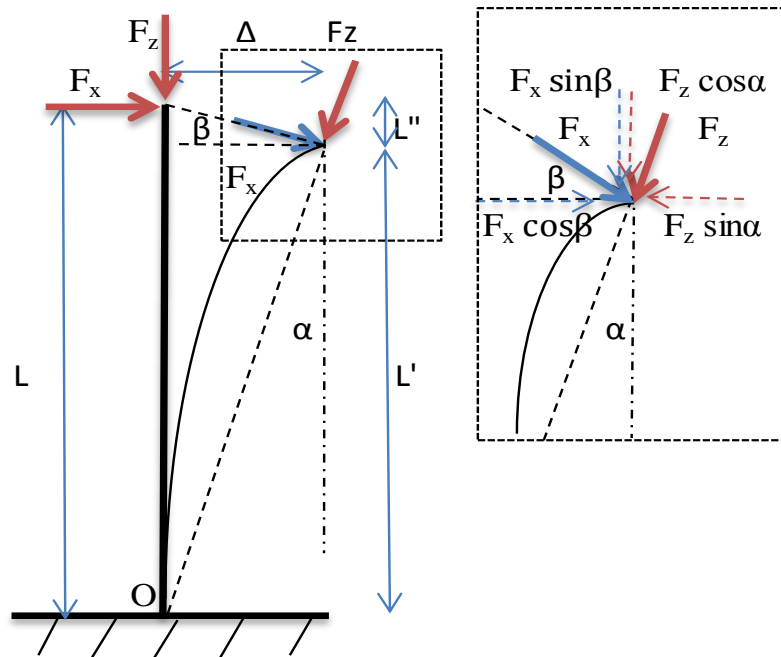


Figure 60 - Static scheme of column with fully fixed support at one end

Since the axial force is applied on the column, the axial force resolves in vertical and horizontal directions. The presence of the axial force creates an incremental increase in the internal moment that is originally computed from the horizontal force. The incremental increase in moment is equal to axial force times the deflection (P-delta effect or second-order).

Assuming an unstable column motion:

$$\sin \alpha = \frac{\Delta}{L}, \quad (85)$$

$$\cos \alpha = \frac{L - L''}{L} = \frac{L'}{L}, \quad (86)$$

$$\tan \beta = \frac{L''}{\Delta} = \frac{(L - L')}{\Delta}. \quad (87)$$

The moment at point O:

$$M_0 - F_x \cdot L' \cdot \cos \beta - F_x \cdot \Delta \cdot \sin \beta - F_z \cdot \Delta \cdot \cos \alpha + F_z \cdot L' \cdot \sin \alpha = 0 \quad (88)$$

$$\rightarrow M_0 = F_x \cdot (L' \cdot \cos \beta + \Delta \cdot \sin \beta) + F_z (\Delta \cdot \cos \alpha - L' \cdot \sin \alpha)$$

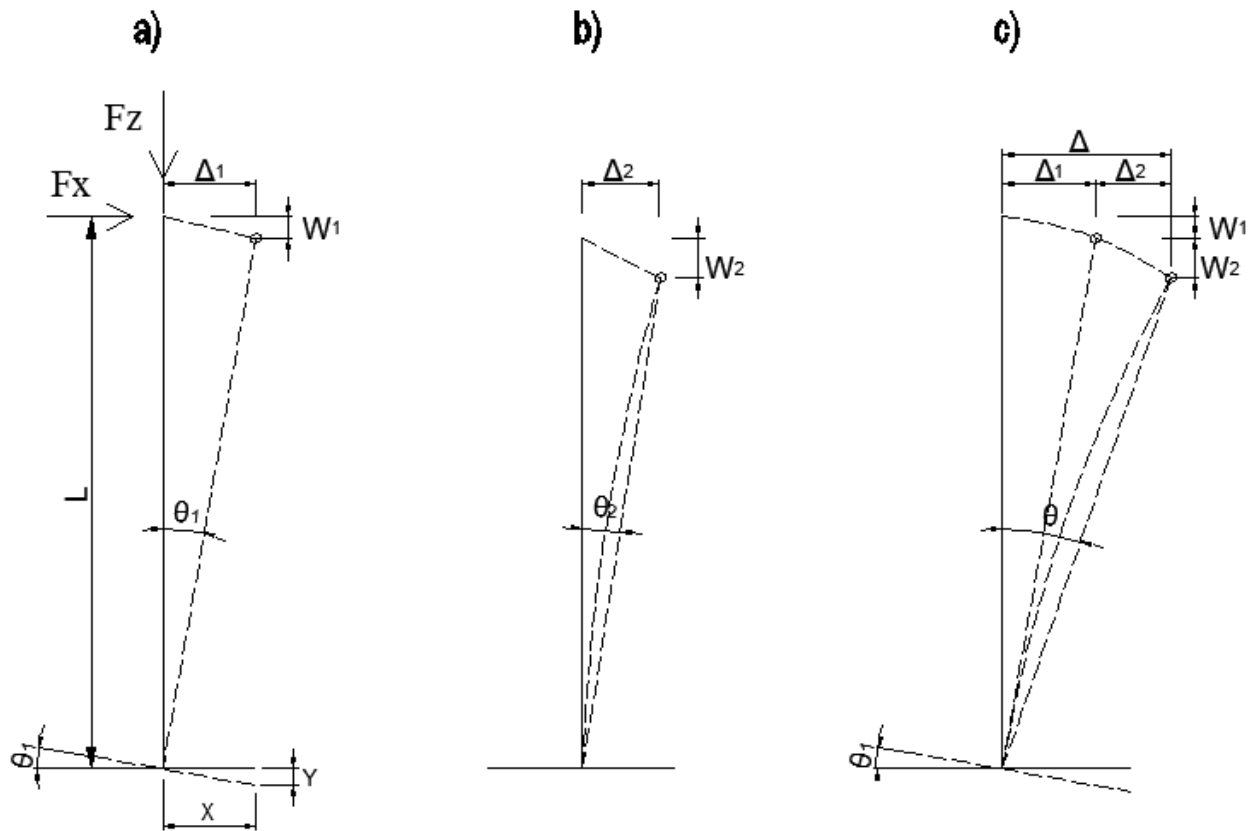


Figure 61 – a) deformation and uplift due to 1st order analysis b) deformation due to 2nd order analysis c) final status

Total measured deformation of column:

$$\Delta = \Delta_1 + \Delta_2 \quad (89)$$

Total rotation of column:

$$\sin \theta \approx \theta = \theta_1 + \theta_2 = \frac{\Delta_1 + \Delta_2}{L - W_1 - W_2} \quad (90)$$

Measured base uplift:

$$\tan \theta_1 \approx \theta_1 = \frac{Y}{X}, \quad (91)$$

where X is the distance of the centre of column to the edge of the base, and Y is the distance vertical translation as shown in *Figure 61*.

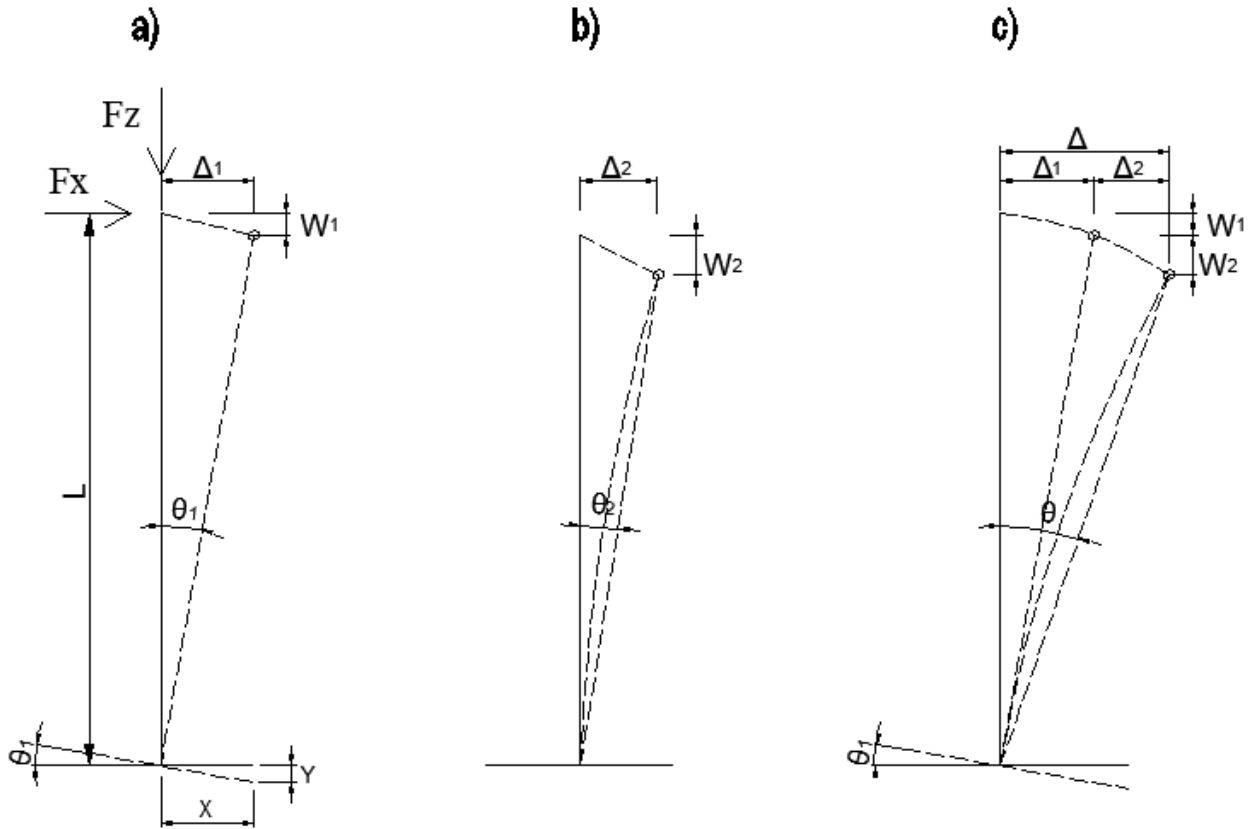


Figure 61

$$\tan \theta_1 \approx \theta_1 = \frac{\Delta_1}{L} \quad (92)$$

Expression of Δ_2 and θ_2 :

$$\theta_2 = \theta - \theta_1 = \frac{\Delta}{L - W_1 - W_2} - \frac{Y}{X}, \quad (93)$$

$$\Delta_2 = \Delta - \Delta_1 \quad (94)$$

During the experiment and the application of loads the uplift were measured considering the procedures shown above to calculate the uplift and the rotation of the column base as illustrated in the following paragraphs.

3.4. TEST RESULTS AND DISCUSSION

In this part, results and observations of the experimental tests are presented and summarized. The performance of each specimen was evaluated based on fatigue and hysteretic behaviour. Load-displacement data of high and low-cycle loading tests for all test specimens (unconfined and confined columns) was recorded, compared and discussed. In the results discussion, negative lateral loads are associated with pulling of the column into the hydraulic actuator direction.

3.4.1 UNCONFINED SPECIMEN – COLUMN TYPE C1 (CONTROL SPECIMEN)

Column type C1 was designed to be representative of a control specimen without CFRP confinement. Its details are mentioned previously in *Table 16* and *Figure 46*. The performance of this control specimen was compared to confined specimens to evaluate the effectiveness of the applied CFRP wraps on the columns behavior and to another unconfined specimen subjected only to low-cycle load to evaluate the effect of high-cycle load on the column behavior.

3.4.1.1 HIGH-CYCLE LOADING TEST-COLUMN TYPE C1

The column type C1 was oscillated approximately one million cycles under constant axial force of 450 kN and lateral force of 6.0 kN, which simulate the high-cycle loading acting on un-strengthened column. During the high-cycle loading test, no cracks were observed at the lower region of the column. Concrete strains at compression and tension zones were measured by strain gauges in both directions, vertical and horizontal. The deformation of the column and the uplift of the column base were measured by Linear Variable Differential Transformers (LVDT) and Dial Test Indicator (DTI) respectively. The measured uplift of the column base was 0.11 mm.

The lateral force-displacement at top of column (at level 1.85 m from the top of steel column footing) for number of cycles of 2×10^5 , 4×10^5 , 6×10^5 , 8×10^5 and 1×10^6 is represented in the *Figure 62*, Fx-X-010-C1 till Fx-X-050-C1 respectively. The figure shows that the lateral displacement of column increases with the increase of number of cycles at the same level of lateral loading.

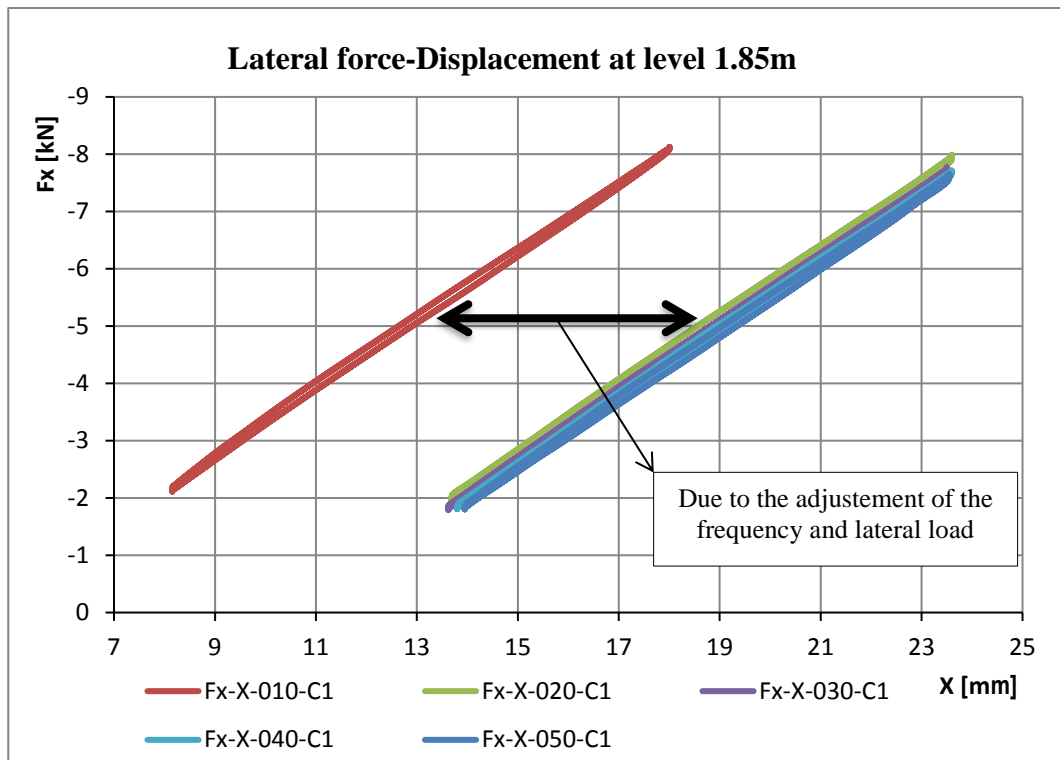
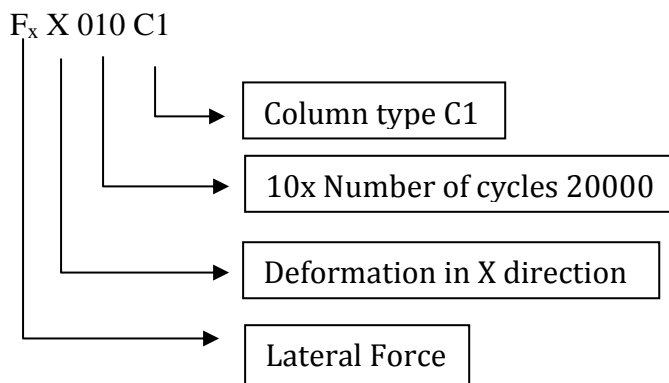


Figure 62 - Lateral force (F_x) vs. displacement (X) for unstrengthen column C1 (high-cycle loading test)



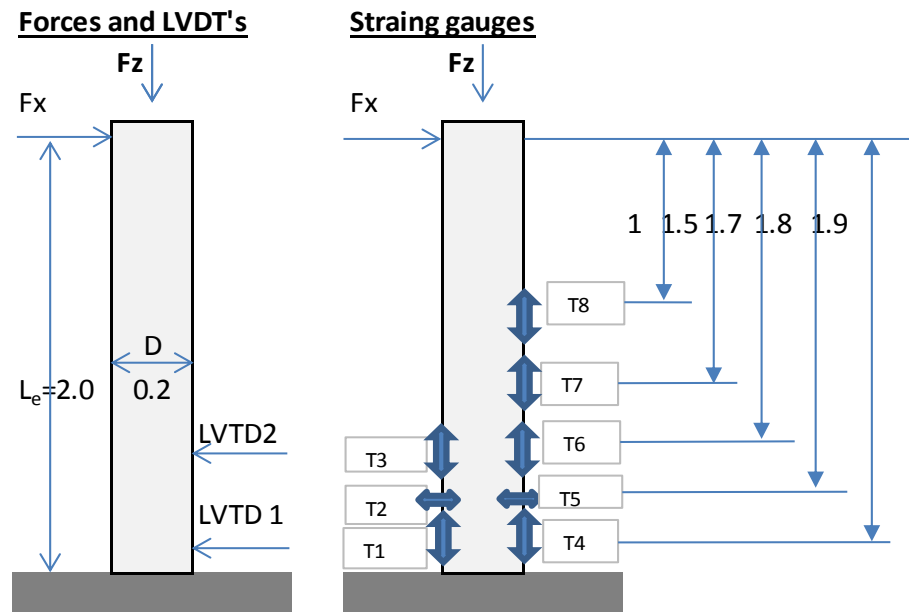
During the high-cyclic loading application, the test has been stopped for a while to adjust and regulate the frequency of the cyclic loading and the lateral load based on the test configuration shown in Figure 54. Therefore, a gap in the lateral force-displacement between the number of cycles 200000 and others has been resulted as shown in the figure above.

In general, a structure to be in equilibrium, all forces or moments acting upon it are balanced. This means that each and every force acting upon a column is resisted by either another equal or opposite forces or set of forces whose net result is zero. Table 22 shows the bending

moments ($M_2 = \sigma \cdot W$) contribution from the measured stresses (σ) in the concrete fibres in tension and compression zones multiplied by the section modulus of the column (W) compared with those resulted from the maximum applied external force multiplied by the arm ($M_1 = F_x \cdot H$) during the high-cycle loading test. As illustrated in *Figure 64* and *Figure 65* the bending moments due to stresses in the concrete fibres at compression and tension zones (M_2), which are measured by the strain gauges positioned at different level (values considered for H – see *table 22*), are smaller than the acting external force (M_1). Therefore, the moment due to the uplift of the column base ($M_3 = K \cdot \theta$) has been calculated and combined with the internal bending moments contributed from the measured stresses. The moment (M_3) is equal to the column stiffness (K) multiplied by the rotation angle (θ) due to the uplift. The summary of the moments (M_2) and (M_3) should be equal to the moment (M_1) in case the column support acts as fully fixed support. As shown in the table below that some losses of the bending moments take place due to the connections of the concrete column to steel footing and the steel footing to the ground of the laboratory, which concludes that the support in the column base is not fully fixed support.

The deformation of the column C1 due to high-cycle loading test is small; therefore the moment results due to P- Δ effect were not taken into consideration.

Circular RC column-high-cycle loading test- Column C1- specimen no.12



Remarks

Strain gauges T1 and T4 are placed 10 cm from the base. The distance between strain gauges is 10 cm and between T6 and T7 is 20 cm. T8 is placed at mid-height of the column(1,0 m from the base). Two LVDTs (V1 and V2) are installed with distance of 2 cm and 40 cm from the base.

Measured uplift at base = 0,55 mm, drift at top of column caused by uplift = $h \times \text{uplift} / b = 2350 \times 0,55 / 225 = 5,75$ mm

Figure 63 – high-cycle loading test configuration for unstrengthen column C1

Table 22 - Bending moments- Test specimen C1

Test specimen - column type C1(12) (unconfined)														
No. of cycles	Zone	Strain gauges	$\Delta\epsilon$ [$\mu\text{m}/\text{m}$]	H [m]	F_z [kN]	F_x [kN]	E [MPa]	W [m^3]	Stiffness K [kN/m]	$\sigma = E\Delta\epsilon$ [MPa]	$M_1 = F_x \cdot H$ [kN.m]	$M_2 = \sigma \cdot W$ [kN.m]	$M_3 = K \cdot \theta$ [kN.m]	$M = M_2 + M_3$ [kN.m]
2x10 ⁵	Compression (-)	T1	341,09	1,90	441,03	8,13	3,73E+04	7,85E-04	1,28E+03	12,73	15,44	10,00	3,138	13,13
		T3	316,13	1,70	441,03	8,13				11,80	13,82	9,26	2,808	12,07
	Tension (+)	T4	376,18	1,90	441,03	8,13				14,04	15,44	11,02	3,138	14,16
		T6	331,71	1,70	441,03	8,13				12,38	13,82	9,72	2,808	12,53
		T7	290,60	1,50	441,03	8,13				10,85	12,19	8,52	2,477	10,99
		T8	185,53	1,00	441,03	8,13				6,93	8,13	5,44	1,652	7,09
	Compression (-)	T1	345,46	1,90	453,95	7,99				12,90	15,18	10,12	3,138	13,26
		T3	321,87	1,70	453,95	7,99				12,02	13,58	9,43	2,808	12,24
4x10 ⁵	Compression (-)	T4	380,58	1,90	453,95	7,99	3,73E+04	7,85E-04	1,28E+03	14,21	15,18	11,15	3,138	14,29
		T6	335,58	1,70	453,95	7,99				12,53	13,58	9,83	2,808	12,64
	Tension (+)	T7	294,61	1,50	453,95	7,99				11,00	11,99	8,63	2,477	11,11
		T8	183,71	1,00	453,95	7,99				6,86	7,99	5,38	1,652	7,04
	Compression (-)	T1	343,41	1,90	458,40	7,77				12,82	14,76	10,06	3,138	13,20
		T3	320,37	1,70	458,40	7,77				11,96	13,20	9,39	2,808	12,53
	Tension (+)	T4	378,95	1,90	458,40	7,77				14,15	14,76	11,11	3,138	14,24
		T6	333,58	1,70	458,40	7,77				12,45	13,20	9,78	2,808	12,58
6x10 ⁵	Compression (-)	T7	293,25	1,50	458,40	7,77	3,73E+04	7,85E-04	1,28E+03	10,95	11,65	8,59	2,477	11,07
		T8	188,58	1,00	458,40	7,77				7,04	7,77	5,53	1,652	7,18
	Compression (-)	T1	340,34	1,90	447,96	7,72				12,71	14,66	9,97	3,138	13,11
		T3	316,60	1,70	447,96	7,72				11,82	13,12	9,28	2,808	12,09
	Tension (+)	T4	375,85	1,90	447,96	7,72				14,03	14,66	11,01	3,138	14,15
		T6	330,58	1,70	447,96	7,72				12,34	13,12	9,69	2,808	12,50
		T7	289,94	1,50	447,96	7,72				10,82	11,57	8,50	2,477	10,97
		T8	186,16	1,00	447,96	7,72				6,95	7,72	5,46	1,652	7,11
1x10 ⁶	Compression (-)	T1	331,40	1,90	460,94	7,65	3,73E+04	7,85E-04	1,28E+03	12,37	14,53	9,71	3,138	12,85
		T3	309,25	1,70	460,94	7,65				11,55	13,00	9,06	2,808	11,87
	Tension (+)	T4	366,26	1,90	460,94	7,65				13,67	14,53	10,73	3,138	13,87
		T6	322,28	1,70	460,94	7,65				12,03	13,00	9,44	2,808	12,25
		T7	282,47	1,50	460,94	7,65				10,55	11,47	8,28	2,477	10,76
		T8	182,14	1,00	460,94	7,65				6,80	7,65	5,34	1,652	6,99

Notation of Symbols in the table

H: Distance between applied lateral force and strain gauge locations;

 F_z : Axial compressive load; F_x : Lateral cyclic load ;E: Modulus of elasticity of concrete = 3.73×10^4 MPa;W: Section modulus of column cross-section = $\pi d^3/32 = 7.85 \times 10^{-4} \text{ m}^3$; σ : Stress in concrete fibers; M_1 : Moment at location of strain gauges due to lateral force- Assumed fully fixed support; M_2 : Effective bending moment due to stress in concrete fibers at strain gauges; M_3 : Bending moment due to rotational stiffness of the base; $\Delta\epsilon$: Strain or deformation per unit length;K: $3EI/L^3$ - Stiffness of columns;

I: Modulus of elasticity of column;

 θ : Δ/L – Lateral deformation/Column length;

V1 and V2: LVDT locations measuring the displacements;

T1 to T8: Strain gauges locations;

 M_{1C} : Summary of M_2 and M_3 for compression zone; M_{1T} : Summary of M_2 and M_3 for tension zone.

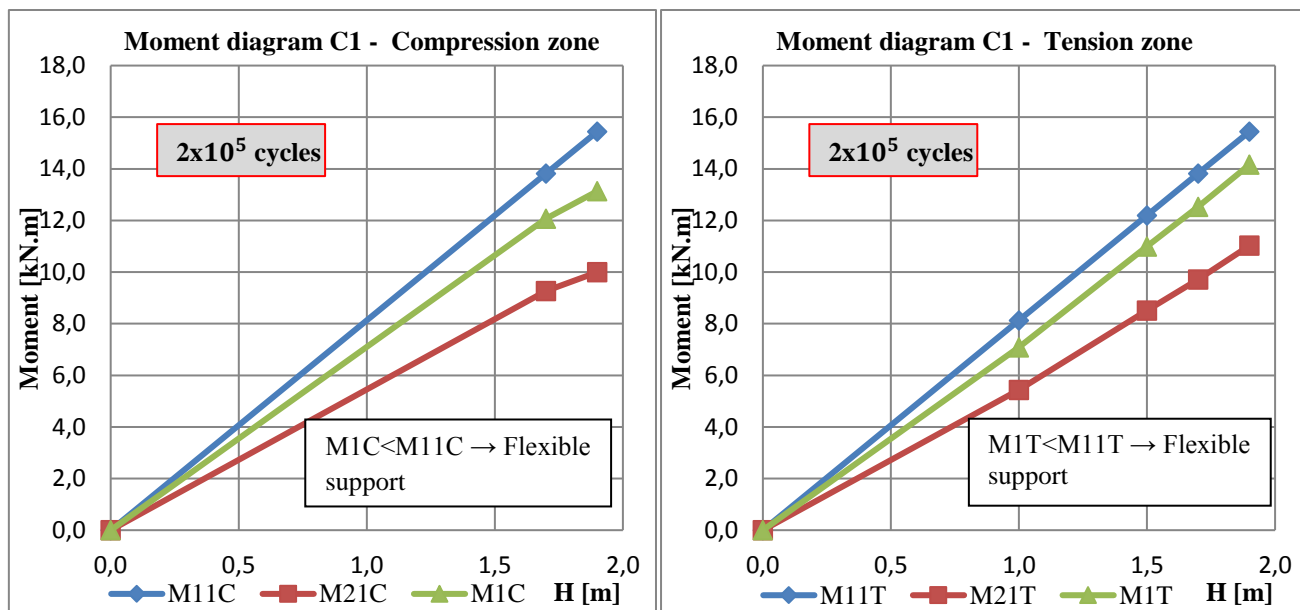


Figure 64 - Moment diagrams of specimen C1 at 2×10^5 cycles

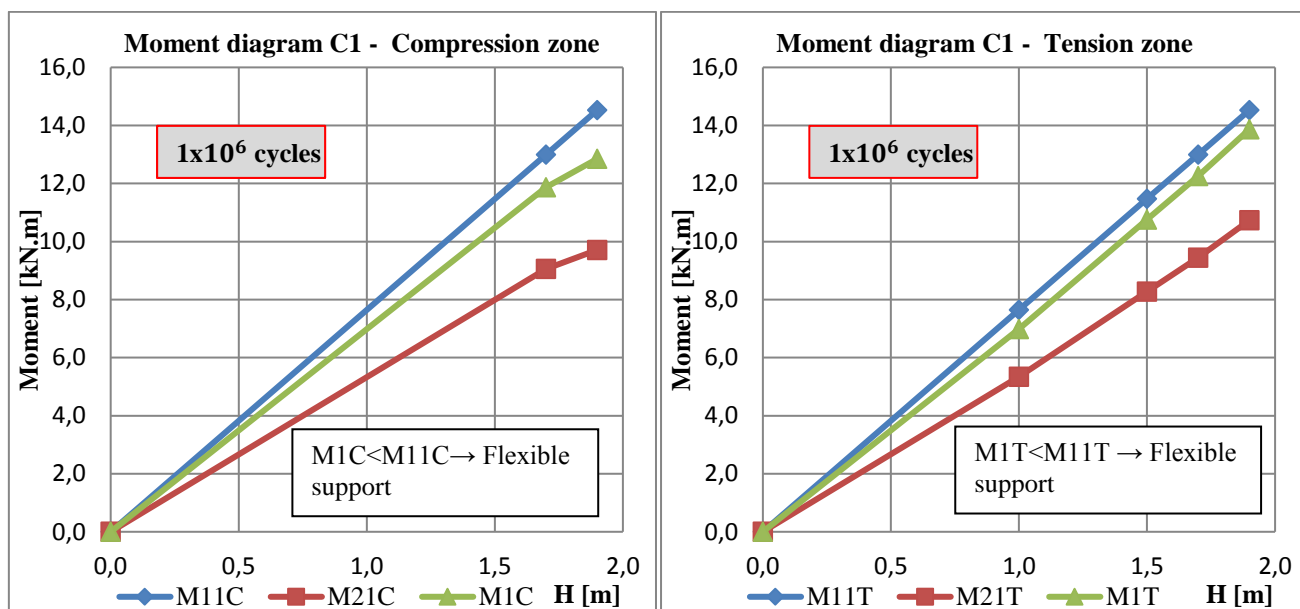
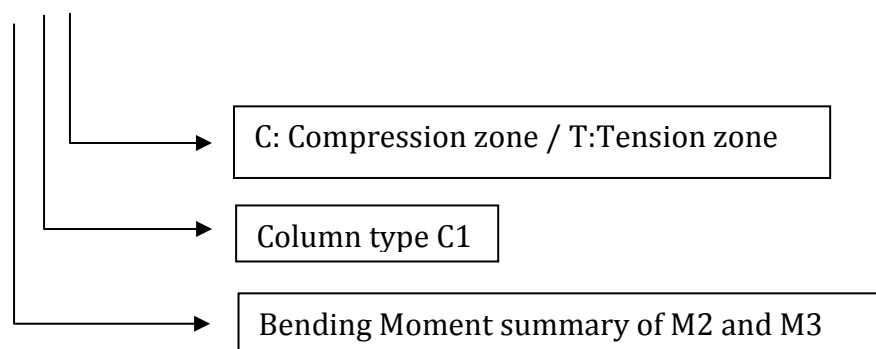
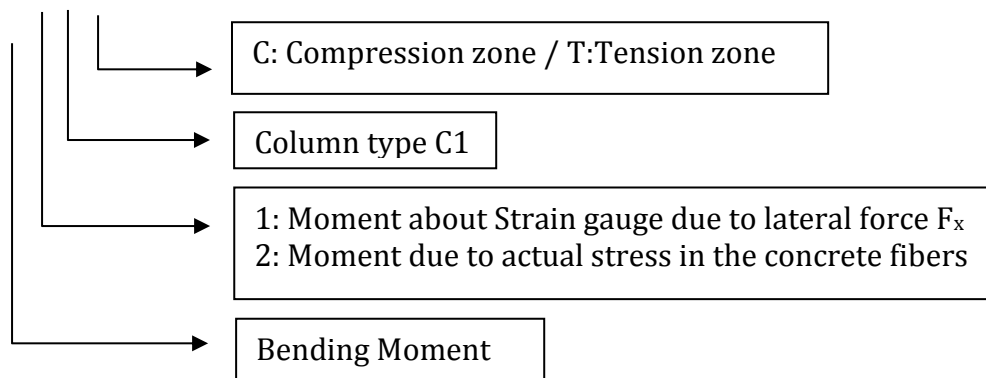


Figure 65 - Moment diagrams of specimen C1 at 1×10^6 cycles

M 1 C



M 1 1 C



3.4.1.2 LOW-CYCLE LOADING TEST-COLUMN TYPE C1

After performing the high-cycle loading test, the column was subjected to reversed cyclic loading test (low-cycle loading test) which simulates the seismic load. Due to the stroke limitation of the hydraulic actuator available in the laboratory, the hydraulic actuator was shifted to a lower position of 1.10 m from the column base as shown below. The configuration and loading test history were mentioned previously. During the loading test, cracks on the bottom surfaces of the column were observed and a cracking sound was heard. Strain gauges were disrupted due to cracks development. The formation of flexural cracks continued with increasing levels of lateral displacement. The spalling of concrete cover of the column began due to lateral loading, exposing the column reinforcement as shown in *Figure 66a*. The loading test was terminated when the displacement level was approximately ± 40 mm (maximum stroke of the hydraulic actuator), and the damage occurred at the lower region of the column. Numerous cracks were observed approximately up to 50 cm of the column height from the column base as shown in *Figure 66b*. Load-displacement (at level 0.90 m from the column base) of column data of reversed cyclic tests were recorded and used to plot the hysteresis curves. Additionally, the uplift of column base during the reversed cyclic loading test was recorded as illustrated in *Figure 69*.

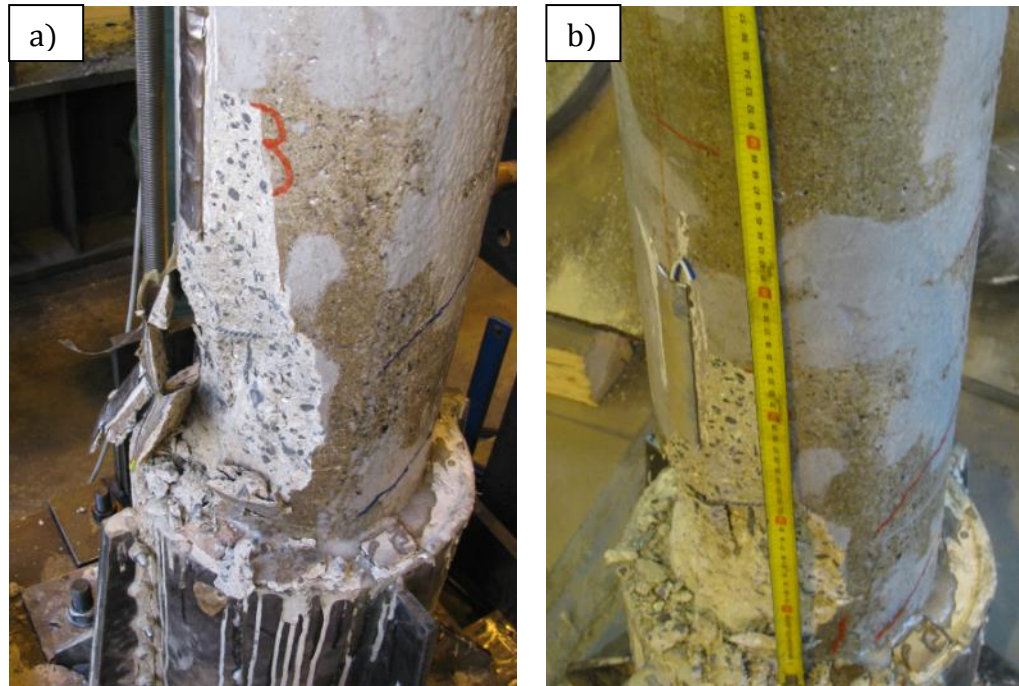
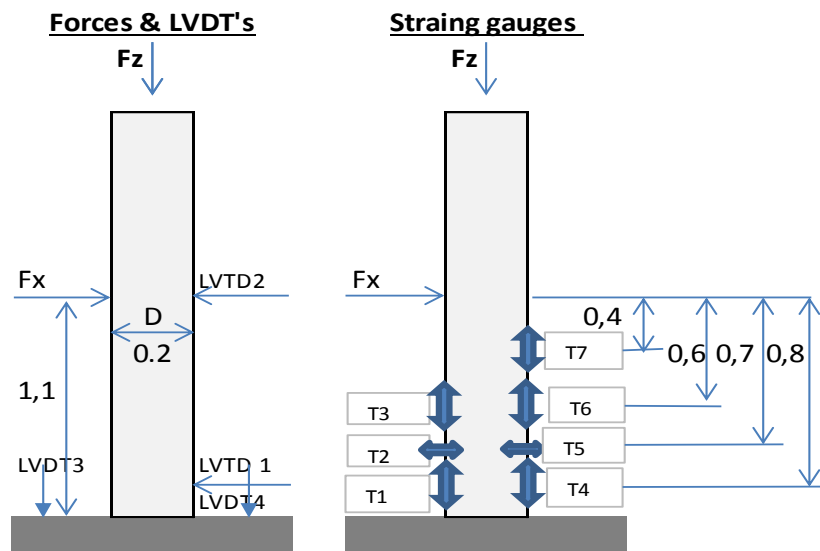


Figure 66 - Failure of Specimen C1; a) Exposing of reinforcement, b) Cracks and damage

Circular RC column-low-cycle fatigue test- Column C1- specimen no.12



Remarks

Strain gauges T1 and T4 are placed 10 cm from the base. The distance between strain gauges is 10 cm and between T6 and T7 is 20 cm. Two LVDTs (V1 and V2) are installed with distance of 2 cm and 110 cm from the base.

Additional two LVDTs V3 and V4 are installed on the steel base to measure the uplift of the footing during the reversed cyclic loading test. Strain gauge T8 was removed due to hydraulic actuator shift (level 1,0 m from the base).

Figure 67 – low cycle loading test configuration for unstrengthen column C1

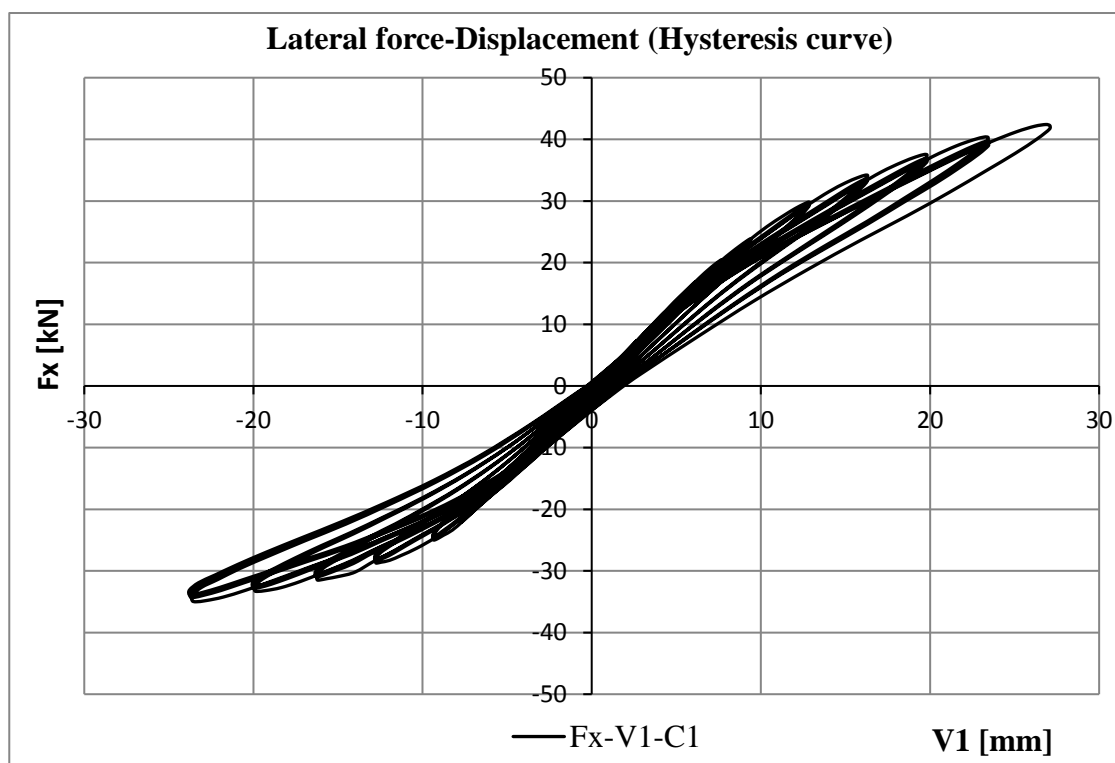


Figure 68 - Lateral force (F_x) vs. displacement (V_1) Hysteresis curve for unstrengthen specimen C1 (low-cycle loading test)

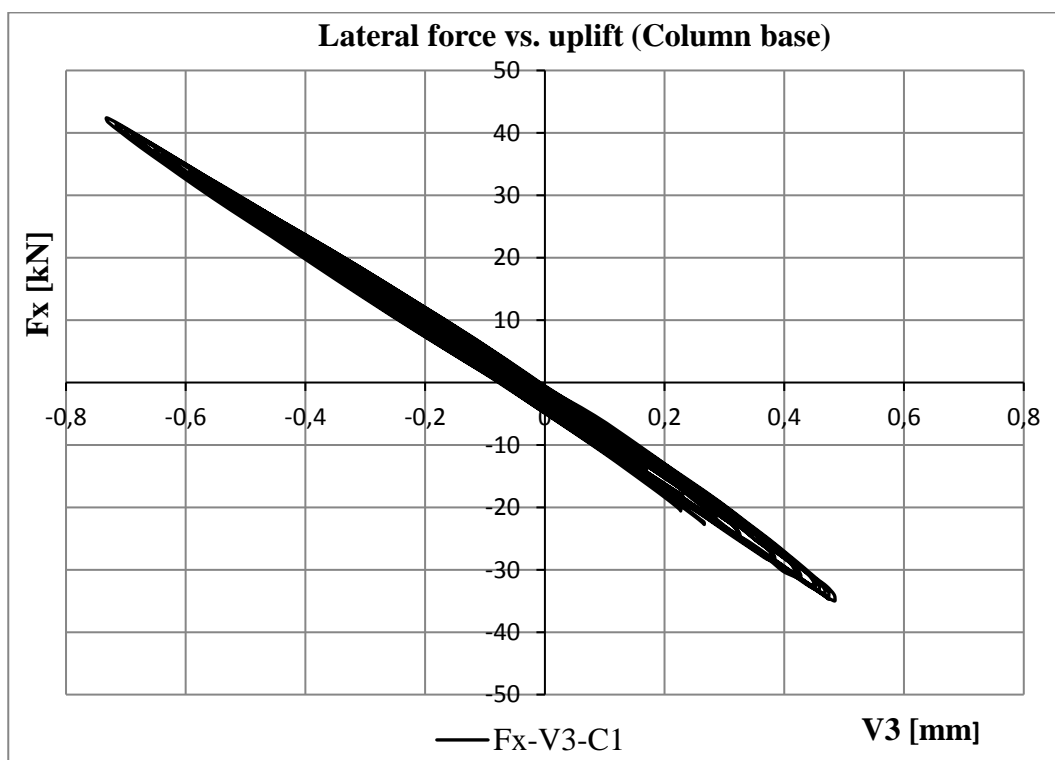
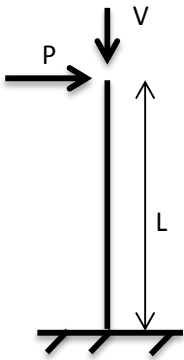


Figure 69 - Lateral force (F_x) vs. uplift of column base (V_3) for unstrengthen specimen C1

Horizontal force:	P =	42,11 [kN]	Free end column subjected to horizontal and vertical forces at top $\Delta_{max} = \frac{PL^3}{3EI - VL^2}$ P - Horizontal force V - Vertical force L - length of column E - modulus of elasticity of concrete column I - moment of inertia Δ_{max} - maximum deflection at top of the column	
Vertical force:	V =	450,00 [kN]		
Length of column:	L =	1,10 [m]		
Diameter of column:	D =	0,20 [m]		
Modulus of elasticity:	E =	37333,00 [MPa]		
Effective Moment of inertia:	I =	3,93E-05 [m ⁴]		
Max.deflection at top:	Δ_{max} =	14,54 [mm]		

The theoretical maximum deflection of the cantilever column subjected to axial and lateral forces simultaneously as shown in the calculation above is 14.54 mm which is smaller than the deflection during the experiment which is 26.11 mm in *Figure 68*. It derives that there is a rotation in the column support and the column base is not acting as fully support.

3.4.2 CONFINED SPECIMEN – COLUMN TYPE C2 AND C3 (6x CFRP)

Column type C2 and C3 were designed to be representative of the confined specimens with CFRP wraps. Details of the column type C2 and C3 are mentioned previously in *Table 16* and *Figure 46*. The performance of these confined specimens was compared to control specimen C1 to evaluate the effectiveness of the applied CFRP wraps on the columns behavior. Test configurations of column type C1 for high and low cycle loading tests were implemented, the same for columns type C2 and C3.

3.4.2.1 HIGH-CYCLE LOADING TEST-COLUMN TYPE C2 AND C3

As the column type C1, the same loading history of high-cycle loading test and number of cycles were conducted on the column type C2 and C3. During the high-cycle loading test, no cracks were observed on the lower surface of the columns. Strains of the concrete and FRP surfaces were measured by strain gauges. The deformation of the columns and the uplift of the column bases were measured by LVDTs and DTI, respectively. The measured uplift under to the same loads (Axial and lateral) of the column base of C2 was 0.55 mm, which was bigger than in the previous column (column type C1). To make the support of columns stiffer and to decrease the uplift of the base, steel stiffeners were provided to column base C3. Afterwards, the measured uplift decreased to 0.11 mm for column C3.

The lateral force- displacement at top of columns C2 and C3 (at level 1.85 m from the top of steel column footing) for number of cycles of 2×10^5 , 4×10^5 , 6×10^5 , 8×10^5 and 1×10^6 which are

represented in the figure by Fx-X-010-C2 till Fx-X-050-C2 respectively. *Figure 70*, shows that the lateral displacement of columns increases with the increase of number of cycles at the same level of lateral loading. The descriptions of subscripts in details are mentioned in the previous paragraph 3.4.1.1.

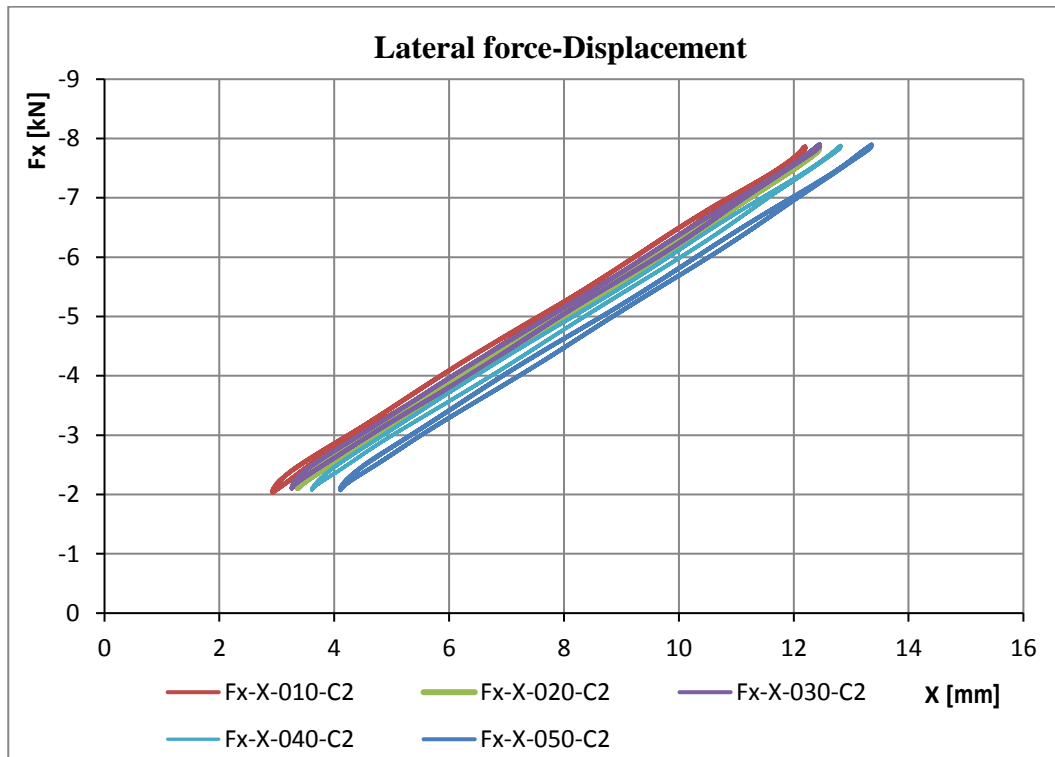


Figure 70 - Lateral force (F_x) vs. displacement (X) for column type C2 (high-cycle loading test)

Table 23 and Table 24 show the bending moment ($M_2 = \sigma \cdot W$) contribution from the measured stresses (σ) in the concrete fibers compared in tension and compression zones multiplied by the section modulus of the column (W) compared with those resulted from the maximum applied external force multiplied by the arm ($M_1 = F_x \cdot H$) during the high-cycle loading test. As illustrated in *Figure 72*, *Figure 73*, *Figure 74*, and *Figure 75* respectively for column type C2 and C3, the bending moments (M_2) due to stresses in the concrete fibers at compression and tension zones, which are measured by the strain gauges positioned at different level (values considered for H – see Table 23 and Table 24), are smaller than due to the acting external force (M_1). Therefore, the moment due to the uplift of the column base ($M_3 = K \cdot \theta$) has been calculated and combined with the internal bending moments contributed from the measured stresses. The moment (M_3) is equal to the column stiffness (K) multiplied by the rotation angle (θ) due to the uplift. The summary of the moments (M_2) and (M_3) should be equal to the moment (M_1) in case the column support acting as fully fixed support. As shown in the tables below that some losses of the bending moments take

place due to the connections of the concrete column to steel footing and the steel footing to the ground of the laboratory, which concludes that the support in the column base for type C2 and C3 is not fully fixed support similarly to column type C1.

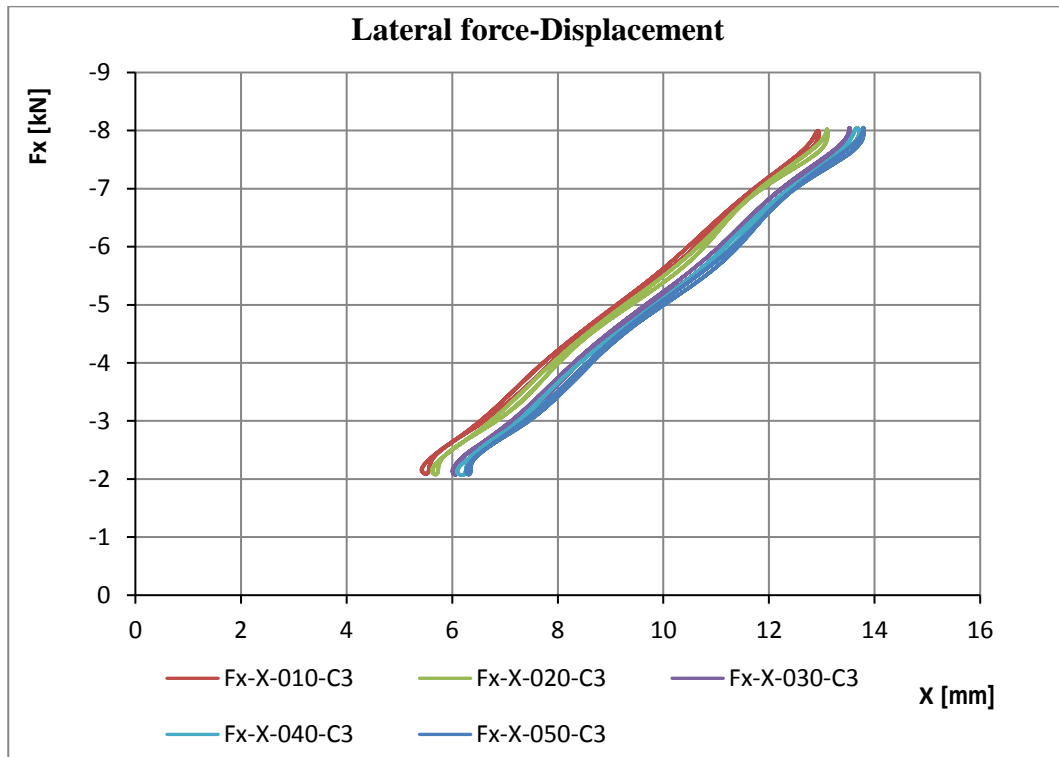


Figure 71 - Lateral force (F_x) vs. displacement (X) for type C3 (high-cycle loading test)

The deformation of the column C2 and C3 due to high-cycle loading test is small, therefore the moment results due to P- Δ effect was not taken into consideration.

Table 23 - Bending moments- Test specimen C2

Test specimen - column type C2(19) (confined with 6x FRP wraps)														
No. of cycles	Zone	Strain gauges	$\Delta\epsilon$ [$\mu\text{m/m}$]	H [m]	F_z [kN]	F_x [kN]	E [MPa]	W [m ³]	Stiffness K [kN/m]	$\sigma = E \cdot \Delta\epsilon$ [MPa]	$M_1 = F_x \cdot H$ [kN.m]	$M_2 = \sigma \cdot W$ [kN.m]	$M_3 = K \cdot \theta$ [kN.m]	$M = M_2 + M_3$ [kN.m]
2x10 ⁵	Compression (-)	T1	291,14	1,90	450,48	7,85	3,38E+04	7,85E-04	1,51E+03	9,84	14,92	7,72	3,69	11,42
		T3	262,15	1,70	450,48	7,85				8,86	13,35	6,96	3,30	10,26
	Tension (+)	T4	312,47	1,90	450,48	7,85				10,56	14,92	8,29	3,69	11,98
		T6	290,95	1,70	450,48	7,85				9,83	13,35	7,72	3,30	11,02
		T7	248,13	1,50	450,48	7,85				8,39	11,78	6,58	2,92	9,50
		T8	181,18	1,00	450,48	7,85				6,12	7,85	4,81	1,94	6,75
4x10 ⁵	Compression (-)	T1	287,59	1,90	454,89	7,86	3,38E+04	7,85E-04	1,51E+03	9,72	14,93	7,63	3,69	11,32
		T3	257,77	1,70	454,89	7,86				8,71	13,36	6,84	3,30	10,14
	Tension (+)	T4	308,27	1,90	454,89	7,86				10,42	14,93	8,18	3,69	11,87
		T6	286,08	1,70	454,89	7,86				9,67	13,36	7,59	3,30	10,90
		T7	242,20	1,50	454,89	7,86				8,19	11,79	6,43	2,92	9,34
		T8	179,15	1,00	454,89	7,86				6,06	7,86	4,75	1,94	6,70
6x10 ⁵	Compression (-)	T1	290,37	1,90	453,16	7,90	3,38E+04	7,85E-04	1,51E+03	9,81	15,01	7,70	3,69	11,40
		T3	260,96	1,70	453,16	7,90				8,82	13,43	6,92	3,30	10,23
	Tension (+)	T4	311,49	1,90	453,16	7,90				10,53	15,01	8,26	3,69	11,96
		T6	289,21	1,70	453,16	7,90				9,78	13,43	7,67	3,30	10,98
		T7	247,63	1,50	453,16	7,90				8,37	11,85	6,57	2,92	9,49
		T8	181,00	1,00	453,16	7,90				6,12	7,90	4,80	1,94	6,75
8x10 ⁵	Compression (-)	T1	290,26	1,90	450,74	7,88	3,38E+04	7,85E-04	1,51E+03	9,81	14,97	7,70	3,69	11,39
		T3	260,90	1,70	450,74	7,88				8,82	13,40	6,92	3,30	10,23
	Tension (+)	T4	312,19	1,90	450,74	7,88				10,55	14,97	8,28	3,69	11,98
		T6	289,73	1,70	450,74	7,88				9,79	13,40	7,69	3,30	10,99
		T7	248,01	1,50	450,74	7,88				8,38	11,82	6,58	2,92	9,50
		T8	181,03	1,00	450,74	7,88				6,12	7,88	4,80	1,94	6,75
1x10 ⁶	Compression (-)	T1	290,86	1,90	458,19	7,88	3,38E+04	7,85E-04	1,51E+03	9,83	14,97	7,72	3,69	11,41
		T3	261,33	1,70	458,19	7,88				8,83	13,40	6,93	3,30	10,24
	Tension (+)	T4	313,49	1,90	458,19	7,88				10,60	14,97	8,32	3,69	12,01
		T6	291,08	1,70	458,19	7,88				9,84	13,40	7,72	3,30	11,03
		T7	250,00	1,50	458,19	7,88				8,45	11,82	6,63	2,92	9,55
		T8	181,07	1,00	458,19	7,88				6,12	7,88	4,80	1,94	6,75

Notations of symbols in the table above are similar to that mentioned in table 22.

E: Modulus of elasticity of concrete = 3.38×10^4 MPa.

Table 24- Bending moments- Test specimen C3

Test specimen - column type C3(18) (confined with 6x FRP wraps)														
No. of cycles	Zone	Strain gauges	$\Delta\epsilon$ [$\mu\text{m/m}$]	H [m]	F_z [kN]	F_x [kN]	E [MPa]	W [m ³]	Stiffness K [kN/m]	$\sigma = E \cdot \Delta\epsilon$ [MPa]	$M_1 = F_x \cdot H$ [kN.m]	$M_2 = \sigma \cdot W$ [kN.m]	$M_3 = K \cdot \theta$ [kN.m]	$M = M_2 + M_3$ [kN.m]
2x10 ⁵	Compression (-)	T1	329,23	1,90	450,65	7,99	3,45E+04	7,85E-04	1,54E+03	11,36	15,18	8,92	3,77	12,69
		T3	316,68	1,70	450,65	7,99				10,93	13,58	8,58	3,37	11,95
	Tension (+)	T4	328,84	1,90	450,65	7,99				11,35	15,18	8,91	3,77	12,68
		T6	323,19	1,70	450,65	7,99				11,15	13,58	8,75	3,37	12,13
		T7	273,72	1,50	450,65	7,99				9,44	11,99	7,41	2,98	10,39
		T8	199,97	1,00	450,65	7,99				6,90	7,99	5,42	1,98	7,40
4x10 ⁵	Compression (-)	T1	328,90	1,90	463,86	8,00	3,45E+04	7,85E-04	1,54E+03	11,35	15,21	8,91	3,77	12,68
		T3	316,06	1,70	463,86	8,00				10,90	13,61	8,56	3,37	11,93
	Tension (+)	T4	329,10	1,90	463,86	8,00				11,35	15,21	8,91	3,77	12,68
		T6	322,44	1,70	463,86	8,00				11,12	13,61	8,73	3,37	12,11
		T7	273,88	1,50	463,86	8,00				9,45	12,01	7,42	2,98	10,39
		T8	200,28	1,00	463,86	8,00				6,91	8,00	5,42	1,98	7,41
6x10 ⁵	Compression (-)	T1	332,58	1,90	454,87	8,05	3,45E+04	7,85E-04	1,54E+03	11,47	15,29	9,01	3,77	12,78
		T3	319,16	1,70	454,87	8,05				11,01	13,68	8,64	3,37	12,02
	Tension (+)	T4	331,62	1,90	454,87	8,05				11,44	15,29	8,98	3,77	12,75
		T6	325,60	1,70	454,87	8,05				11,23	13,68	8,82	3,37	12,19
		T7	276,11	1,50	454,87	8,05				9,53	12,07	7,48	2,98	10,45
		T8	201,37	1,00	454,87	8,05				6,95	8,05	5,45	1,98	7,44
8x10 ⁵	Compression (-)	T1	333,62	1,90	445,59	8,03	3,45E+04	7,85E-04	1,54E+03	11,51	15,26	9,04	3,77	12,81
		T3	319,08	1,70	445,59	8,03				11,01	13,66	8,64	3,37	12,01
	Tension (+)	T4	331,60	1,90	445,59	8,03				11,44	15,26	8,98	3,77	12,75
		T6	326,47	1,70	445,59	8,03				11,26	13,66	8,84	3,37	12,21
		T7	276,60	1,50	445,59	8,03				9,54	12,05	7,49	2,98	10,47
		T8	202,13	1,00	445,59	8,03				6,97	8,03	5,47	1,98	7,46
1x10 ⁶	Compression (-)	T1	333,51	1,90	449,33	8,05	3,45E+04	7,85E-04	1,54E+03	11,51	15,30	9,03	3,77	12,80
		T3	319,50	1,70	449,33	8,05				11,02	13,69	8,65	3,37	12,03
	Tension (+)	T4	331,96	1,90	449,33	8,05				11,45	15,30	8,99	3,77	12,76
		T6	326,70	1,70	449,33	8,05				11,27	13,69	8,85	3,37	12,22
		T7	276,81	1,50	449,33	8,05				9,55	12,08	7,50	2,98	10,47
		T8	201,78	1,00	449,33	8,05				6,96	8,05	5,46	1,98	7,45

Notations of symbols in the table above are similar to that mentioned in table 22.

E: Modulus of elasticity of concrete = 3.45x10⁴ MPa.

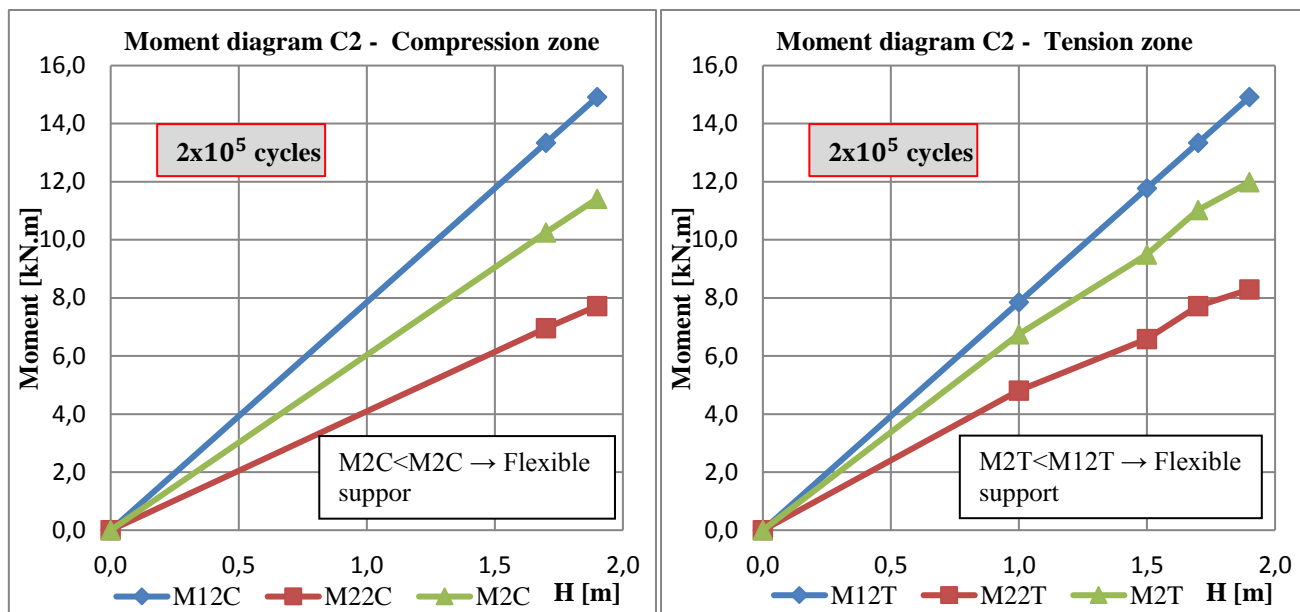


Figure 72 - Moment diagrams of specimen C2 at 2×10^5 cycles

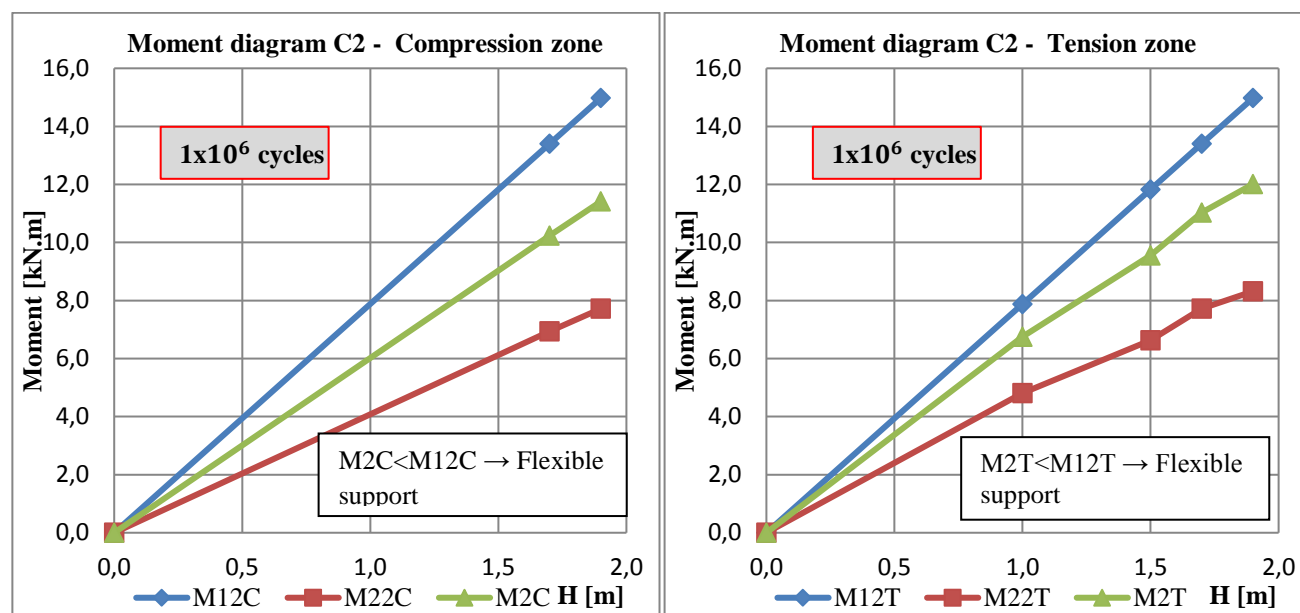


Figure 73 - Moment diagrams of specimen C2 at 1×10^6 cycles

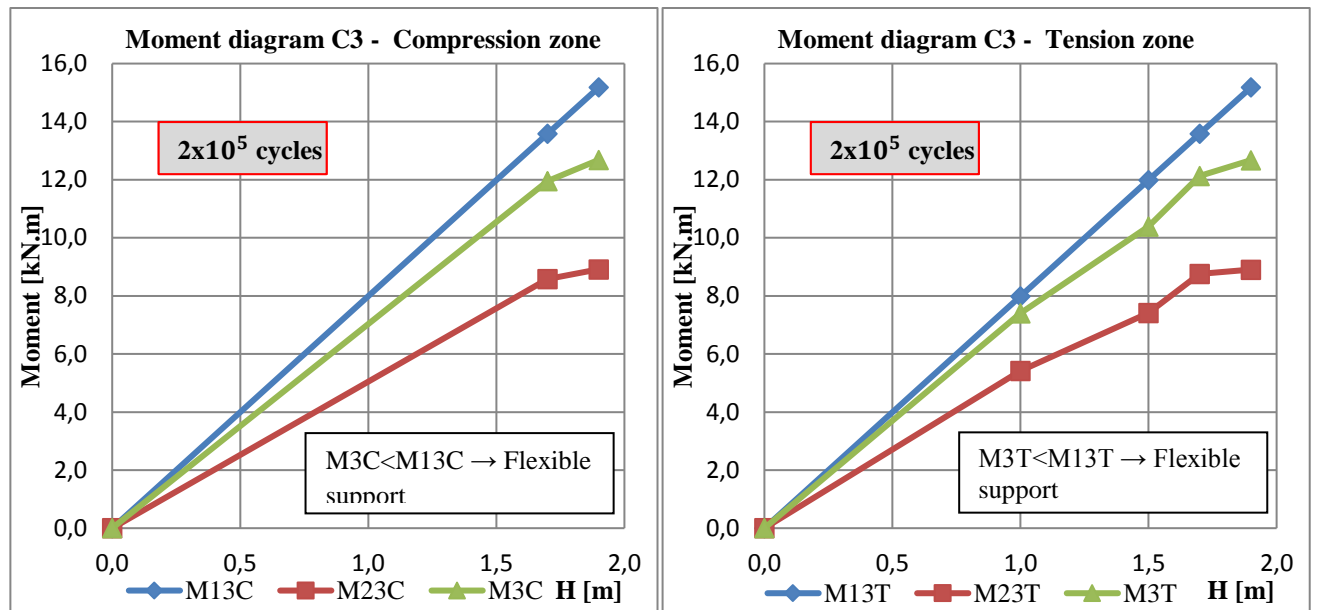


Figure 74 - Moment diagrams of specimen C3 at 2×10^5 cycles

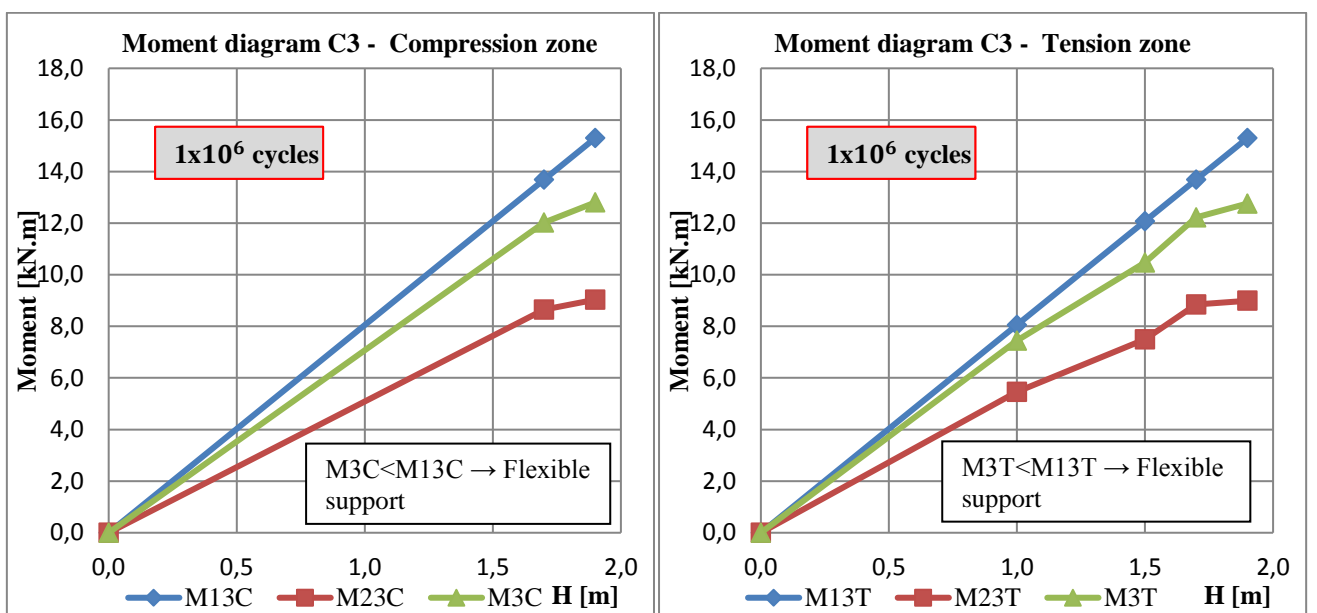


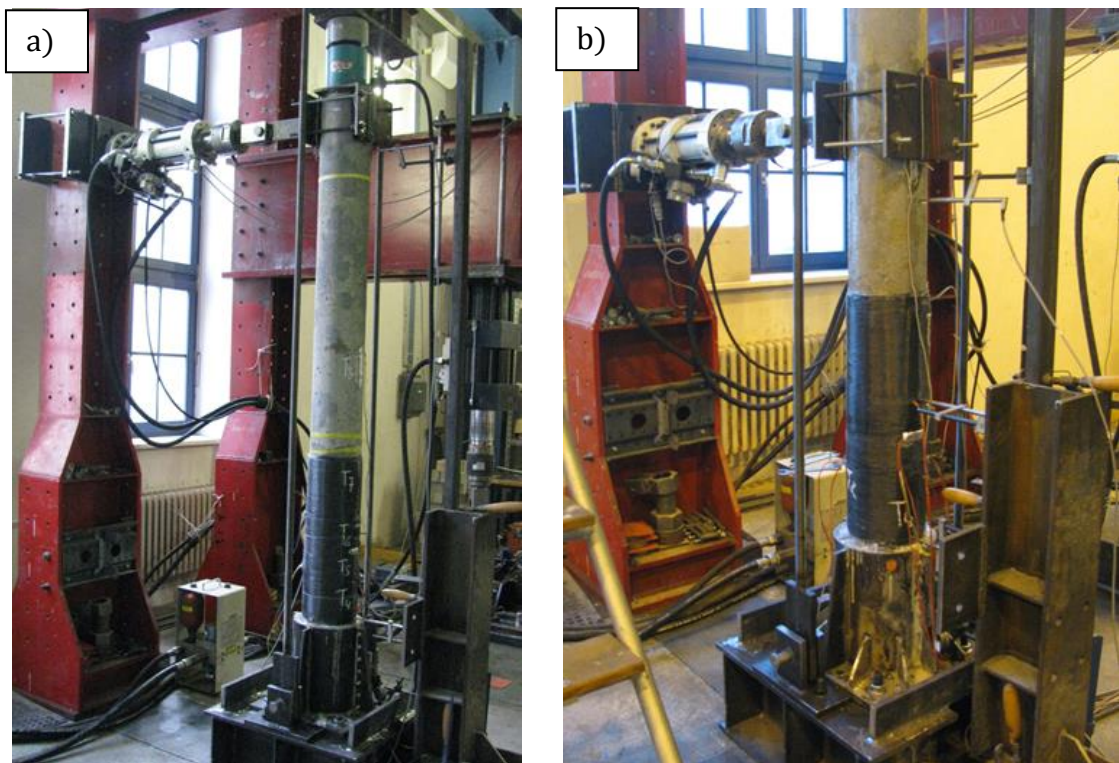
Figure 75 - Moment diagrams of specimen C3 at 1×10^6 cycles

Additionally to the conclusion above, it get out of it that there is no equilibrium between the external and internal forces due to these reasons that, the base of the columns are inherently flexible due to the oversized holes of the anchor bolts connected to the ground and the fact that the anchor bolts cannot be fully and perfectly pre-tensioned and to the connection of the concrete columns to the steel pocket foundation.

3.4.2.2 LOW-CYCLE LOADING TEST-COLUMN TYPE C2 AND C3

After performing the high-cycle loading test, the column was subjected to reversed cyclic loading test (low-cycle test) which simulates the seismic load. Due to the stroke limitation of the hydraulic actuator available in the laboratory, the actuator was shifted to a lower position of 1.10 m from the column base as shown in *Figure 76b*. The configuration and loading test history were mentioned previously. During the loading test, some of strain gauges were disrupted due to cracks development and a popping sound was heard. The loading test was terminated when the stroke of the hydraulic actuator reached the maximum distance of ± 40 mm.

Load-displacement data of reversed cyclic (low-cycle test at level 0.90 m from the column base) tests was recorded and used to plot the hysteresis curves for columns C2 and C3 see *Figure 77* and *Figure 79* respectively. Additionally, the uplift of column base during the reversed cyclic loading test was recorded as illustrated in *Figure 78* and *Figure 80*.



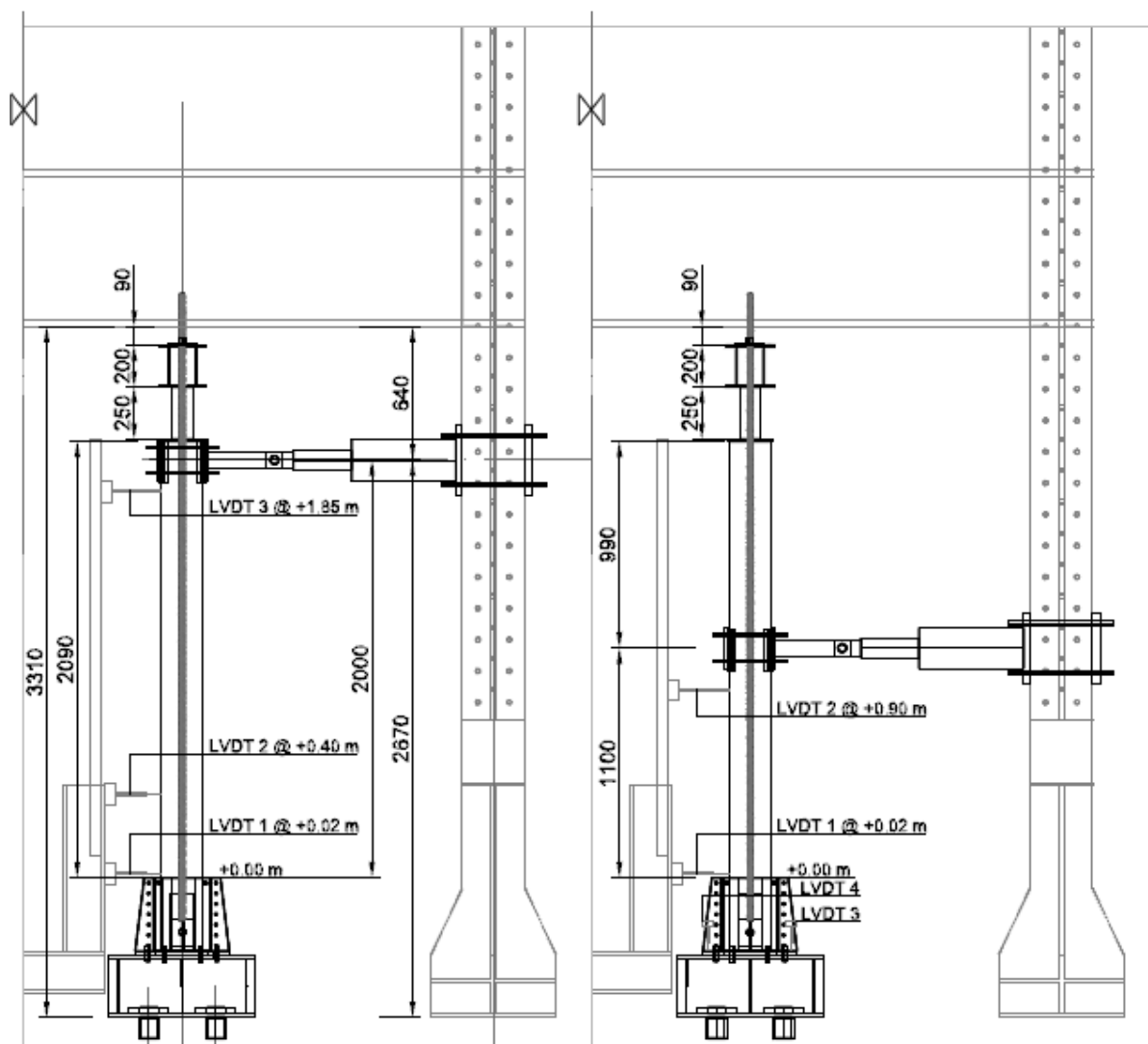


Figure 76 - Specimen C2 and C3 a) High-cycle loading test, b) Reversed cyclic loading test and corresponding schemes

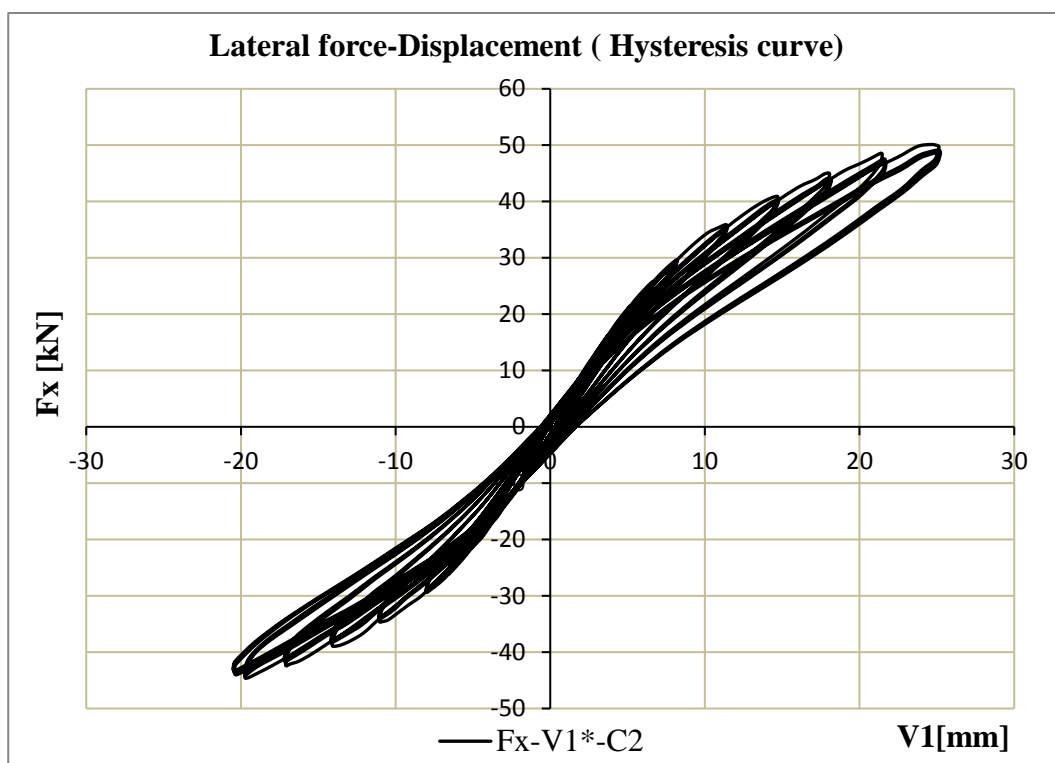


Figure 77 - Lateral force (F_x) vs. Displacement ($V1$) Hysteresis curve for specimen C2

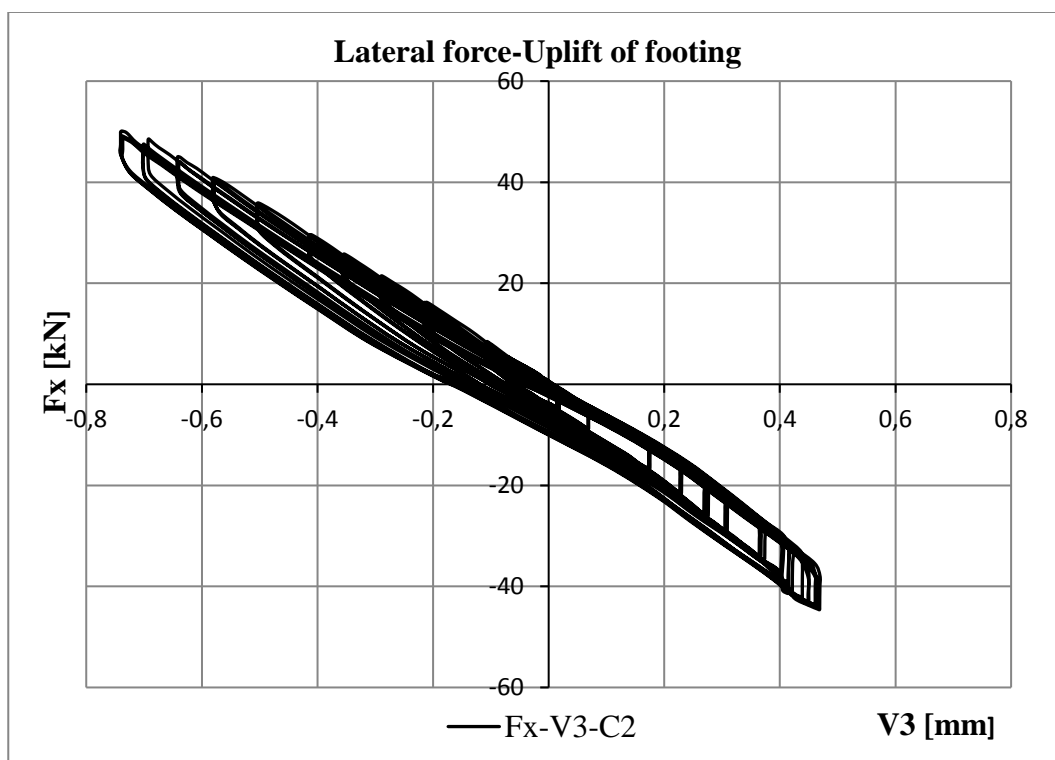


Figure 78 - Lateral force (F_x) vs. uplift of column base ($V3$) for specimen C2

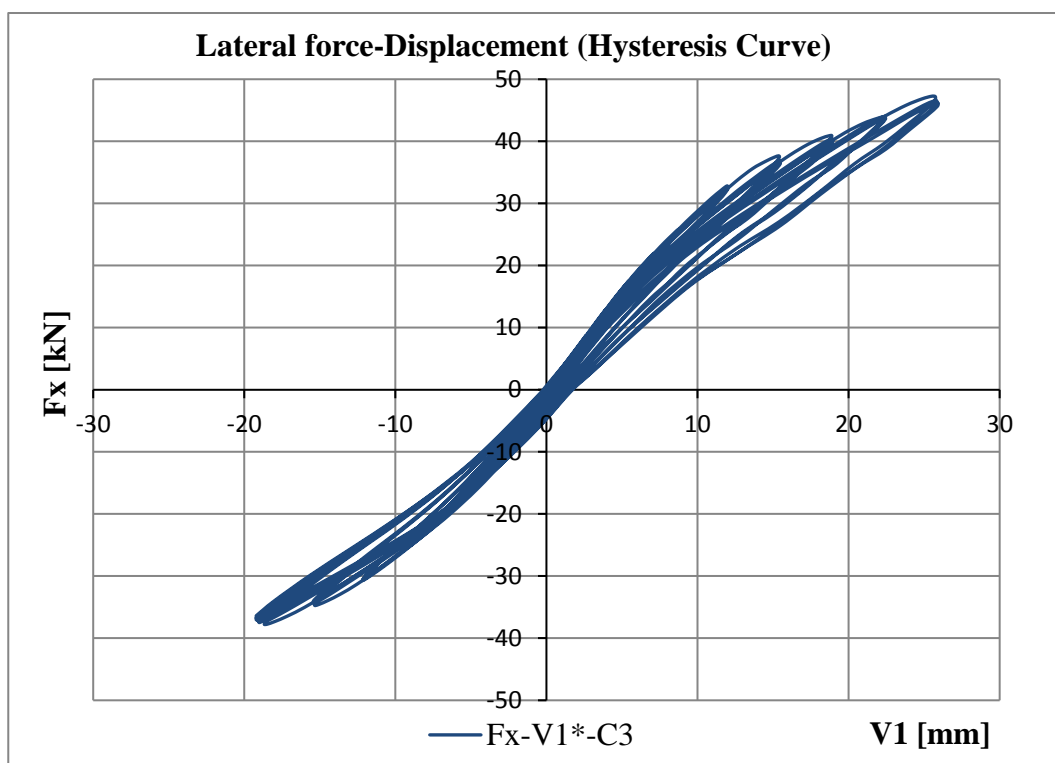


Figure 79 - Lateral force (F_x) vs. Displacement ($V1$) - Hysteresis curve for specimen C3

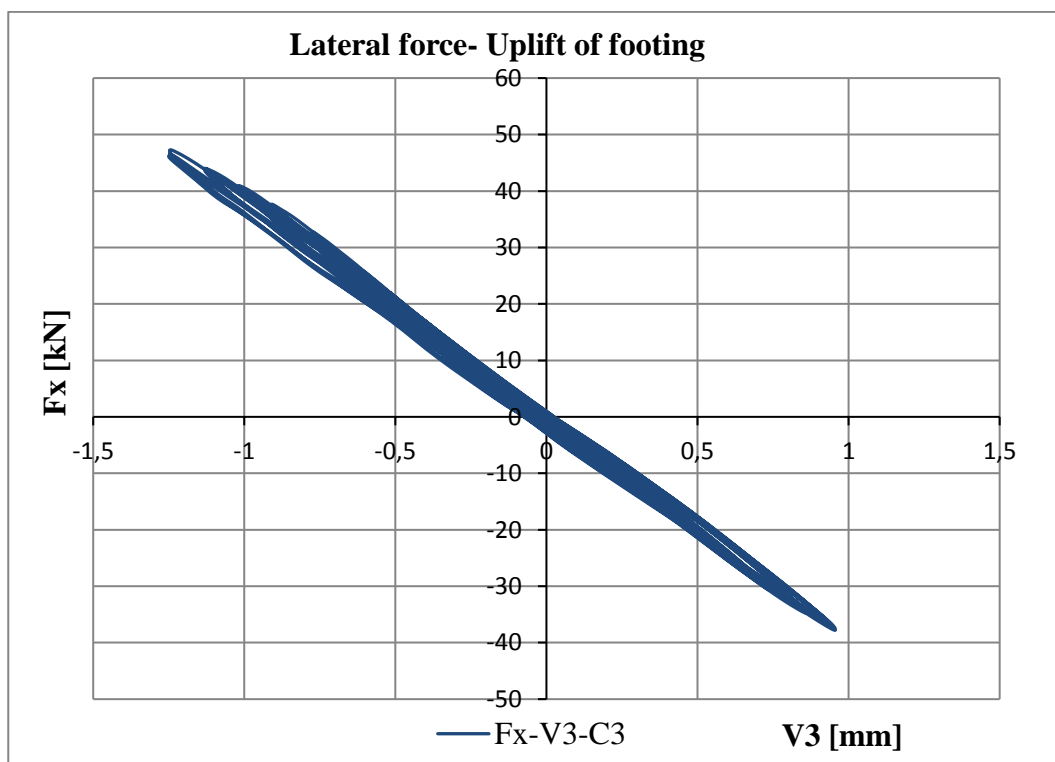


Figure 80 - Lateral force (F_x) vs. uplift of column base ($V3$) for specimen C3

3.4.3 UNCONFINED SPECIMEN – COLUMN TYPE C4

Column type C4 was designed to be representative of specimen without CFRP confinement. Details of the column type C4 are in *Table 16* and *Figure 46*. Specimen C4 was subjected only to reversed cyclic load (low-cycle load as defined in paragraph 3.3.8), and the performance of this specimen was compared to specimen C1, C2 and C3 to evaluate the effectiveness of the high cycle load on the column behavior.

The configuration and loading test history of low cycle load were conducted in the same way as specimens C1, C2 and C3. The behavior of specimen C4 was similar to specimen C1. The formation of flexural cracks continued with increasing levels of lateral displacement. The loading test was terminated when the displacement level was approximately ± 40 mm (maximum stroke of the hydraulic actuator). The spalling of concrete cover of the column began due to lateral loading, exposing the column reinforcement as shown in *Figure 81*, and the damage occurred at the lower region of column.

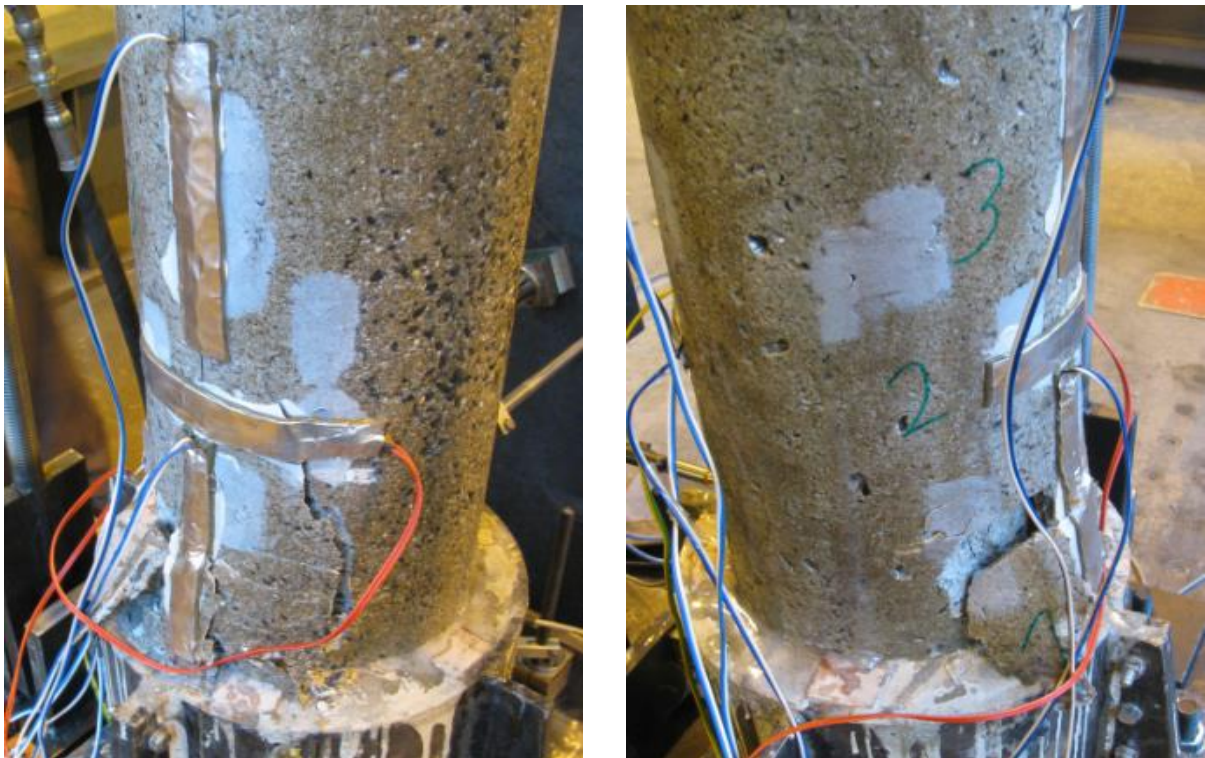


Figure 81 - Failure of specimen C4- Development of cracks

Load-displacement (at level 0.90 m from the column base) of column data of reversed cyclic test was recorded and used to plot the hysteresis curves.

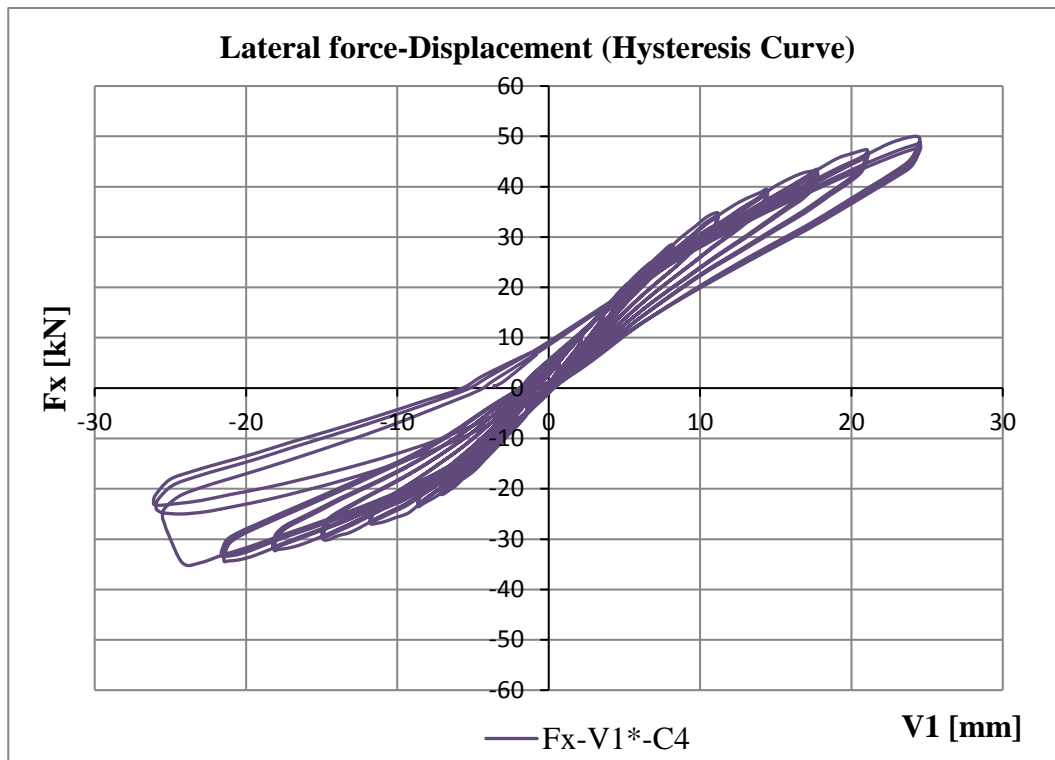


Figure 82 - Lateral force vs. Displacement-Hysteresis curve for specimen C4

Horizontal force:	P =	49,64 [kN]	<p>Free end column subjected to horizontal and vertical forces at top</p> $\Delta_{max} = \frac{PL^3}{3EI - VL^2}$ <p>P - Horizontal force V - Vertical force L - length of column E - modulus of elasticity of concrete column I - moment of inertia Δ_{max} - maximum deflection at top of the column</p>	
Vertical force:	V =	450,00 [kN]		
Length of column:	L =	1,10 [m]		
Diameter of column:	D =	0,20 [m]		
Modulus of elasticity:	E =	34766,00 [MPa]		
Moment of inertia:	I =	3,93E-05 [m ⁴]		
Max.deflection at top:	Δ_{max} =	18,60 [mm]		

The theoretical maximum deflection of the cantilever column subjected to axial and lateral forces as shown in the calculation above is 18.60 mm which is smaller than the deflection during the experiment which is 23.56 mm. It derives that there is a rotation in the column support and the column base is not acting as fully support.

3.5 NUMERICAL ANALYSIS

3.5.1 FINITE ELEMENT METHOD

Parallel to conducting the experimental investigations, it is necessary to use a method of analysis in order to simulate the behavior of test specimen. Finite element method is widely used method to understand and to simulate the behavior of circular reinforced concrete columns under monotonic and quasi-static cyclic loading.

The common problem arising in structural analysis is to determine the deflection arising from a set of static loads. If the loads at a number of points about a structure – or degrees of freedom are defined by a vector ΔR and the displacements at the corresponding points are Δr , matrix stiffness $[k]$.

$$[k]\Delta r = \Delta R, \quad (95)$$

Of most interest to dynamic is a similar formulation that includes inertia and damping terms

$$[M]\{\ddot{X}\} + [C]\{\dot{X}\} + [K]\{X\} = \{F\}, \quad (96)$$

where

$[M]$ – The mass matrix,

$\{\ddot{X}\}$ and $\{\dot{X}\}$ - the first and second derivatives of the displacement with respect to time.

The force applied to the system is a function of time. While mass and stiffness of a structure are measured and relatively easily derived, the mechanism whereby energy is lost through damping is less easily modelled. The viscous damping model represented by matrix $[C]$ in *equation (95)* is commonly used but by no means exclusively used, being proportional to velocity.

The basic solution procedure of *equation (94)* is the well-known Newton-Raphson method. In the Newton-Raphson method, depicted in *Figure 84* and *equation (94)* is solved by a recurrence relation

$$[k_T]^k \cdot \Delta r_n^k = \Delta R_n^{k-1} = (\Delta R_E)_n - (\Delta R_I)^{k-1}, \quad (97)$$

$$r_{n+1}^k = r_{n+1}^{k-1} + \Delta r_n^k, \quad (98)$$

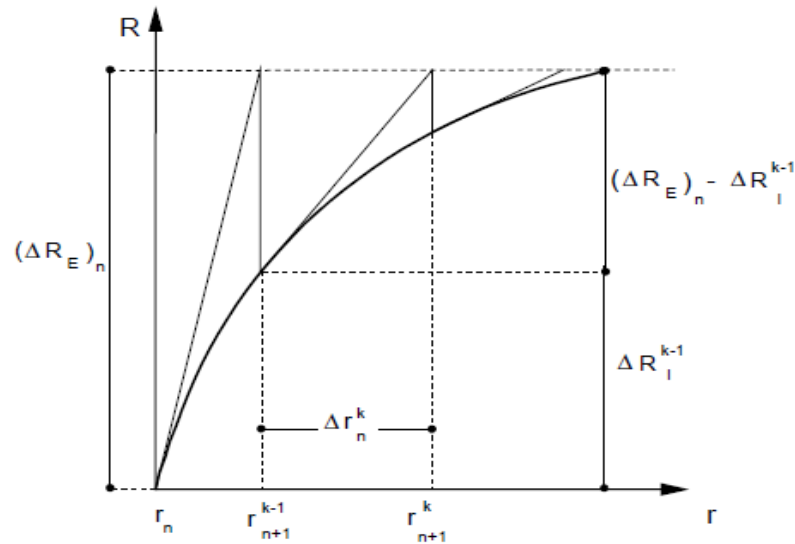


Figure 84 - Newton-Raphson method of nonlinear analysis [43]

until a suitable norm of the vector on the right-hand side of *equation (95)* becomes smaller than the specified tolerance. Subscript index n refers to the load step, while superscript index k refers to the iteration within a particular load step. ΔR_n^{k-1} is the difference between $(\Delta R_E)_n$, the externally applied load increments at step n , and $(\Delta R_I)^{k-1}$, the internal resisting load increments.

The basic Newton-Raphson method is not necessarily the most economical solution scheme and does not always provide rapid or reliable convergence. To improve upon some of the limitations of the basic Newton-Raphson method, several modifications have been proposed over the years. Some of these methods involve modifications of the stiffness matrix in *equation (96)* and are then classified as Modified Newton or Quasi-Newton methods.

In Newton-Raphson approach, the load is subdivided into a series of load increments. The load increments can be applied over several load steps. Before each solution, the Newton-Raphson method evaluates the out-of-balance load vector, which is the difference between the restoring forces (the loads corresponding to the element stresses) and the applied loads. The program then performs a linear solution, using the out-of-balance loads, and checks for convergence. If convergence criteria are not satisfied, the out-of-balance load vector is re-evaluated, the stiffness matrix is updated, and a new solution is obtained. This iterative procedure continues until the problem converges.

In some nonlinear static analyses, if the Newton-Raphson method is used alone, the tangent stiffness matrix may become singular (or non-unique), causing severe convergence difficulties.

Such occurrences include nonlinear buckling analyses in which the structure either collapses completely or "snaps through" to another stable configuration.

For such situations, the arc-length method is useful to avoid bifurcation points and track unloading. The arc-length method causes the Newton-Raphson equilibrium iterations to converge along an arc, as can be seen in *Figure 85*, thereby often preventing divergence, even when the slope of the load vs. deflection curve becomes zero or negative. The constraint equation is forced to be satisfied at each iteration.

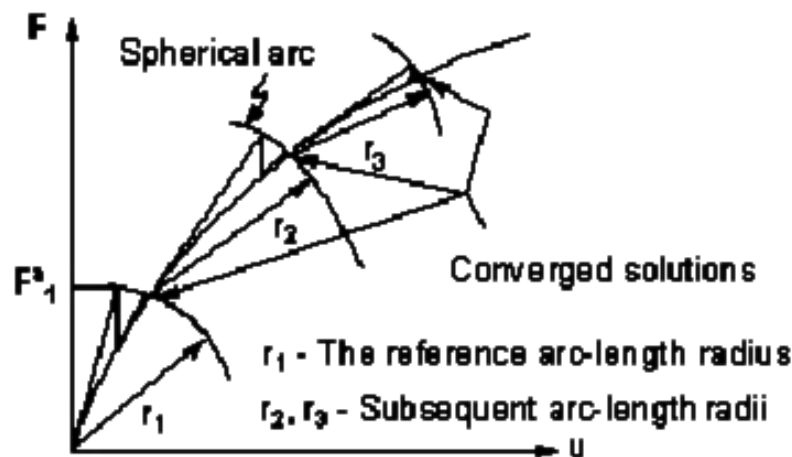


Figure 85 - Arc length method [43]

Unlike traditional non-linear solution methods, continuation methods can handle post yielding non-linear behaviour of materials, which show strain softening after yield point. They cannot be trapped in an infinite loop at the unstable region of the solution curve (since the stiffness matrix is updated based on both load increment and displacement increment).

3.5.2 NUMERICAL ANALYSIS BY ATENA 3D

ATENA recognizes two models, geometrical and numerical. Geometrical model represents dimensions, properties and loading. It consists of macro-element. Each macro-element is an independent element defined by joints, lines and surfaces. The interaction between macro-elements is provided by contacts. Numerical model is based on geometrical model and represents a numerical approximation of the structural analysis. It is a result of discretization made by the finite element method. Because of independent macro-elements, the finite element meshes are generated for each macro-element independently. Two default methods are defined for solution of nonlinear equations; standard Newton-Raphson method and standard arc-length method. Newton-

Raphson method keeps the increment unchanged and iterates displacements until equilibrium is satisfied within the given tolerance. Arc-length method keeps the solution path constant and iterates both increments of displacement and forces. Therefore, it changes both, displacements and forces.

3.5.3 ANALYSIS PROCEDURE OF TESTED SPECIMENS

3.5.3.1 ELEMENT FORMULATION OF THE SPECIMENS

3D structural elements are used to model the materials of the columns. The model was developed from 3D macro-elements and reflects the actual geometry of the column, its material composition and boundary conditions (column supporting and type of loading). The concrete was modelled as quasi-brittle material, which considers the formation and development of cracks; it was defined as 3D nonlinear Cementitious. The longitudinal and transverse reinforcements were modelling as elastic-plastic material.

3.5.3.2 GEOMETRY AND MATERIALS OF SPECIMENS

Three specimens of circular concrete column (C1, C3, and C4) were considered for numerical study. The material properties of specimen (compressive strength of concrete, yield strength of reinforcement) in numerical study were selected the same according to the experimental study.

More details about the geometry and material properties of specimen are mentioned in the following paragraph (experimental part).

3.5.3.3 LOADING, SUPPORTING, AND MONITORING

Two load cases are defined, supporting and loading. First contains the supports; the support at the bottom end is provided as fixed end support to prevent movement in three directions, and the top end is free. Second contains the axial compressive force at the top end in Z (-) direction and lateral cyclic load in X direction. In nonlinear analysis, it is necessary to avoid any unrealistic stress concentration, which may cause premature failure or cracking at the end locations of columns. Therefore, a steel plate as a macro-element of diameter of 200 mm and height of 100 mm is modeled at both ends of the column, and another steel plate of height of 200 mm and thickness of 50 mm is modeled at both parts where cyclic loading is applied.

The loading history consists of load steps. Each load step is defined as a combination of load cases as defined previously (supporting and loading). Each load step contains also a

definition of solution parameters, which define solution methods that are to be used during the load steps; in our case Newton-Raphson, method was considered.

Monitoring is useful during nonlinear analysis, to monitor forces, deformations or stresses in the model. Four monitoring points are placed on each column at the ends of column to monitor deformation and applied forces and to be able to define the load curve.

3.5.3.4 BOUNDARY CONDITIONS

To determine and find-out an appropriate boundary condition for the ATENA MODEL similar to that used in the experiment. Columns were modelled with different base plate thicknesses having different modulus of elasticity, and it was considered an elastic material with the same modulus of elasticity as steel 2.0×10^5 MPa for all macro-elements used in the model except the base plate with lower modulus of elasticity of 3.70×10^4 MPa. This value was reached after many trials, to observe the appropriate support in case the material was behaving linearly.

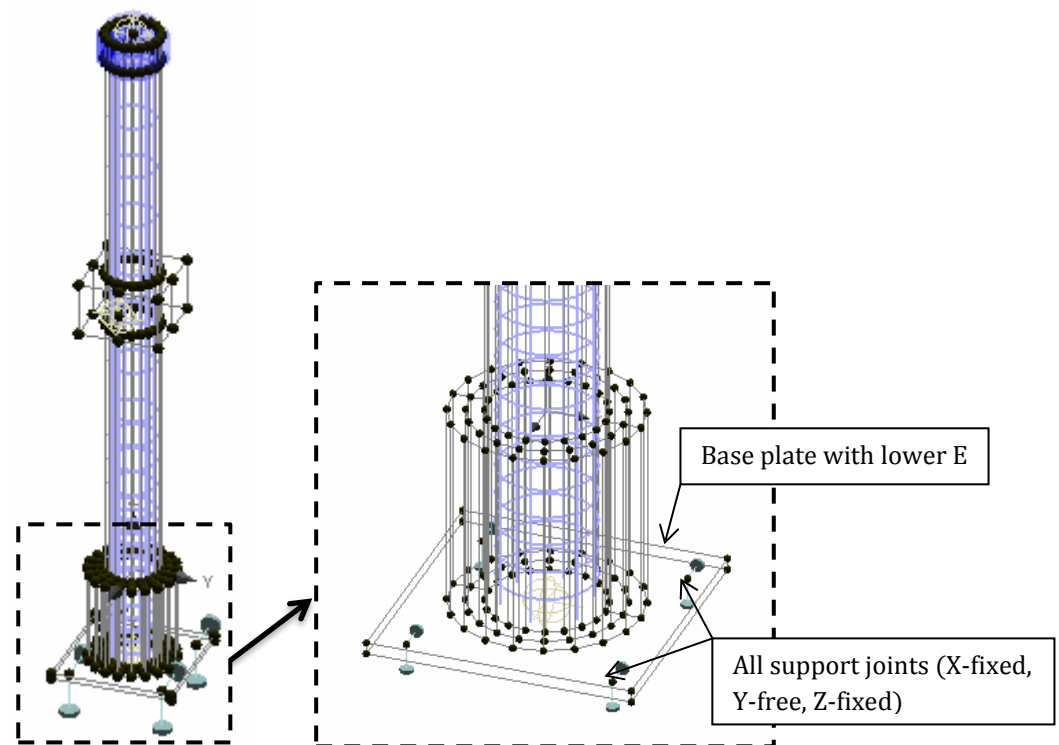


Figure 86 - Boundary Conditions – Column Type C4

Figure 86 above shows the boundary conditions of the columns selected for ATENA model. As shown Figure 87, at displacement 10 mm the force is 33.7 kN which is very close to the value obtained from the experiment.

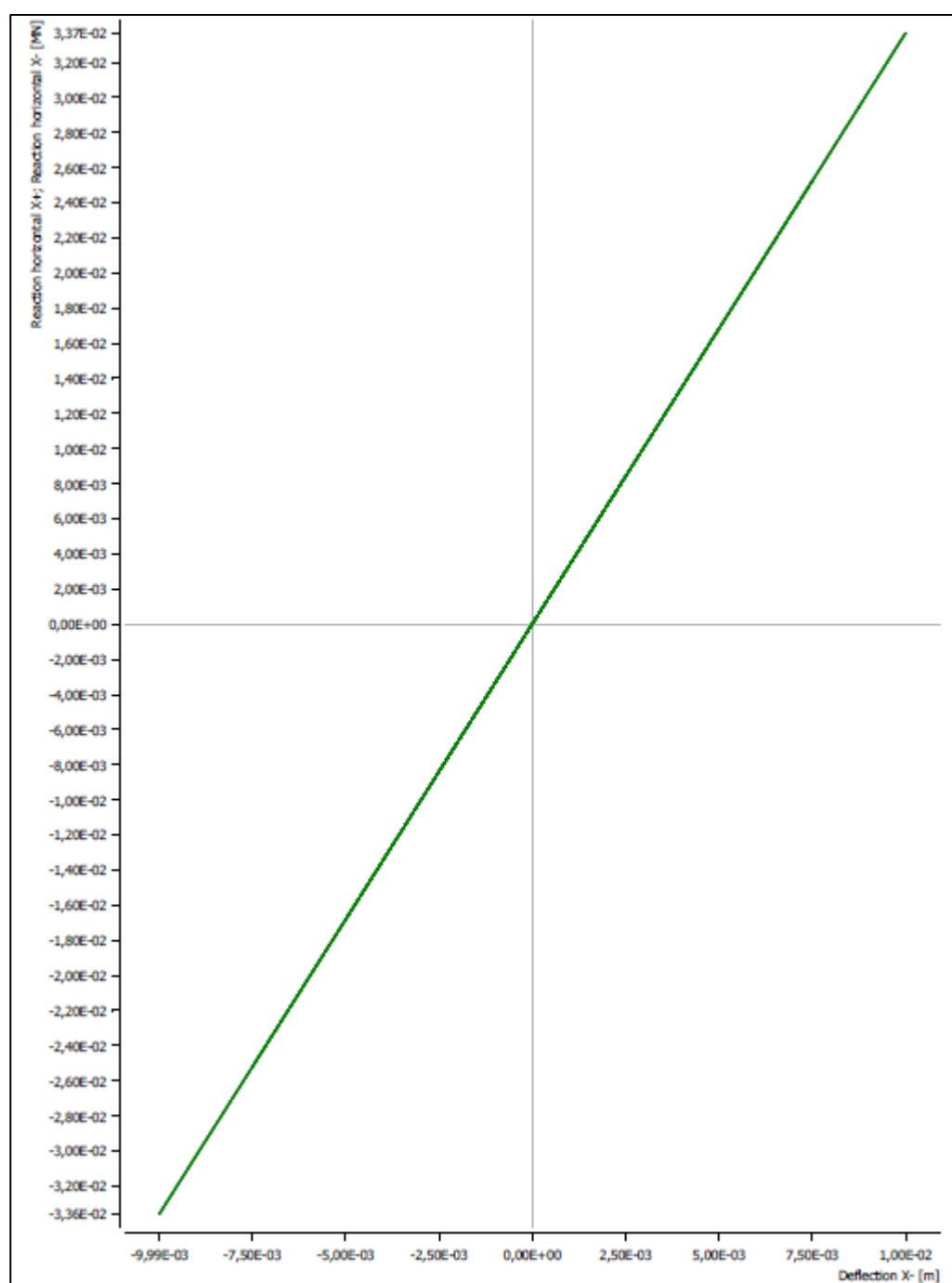


Figure 87 - Hysteresis Diagram– Column Type C4 - Atena (Elastic Behavior)

CHAPTER 4-EVALUATION AND COMPARISON OF EXPERIMENTAL AND NUMERICAL RESULTS

4.1 INTRODUCTION

This chapter discusses the results of the experimental tests presented in the previous chapter and presents a comparison of the experimental and numerical results; this comparison is made between specimens with different configuration to analyze the effect of FRP wraps and low/high-cycle load. The experimental results are introduced in form of hysteresis force-displacement envelope diagrams, energy dissipation-displacement diagrams, energy dissipation-drift, and lateral force-drift. Moreover, a numerical and experimental comparison of column type C1, C3, and C4 were provided.

4.2 FORCE -DISPLACEMENT ENVELOPE DIAGRAMS

The summary of the experimental test configuration of the columns type C1, C2, C3, and C4 is shown in *Table 26*. The CFRP wraps were installed for columns type C2 and C3 and both high and low-cycle loading was applied. Columns type C1 and C4 were unconfined columns and the difference between them was the load configuration, both high and low-cycle fatigue loading was applied on column C1 and only high-cycle loading was applied on column C4.

Table 26 – Summary of Experimental Test Configuration

Experimental test configuration		
Type of column	Confinement	Loading
C1	Unconfined	Both loading (high and low cycle fatigue load) are applied
C2	Confined	Both loading (high and low cycle fatigue load) are applied
C3	Confined	Both loading (high and low cycle fatigue load) are applied
C4	Unconfined	Only high cycle fatigue load is applied

Figure below illustrates the comparison of the experimental results of lateral force-displacement envelope diagrams (hysteresis envelope lines) among all specimens.

The test results for the unconfined and confined specimens are compared to quantify the improvement in column behavior provided by the FRP wraps and the effect of high and low cycle loading. *Figure 88* illustrates the comparison between unconfined specimen C1 and confined specimens C2 and C3 subjected to high and low-cycle load, and unconfined specimen C4 subjected to low-cycle load only. The behavior of column C4 is different from the specimen C1 due to the loading pattern. It shows that column type C4 has higher ductility than C1.

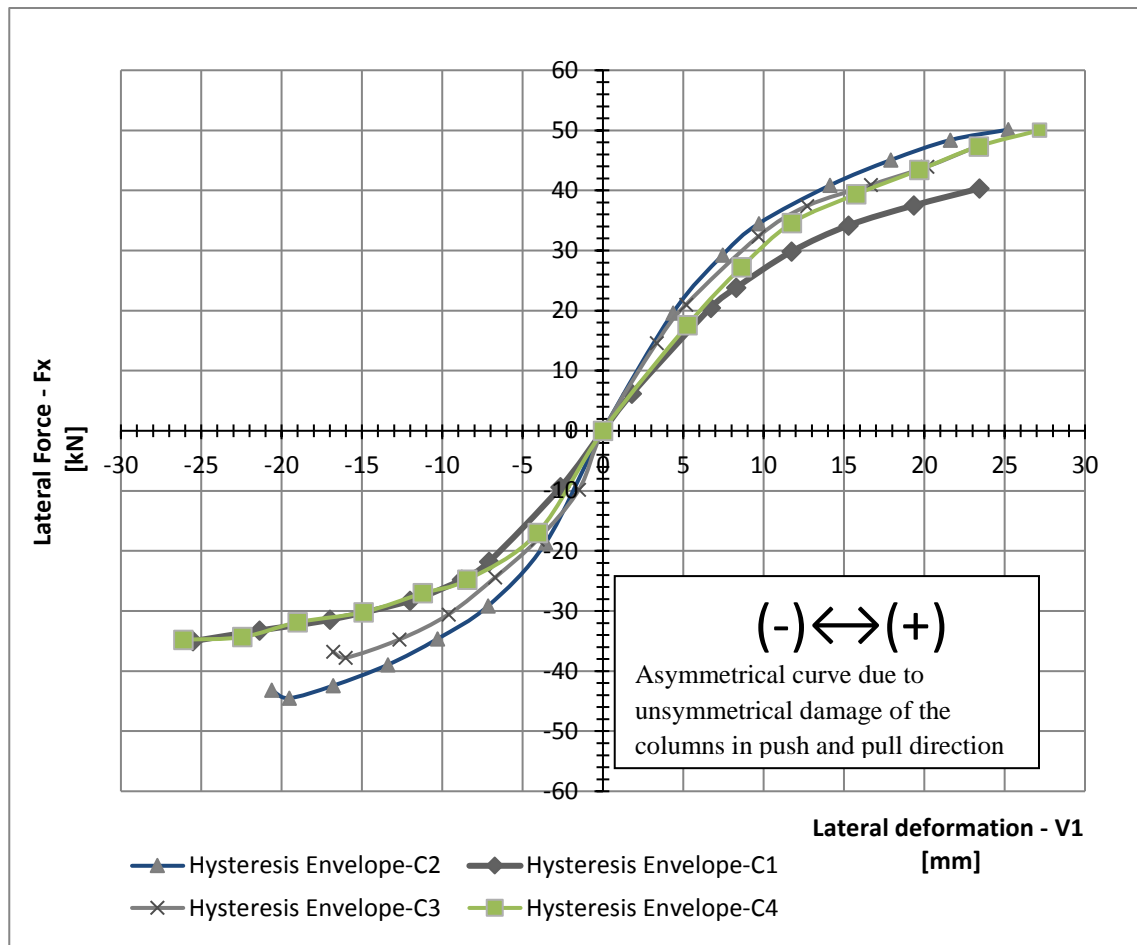


Figure 88 - Force-Displacement Envelope Diagrams for all specimens-Experimental

The fatigue occurs in the specimen C1 due to high-cycle (one million cycles) and low-cycle; and a progressive structural damage occurs when a material is subjected to both cyclic loadings (high and low). Same configuration has been implemented for columns type C2 and C3, and even though a small difference in the results occurred due to the difference in the mechanical properties of the concrete (material characteristics; i.e. the compressive strength and modulus of elasticity of concrete).

The comparison between unconfined specimen C1 and confined specimens C2 and C3 subjected to high and low-cycle load shows that FRP wraps in hoop direction provide an improvement in the ductility, i.e. means adding of FRP wraps to columns changes the mechanical properties of materials which improves the fatigue resistant and the life of columns.

The initial slope of the load vs. displacement response curve defines the stiffness of the column specimens. The initial slope of the load vs. displacement response curves for the unconfined specimen C1 and confined specimens C2 and C3 is not similar, i.e. that the FRP wraps have an influence on the stiffness of the columns.

The hysteresis curve of the columns shows that the ultimate force of the unconfined column C1 reached about 40 kN for displacement of 23 mm and for the confined column C2 and C3 47 kN and 49 kN respectively for the same displacement in the push direction (positive zone). It means that FRP wraps enhance the capacity of the unconfined column C1 approximately by 20% (considering the average of confined columns C2 and C3). The ultimate lateral forces in the push and pull directions are not matching.

The asymmetrical of the curve in the positive (push direction) and negative zone (pull direction) may be probably caused by unsymmetrical damage of the columns during the test in push and pull directions as shown in the *Figure 66* and *Figure 81* and to the effect of inhomogeneity of concrete. The reason of the symmetrical envelope line in the numerical simulation and not in the experiment is the loose fitting of the connection between the stroke of the electrical hydraulic actuator and the concrete columns which it was not faced in the numerical simulation.

4.3 ENERGY DISSIPATION -DISPLACEMENT ENVELOPE DIAGRAMS

Energy dissipation is a fundamental structural property of structural elements subjected to cyclic loading. The failure mechanism of reinforced concrete columns is dependent on the load path history and affects the ductility and energy dissipation capacity of the columns. The energy dissipation of the column is derived from the work done in deforming the column. This can be defined either in function of bending moment and rotation, or shear force and lateral displacement. Deriving energy dissipation from shear and lateral displacement is more stable consideration. The energy dissipated by the specimens was calculated by integrating the lateral load-displacement curve. The energy released due to change in displacement caused by a lateral force in an interval time $E_{si}(t)$ and the total energy E_{si} are defined by

$$E_{si}(t) = \frac{1}{2} \frac{\Delta X_i}{\Delta t} [F_i(t) + F_{i+1}(t)] \quad (99)$$

$$E_{si} = \int_{t=0}^n E_{si}(t) \cdot \Delta t \quad (100)$$

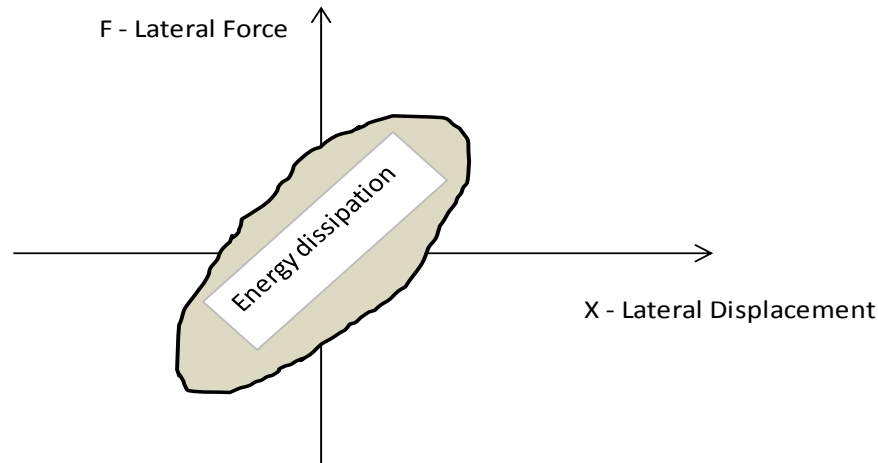


Figure 89 - Energy Dissipation in a cycle of Hysteresis diagram

Table below shows the summary of the energy dissipation and drift of the column type C1, C2, C3 and C4.

Table 27 - Energy Dissipation and Drift of un-strengthened column type C1

Column Type C1 - Unconfined (10^6 cycles)							
Point	Displacement X_i [mm]	Lateral Force F_i [kN]	$X_2 - X_1$ [mm]	$(F_1 + F_2)/2$ [kN]	Area Under Curve $(X_2 - X_1)(F_1 + F_2)/2$ [kN.mm]	Drift = X_i/L [%]	Energy Dissipation [kN.mm]
1	0,000	0,000	0,000	0,000	0,000	0,000	0,000
2	1,801	6,169	1,801	3,085	5,555	0,157	5,555
3	6,702	20,471	4,901	13,320	65,285	0,583	70,840
4	8,287	23,812	1,585	22,142	35,100	0,721	105,939
5	11,738	29,822	3,451	26,817	92,540	1,021	198,480
6	15,283	34,175	3,545	31,999	113,421	1,329	311,900
7	19,341	37,499	4,058	35,837	145,437	1,682	457,337
8	23,426	40,330	4,085	38,914	158,977	2,037	616,314
Total Dissipated Energy E(C1)=					616,314		

Table 28 - Energy Dissipation and Drift of strengthened column type C2

Column Type C2 - Confined (10^6 cycles)							
Point	Displacement X_i [mm]	Lateral Force F_i [kN]	$X_2 - X_1$ [mm]	$(F_1 + F_2)/2$ [kN]	Area Under Curve $(X_2 - X_1)(F_1 + F_2)/2$ [kN.mm]	Drift = X_i/L [%]	Energy Dissipation [kN.mm]
1	0,000	0,000	0,000	0,000	0,000	0,000	0,000
2	4,351	19,623	4,351	9,811	42,693	0,378	42,693
3	7,447	29,234	3,096	24,429	75,619	0,648	118,312
4	9,703	34,503	2,256	31,868	71,900	0,844	190,211
5	14,129	40,852	4,426	37,677	166,765	1,229	356,976
6	17,913	45,058	3,784	42,955	162,545	1,558	519,521
7	21,619	48,389	3,705	46,724	173,130	1,880	692,651
8	25,227	50,116	3,609	49,253	177,735	2,194	870,386
Total Dissipated Energy E(C2)=					870,386		

Table 29 - Energy Dissipation and Drift of strengthened column type C3

Column Type C3 - Confined (10 ⁶ cycles)							
Point	Displacement X_i [mm]	Lateral Force F_i [kN]	$X_2 - X_1$ [mm]	$(F_1+F_2)/2$ [kN]	Area Under Curve $(X_2 - X_1)(F_1+F_2)/2$ [kN.mm]	Drift = X_i/L [%]	Energy Dissipation [kN.mm]
1	0,000	0,000	0,000	0,000	0,000	0,000	0,000
2	3,336	14,611	3,336	7,305	24,370	0,290	24,370
3	5,171	21,013	1,835	17,812	32,684	0,450	57,054
4	9,671	32,339	4,500	26,676	120,035	0,841	177,089
5	12,703	37,426	3,032	34,882	105,769	1,105	282,858
6	16,673	40,934	3,970	39,180	155,547	1,450	438,405
7	20,181	43,969	3,509	42,452	148,943	1,755	587,348
8	23,226	47,267	3,045	45,618	138,908	2,020	726,256
Total Dissipated Energy E(C3)=					726,256		

Table 30 - Energy Dissipation and Drift of un-strengthened column type C4

Column Type C4 - Unconfined							
Point	Displacement X_i [mm]	Lateral Force F_i [kN]	$X_2 - X_1$ [mm]	$(F_1+F_2)/2$ [kN]	Area Under Curve $(X_2 - X_1)(F_1+F_2)/2$ [kN.mm]	Drift = X_i/L [%]	Energy Dissipation [kN.mm]
1	0,000	0,000	0,000	0,000	0,000	0,000	0,000
2	5,258	17,589	5,258	8,795	46,247	0,457	46,247
3	8,622	27,217	3,364	22,403	75,361	0,750	121,608
4	11,748	34,563	3,126	30,890	96,549	1,022	218,157
5	15,764	39,369	4,016	36,966	148,475	1,371	366,631
6	19,688	43,422	3,924	41,395	162,430	1,712	529,061
7	23,378	47,343	3,690	45,382	167,439	2,033	696,501
8	27,179	50,013	3,801	48,678	185,040	2,363	881,540
Total Dissipated Energy E(C4)=					881,540		

Figure below illustrates the evolution of total energy dissipation of specimens and the comparison between them. The area under the lateral force-displacement diagrams presents the total energy dissipation. The energy dissipation of unconfined and confined circular columns is investigated under low and high-cyclic loadings.

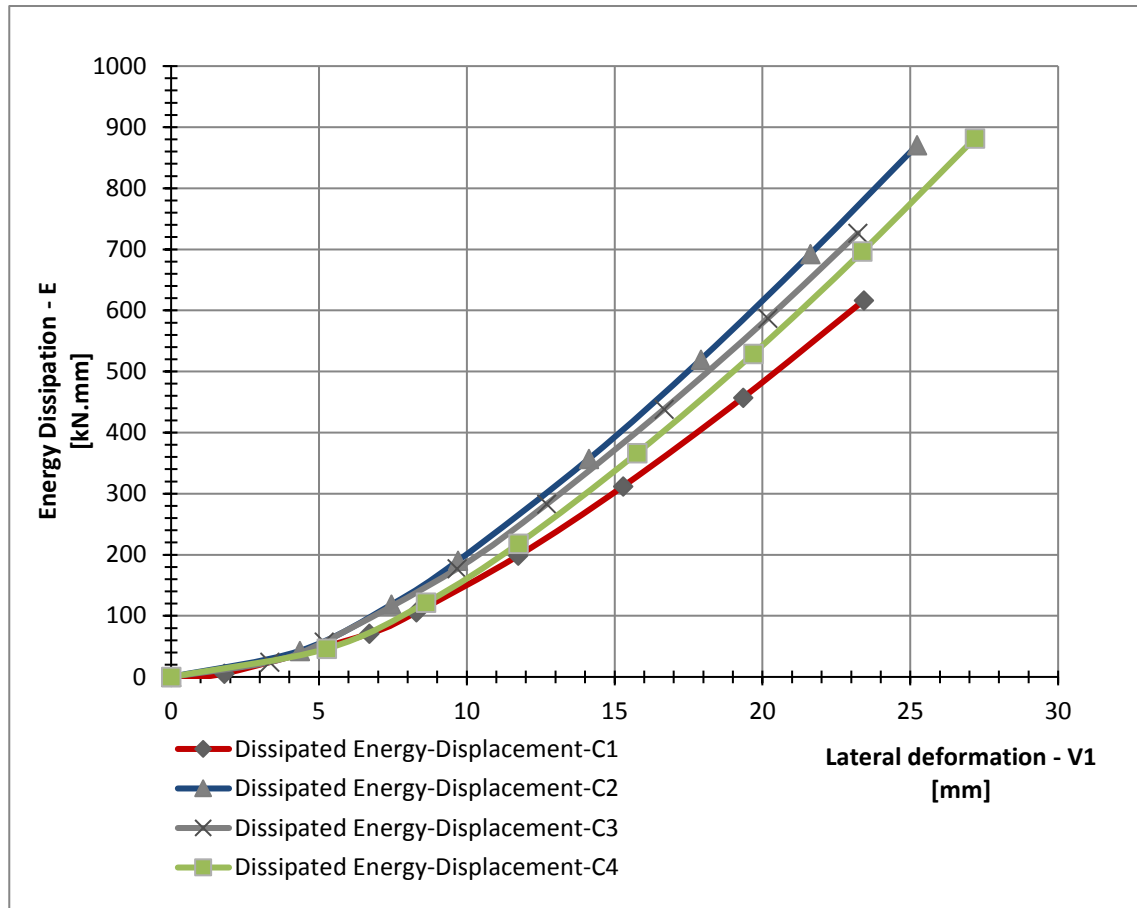


Figure 90 - Energy Dissipation-Displacement Envelope Diagrams for all Specimens-Experimental

Specimen type C1 (control specimen- unconfined) subjected to high and low-cycle load dissipates less than the specimen C4, which is subjected to low-cycle loading only. The total energy dissipated by the specimen C1 and C4 are 616,314 KN.mm and 881,540 KN.mm respectively, which is 43% higher. Additionally, the confined specimens with FRP wraps C2 and C3 subjected to high and low-cycle loading (same loading configurations as specimen type C1) have higher dissipated energy level than specimen type C1. The total average energy dissipated by the specimens C2 and C3 is 798,321 KN.mm, which is higher 29,50 % than the total energy dissipated by the specimen C1. The difference in the energy dissipation between columns type C2 and C3 is due to the variance in the material properties (the compressive strength and the modulus of elasticity of the concrete). It can be concluded that the ductility and energy dissipating capacity increase when the confinement is presented. Additionally, the low-cycle loading decreases the ductility and the energy dissipating capacity of the columns. It can be concluded that the high-cycle loading and the FRP wraps have a significant effect of the behavior of the concrete columns.

4.4 LATERAL FORCE-DRIFT DIAGRAMS

The lateral drift ratio of the cantilever column is defined as the ratio of maximum lateral displacement (Δ_{\max}) deriving from lateral force to total height (L) of the specimen.

$$Drift = \mu = \frac{\Delta_{\max}}{L} \quad (101)$$

Figure below illustrates lateral force-drift of unconfined and confined specimens.

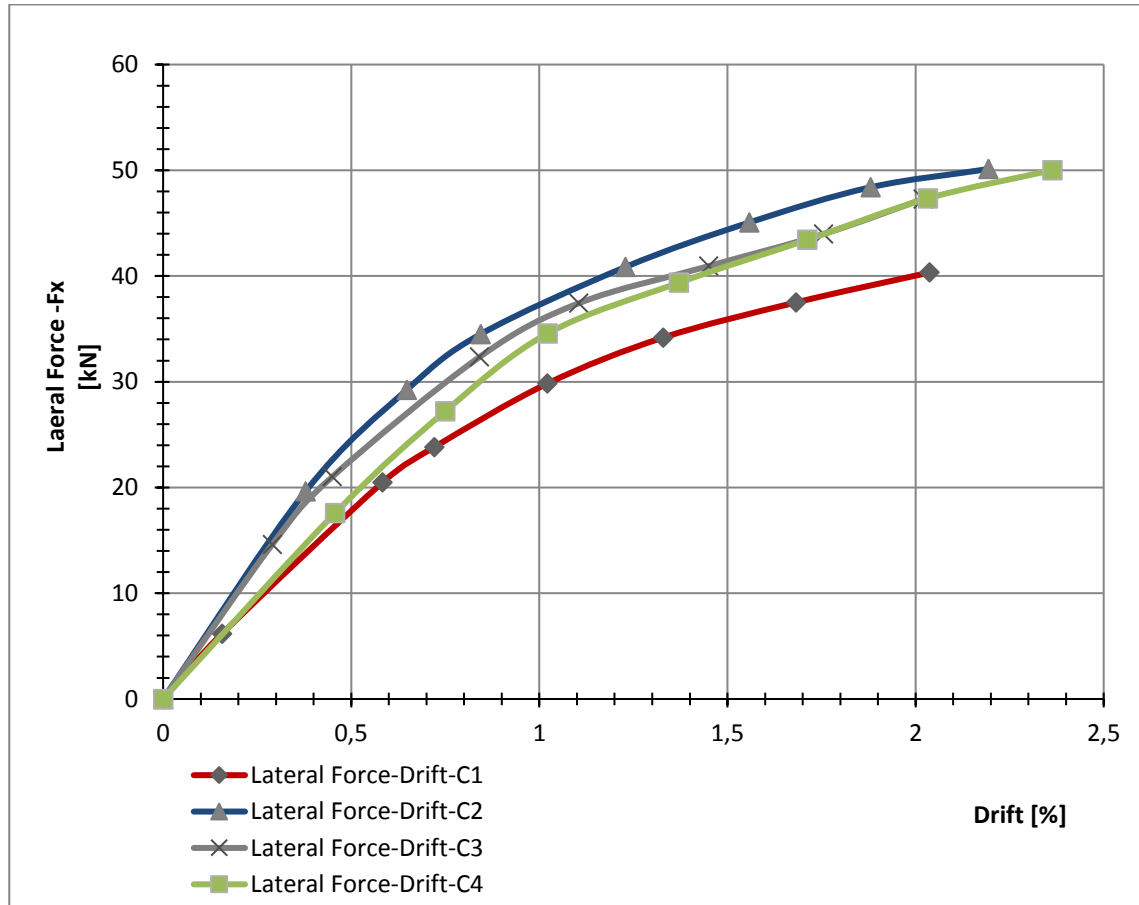


Figure 91 - Lateral Force-Drift Ratio for all Specimens-Experimental

Figure above illustrates the comparison between the unconfined columns C1 and C4, and the confined columns with FRP wraps C2 and C3. The test data and figure above indicate that the drift capacity of unconfined column type C1 subjected to high and low-cycle load is lower than the drift of unconfined column type C4 subjected to low-cycle load only. Additionally, the drift capacity increases when the confinement is presented as shown in the comparison between columns C1 and confined columns C2 and C3. The difference in drift between columns type C2 and C3 is due to the variance in the material properties (the compressive strength and the modulus of elasticity of the concrete).

Table 31 - Summary of Maximum Load and Displacement Test Results

Column	Max. Lateral Force [kN]	Max. Displacement [mm]	Drift [%]	Energy Dissipation [kN.mm]	Performance [%]
Type C1	40,33	23,43	2,04	616,31	-
Type C2	50,12	25,23	2,19	870,39	29,19
Type C3	47,27	23,23	2,02	726,26	15,14
Type C4	50,01	27,18	2,36	881,54	30,09

4.5 EMPIRICAL MODEL FOR FRP CONFINED CONCRETE SUBJECTED TO CYCLIC LOADING

One of the main objectives of this dissertation work is to develop an empirical model (design-oriented model) of the confined concrete subjected to cyclic loading and to predict the confined compressive strength of concrete wrapped with CFRP. The typical form of design-oriented expressions is

$$\frac{f_{cc}}{f_{co}} = k_1 + k_2 \left(\frac{\sigma_{l,eff}}{f_{co}} \right)^{k_3}, \quad (102)$$

where k_1, k_2, k_3 are constants, the value of k_1 is usually 1, the values of k_2 and k_3 are unknown parameters based on the results of loading test and the various compressive strength of the concrete. f_{cc} , f_{co} , and $\sigma_{l,eff}$ are the predicted confined compressive strength of the concrete, the compressive strength of the unconfined concrete and the effective lateral pressure contributed by the FRP wraps respectively. For the compressive strength subjected to cyclic loading a similar expression will be adopted within consideration the FRP wraps contribution on the enhancement of the unconfined concrete. The relationship mentioned above is describing the development of the strength of the confined concrete which depending on the amount of the lateral pressure contributed by the FRP warps.

Based on the results obtained from the experimental study among specimens C1, C2 and C3, the enhancement of the FRP wraps on the behavior of the unconfined concrete is approximately 20 % (taken the average between of C2 and C3). As shown in *Table 18*, the properties of concrete for test specimens are different from one specimen to another; therefore, a calibration shall be conducted. After performing the calibration, the enhancement of the FRP wraps on the unconfined column increased approximately 10 %. The unknown parameters k_2 and k_3 were determined based on the results and the behavior of the unconfined and confined concrete columns subjected to

cyclic loading by defining one unknown and finding the second unknown using the logarithm functions . For $k_2 = 1.5$, respectively $k_3 = 1.30$. The design oriented expression to predict the strength of the confined concrete can be written in the following form

$$\frac{f_{cc}}{f_{co}} = 1 + 1.5 \left(\frac{\sigma_{l,eff}}{f_{co}} \right)^{1.30} . \quad (103)$$

Various models for confinement of concrete with FRP have been developed. The majority of these models were performed on plain concrete specimens' test. Most of the existing strength models for FRP confined concrete adopted the concept of Richart et al. (1929) [53], in which the strength at failure for concrete confined by hydrostatic fluid pressure. In addition, limited models have been conducted on confined concrete subjected to high cycle loading.

To validate the proposed model, the compressive strength of FRP confined columns of various models proposed by other authors was compared with the compressive strength of the proposed model. The compressive strength of columns type C2 and C3 was adopted and the fatigue compressive strength of concrete was computed according to EN 1992-1-1. The lateral confining pressure provided by 6 layers of CFRP wraps was evaluated. The comparison shown in *Table 32* that the present model is more conservative in predicting the concrete compressive strength subjected to cyclic loading (high and low cycle loading).

A comparison of strengthening ratio versus confinement ratio of various proposed models is presented in *Table 33* and *Figure 92*. The confinement lateral pressure was calculated for confined concrete column with CFRP wraps by 1x till 6x layers. The unconfined compressive strength of concrete with fatigue was considered 35 MPa.

Table 32 – Compressive strength comparison of the proposed models

Author of proposed models	Unconfined Compressive Strength	Lateral Pressure	Confined compressive strength	Unconfined compressive strength with fatigue	Confined compressive strength with fatigue
	f_{cm} (MPa)	$\sigma_{l,eff}$ (MPa)	$f_{cm,c}$ (MPa)	$f_{cm,fat}$ (MPa)	$f_{cm,c,fat}$ (MPa)
Richart et al. 1928	52,00	17,62	124,22	35,01	107,23
	58,00		130,22	37,86	110,09
Mander et al. 1988	52,00	17,62	124,70	35,01	97,23
	58,00		133,50	37,86	102,19
Cusson & Paultre 1995	52,00	17,62	103,19	35,01	80,46
	58,00		110,89	37,86	84,40
Karbhari & Gao 1997	52,00	17,62	94,58	35,01	75,45
	58,00		101,19	37,86	78,72
kono et al. 1998	52,00	17,62	104,40	35,01	70,28
	58,00		116,44	37,86	76,01
Samaan et al. 1998	52,00	17,62	96,70	35,01	79,70
	58,00		102,70	37,86	82,56
Spoelstra & Monti 1999	52,00	17,62	142,80	35,01	109,50
	58,00		153,89	37,86	115,34
Toutanji 1999	52,00	17,62	124,52	35,01	103,35
	58,00		131,72	37,86	107,02
Saafi et al. 1999	52,00	17,62	98,08	35,01	78,26
	58,00		104,89	37,86	81,66
Yousef et al. 2007	52,00	17,62	82,24	35,01	68,39
	58,00		87,42	37,86	70,60
Lam & Teng 2003	52,00	17,62	110,13	35,01	93,14
	58,00		116,13	37,86	95,99
EN 1992	52,00	17,62	102,54	35,01	83,42
	58,00		109,29	37,86	86,63
Mansour 2018	52,00	17,62			71,10
	58,00				76,48

Table 33 – Comparison of the strengthening ratio of various proposed models

	Lam & Teng (2003)	Cusson & Paultre (1995)	Richart et al. (1928)	Mander et al. (1988)	Eurocode 2 (1992)	Mansour (2018)
Confinement ratio	Strengthening ratio					
$\sigma_l / f_{co,fat}$	$f_{cc,fat} / f_{co,fat}$	$f_{cc,fat} / f_{co,fat}$	$f_{cc,fat} / f_{co,fat}$	$f_{cc,fat} / f_{co,fat}$	$f_{cc,fat} / f_{co,fat}$	$f_{cc,fat} / f_{co,fat}$
0,08	1,28	1,37	1,34	1,49	1,42	1,54
0,17	1,55	1,60	1,69	1,85	1,54	1,60
0,25	1,83	1,80	2,03	2,15	1,75	1,67
0,34	2,11	1,98	2,38	2,39	1,96	1,74
0,42	2,38	2,14	2,72	2,60	2,17	1,82
0,50	2,66	2,30	3,06	2,78	2,38	1,91

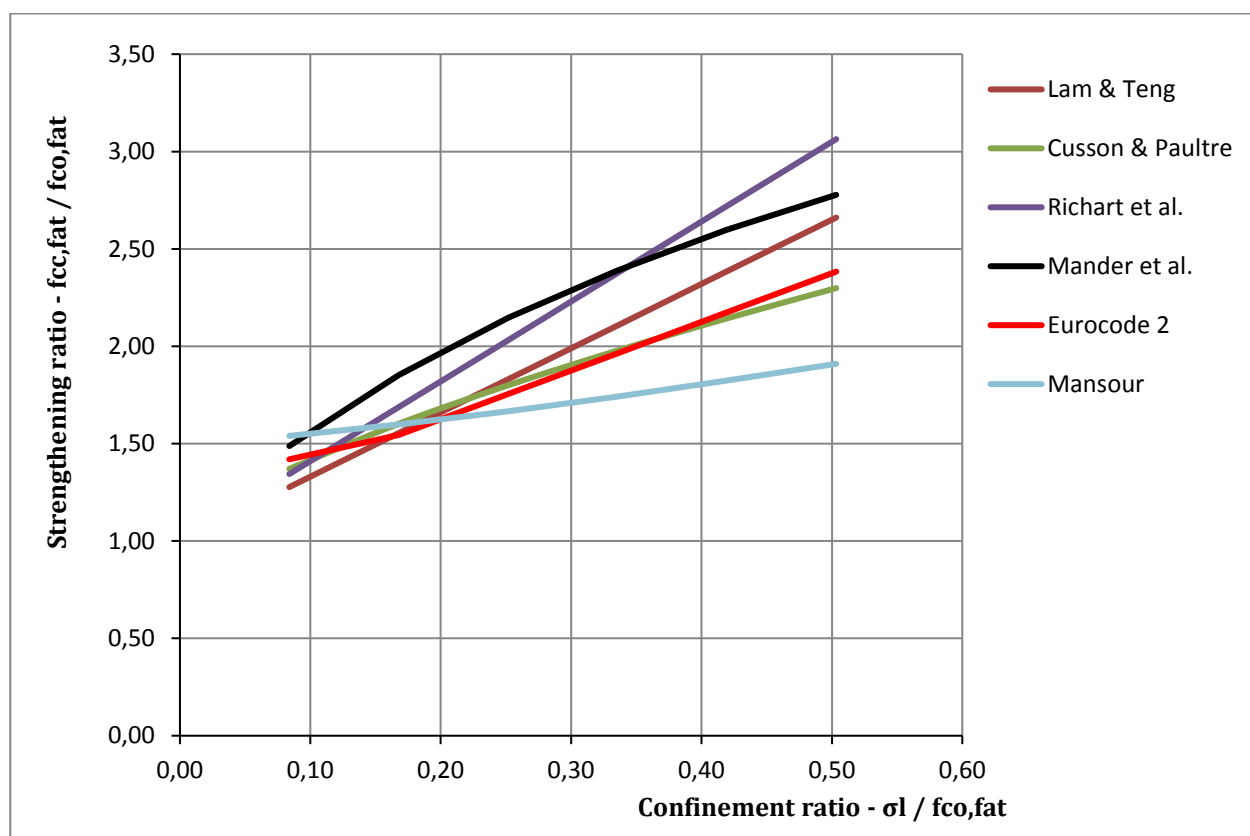


Figure 92 – Strengthening ratio vs Confinement ratio comparison of various proposed models

4.6 NUMERICAL RESULTS OF COLUMNS TYPE C1, C3 AND C4-ATENA

The numerical results of columns type C1 (unconfined with low and high-cycle loading), C3 (confined with low and high-cycle loading), and C4 (unconfined with low-cycle loading) carried out by Atena in form of hysteresis diagram are introduced hereby. Figures below illustrate the envelope line, energy dissipation vs displacement, and energy dissipation vs drift diagrams. The following paragraph illustrates the comparison of the numerical analysis.

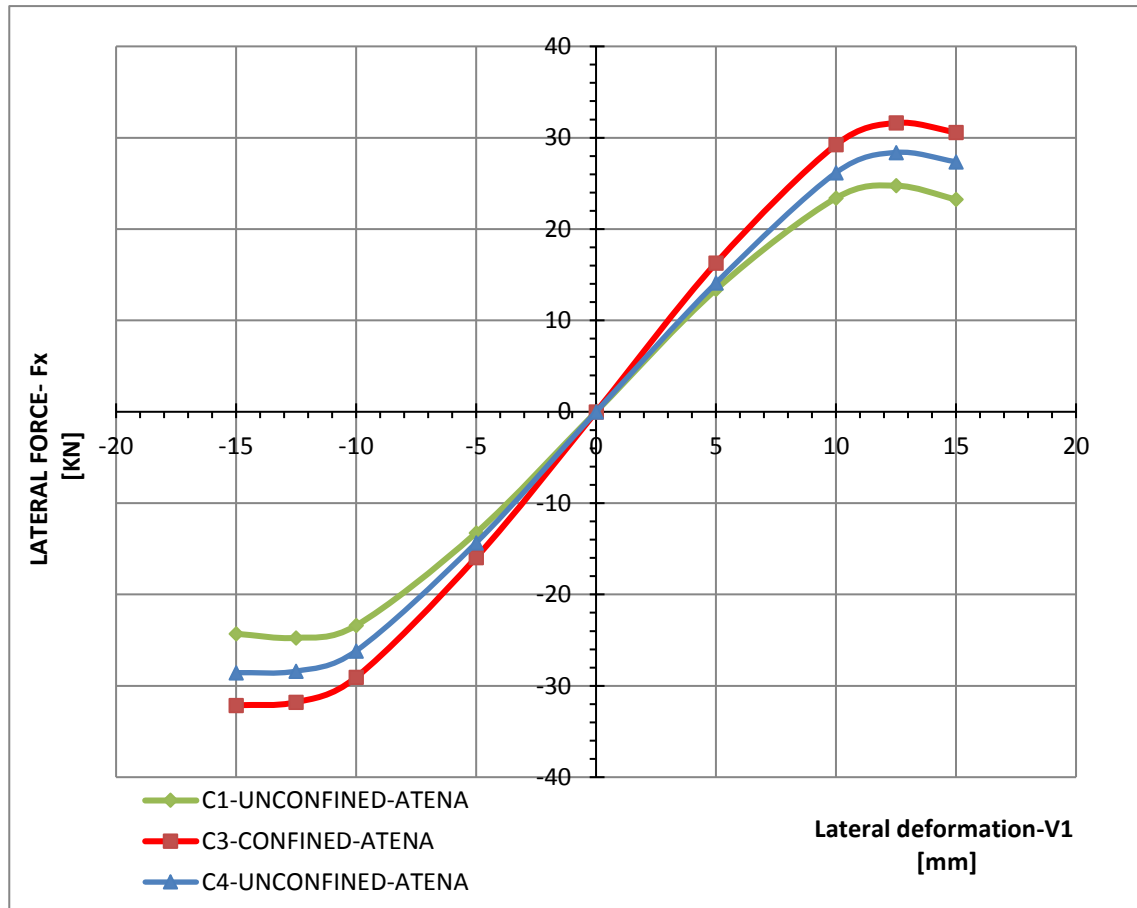


Figure 93 - Force-Displacement Envelope Diagrams for all specimens-Atena

The comparison of the experimental and numerical results is presented in the paragraph 4.7 which covers the followings:

- Envelope line (Lateral force vs lateral deformation);
- Energy dissipation vs lateral deformation;
- Energy dissipation vs drift.

The reason of the symmetrical envelope line in the numerical simulation and not in the experiment is the loose fitting of the connection between the stroke of the electrical hydraulic actuator and the concrete columns which it was not faced in the numerical simulation.

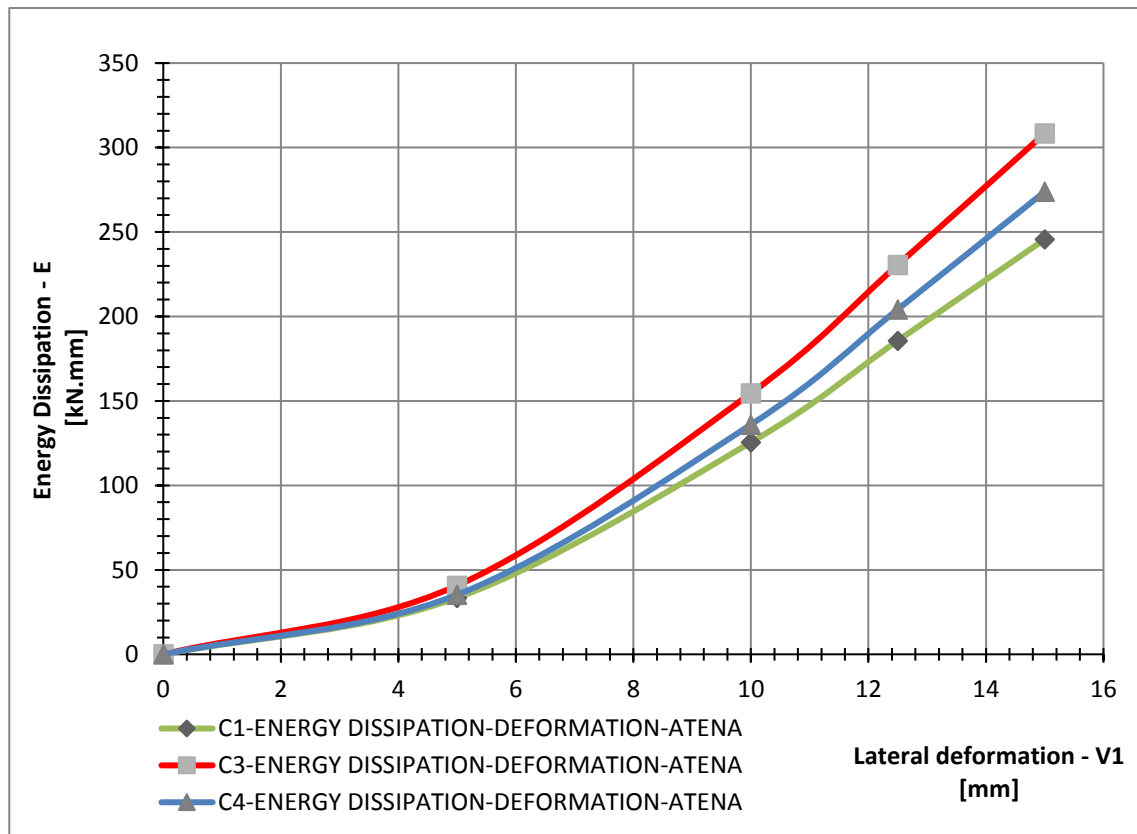


Figure 94 - Energy Dissipation-Displacement Envelope Diagrams for all Specimens-Atena

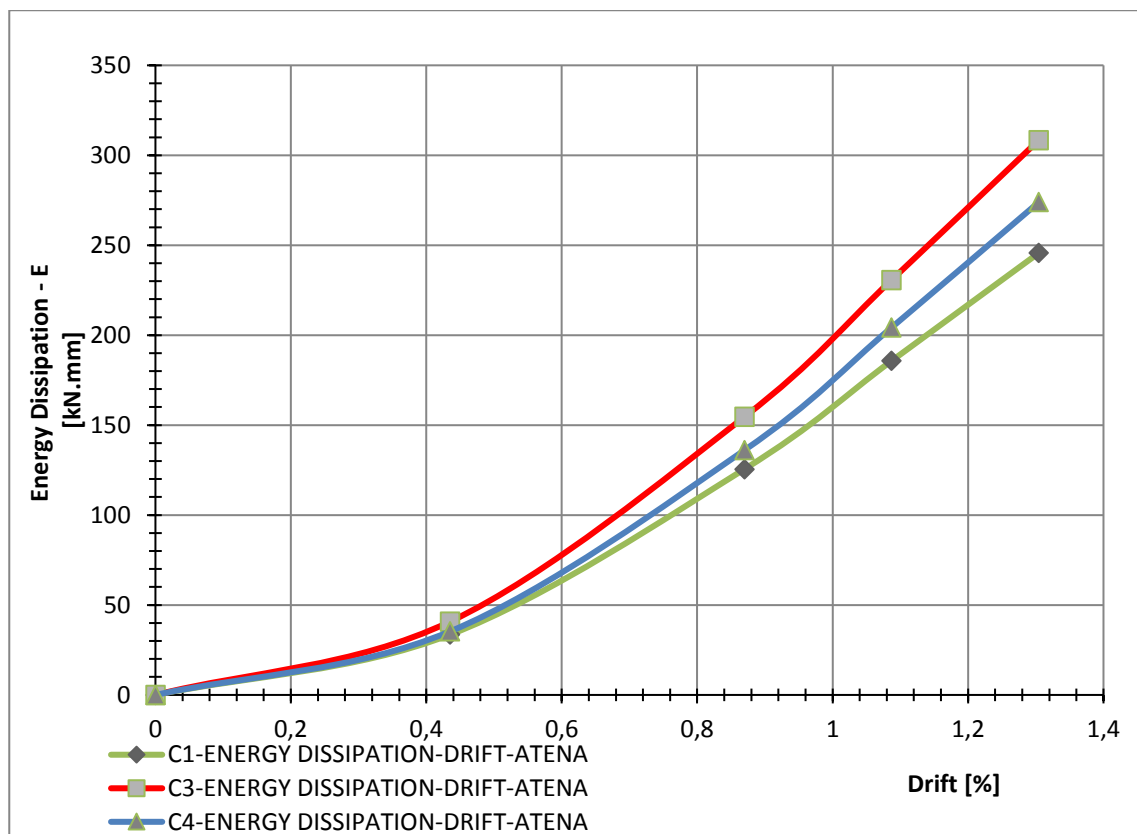


Figure 95 - Energy Dissipation-Drift Envelope Diagrams for all Specimens-Atena

4.7 COMPARISON OF THE EXPERIMENTAL AND NUMERICAL RESULTS

The following figures illustrate the comparison between the experimental and numerical results provided by ATENA which covers the followings:

- Envelope line (Lateral force vs lateral deformation);
- Energy dissipation vs lateral deformation;
- Energy dissipation vs drift.

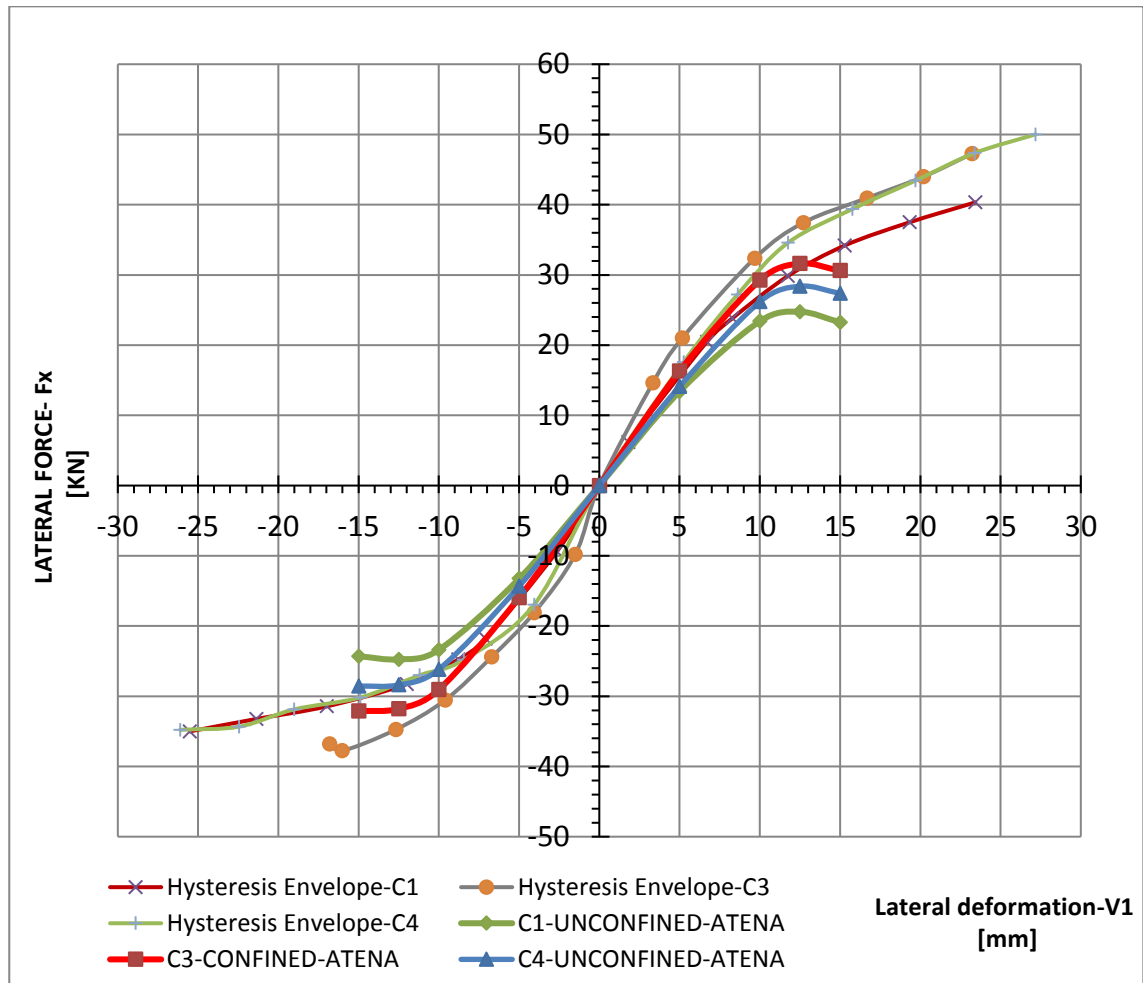


Figure 96 - Envelope line - Experimental vs. Atena

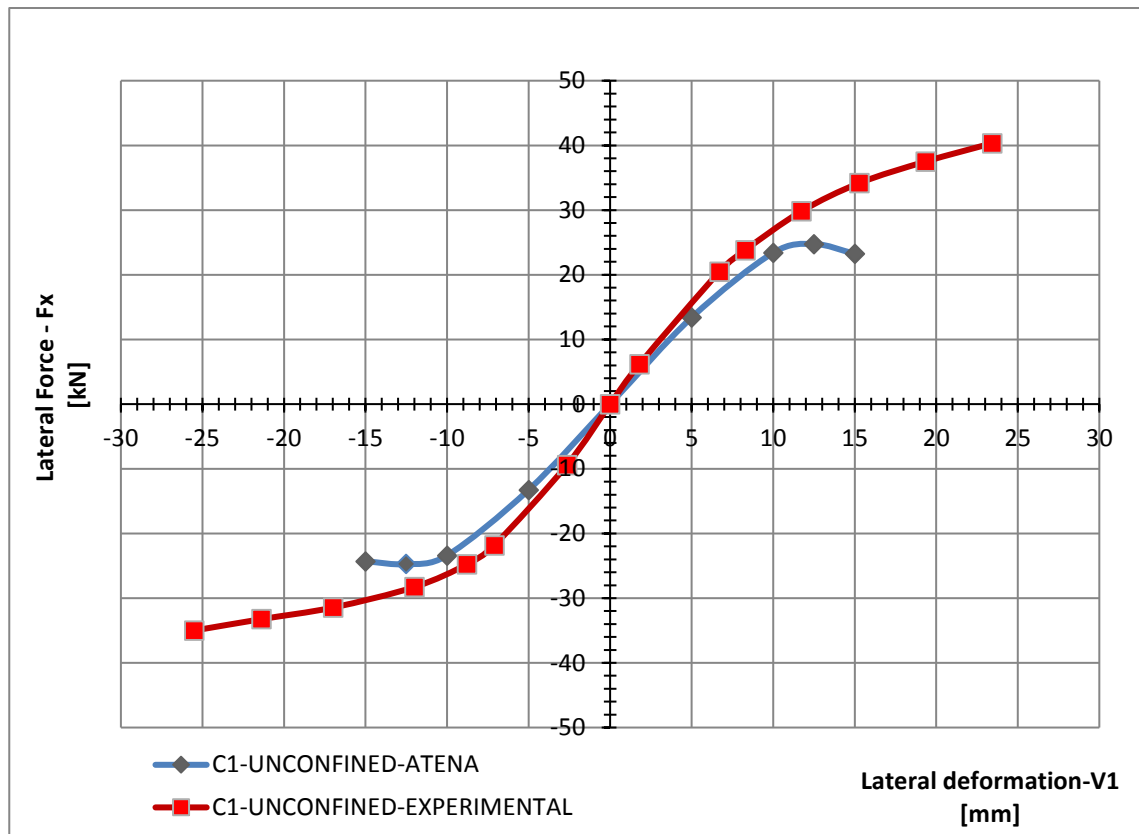


Figure 97 - Envelope line for Columns C1 - Experimental vs. Atena

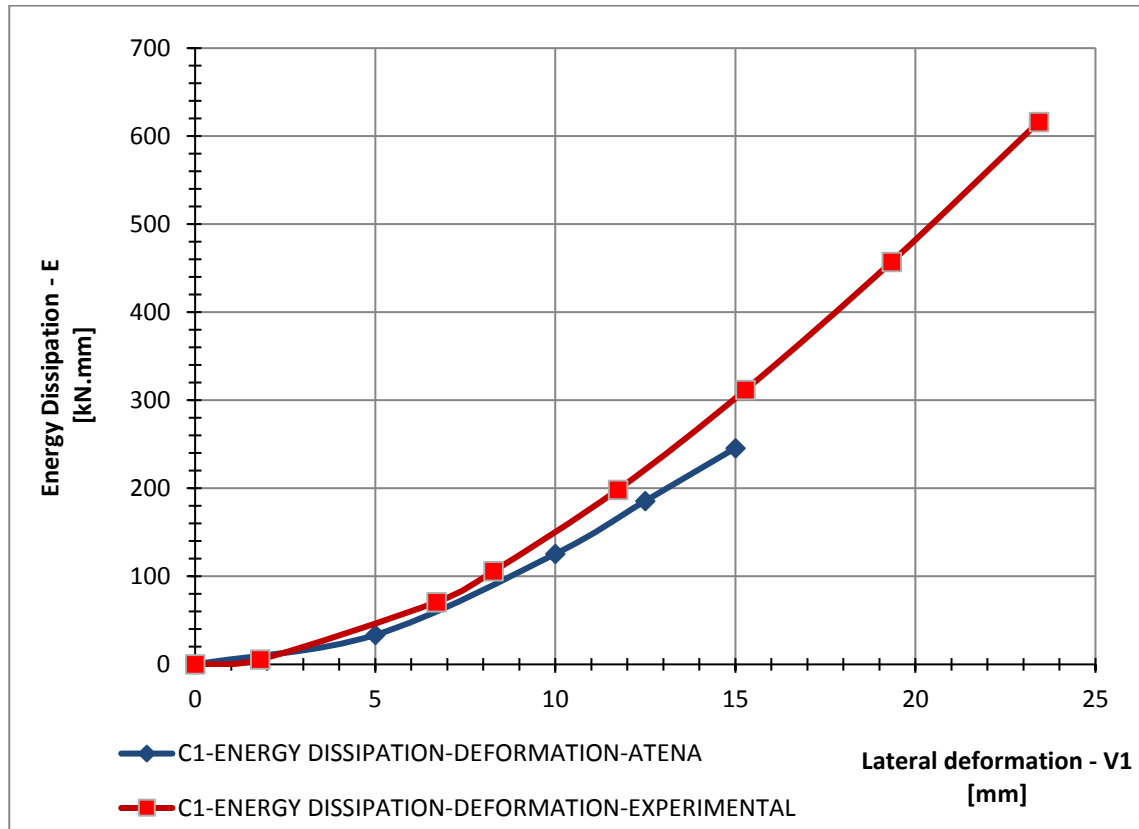


Figure 98 - Energy dissipation - deformation for Columns C1- Experimental vs. Atena

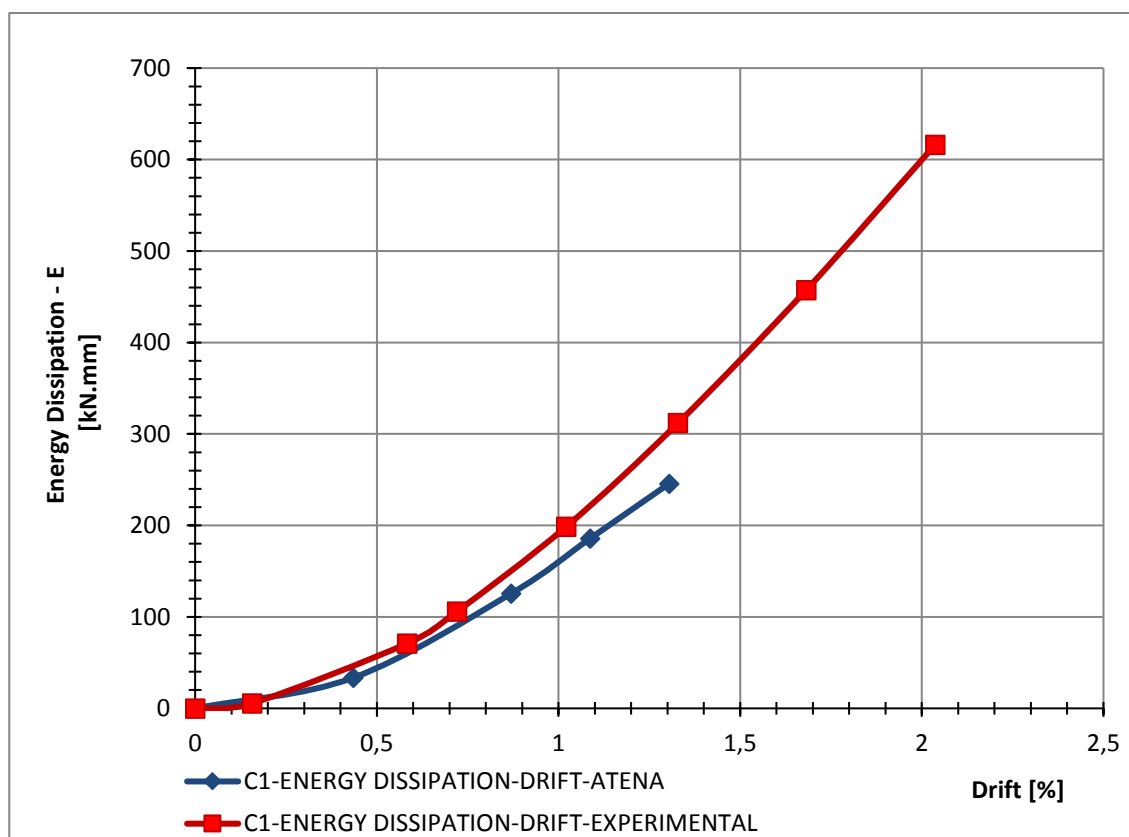


Figure 99 - Energy dissipation - drift for Columns C1- Experimental vs. Atena

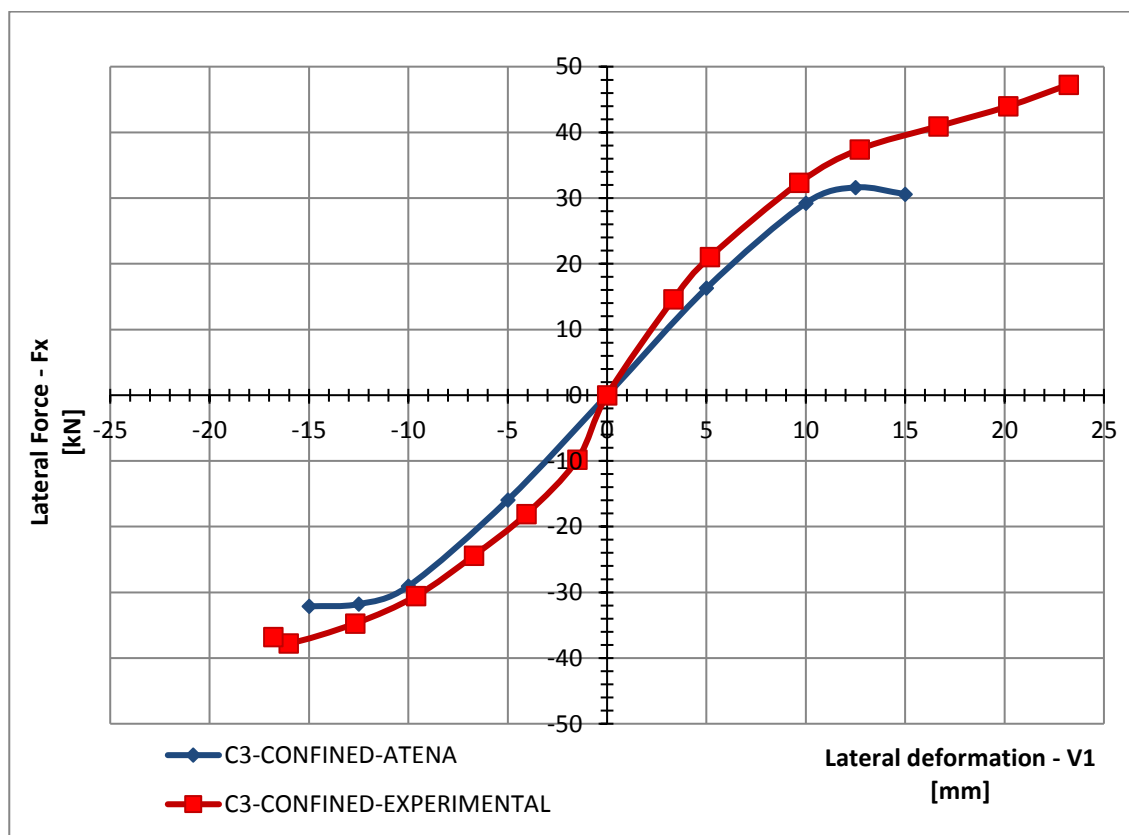


Figure 100 - Envelope line for Columns C3 - Experimental vs. Atena

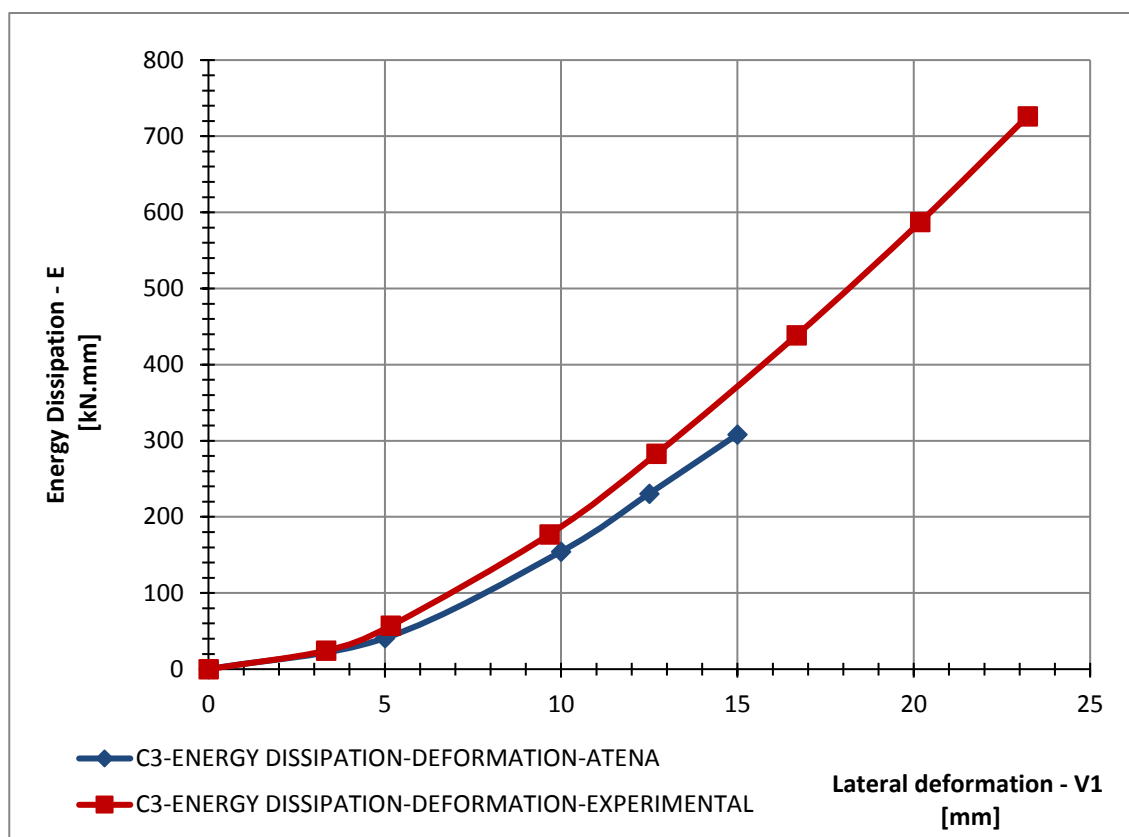


Figure 101 - Energy dissipation - deformation for Columns C3- Experimental vs. Atena

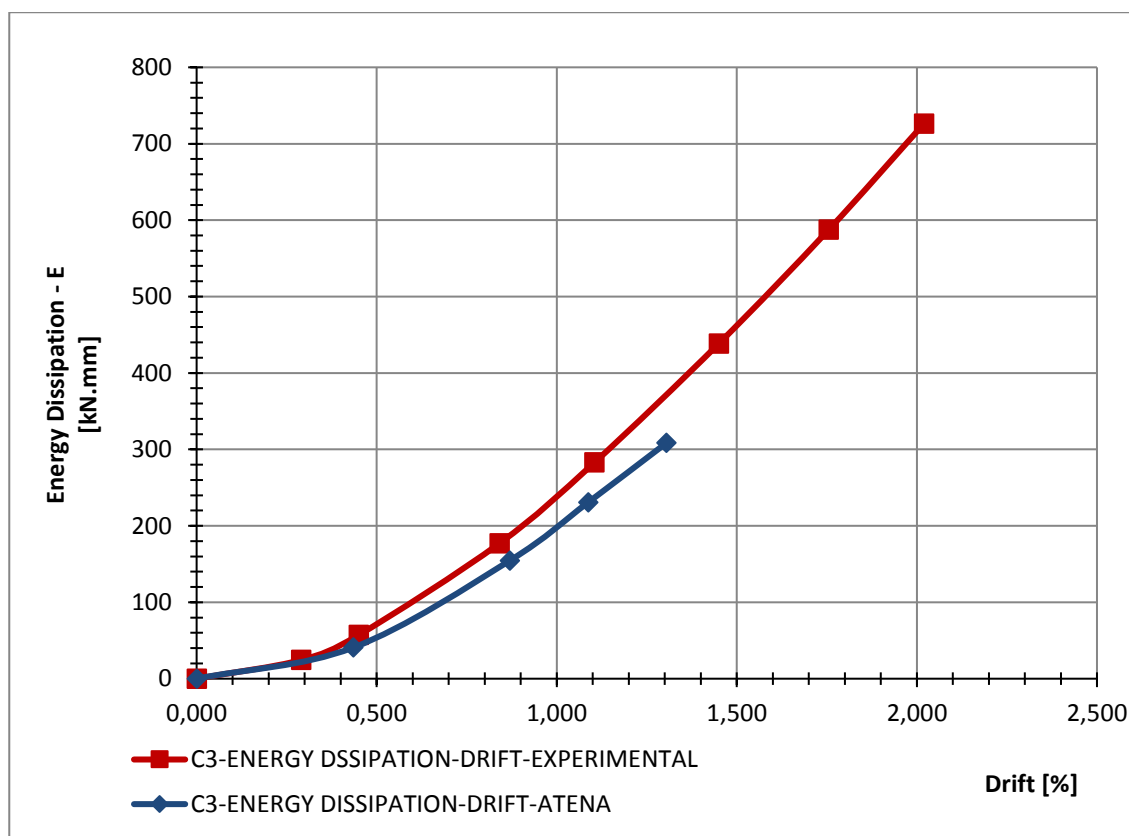


Figure 102 - Energy dissipation - drift for Columns C3- Experimental vs. Atena

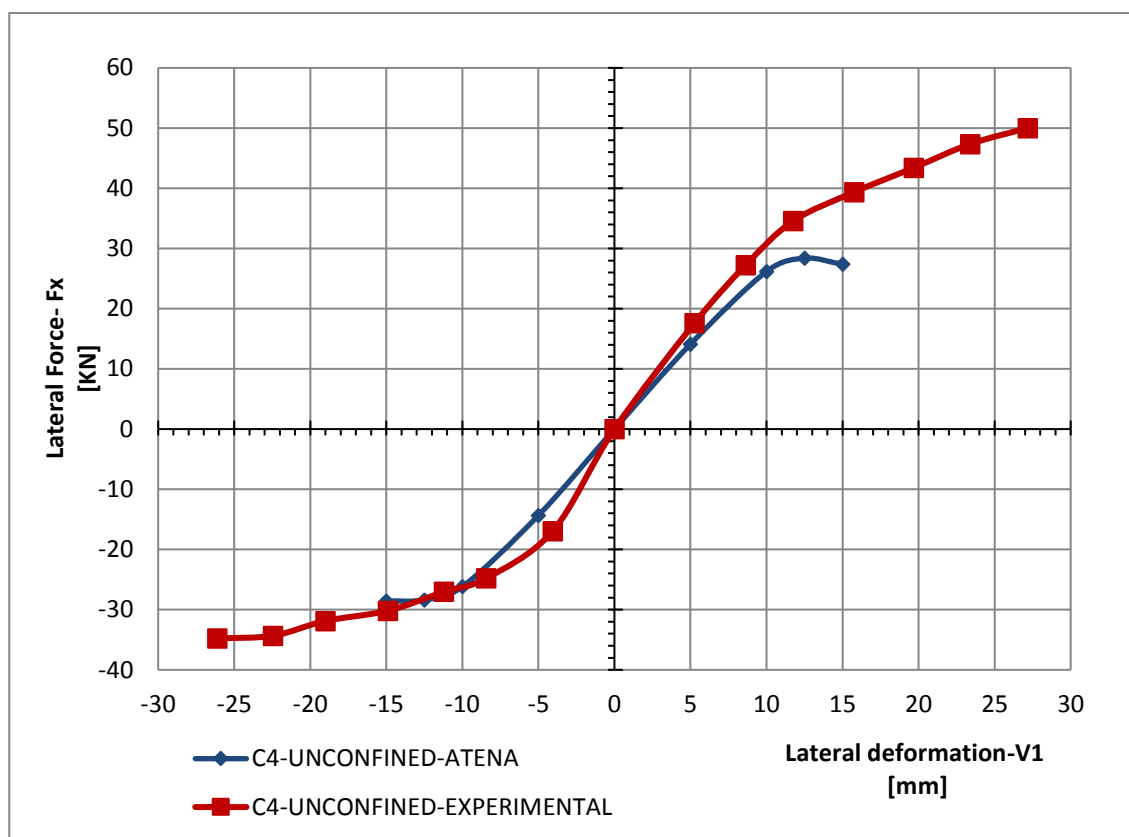


Figure 103 - Envelope line for Columns C4 - Experimental vs. Atena

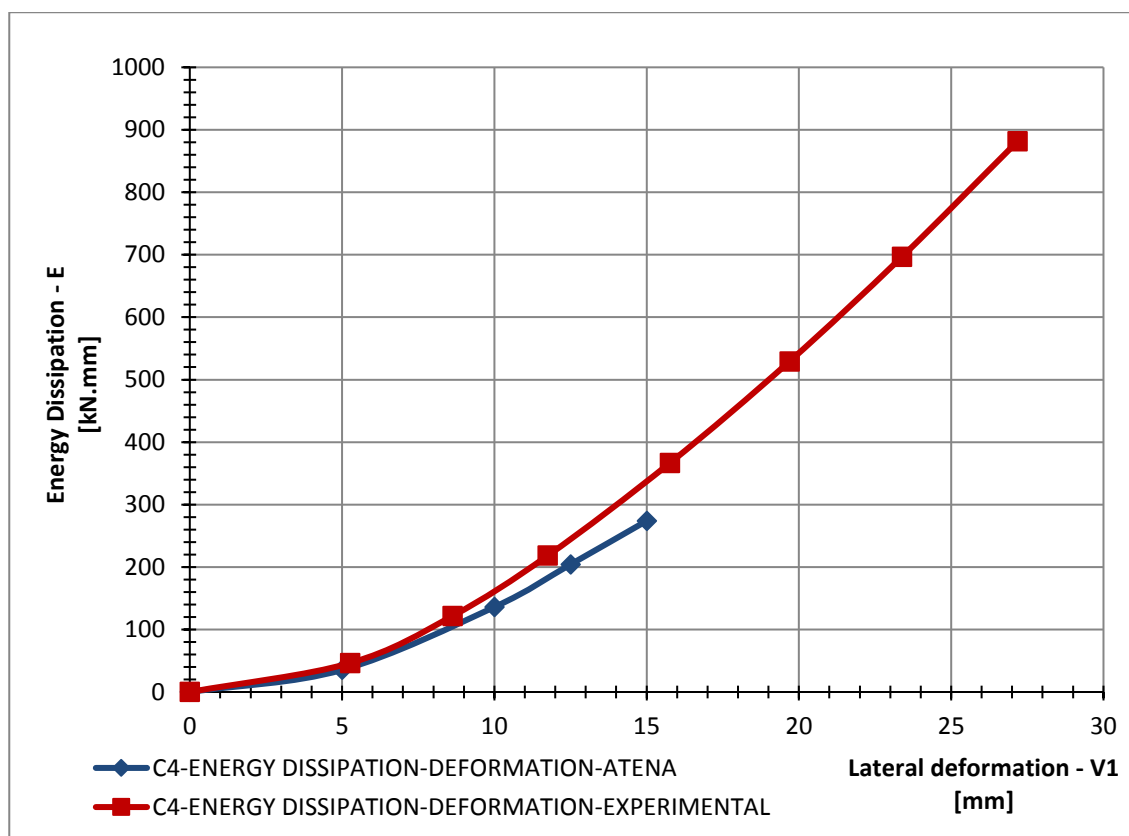


Figure 104 – Energy dissipation- deformation for Columns C4 - Experimental vs. Atena

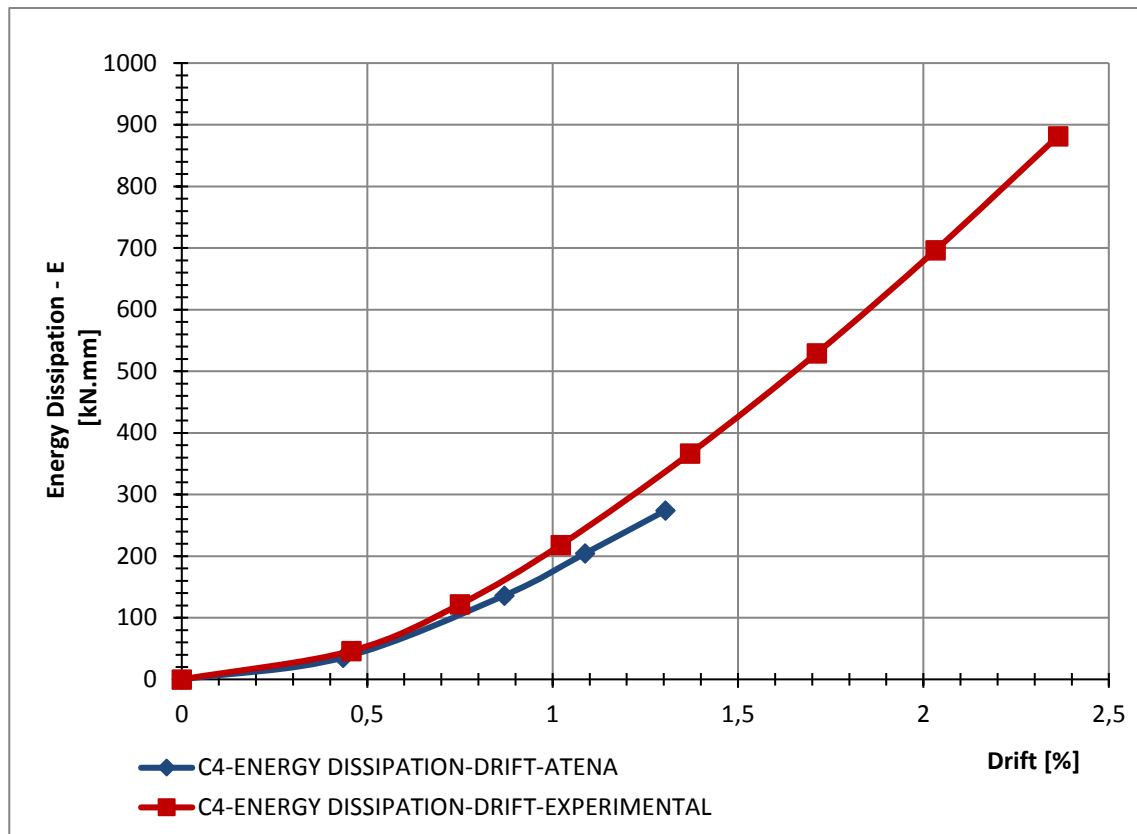


Figure 105 - Energy dissipation - drift for Columns C4- Experimental vs. Atena

As shown in the envelope line diagram obtained from the experimental and numerical results, the behaviour of the unconfined column type C1 and C4, and confined column type C3 subjected to constant axial force, lateral cyclic force is similar, and the energy dissipation versus lateral deformation and drift are coincident. During the experiment, the columns continued to deform until stopping the test. In the numerical simulation, the columns stopped deformation while large cracks appeared at the bottom zone of the column. The ultimate lateral forces in the push and pull directions are not matching as shown in *Figure 88* and *Figure 96* of the experimental results. The asymmetrical of the curve in the positive (push direction) and negative zone (pull direction) was probably caused by unsymmetrical damage of the columns during the test in push and pull directions and due to the effect of inhomogeneity of concrete. Additionally, the reason of the symmetrical envelope line in the numerical simulation and not in the experiment is the loose fitting of the connection between the stroke of the electrical hydraulic actuator and the concrete columns which it was not faced in the numerical simulation.

4.8 DESIGN PROCEDURE

Ductility equivalent to chord rotation of columns is the most important aspect for structural elements subjected to seismic load. The main aim of retrofitting in seismic is to increase the ductility of structural elements/ columns.

The design of FRP jackets for a defined or target displacement ductility. This is achieved by the following procedure:

1. Determine the plastic hinge length based on Eurocode 2 (refer to paragraph 2.8.5, equation 60 to 62),

$$L_{pl} = \frac{L_v}{30} + 0.2D + 0.11 \frac{f_y}{\sqrt{f_{co}}} d_{bl}$$

2. Compute the yield curvature based on cross-section analysis (refer to paragraph 2.8.5, equation 67),

$$\phi_y = 2.25 \frac{\varepsilon_y}{D}$$

3. Curvature capacity of the reinforced concrete columns based on the required or target displacement ductility can be expressed (refer to chapter 2, section 2.8.5.)

$$\mu_\phi = \frac{(\mu_\Delta - 1)}{3 \left(\frac{L_{pl}}{L_v} \right) \left(1 - 0.5 \frac{L_{pl}}{L_v} \right)} + 1$$

4. Ultimate curvature capacity of the reinforced concrete columns can be expressed (refer to section 2.8.2 equation 45)

$$\mu_\phi = \frac{\phi_u}{\phi_y} \rightarrow \phi_u = \mu_\phi \phi_y$$

5. Ultimate strain of the reinforced concrete columns can be expressed (refer to section 2.8.2 equation 45)

$$\varepsilon_{ccu} = \phi_u x$$

6. Effective lateral confining pressure contributed by the FRP wraps can be expressed based on Eurocode 2 (refer to section 2.7.1 equation 32)

$$\sigma_l = \frac{(\varepsilon_{ccu} - \varepsilon_{co})}{0.2} f_{co}$$

7. Required thickness of FRP wraps can be expressed (refer to section 2.4.1 equation 1)

$$t_f = \frac{\sigma_l D}{2 E_f \varepsilon_{f, rup}}$$

f_{co} : unconfined compressive strength of concrete

f_y : yielding strength of steel

ε_{co} : strain of concrete

ε_y : strain of steel

E_f : elastic modulus of FRP

f_f : tensile strength of FRP

$\varepsilon_{f, rup}$: strain rupture of FRP

D : diameter of column

d_{bl} : diameter of rebars

L_{pl} : plastic hinge length

L : length of column

x : depth of neutral axis

σ_l : effective lateral pressure due to FRP

ε_{ccu} : ultimate strain of concrete due to FRP

ϕ_y : yield curvature

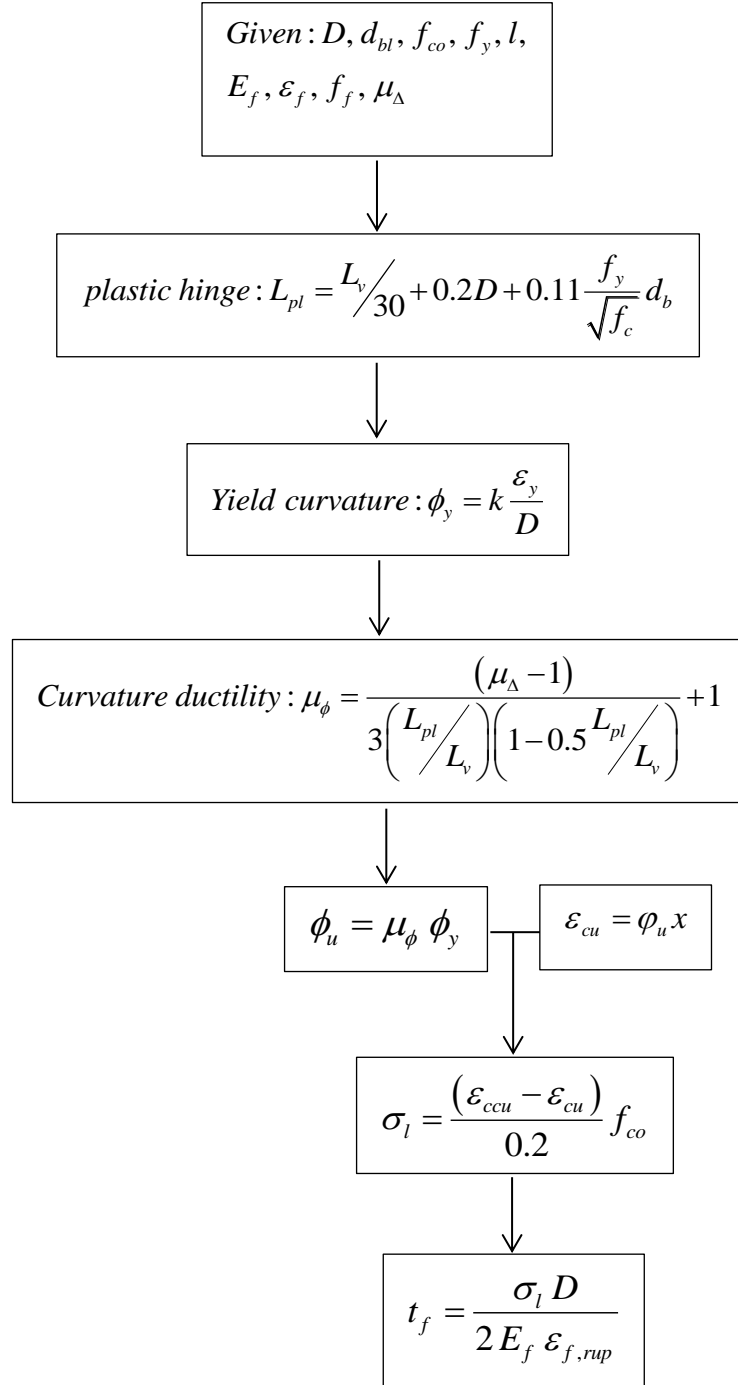
ϕ_u : ultimate curvature

μ_ϕ : curvature ductility

μ_Δ : displacement ductility

t_f : thickness of FRP

k : 2.25 for circular columns, 2.10 for square columns



DESIGN OF FRP CONFINEMENT FOR A CIRCULAR COLUMN FOR A SEISMIC RETROFIT
INPUT

Geometry of column	Diameter of column	D =	200	[mm]
	Gross area of column	A _g =	31415,93	[mm ²]
	Length of column	L =	2000	[mm]
	Concrete cover	CC =	20	[mm]

Concrete properties	Compressive strength of concrete	f _{co} =	35	[MPa]
	Axial strain of concrete	ε _{cu} =	0,002	[%]

Reinforcing steel properties	Diameter of longitudinal bars	d _{bl} =	8	[mm]
	Number of longitudinal bars	n =	6	
	Total area of longitudinal bars	A _s =	301,59	[mm ²]
	Diameter of hoops	dt =	6	[mm]
	Spacing of hoops/ pitch for spiral	s =	150	[mm]
	Yield strength of bars	f _y =	500	[MPa]
	Modulus of elasticity of bars	E _s =	200000	[MPa]
	Yield strain	ε _y =	0,0025	[-]

FRP wrap properties	Modulus of elasticity of FRP	E _f =	140000	[MPa]
	Tensile strength of FRP	f _f =	1870	[MPa]
	Thickness of one layer of FRP	t _f =	0,125	[mm]
	Ratio	ε _{f,rupt} /ε _{fu} =	0,7	[%]
	Strain of FRP at rupture	ε _{f,rupt} =	0,00935	[%]
	Reduction factor	ψ _f =	0,9	

Column Configuration	Displacement ductility	μ _Δ =	4	
	Axial force	F _z =	450	[kN]
	Effective depth of cross-section	d =	170	[mm]

OUTPUT

Plastic hinge length	L _{pl} = L _v /30+0.2D+0.11d _{bl} f _y /√f _{co}	181	[mm]
Required curvature ductility	μ _φ = (μ _Δ - 1)/3(L _p /L)(1-0.5(L _p /L)) + 1	12,57	[-]
Yielded curvature of the section	φ _y = 2.25 ε _y /D	0,0281	[1/m]
Required ultimate curvature	φ _u = μ _φ φ _y	0,354	[1/m]
Depth of the neutral axis of unconfined concrete	C _u = d [ε _{co} /(ε _{co} +ε _y)]	75,56	[mm]
Ultimate strain of the column	ε _{ccu} = φ _u C _u	0,0267	[%]
Actual maximum confining stress	f _{la} = (ε _{ccu} - ε _{co}) f _{co} /0.2	4,32	[MPa]
Required thickness of FRP jacket	t _f = (f _{la} D)/(2E _f ε _{f,rupt})	0,33	[mm]

A design algorithm and code is part of the dissertation work. The Language used is C#.net, was developed using Visual Studio Community 2017 edition, which is a free version of Visual Studio. It can be downloaded at the following link:

<https://www.visualstudio.com/downloads/>

This software was made to determine the shear capacity of the reinforced concrete circular column confined with FRP in seismic zones.

It consists of inputting data to a form and getting results using the following three methods:

1. Shear strength retrofit,
2. Flexural plastic hinge confinement,
3. Clamping of lap splices.

The software will automate the calculations needed to return the required results.

The structure of the code is shown in detail in the appendix.

4.9 SUMMARY AND CONCLUSION OF THE INVESTIGATION

The submitted dissertation work is dealing with the behaviour of unconfined and confined circular concrete columns subjected to axial static load and lateral cyclic load (high and low-cyclic loading). Two main issues are required for consideration for the column subjected to lateral load; one is strength capacity enhancement and the second is ductility enhancement. FRP wraps provide additional strength capacity, which reduces the risk of a brittle failure, and increases the strain capacity of concrete in compression, leading to enhancing the member ductility.

Fulfilling the objective of the dissertation work

This investigation work focused on the available knowledge required to strengthen the circular concrete column with FRP wraps subjected to lateral cyclic loading (high and low-cyclic loading). The majority of standards and codes provide numerical equations to predict the confinement lateral pressure contributed by wrapping. These standards do not consider the degradation of concrete compressive strength due to preloading and especially cyclic load (high cyclic loading). Thereby, the degradation of the concrete compressive strength of the existing structures has to be considered due to the material fatigue by finding out the actual concrete compressive strength of the existing structures and by verifying the results with the theoretical value predicted by the codes and standards. The aim of this work was to predict the enhancement of the FRP wraps on the behaviour of the circular concrete columns subjected to lateral cyclic loading (predicting of design-oriented model) and to introduce the strengthening procedure of a circular column by FRP wraps. The main two issues mentioned above are the key to a successful procedure to strengthening design. Therefore, an experimental and numerical study are presented here to investigate the behaviour of unconfined and CFRP confined circular concrete columns subjected to combined axial load and reversed lateral cyclic loads. The experimental procedures are reported here in detail for four specimens unconfined and confined circular columns under axial static load and lateral high and low-cycle loadings. The axial load was applied prior to lateral

load. The lateral loads were applied in two different methods; first, the force control fatigue method that column, simultaneously with axial static load, is subjected to one direction pulling lateral force for one million cycles (high-cycle load), and second, the displacement control reversed cyclic method (low-cycle load) is based on a pattern of progressively increasing displacements. The hysteresis loops vs. deflection, energy dissipation vs. deflection and energy dissipation vs. drift for each specimen were presented. The experimental results evaluation and comparison between specimens were introduced. Part of the work is theoretical, which was presented by the interaction diagrams and moment-curvature diagrams of the circular concrete column cross-sections and the static scheme of the cantilever column with axial and lateral loads, and a mathematical model of the unconfined and confined columns conducted by ATENA 3D presented the numerical study. Additionally, a design code developed by C# programming language presented the design algorithm.

Based on the experimental results and research of the theoretical study, the following outlines were obtained:

- The enhancement contributed by FRP jackets on the section analysis of circular reinforced concrete columns by using the interaction diagrams was verified (paragraph 3.2.1.2), and the ultimate compressive strength and bending moment enhancement of a concrete section depends on the number of FRP layers provided.
- The ductility enhancement of unconfined and confined columns, moment-curvature analysis of test specimens conducted by software SAP2000 (paragraph 3.2.1.5) was evaluated and it shows that the ductility performance of the unconfined columns can be improved by the confinement of concrete conducted by FRP wraps and spiral reinforcement.
- The plastic hinge length is a significant factor between the displacement, rotation, and curvature ductility factors of the cantilever column (paragraph 3.2.1.6).

- The use of FRP jackets for the ductility and load capacity enhancement in unconfined reinforced concrete columns subjected to axial load and lateral cyclic loading was verified experimentally, based on the comparison between unconfined specimen C1 and confined specimens C2 and C3.
- There is a difference in the behaviour of reinforced concrete columns subjected to low and high-cycle loadings. As listed earlier in the experimental results, the unconfined column C1 subjected to high-cycle loading (approximately 1 million cycles) before exposing to low-cycle loading can dissipate lower energy than the column C4 exposed to low-cycle loading only due to the fatigue of materials. Additionally, providing FRP wraps to columns exposed to high-cycle loading improve their energy dissipation and ductility as shown in the comparison between unconfined column C1 and confined columns C2 and C3 (paragraph 4.3).
- During high-cycle loading (in the experiment, a lateral force of a minimum of 2.0 kN and a maximum of 8.0 kN was selected) of 1 million cycles, specimens C1, C2, and C3 do not display any sign of failure. The performing of a fatigue life assessment of the column based on a pattern of progressively increasing displacements, few cycles are enough for the strength degradation and failure of the specimens.
- The experimental results illustrated in table 22, 23, and 24 and figures 63, 64, 65, 70, 71, 72, and 73 show that some losses in the moments at fixed support were presented due to the elastic behaviour of the column's support.
- Prediction of a new empirical model for FRP confined concrete circular column subjected to axial static loading and lateral cyclic loadings (high and low- cyclic loading) is presented in the paragraph 4.5.
- The mathematical model based on FEM conducted by ATENA 3D software, which simulates the behaviour of unconfined and confined reinforced concrete columns subjected

to axial static load and reversed cycle lateral load was evaluated by the line envelope and energy dissipation versus lateral displacement and compared to the experimental results, which provide a good agreement with the experimental results.

- The strength degradation due to the high-cycle loading (comparison between unconfined specimens C1 and C4) should be taken into consideration while the strengthening of existing concrete column is carried out.
- During low-cyclic loading, once displacement ductility reaches values between 2 and 3, the strains of the concrete in the plastic hinge length exceed the unconfined concrete limit, causing spalling of the cover concrete then the crushing extends to the core, causing buckling in the longitudinal reinforcements, this failure mode occurred at specimens C1 and C4. In the confined columns C2 and C3, many layers of FRP wraps may provide sufficient confinements to prevent such failure.
- The stress-strain properties of concrete and steel become quite different from that purely tensile or compressive stress due to the reversed cyclic loading (1 million cycles). This conclusion is drawn from the comparison of specimens C1 and C4. The concrete compressive strength decreases due to fatigue, which leads to the shear strength degradation of the concrete columns. It is the reason of shear failure of concrete columns under cyclic loading. It is significant to lateral deformation-based design to evaluate the degraded shear strengths after each load cycle.
- The energy dissipation of the test specimens increased with providing the FRP wraps. The energy dissipation of the FRP confined columns is between 17% and 28% larger than the unconfined column subjected to high and cycle loadings, and 13% larger for the unconfined column subjected to low-cycle loading only.
- The required amount of transverse confinement of columns should be provided to achieve certain level of ductility and strength of concrete columns.

- The displacement ductility capacity of the concrete columns was significantly improved by the contribution of the FRP wraps at the plastic hinge location of the columns, and the ductility was controlled by the strength of the FRP wraps.

The above-mentioned outcomes which based on the theoretical and experimental studies fulfil the main objective of the dissertation work presented in paragraph 1.3.

4.10 FUTURE RESEARCH AND RECOMMENDATIONS

Due to complexity of operation to perform such tests under realistic loads in large quantities especially on large-scale concrete columns, the available investigations and researches are still limited. Many different philosophies and proceedings have been suggested for the FRP strengthening of concrete columns under cyclic loading, and the relevant provisions differ in various design codes. Therefore, it is recommended to enlarge researches and investigations and to describe relevant parameters to seismic behaviour of concrete columns; such as curvature ductility factor, displacement ductility factor, and lateral drift ratio, which are used by many standards and seismic design criteria. It has been found that the design procedures vary due to different design criteria. Due to variations in the seismic design provisions in current design codes to determine the confinement of concrete columns, a comprehensive database and large parameters of the columns simulated seismic loads are significant for supplementary development of analysis and design provisions. The ranges of important parameters such as the geometry, strength of concrete (NSC and HPC), jacketing materials (CFRP, GFRP, etc.), additional effect of transverse reinforcement on confinement and different loadings (monotonic and cyclic), should be studied and investigated.

Based on the experimental results and complication faced during the testing, hereby the following recommendations:

1. To prevent moment loses at the column support and to realize the fixity of the column base, it is recommended to have concrete column and base as one piece and cast in one go.
2. To have statistically significant results, a larger number of columns with the same configuration to be tested and to be able to quantify the shear strength degradation of the concrete columns subjected to cyclic loading.
3. The selection of the geometry and the size of the specimens to be based on the available equipment in the laboratory.

4. To study larger number of parameters in the experimental study affecting the columns subjected to cyclic loading such as frequency, number of layers of the FRP, the magnitude of the lateral force, the number of cycles and the fatigue of FRP wraps.

APPENDIX



Figure 106 - Specimen type C1

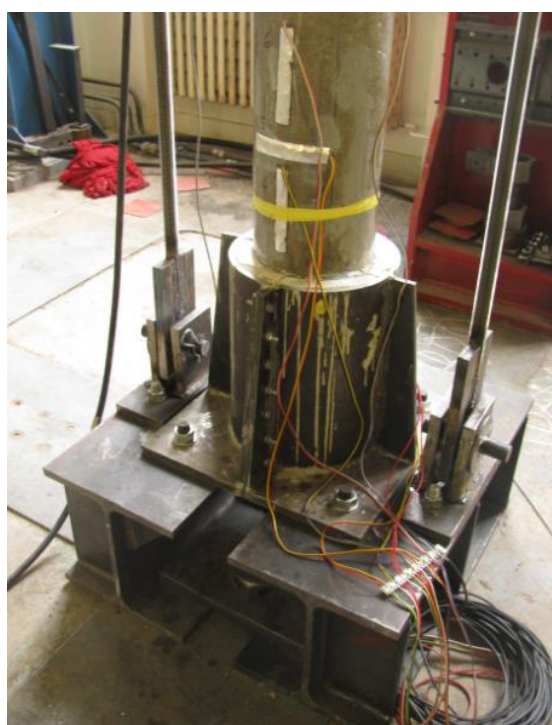


Figure 107 - Specimen Type C1- Footing

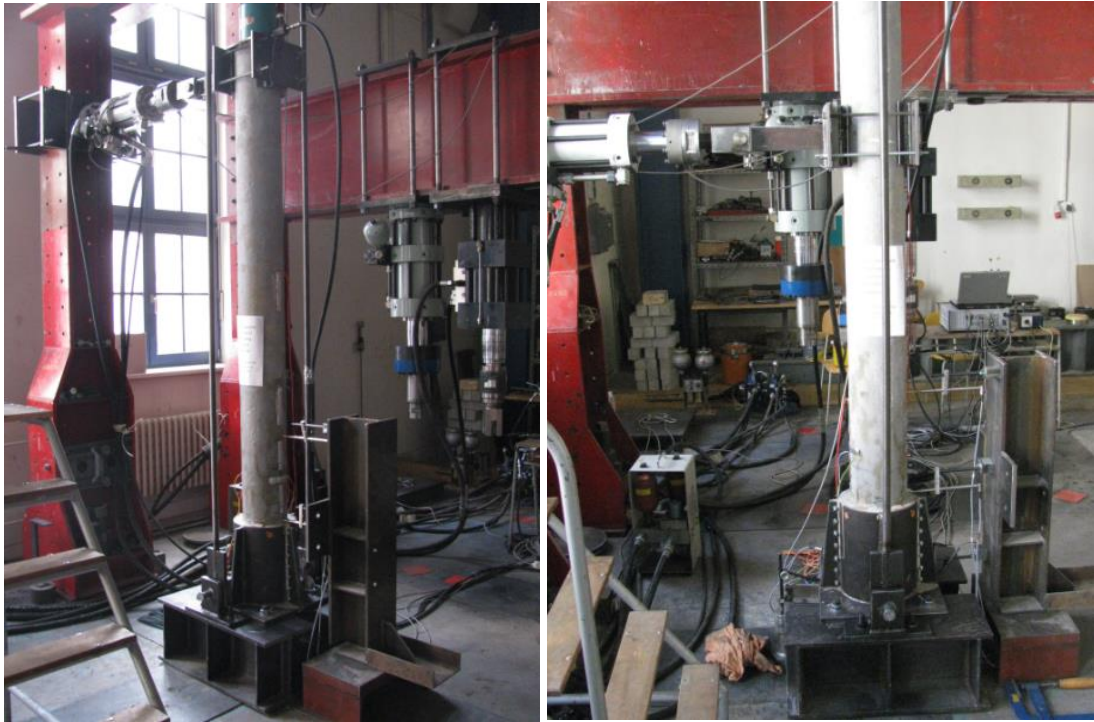


Figure 108 - Specimen Type C1- Test Configurations



Figure 109 - Specimen Type C1- Axial and Lateral Loads Application



Figure 110 - Strain gauges installation

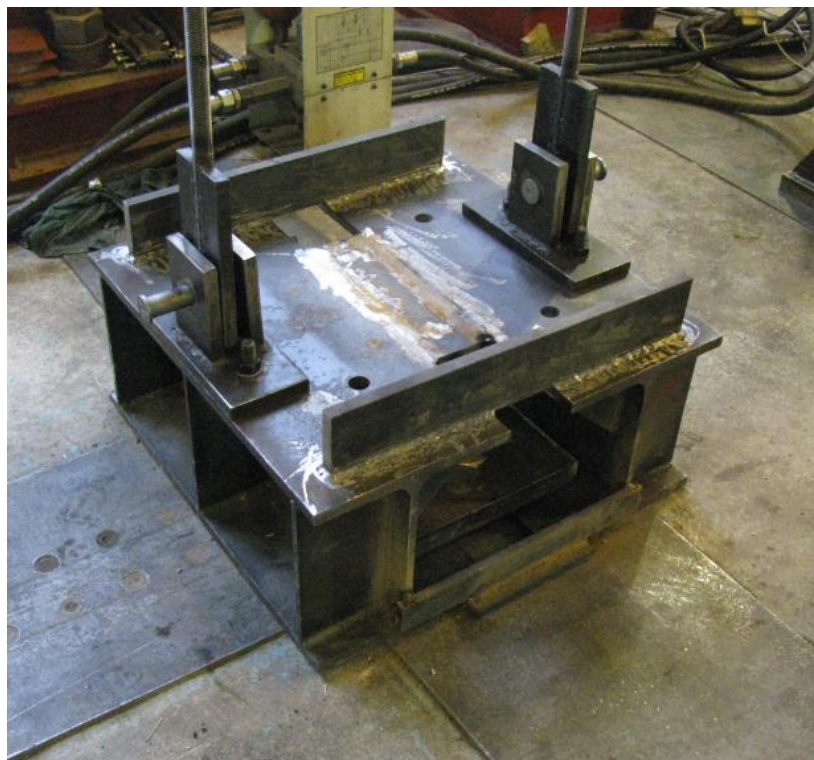


Figure 111 – Steel footing fixed to ground by anchor bolts



Figure 112 – Specimen Type C3- Confined with FRP wraps



Figure 113 – Specimen Type C2- Confined with FRP wraps

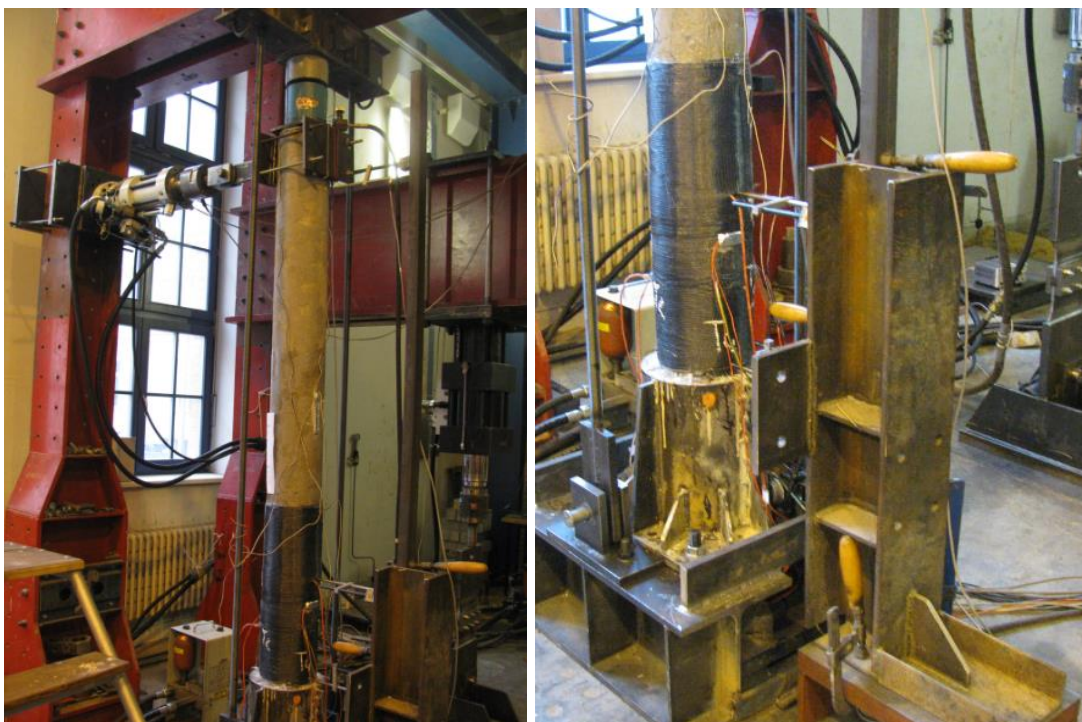


Figure 114 – Specimens Type C2 and C3- Test Configurations

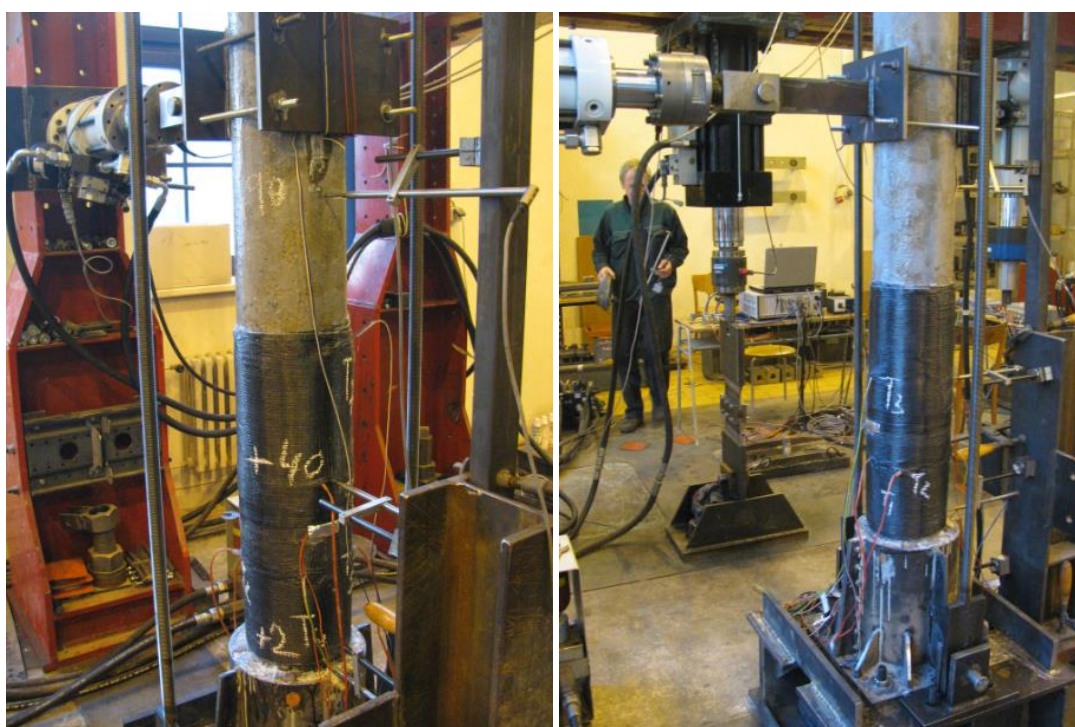


Figure 115 – Specimens Type C2 and C3- Loads application at lower level

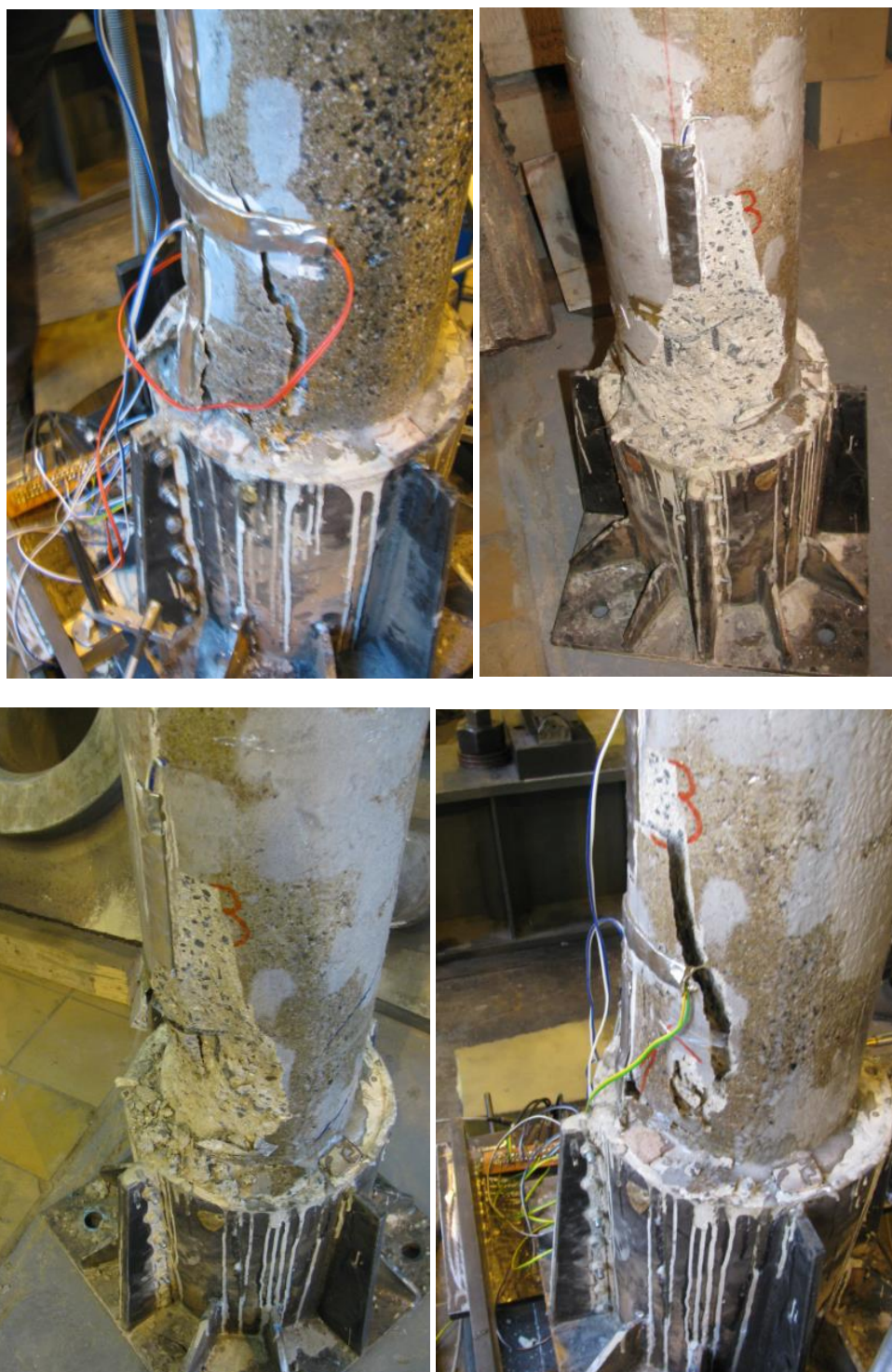


Figure 116 – Specimen Type C1- Failure mode

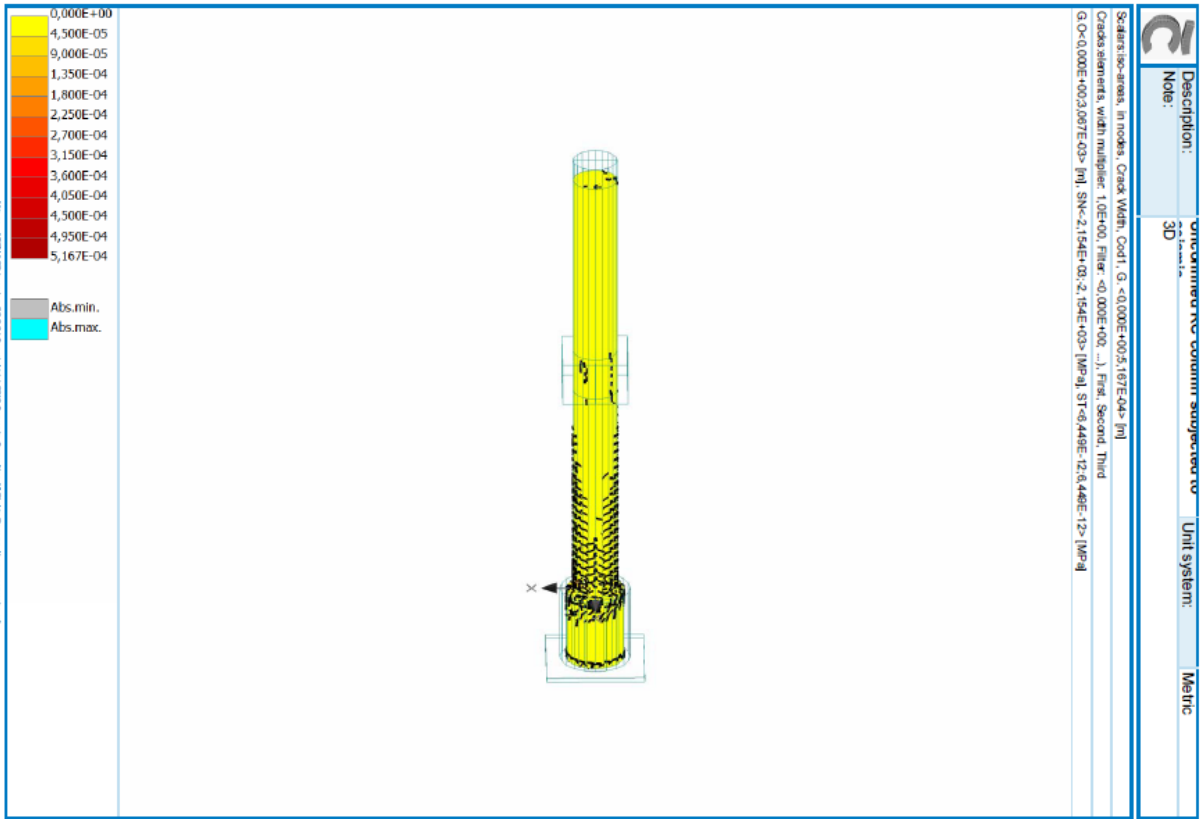


Figure 117 – Specimen Type C1- Atena – Cracks Element

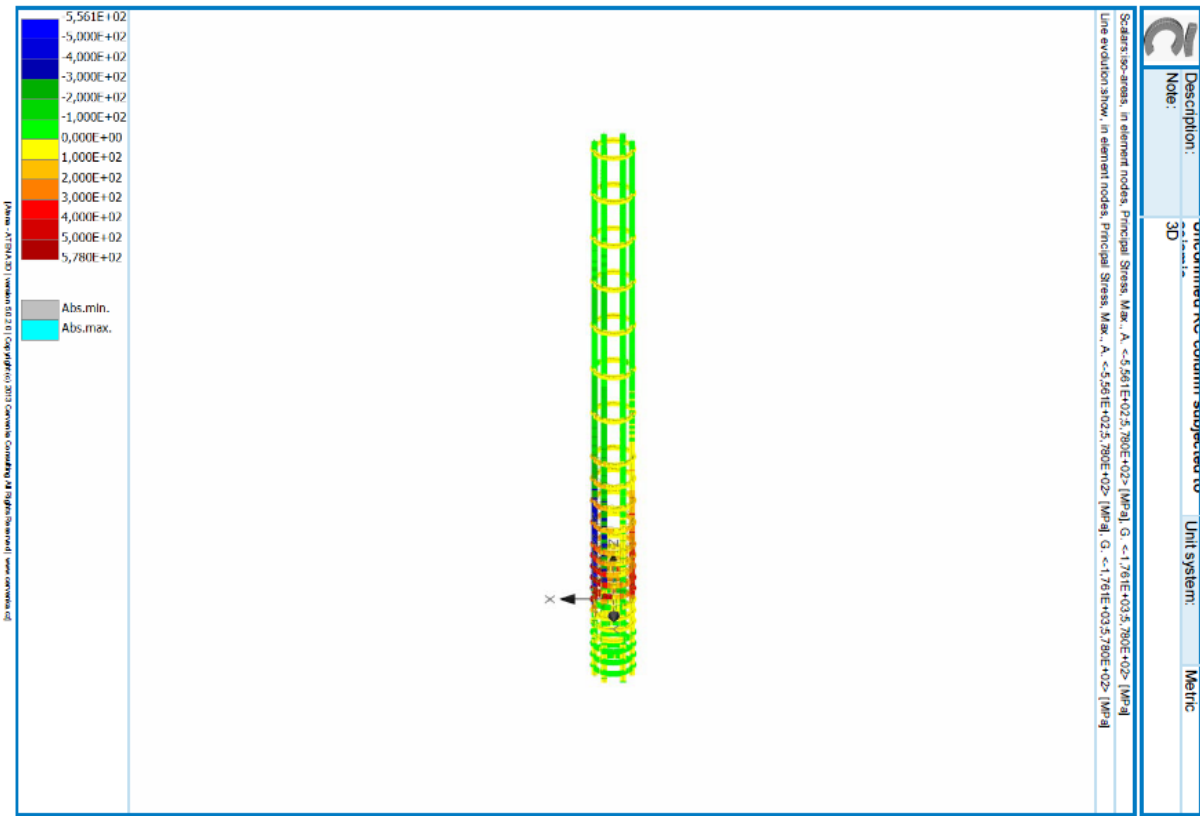


Figure 118 – Specimen Type C1- Atena – Principal Stresses in Reinforcements

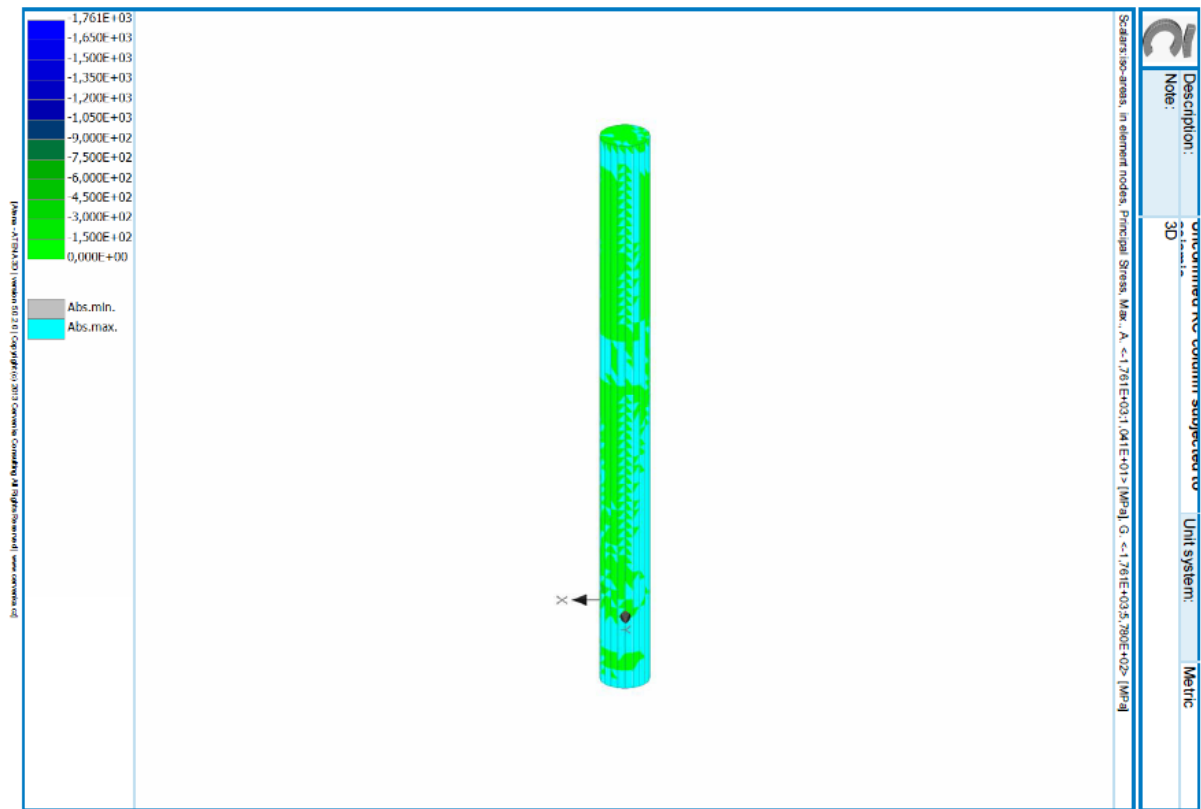


Figure 119 – Specimen Type C1- Atena – Principal Stresses in Concrete

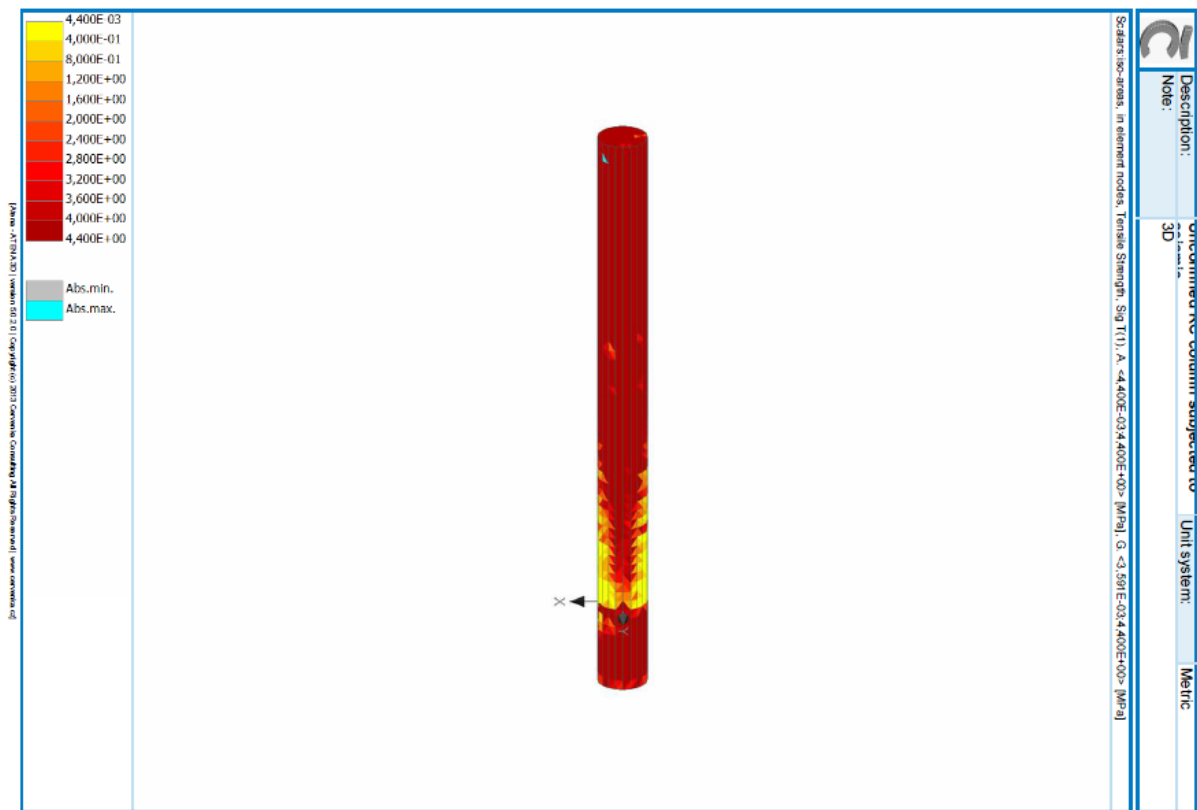


Figure 120 – Specimen Type C1- Atena – Tensile Strength SIG T(1)

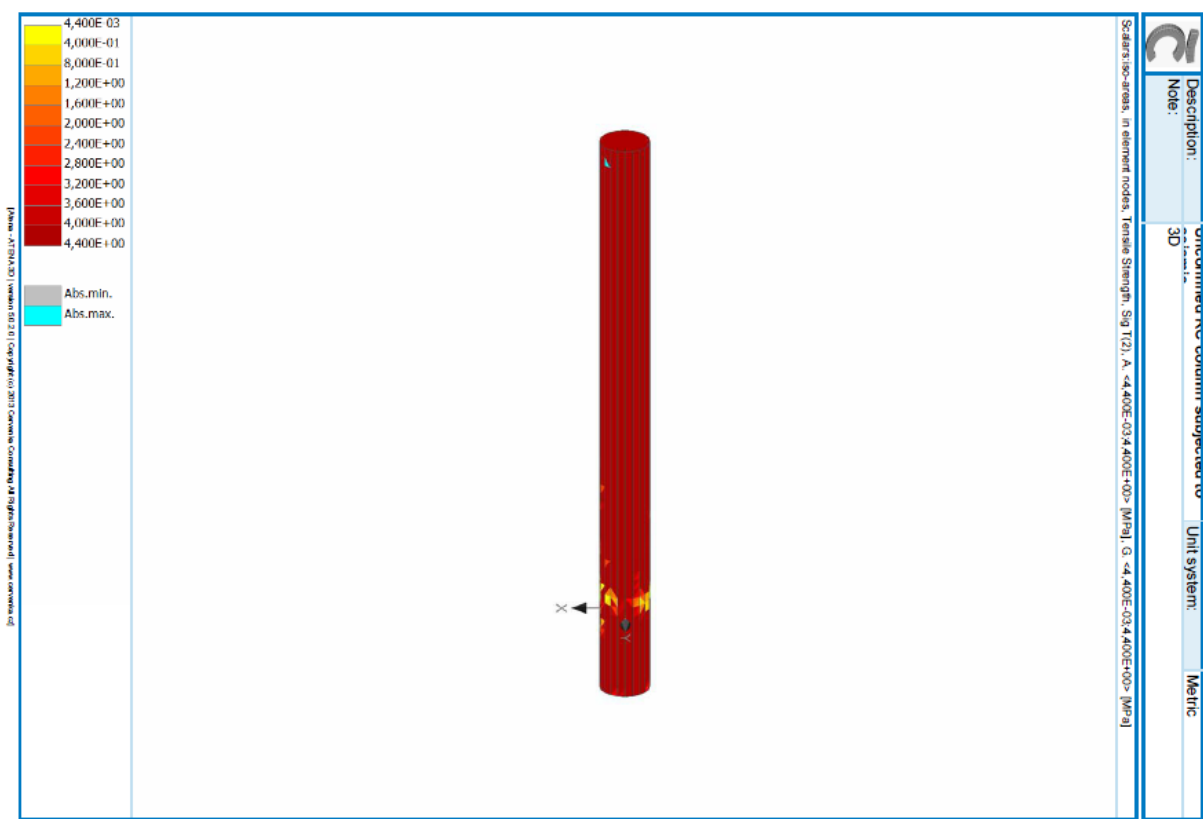


Figure 121 – Specimen Type C1- Atena – Tensile Strength SIG T (2)

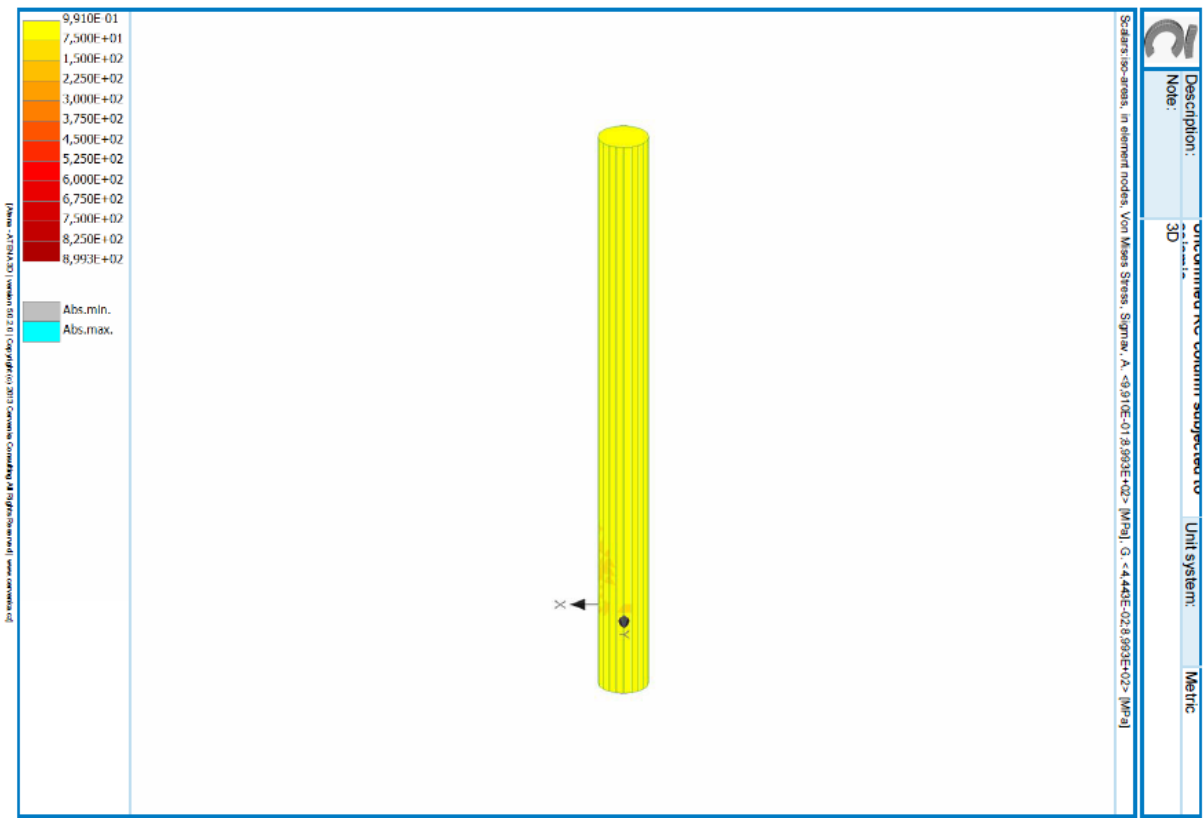


Figure 122 – Specimen Type C1- Atena – Von Mises Stresses in Concrete

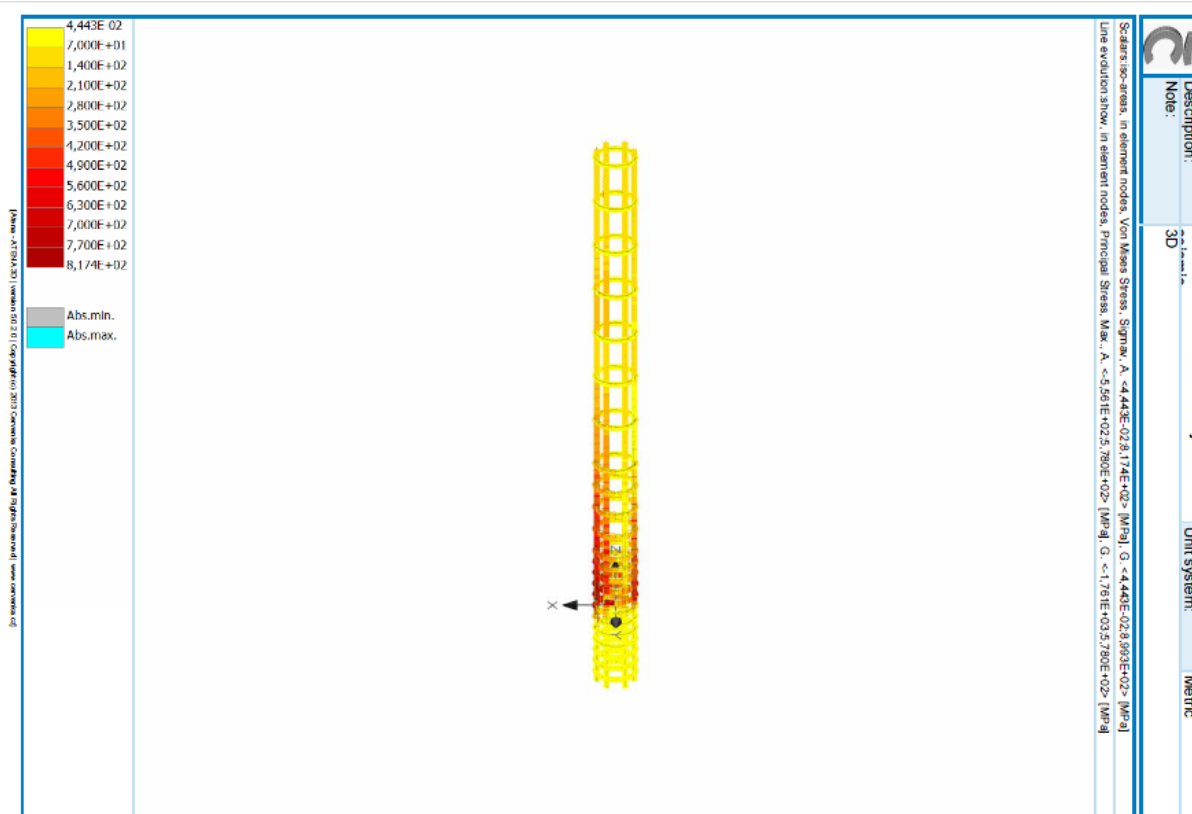


Figure 123 – Specimen Type C1- Atena – Von Mises Stresses in Reinforcements

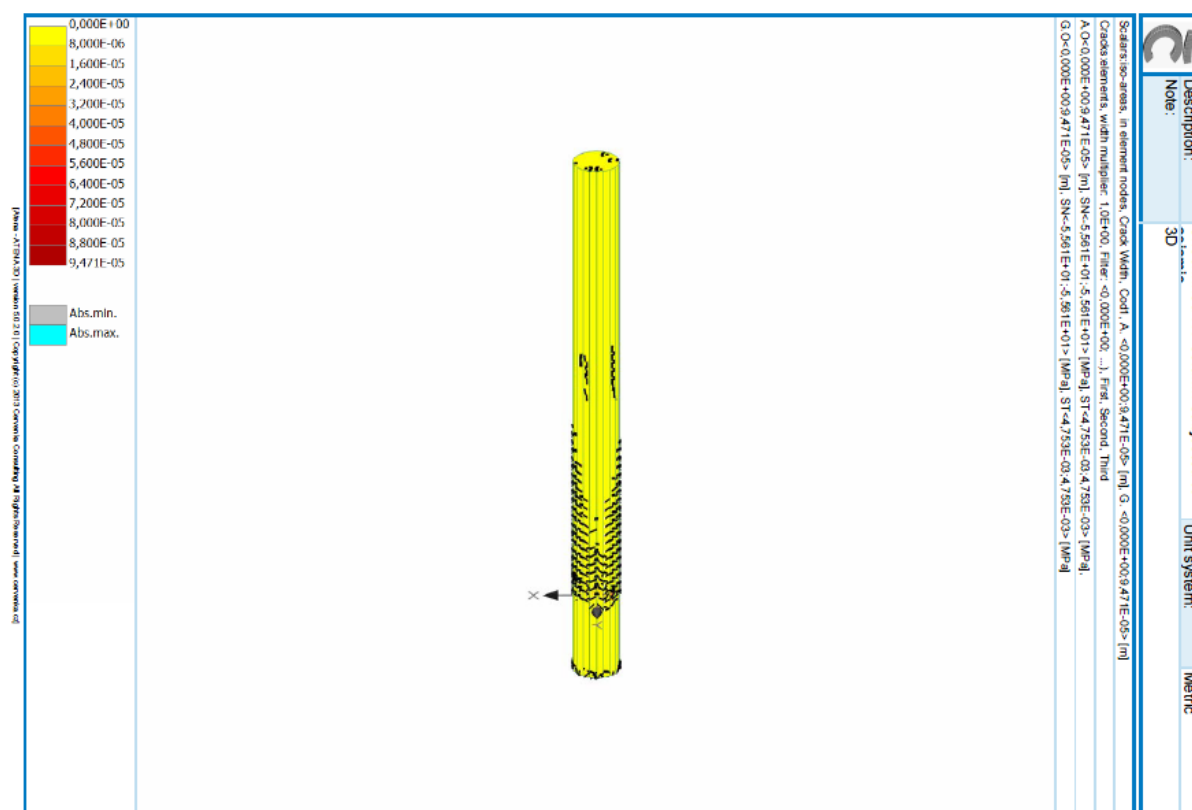


Figure 124 – Specimen Type C3- Atena – Cracks Element

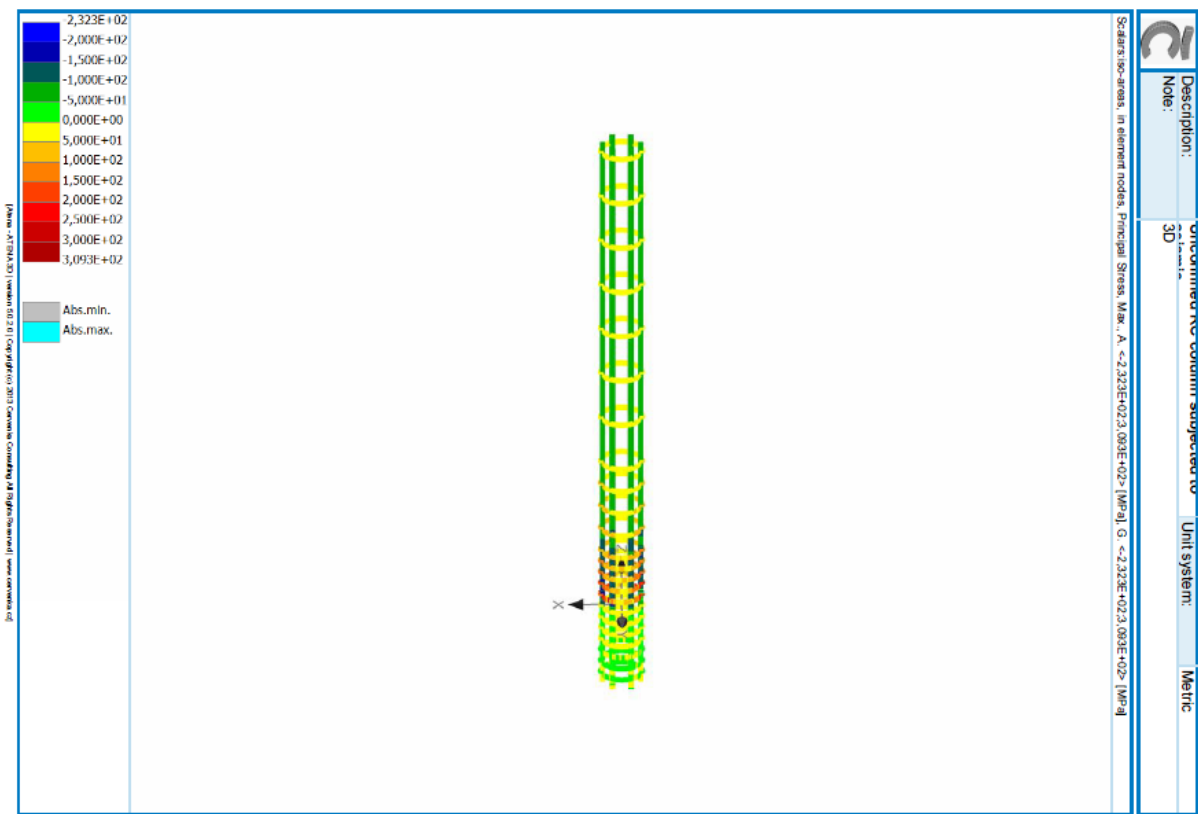


Figure 125 – Specimen Type C3- Atena – Principal Stresses in Reinforcements

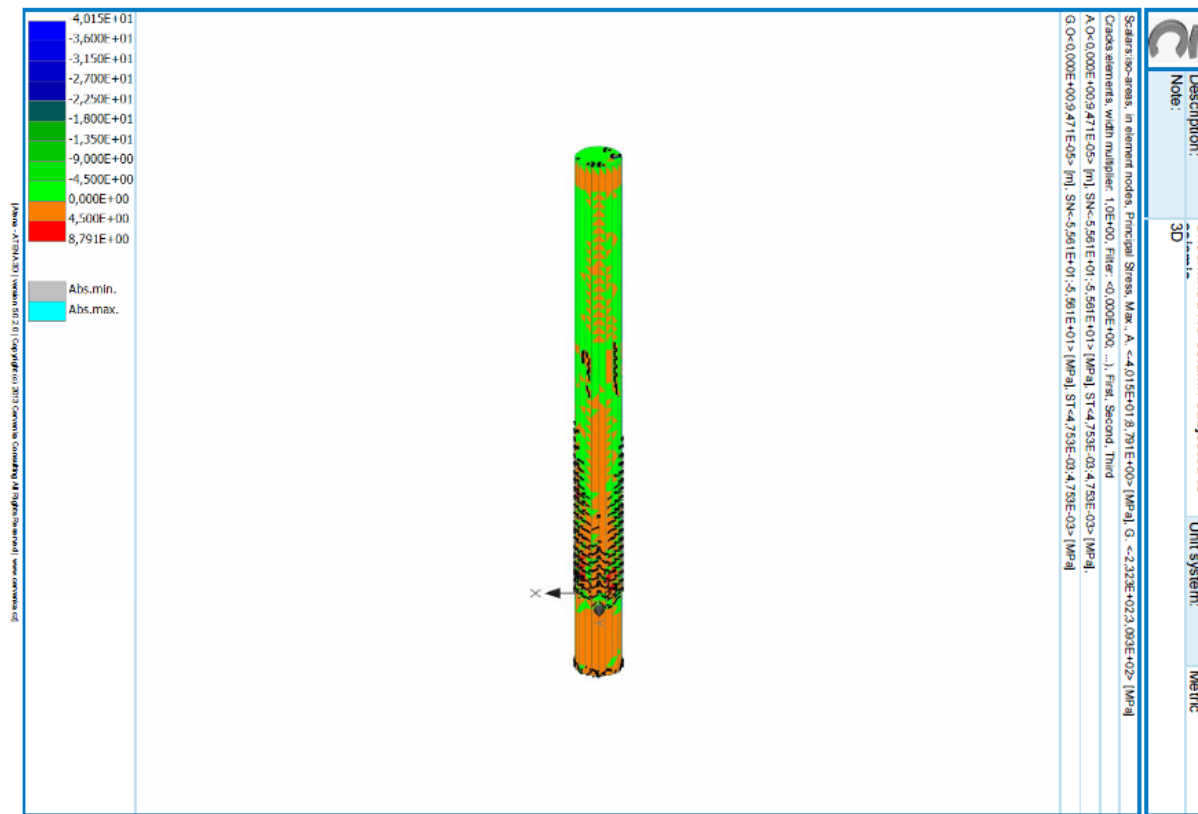


Figure 126 – Specimen Type C3- Atena – Principal Stresses in Concrete

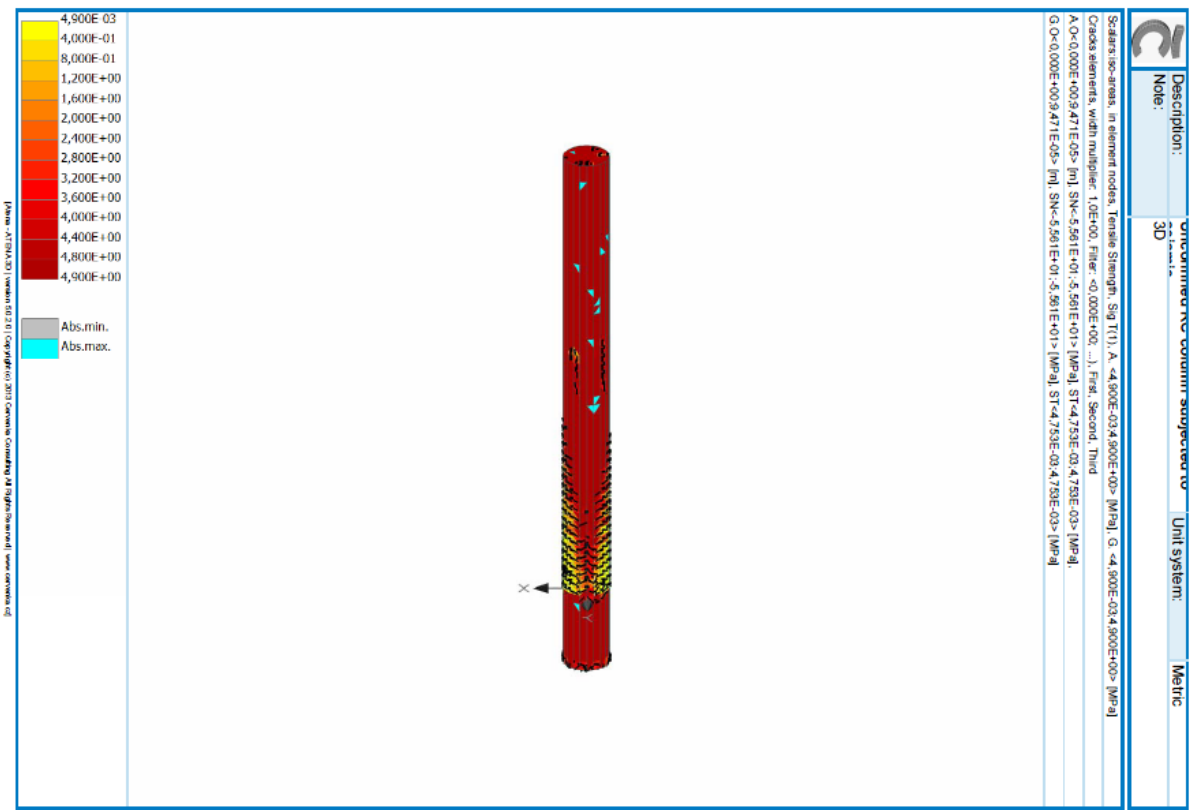


Figure 127 – Specimen Type C3- Atena – Tensile Strength SIG T (1)

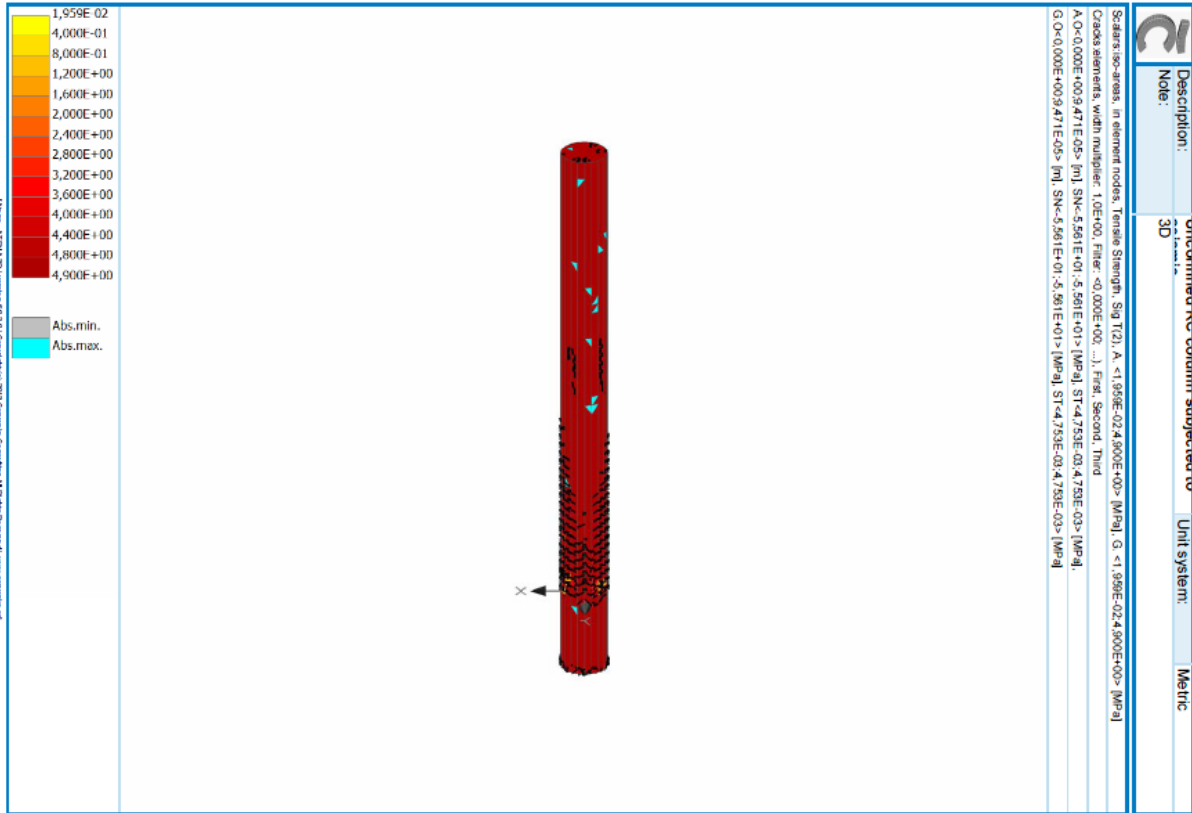


Figure 128 – Specimen Type C3- Atena – Tensile Strength SIG T (2)

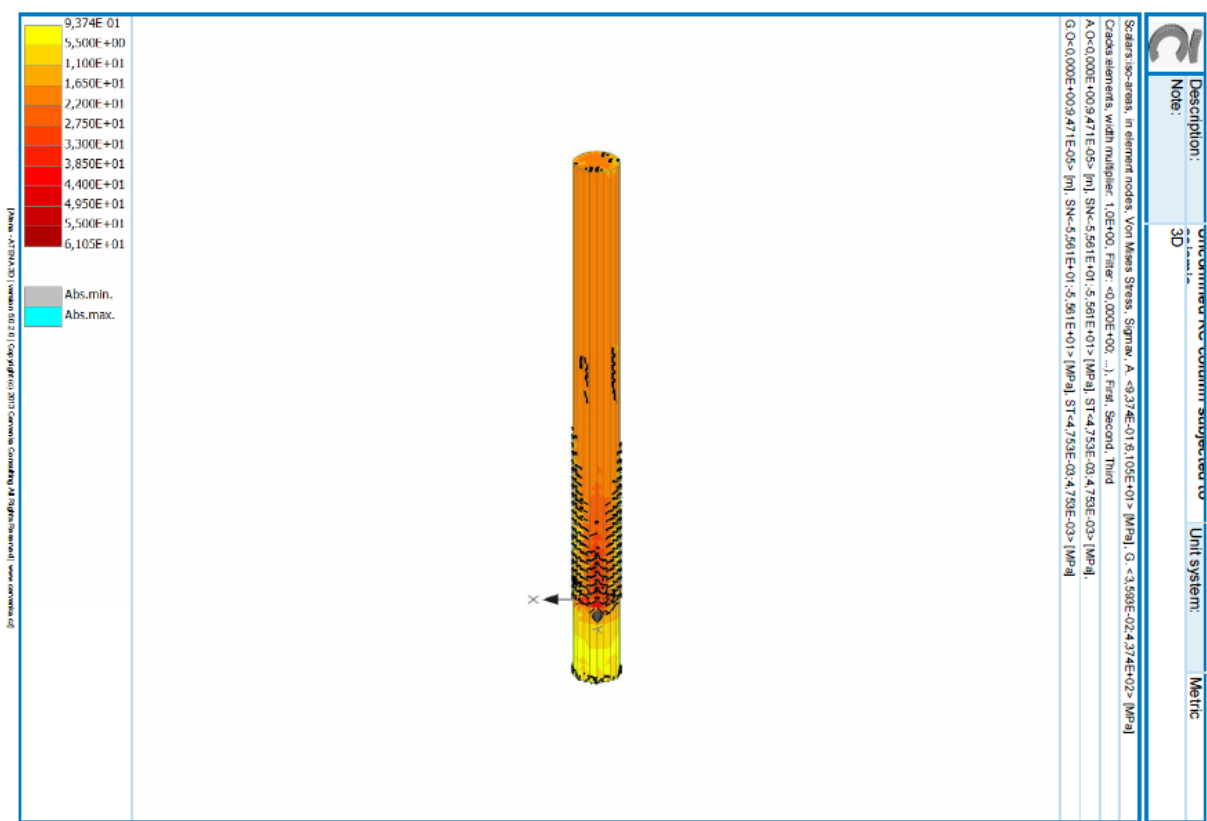


Figure 129 – Specimen Type C3- Atena – Von Mises Stresses in Concrete

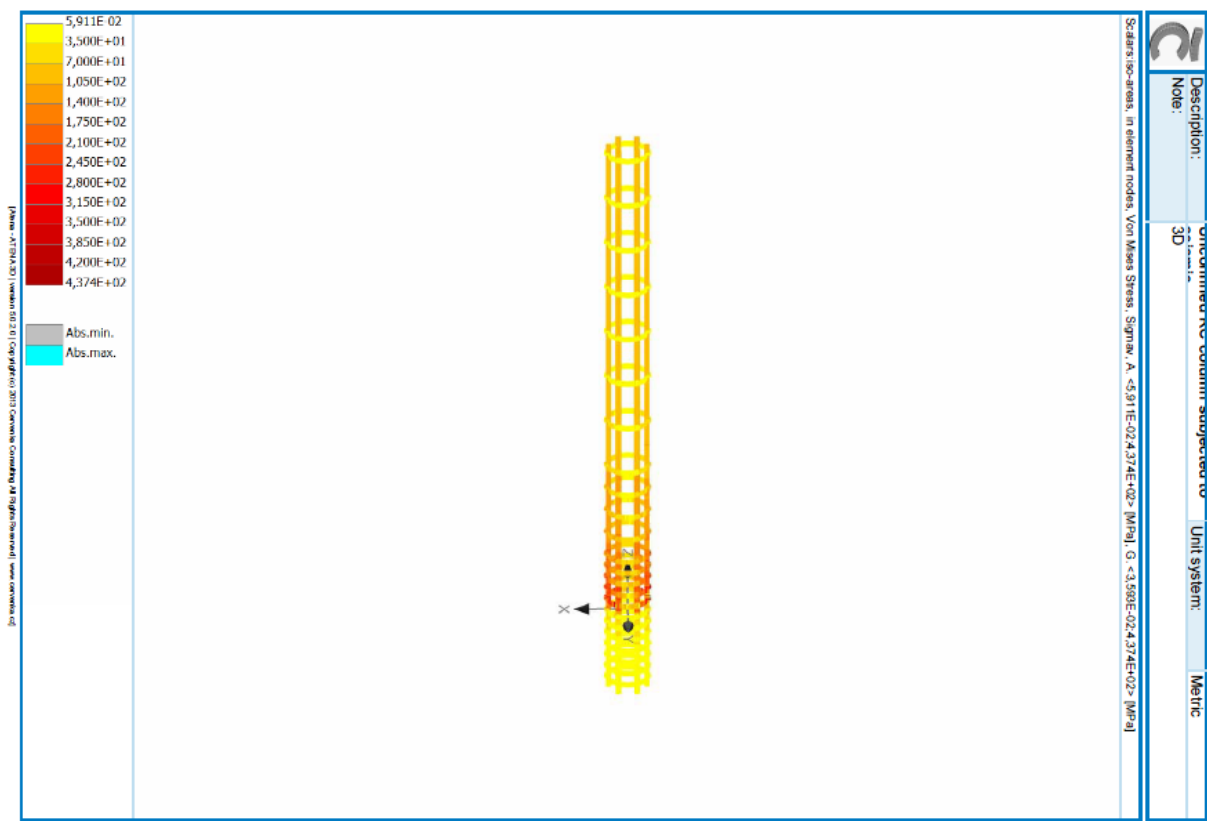


Figure 130 – Specimen Type C3- Atena – Von Mises Stresses in Reinforcements

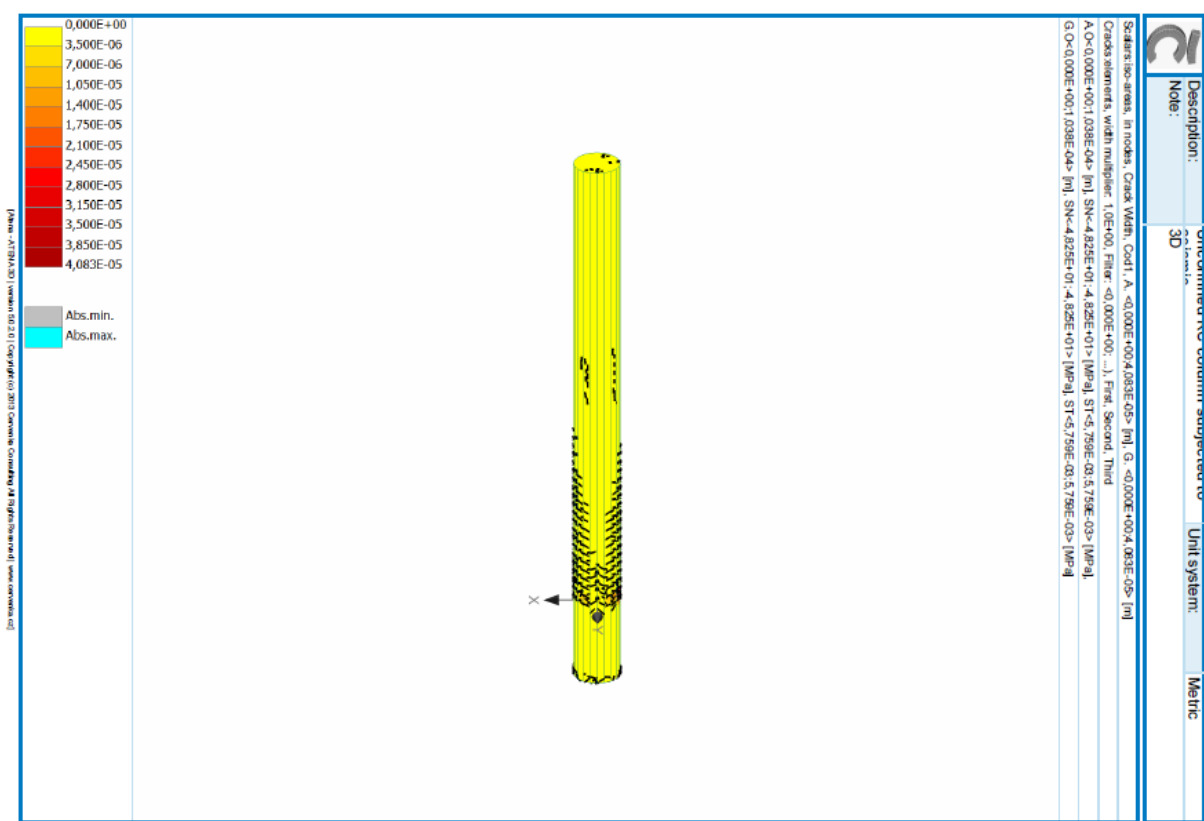


Figure 131 – Specimen Type C4- Atena – Cracks Element

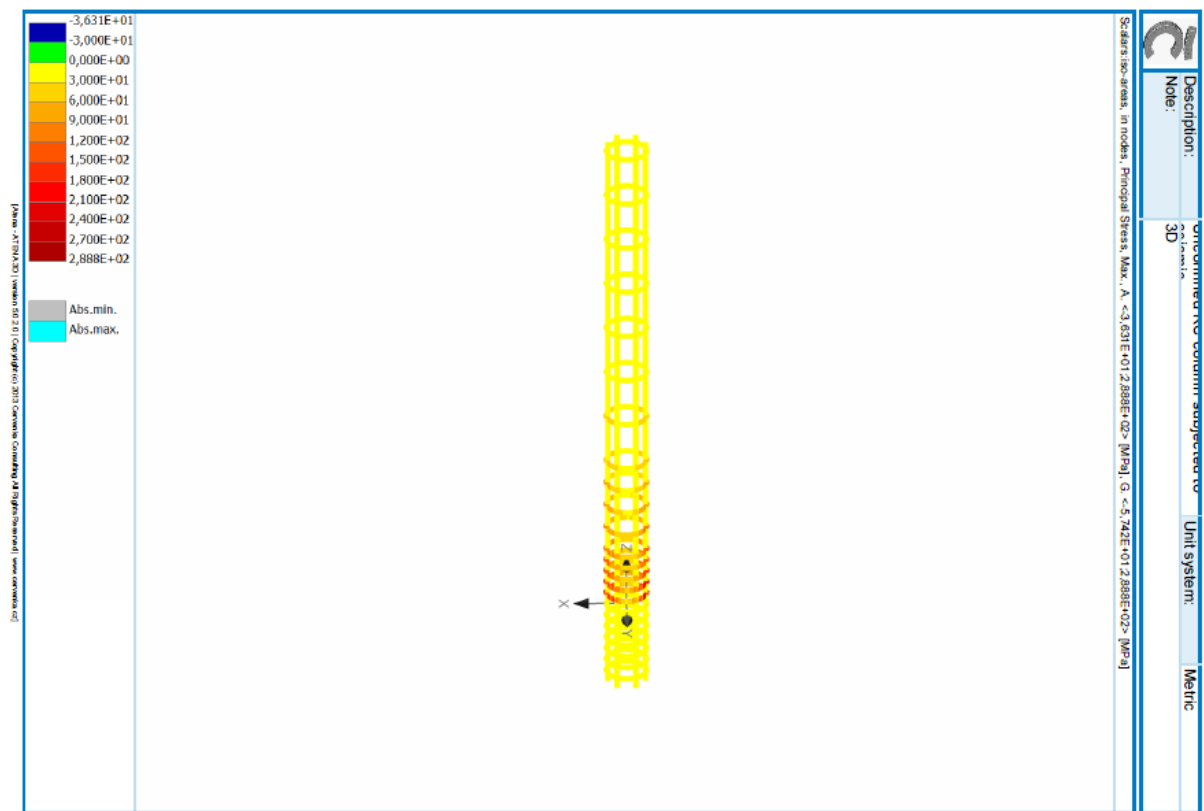


Figure 132 – Specimen Type C4- Atena – Principal Stresses in Reinforcements

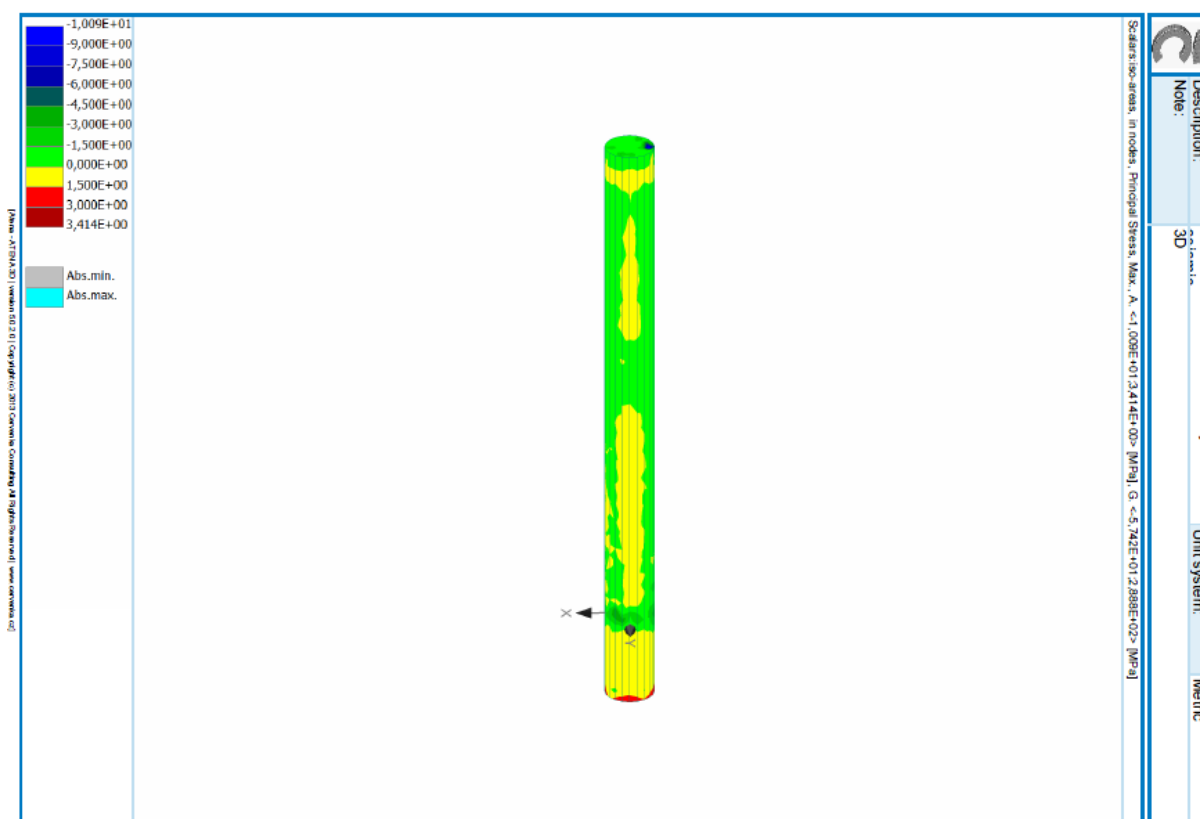


Figure 133 – Specimen Type C4- Atena – Principal Stresses in Concrete

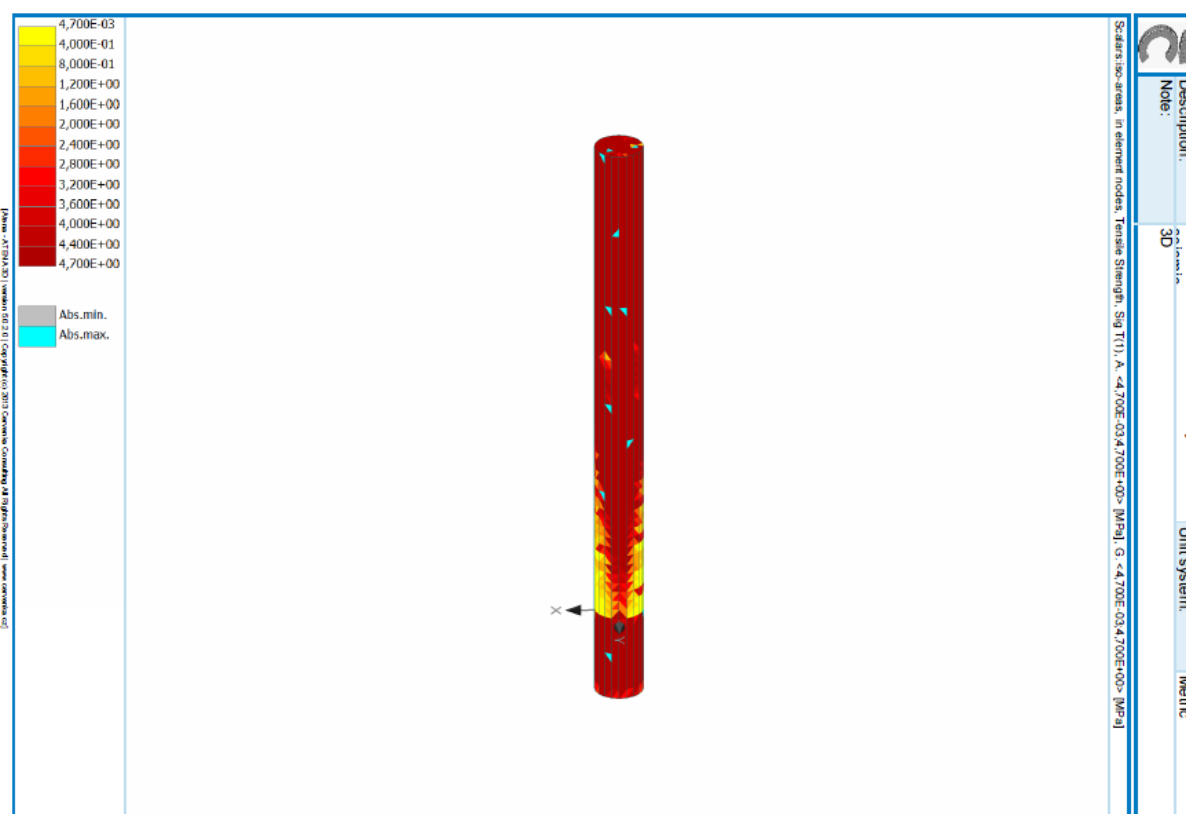


Figure 134 – Specimen Type C4- Atena – Tensile Strength SIG T (1)

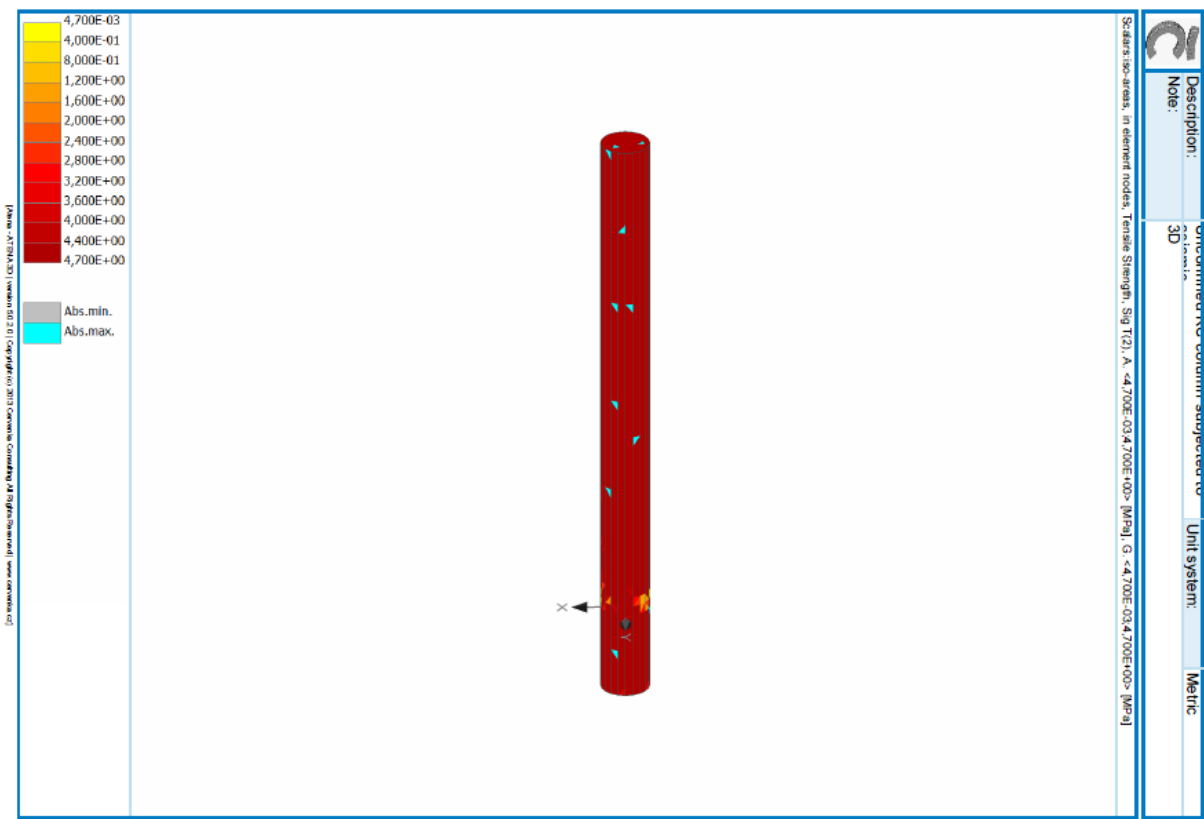


Figure 135 – Specimen Type C4- Atena – Tensile Strength SIG T (2)

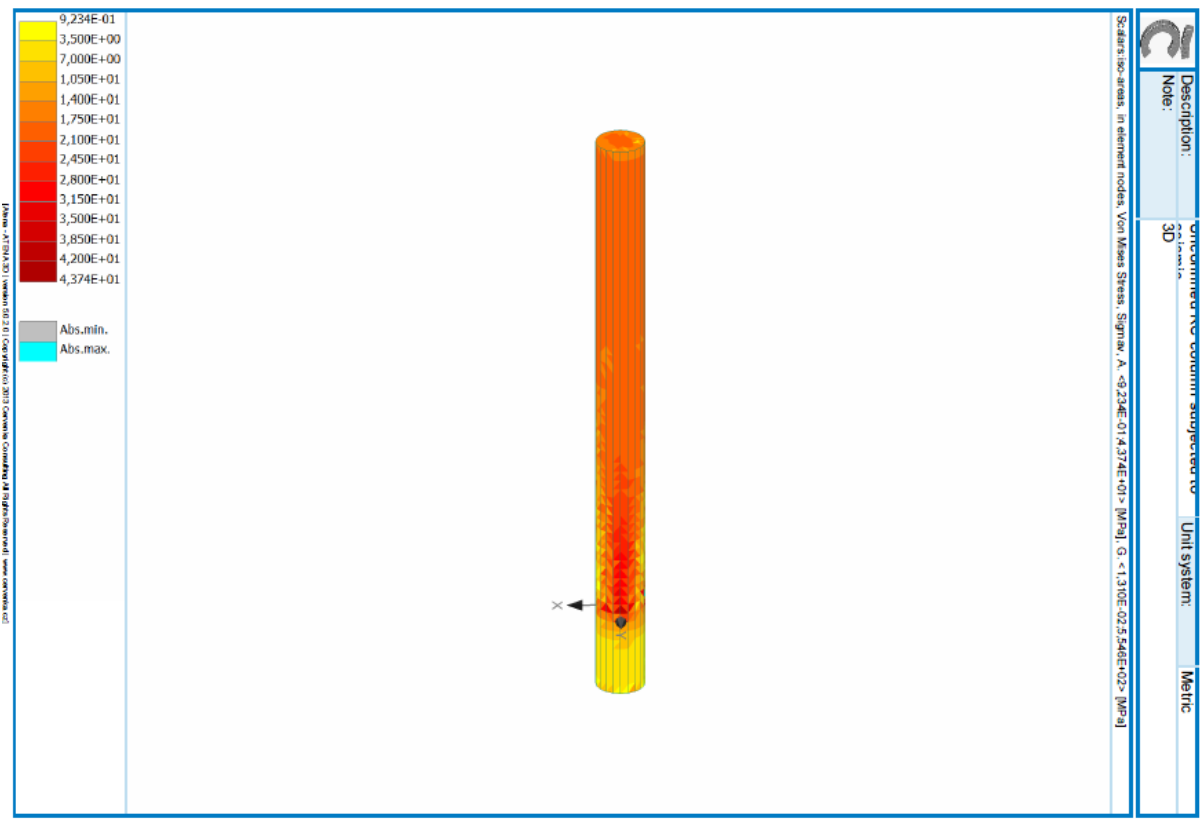


Figure 136 – Specimen Type C4- Atena – Von Mises Stresses in Concrete

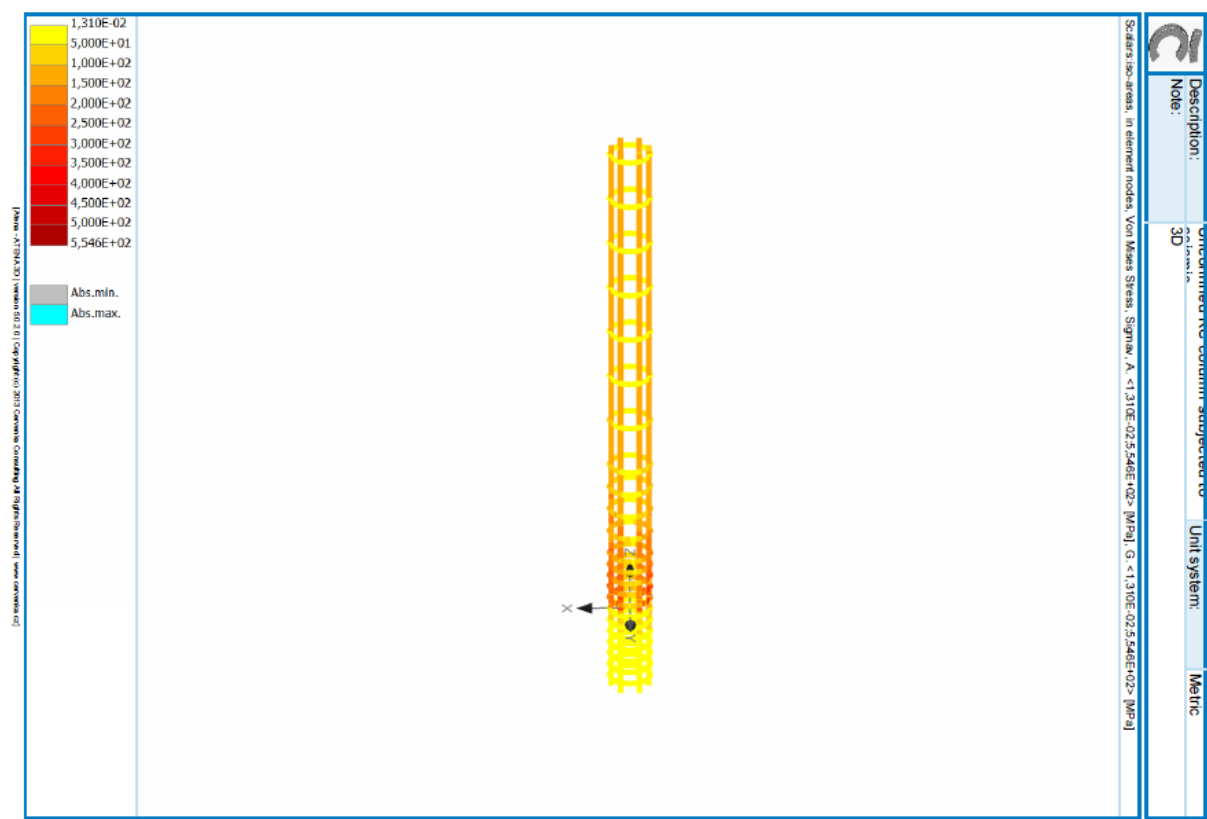


Figure 137 – Specimen Type C4- Atena – Von Mises Stresses in Reinforcements

This software was made to automate the process of calculations needed during design procedure for circular columns in seismic zones.

It consists of entering the given data to a form and get results using three methods:

4. Shear strength Retrofit,
5. Flexural Plastic Hinge Confinement
6. Clamping of Lap Splices.

The software will automate the calculations needed to return the required results.

The Language used is C#.net, was developed using Visual Studio Community 2017 edition, which is a free version of Visual Studio. It can be downloaded at the following link:

<https://www.visualstudio.com/downloads/>

GRAPHICAL USER INTERFACE

Since we have 3 methods, the interface was divided into 3 Tabs, one for each method, having inside each only the related data, the formulas and results of calculations. A **Calculate** button will call all the required functions in the code behind and display the results back to the form.

1. Shear Strength Retrofit Tab

Design Procedure for circular column in seismic zones

Shear Strength Retrofit | Flexural Plastic Hinge Confinement | Clamping of Lap Splices

Data to be entered:

- Compressive strength of concrete (MPa) f_c
- Diameter of longitudinal Bars (mm) db
- Spiral Pitch (spacing of horizontal reinforcement) s
- Carbon Jacket Thickness (mm) t_j
- Diameter of Column (mm) D
- Diameter of Horizontal Bars (mm) ds
- Axial Force (N) P
- Modulus of elasticity of FRP E_f
- Column Displacement Ductility μ_d
- Yielding Strength of Bar (MPa) f_y
- Distance between neutral axis and fiber (mm) e
- Reduction Factor 0.85
- Concrete Cover CC (mm) cc
- Shear crack Inclination (degrees) θ
- Length of column (mm) L

Calculate

Result

Vc Shear Contributed by Concrete

$$\frac{V'_c}{N} = 0.083k \sqrt{\frac{f'_c}{MPa}} \frac{A_g}{mm^2}$$

Vc=

Shear contributed by shear reinforcement

$$V_s = \frac{\pi A_h f_{hy} D'}{2s} \cot \theta \quad (N)$$

where $D' = D - 2cc - db$

Vs=

Nominal Shear Capacity

$$V_n = V_c + V_s + V_p + V_j \geq \frac{V_0}{\phi}$$

Vn=

Shear contributed by FRP jacket

$$V_j = \frac{\pi}{2} f_{ja} t_j D \cot \theta \quad (N)$$

Vj=

Axial Load shear contribution

$$V_p = P \tan \alpha \quad (N)$$

where $\tan \alpha = \frac{D - c}{2L}$

Vp=

Applied Shear Force (N) V_0

Check Safety

Formulas

Design Procedure for circular column in seismic zones

Shear Strength Retrofit Flexural Plastic Hinge Confinement Clamping of Lap Splices

Compressive strength of concrete (MPa) <input type="text"/> f_c	Diameter of longitudinal Bars (mm) <input type="text"/> d_b	Spiral Pitch (spacing of horizontal reinforcement) <input type="text"/> s	Carbon Jacket Thickness (mm) <input type="text"/> t_j
Diameter of Column (mm) <input type="text"/> D	Diameter of Horizontal Bars (mm) <input type="text"/> d_s	Axial Force (N) <input type="text"/> P	Modulus of elasticity of FRP <input type="text"/> E_j
Column Displacement Ductility <input type="text"/> μ_d	Yielding Strength of Bar (MPa) <input type="text"/> f_y	Distance between neutral axis and fiber (mm) <input type="text"/> c	Reduction Factor 0.85 ϕ
Concrete Cover CC (mm) <input type="text"/> cc	Shear crack Inclination (degrees) 45 θ	Length of column (mm) <input type="text"/> L	<input type="button" value="Calculate"/>

Result

Vc Shear Contributed by Concrete

$$\frac{V'_c}{N} = 0.083k \sqrt{\frac{f'_c}{\text{MPa}}} \frac{A_g}{\text{mm}^2}$$

Vc=

Shear contributed by shear reinforcement

$$V_s = \frac{\pi A_h f_{hy} D'}{s} \cot \theta \quad (N)$$

where $D' = D - 2cc - d_b$

Vs=

Nominal Shear Capacity

$$V_n = V_c + V_s + V_p + V_j \geq \frac{V_u}{\phi}$$

Vn=

Shear contributed by FRP jacket

$$V_j = \frac{\pi}{2} f_{jd} t_j D \cot \theta \quad (N)$$

Vj=

Axial Load shear contribution

$$V_p = P \tan \alpha \quad (N)$$

where $\tan \alpha = \frac{D - c}{2L}$

Vp=

Applied Shear Force (N)
 V_0

Checking if thickness is safe, otherwise calculating thickness by changing V0

Results

2. Flexural Plastic Hinge Confinement Tab

The Values to be entered here are needed for this method only; any other value needed should be entered in the previous tab (Shear Strength Retrofit Tab).

If anything is missing when calculate button is pressed, a hint will appear to help show what is missing.

Design Procedure for circular column in seismic zones

Shear Strength Retrofit Flexural Plastic Hinge Confinement **Clamping of Lap Splices**

Tensile strength of FRP jacket (MPa)
 f_{ju}

Strain of FRP jacket (%)
 ϵ_{ju}

Number of Bars
 n

Results

$$t_j = \frac{D f'_c}{5 f_{ju}} \left[0.5 + 1.25 \frac{P}{f'_c A_g} \right] + 0.13 (\rho_\lambda - 0.01) \text{ (mm)} \quad t_{j \min} = \frac{6.9nD}{E}$$

Carbon Jacket Thickness

Result

$$\epsilon_{cu} = 0.004 + \frac{2 \times 1.4 \rho_j f_{ju} \epsilon_{ju}}{f'_{cc}} \quad \text{having} \quad \rho_j = \frac{4t_j}{D}$$

Ultimate Compression Strain

Results

3. Clamping for Lap Splices Tab:

The Values to be entered here are needed for this method only, any other value needed should be entered in the previous tab (Shear Strength Retrofit Tab).

If anything is missing a hint will appear to help show what's missing.

Design Procedure for circular column in seismic zones

Shear Strength Retrofit Flexural Plastic Hinge Confinement **Clamping of Lap Splices**

Lap Splice Length (mm)

 L_s

Inside Crack Perimeter (mm)

 p

Modulus of Steel Bars (MPa)

 E_h

Calculate

Result

$$t_j = 500 \frac{D(f_\lambda - f_h)}{E_j} \text{ (mm)} \quad \text{having} \quad f_\lambda = \frac{A_s f_{sy}}{\left(\frac{p}{2n} + 2(d_b + cc)\right) L_s}$$

$$f_h = \frac{0.002 A_h E_h}{D s}$$

Carbon Jacket Thickness

Result

CODE

Form1.cs

```
1. using DesignProcedure;
2. using System;
3. using System.Collections.Generic;
4. using System.ComponentModel;
5. using System.Data;
6. using System.Drawing;
7. using System.Linq;
8. using System.Text;
9. using System.Threading.Tasks;
10. using System.Windows.Forms;
11. namespace ShearRetrofit {
12.     public partial class Form1: Form {
13.         //defining variables
14.         double diameter;
15.         double fc;
16.         double ductility;
17.         double cc;
18.         double fhy;
19.         int  $\theta$ ;
20.         double spiral_pitch;
21.         double P;
22.         double c;
23.         double L;
24.         double tj_shear;
25.         double Ej;
26.         double fju;
27.         double  $\epsilon_{ju}$ ;
28.         double db;
29.         double ds;
30.         double Vc, Vs, Vp, Vj;
31.         double n;
32.         double p;
33.         double Ls;
34.         double Eh;
35.         double Vn;
36.         //constructor
37.         public Form1() {
38.             InitializeComponent();
39.             CustomToolTip tip = new CustomToolTip();
40.             tip.SetToolTip(label16, "text");
41.             label16.Tag = DesignProcedure.Properties.Resources.ductility; //toolti
p for ductility
42.         }
43.         /*Getting the values for ShearStrengthRetrofit from the form, checking mis
sing values and marking them in Red          * Returns true if all values are entered,
returns false if any value is missing          */
44.         private Boolean getValuesShearStrengthRetrofit() {
45.             bool is_missing = false; //making all labels black
46.             lbl_fc.ForeColor = Color.Black;
47.             lbl_diameter.ForeColor = Color.Black;
48.             lbl_ductility.ForeColor = Color.Black;
49.             lbl_cc.ForeColor = Color.Black;
50.             lbl_db.ForeColor = Color.Black;
```

```
51.         lbl_ds.ForeColor = Color.Black;
52.         lbl_fhy.ForeColor = Color.Black;
53.         lbl_θ.ForeColor = Color.Black;
54.         lbl_spiral_pitch.ForeColor = Color.Black;
55.         lbl_P.ForeColor = Color.Black;
56.         lbl_c.ForeColor = Color.Black;
57.         lbl_L.ForeColor = Color.Black;
58.         lbl_tj.ForeColor = Color.Black;
59.         lbl_Ej.ForeColor = Color.Black;
60.     try {
61.         //checking if this value is entered or blank
62.         if (this.txt_fc.Text.Equals("")) {
63.             is_missing = true; //highlighting label in red
64.             lbl_fc.ForeColor = Color.Red;
65.         } else { //getting the value to a variable
66.             fc = Convert.ToDouble(this.txt_fc.Text);
67.         }
68.         if (this.txt_diameter.Text.Equals("")) {
69.             is_missing = true;
70.             lbl_diameter.ForeColor = Color.Red;
71.         } else {
72.             diameter = Convert.ToDouble(this.txt_diameter.Text);
73.         }
74.         if (this.txt_ductility.Text.Equals("")) {
75.             is_missing = true;
76.             lbl_ductility.ForeColor = Color.Red;
77.         } else {
78.             ductility = Convert.ToDouble(this.txt_ductility.Text);
79.         }
80.         if (this.txt_cc.Text.Equals("")) {
81.             is_missing = true;
82.             lbl_cc.ForeColor = Color.Red;
83.         } else {
84.             cc = Convert.ToDouble(this.txt_cc.Text);
85.         }
86.         if (this.txt_db.Text.Equals("")) {
87.             is_missing = true;
88.             lbl_db.ForeColor = Color.Red;
89.         } else {
90.             db = Convert.ToDouble(this.txt_db.Text);
91.         }
92.         if (this.txt_ds.Text.Equals("")) {
93.             is_missing = true;
94.             lbl_ds.ForeColor = Color.Red;
95.         } else {
96.             ds = Convert.ToDouble(this.txt_ds.Text);
97.         }
98.         if (this.txt_fhy.Text.Equals("")) {
99.             is_missing = true;
100.            lbl_fhy.ForeColor = Color.Red;
101.        } else {
102.            fhy = Convert.ToDouble(this.txt_fhy.Text);
103.        }
104.        if (this.txt_θ.Text.Equals("")) {
105.            is_missing = true;
106.            lbl_θ.ForeColor = Color.Red;
107.        } else {
108.            θ = Convert.ToInt32(this.txt_θ.Text);
109.        }
```



```

110.         if (this.txt_spiral_pitch.Text.Equals("")) {
111.             is_missing = true;
112.             lbl_spiral_pitch.ForeColor = Color.Red;
113.         } else {
114.             spiral_pitch = Convert.ToDouble(this.txt_spiral_pitch.T
ext);
115.         }
116.         if (this.txt_P.Text.Equals("")) {
117.             is_missing = true;
118.             lbl_P.ForeColor = Color.Red;
119.         } else {
120.             P = Convert.ToDouble(this.txt_P.Text);
121.         }
122.         if (this.txt_c.Text.Equals("")) {
123.             is_missing = true;
124.             lbl_c.ForeColor = Color.Red;
125.         } else {
126.             c = Convert.ToDouble(this.txt_c.Text);
127.         }
128.         if (this.txt_L.Text.Equals("")) {
129.             is_missing = true;
130.             lbl_L.ForeColor = Color.Red;
131.         } else {
132.             L = Convert.ToDouble(this.txt_L.Text);
133.         }
134.         if (this.txt_tj.Text.Equals("")) {
135.             is_missing = true;
136.             lbl_tj.ForeColor = Color.Red;
137.         } else {
138.             tj_shear = Convert.ToDouble(this.txt_tj.Text);
139.         }
140.         if (this.txt_Ej.Text.Equals("")) {
141.             is_missing = true;
142.             lbl_Ej.ForeColor = Color.Red;
143.         } else {
144.             Ej = Convert.ToDouble(this.txt_Ej.Text);
145.         }
146.     } catch (Exception) {}
147.     return is_missing;
148. } //end
149. /*Getting the values for FlexuralPlasticHinge from the form, checki
ng missing values and marking them in Red * Returns true if all values are ente
red, returns false if any value is missing * */
150. public Boolean getValuesFlexuralPlasticHinge() {
151.     bool is_missing = false;
152.     lbl_fju.ForeColor = Color.Black;
153.     lbl_ε_ju.ForeColor = Color.Black;
154.     lbl_n.ForeColor = Color.Black;
155.     lbl_diameter.ForeColor = Color.Black;
156.     lbl_db.ForeColor = Color.Black;
157.     lbl_fc.ForeColor = Color.Black;
158.     lbl_Ej.ForeColor = Color.Black;
159.     lblHintFlexural.Visible = false;
160.     try {
161.         if (this.txt_diameter.Text.Equals("")) {
162.             lblHintFlexural.Visible = true;
163.             is_missing = true;
164.             lbl_diameter.ForeColor = Color.Red;
165.         } else {

```

```

166.         diameter = Convert.ToDouble(this.txt_diameter.Text);
167.     }
168.     if (this.txt_db.Text.Equals("")) {
169.         lblHintFlexural.Visible = true;
170.         is_missing = true;
171.         lbl_db.ForeColor = Color.Red;
172.     } else {
173.         db = Convert.ToDouble(this.txt_db.Text);
174.     }
175.     if (this.txt_fc.Text.Equals("")) {
176.         lblHintFlexural.Visible = true;
177.         is_missing = true;
178.         lbl_fc.ForeColor = Color.Red;
179.     } else {
180.         fc = Convert.ToDouble(this.txt_fc.Text);
181.     }
182.     if (this.txt_Ej.Text.Equals("")) {
183.         lblHintFlexural.Visible = true;
184.         is_missing = true;
185.         lbl_Ej.ForeColor = Color.Red;
186.     } else {
187.         Ej = Convert.ToDouble(this.txt_Ej.Text);
188.     }
189.     if (this.txt_fju.Text.Equals("")) {
190.         is_missing = true;
191.         lbl_fju.ForeColor = Color.Red;
192.     } else {
193.         fju = Convert.ToDouble(this.txt_fju.Text);
194.     }
195.     if (this.txt_ε_ju.Text.Equals("")) {
196.         is_missing = true;
197.         lbl_ε_ju.ForeColor = Color.Red;
198.     } else {
199.         ε_ju = Convert.ToDouble(this.txt_ε_ju.Text);
200.     }
201.     if (this.txt_n.Text.Equals("")) {
202.         is_missing = true;
203.         lbl_n.ForeColor = Color.Red;
204.     } else {
205.         n = Convert.ToDouble(this.txt_n.Text);
206.     }
207. } catch (Exception) {}
208. return is_missing;
209. }
210. /*Getting the values for ClampingofLapSplices from the form, checki
ng missing values and marking them in Red * Returns true if all values are ente
red, returns false if any value is missing * */
211. public Boolean getValuesClampingofLapSplices() {
212.     bool is_missing = false;
213.     lbl_perimeter.ForeColor = Color.Black;
214.     lbl_Ls.ForeColor = Color.Black;
215.     lbl_Eh.ForeColor = Color.Black;
216.     lbl_db.ForeColor = Color.Black;
217.     lbl_fhy.ForeColor = Color.Black;
218.     lbl_n.ForeColor = Color.Black;
219.     lbl_cc.ForeColor = Color.Black;
220.     lbl_ds.ForeColor = Color.Black;
221.     lbl_diameter.ForeColor = Color.Black;
222.     lbl_spiral_pitch.ForeColor = Color.Black;

```

```
223.         lbl_Ej.ForeColor = Color.Black;
224.         lblHintClamping.Visible = false;
225.         try {
226.             if (this.txt_db.Text.Equals("")) {
227.                 lblHintClamping.Visible = true;
228.                 is_missing = true;
229.                 lbl_db.ForeColor = Color.Red;
230.             } else {
231.                 db = Convert.ToDouble(this.txt_db.Text);
232.             }
233.             if (this.txt_fhy.Text.Equals("")) {
234.                 lblHintClamping.Visible = true;
235.                 is_missing = true;
236.                 lbl_fhy.ForeColor = Color.Red;
237.             } else {
238.                 fhy = Convert.ToDouble(this.txt_fhy.Text);
239.             }
240.             if (this.txt_n.Text.Equals("")) {
241.                 lblHintClamping.Visible = true;
242.                 is_missing = true;
243.                 lbl_n.ForeColor = Color.Red;
244.             } else {
245.                 n = Convert.ToDouble(this.txt_n.Text);
246.             }
247.             if (this.txt_cc.Text.Equals("")) {
248.                 lblHintClamping.Visible = true;
249.                 is_missing = true;
250.                 lbl_cc.ForeColor = Color.Red;
251.             } else {
252.                 cc = Convert.ToDouble(this.txt_cc.Text);
253.             }
254.             if (this.txt_ds.Text.Equals("")) {
255.                 lblHintClamping.Visible = true;
256.                 is_missing = true;
257.                 lbl_ds.ForeColor = Color.Red;
258.             } else {
259.                 ds = Convert.ToDouble(this.txt_ds.Text);
260.             }
261.             if (this.txt_diameter.Text.Equals("")) {
262.                 lblHintClamping.Visible = true;
263.                 is_missing = true;
264.                 lbl_diameter.ForeColor = Color.Red;
265.             } else {
266.                 diameter = Convert.ToDouble(this.txt_diameter.Text);
267.             }
268.             if (this.txt_spiral_pitch.Text.Equals("")) {
269.                 lblHintClamping.Visible = true;
270.                 is_missing = true;
271.                 lbl_spiral_pitch.ForeColor = Color.Red;
272.             } else {
273.                 spiral_pitch = Convert.ToDouble(this.txt_spiral_pitch.T
ext);
274.             }
275.             if (this.txt_Ej.Text.Equals("")) {
276.                 lblHintClamping.Visible = true;
277.                 is_missing = true;
278.                 lbl_Ej.ForeColor = Color.Red;
279.             } else {
280.                 Ej = Convert.ToDouble(this.txt_Ej.Text);
```

```

281.         }
282.         if (this.txt_perimeter.Text.Equals("")) {
283.             is_missing = true;
284.             lbl_perimeter.ForeColor = Color.Red;
285.         } else {
286.             p = Convert.ToDouble(this.txt_perimeter.Text);
287.         }
288.         if (this.txt_Ls.Text.Equals("")) {
289.             is_missing = true;
290.             lbl_Ls.ForeColor = Color.Red;
291.         } else {
292.             Ls = Convert.ToDouble(this.txt_Ls.Text);
293.         }
294.         if (this.txt_Eh.Text.Equals("")) {
295.             is_missing = true;
296.             lbl_Eh.ForeColor = Color.Red;
297.         } else {
298.             Eh = Convert.ToDouble(this.txt_Eh.Text);
299.         }
300.     } catch (Exception) {}
301.     return is_missing;
302. } //function that calculates Vc: Concrete Contribution
303. private double calculateVc() {
304.     double Vc = 0;
305.     double Ag = Math.PI * Math.Pow(diameter, 2) / 4;
306.     double Ae = Ag * 0.8;
307.     double k;
308.     if (ductility < 2) k = 3;
309.     else if (ductility >= 2 && ductility < 4) k = 5 - ductility;
310.     else if (ductility >= 4 && ductility < 8) k = 1.5 -
ductility / 8;
311.     else k = 0.5;
312.     Vc = 0.083 * k * Math.Sqrt(fc) * Ae;
313.     Vc = Math.Round(Vc, 2);
314.     this.lbl_vc.Text = "Vc= " + Convert.ToString(Vc) + " N";
315.     return Vc;
316. } // Function that calculates Vs : horizontal reinforcing steel con
tribution
317. private double calculateVs() {
318.     double Vs = 0;
319.     double d_prime = diameter - 2 * cc - db;
320.     double ah = Math.PI * Math.Pow(ds, 2) / 4;
321.     double radian = 0 * Math.PI / 180.0;
322.     Vs = Math.PI / 2 * ah * fhy * d_prime * (1 / Math.Tan(radian))
/ spiral_pitch;
323.     Vs = Math.Round(Vs, 2);
324.     this.lbl_vs.Text = "Vs= " + Convert.ToString(Vs) + " N";
325.     return Vs;
326. } // Function that calculates Vp : axial load shear contribution
327. private double calculateVp() {
328.     double VP = 0;
329.     VP = P * (diameter - c) / (2 * L);
330.     VP = Math.Round(VP, 2);
331.     this.lbl_vp.Text = "Vp= " + Convert.ToString(VP) + " N";
332.     return VP;
333. } // Function that calculates Vj : carbon jacket shear retrofit
334. private double calculateVj() {
335.     double VJ = 0;
336.     double fjd = 0.004 * Ej;

```

```

337.         double radian =  $\theta$  * Math.PI / 180.0;
338.         double cotan = 1 / Math.Tan(radian);
339.         VJ = (Math.PI / 2) * fjd * tj_shear * diameter * cotan;
340.         VJ = Math.Round(VJ, 2);
341.         this.lbl_vj.Text = "Vj= " + Convert.ToString(VJ) + " N";
342.         return VJ;
343.     } // Function that calculates Vn: Nominal Shear Capacity
344.     private double calculateVn() {
345.         Vc = calculateVc();
346.         Vs = calculateVs();
347.         Vp = calculateVp();
348.         Vj = calculateVj();
349.         return Vc + Vs + Vp + Vj;
350.     } // Function that calculates thickness for flexural plastic hinge
reinforcement
351.     private double calculateTjPlasticHinge() {
352.         double Ag = Math.PI * Math.Pow(diameter, 2) / 4;
353.         double A = Math.PI * Math.Pow(db, 2) / 4;
354.         double  $\rho_\lambda$  = A / Ag;
355.         double tj_plastichinge = ((diameter * fc) / (5 * fju)) * (0.5 +
1.25 * P / (fc * Ag)) + 0.13 * ( $\rho_\lambda$  - 0.01);
356.         return tj_plastichinge;
357.     } // Function that calculates thickness for lap splice clamping
358.     private double calculateTjLapSpliceClamping() {
359.         double tj = 0;
360.         double As = Math.PI * Math.Pow(db, 2) / 4;
361.         double f $\lambda$  = As * fhy / (((p / (2 * n)) + 2 * (db + cc)) * Ls);

362.         double Ah = Math.PI * Math.Pow(ds, 2) / 4;
363.         double fh = 0.002 * Ah * Eh / (diameter * spiral_pitch);
364.         tj = 500 * diameter * (f $\lambda$  - fh) / Ej;
365.         return tj;
366.     } //button Calculate click event for ShearStrengthRetrofit
367.     private void btnCalculate_Click_1(object sender, EventArgs e) {
368.         this.lblTextResult.Text = "";
369.         this.lbl_vn.Text = "Vn= ";
370.         txt_new_thickness.Text = "";
371.         if (!getValuesShearStrengthRetrofit()) //checking if all values
are entered by calling the function getValuesShearStrengthRetrofit()
372.         {
373.             Vn = calculateVn(); //calling function that calculates Vn
374.             Vn = Math.Round(Vn, 2); //rounding to 2 decimal places
375.             this.lbl_vn.Text = "Vn= " + Convert.ToString(Vn) + " N"; //
showing the values in the form
376.         }
377.     } //Button click event for calculating thickness in shear retrofit
design in case result is UNSAFE
378.     private void btnCalculateThickness_Click(object sender, EventArgs e) {
379.         this.lblTextResult.Text = "Calculating...";
380.         if (!this.txtV0.Text.Equals("")) { //getting V0 and  $\phi$  values
381.             double V0 = Convert.ToDouble(this.txtV0.Text);
382.             double  $\phi$  = Convert.ToDouble(this.txt_ $\phi$ .Text);
383.             this.lblTextResult.Text = "";
384.             txt_new_thickness.Text = ""; //comparing
385.             if (Vn >= (V0 /  $\phi$ )) {
386.                 panelResult.Visible = false;
387.                 this.lblTextResult.Text = "SAFE";
388.             } else {

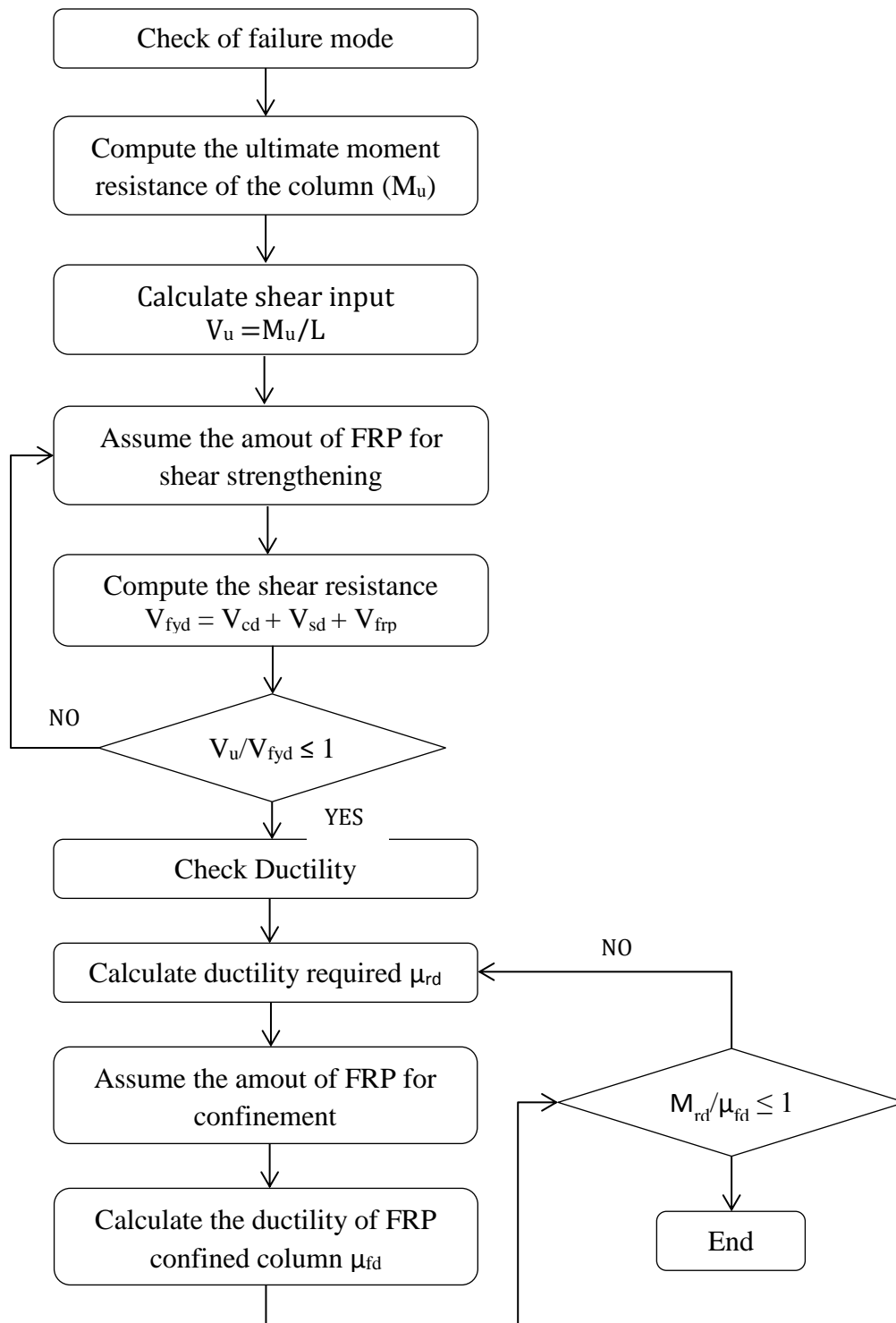
```

```

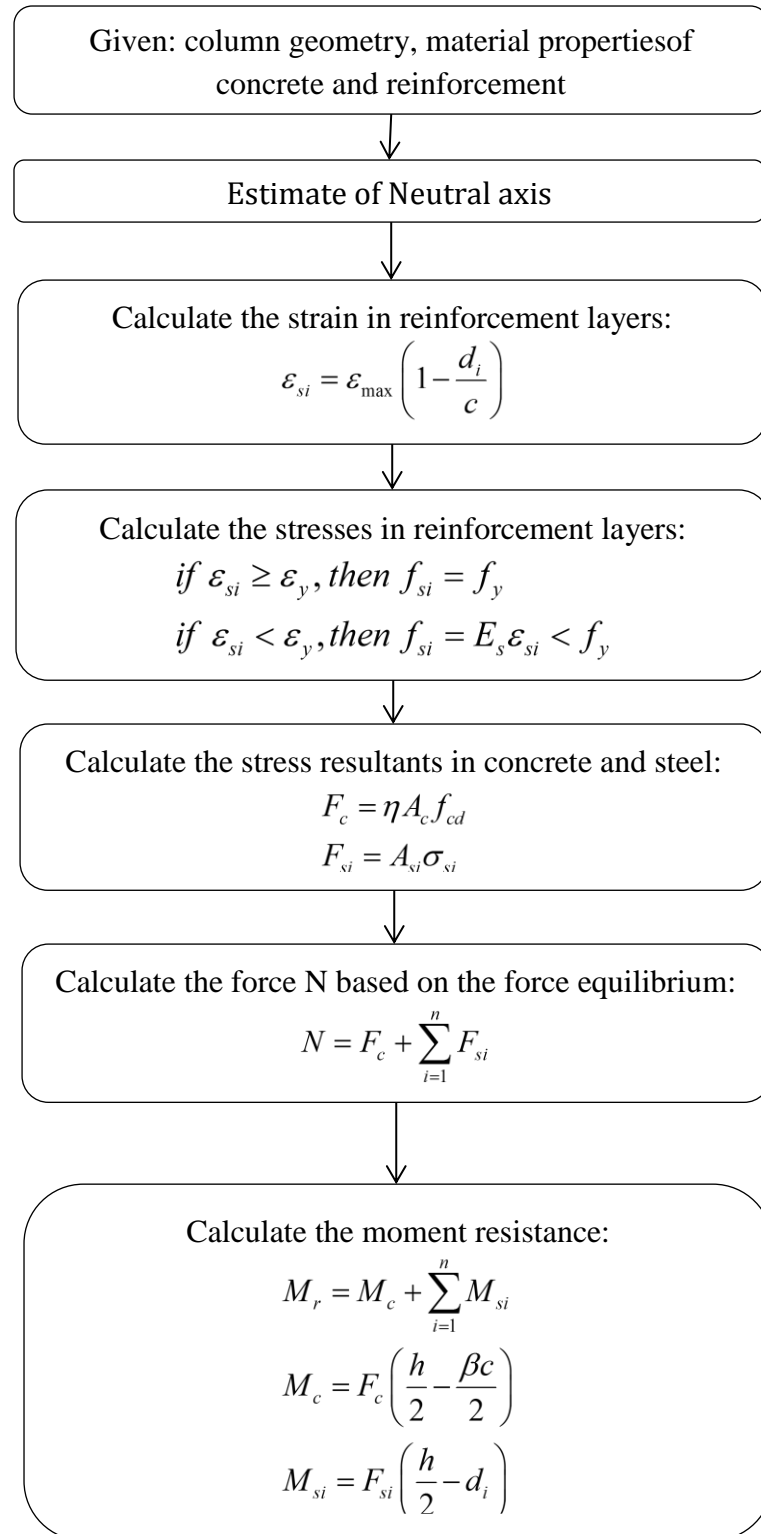
389.         panelResult.Visible = true;
390.         this.lblTextResult.Text = "UNSAFE";
391.         double new_tj = (V0 / φ -
(Vc + Vs + Vp)) / ((Math.PI / 2) * 0.004 * Ej * diameter);
392.         new_tj = Math.Round(new_tj, 2);
393.         txt_new_thickness.Text = Convert.ToString(new_tj) + " m
m";
394.     }
395. }
396. } //Button Calculate Click event for Flexural Plastic Hinge Confine
ment
397. private void btnCalculateflexural_Click(object sender, EventArgs e) {
398.     if (!getValuesFlexuralPlasticHinge()) //checking if all values
are entered by calling the function getValuesFlexuralPlasticHinge()
399.     {
400.         double tj = calculateTjPlasticHinge(); //calculating
401.         double roundTj = Math.Round(tj, 2); //rounding
402.         this.lbl_tj_plastic_hinge.Text = Convert.ToString(roundTj)
+ " mm"; //showing
403.         double minimum = 6.9 * n * diameter / Ej; //calculating min
imum thickness
404.         this.lblResultFelxuralHinge.Visible = false; //comparing th
ickness to minimum
405.         if (tj < minimum) {
406.             this.lblResultFelxuralHinge.Visible = true;
407.             this.lblResultFelxuralHinge.Text = "Thickness is lower
than minium. Minimum Thickness= " + Math.Round(minimum, 2) + " mm";
408.         }
409.         double pj = 4 * tj / diameter;
410.         double εcu = 0.004 + (2 * 1.4 * pj * fju * ε_ju) / (1.5 * f
c);
411.         this.lblResult_εcu.Text = Convert.ToString(εcu) + " N";
412.     }
413. } //Button click for calculation of Clamping of Lap Splices
414. private void btnCalculateClamping_Click(object sender, EventArgs e) {
415.     if (!getValuesClampingofLapSplices()) //checking if all values are
entered by calling the function getValuesClampingofLapSplices()
416.     {
417.         double tj = calculateTjLapSpliceClamping(); //calculating
418.         tj = Math.Round(tj, 2); //rounding
419.         this.lbl_tj_clamping.Text = Convert.ToString(tj) + " mm"; //sho
wing
420.     }
421. }
422. }
423. }

```

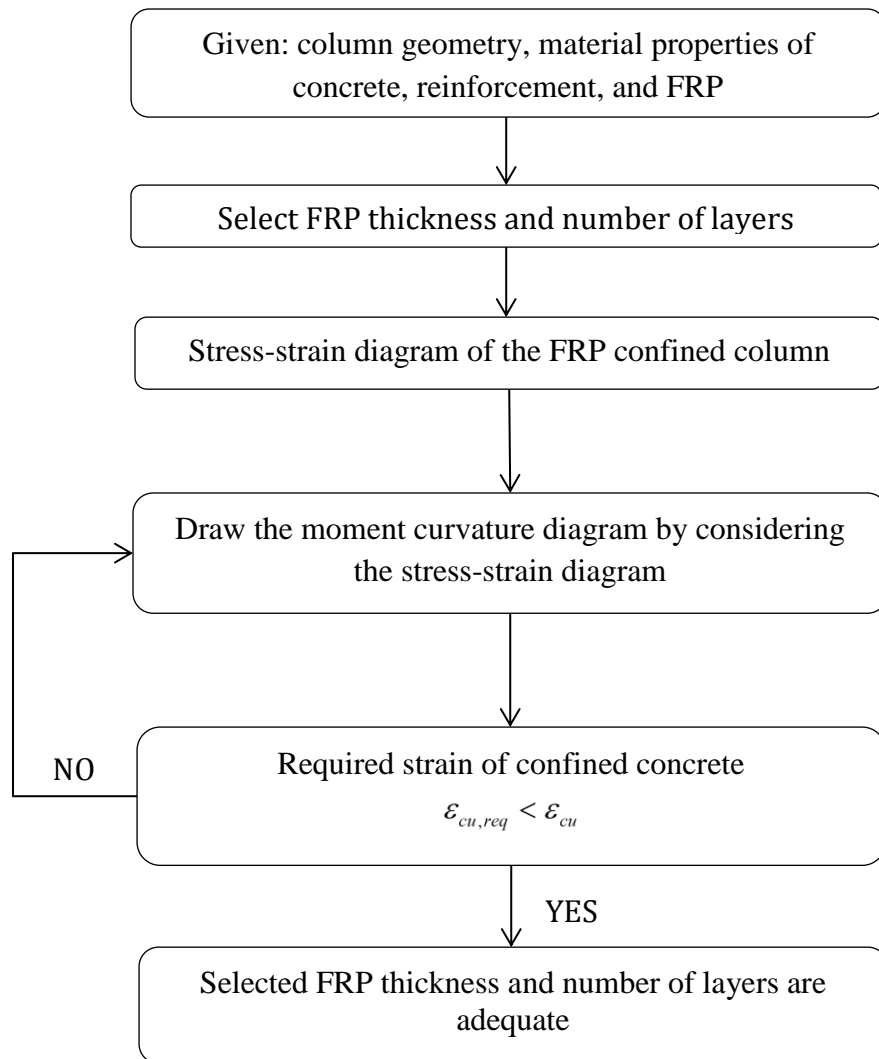
FLOW CHARTS



Flowchart to calculate ductility of confined columns



Flowchart to plot interaction diagram of column



Flowchart to design FRP based on the required strain of concrete

REFERENCES

- [1] ČSN EN 1992-1-1 (73 1201), “Design of concrete structures”. Part 1-1: General Rules and Rules for Buildings.
- [2] ACI 440.2R-02, “Guide for the Design and Construction of Externally Bonded FRP Systems for Strengthening Concrete Structures”, ISBN 0-87031-088-7
- [3] EN 1998-3-3, “Design of Structures for Earthquake Resistance”. Part 3: Strengthening and Repair of Buildings.
- [4] FIB Bulletin, “Design and Use of Externally Bonded FRP Reinforcement (FRP EBR) for Reinforced Concrete Structures”. Bulletin no. 14, prepared by sub-group EBR (Externally Bonded Reinforcement) of fib Task Group 9.3 ‘FRP Reinforcement for Concrete Structures’ (2001).
- [5] FIB Bulletin no. 65, “Model Code 2010 Volume 1, 2”, International Federation for Structural Concrete, 2010, Lausanne, Switzerland, ISBN 978-2-88394-105-2
- [6] Technical report no. 55, “Design Guidance for Strengthening Concrete Structures using Fibre Composite Materials”. UK: The Concrete Society; 2000.
- [7] Hernandez-Barrioas H., Jara J.M., Jara M., “Revision Constitutive Models for Repair of Bridge Columns with Fibre Polymers”, International Journal of Engineering, Science and Technology vol.3, No.4, 2011, pp.48-64.
- [8] Cusson, D., and Paultre, P., “Stress-Strain Model for Confined High Strength Concrete”, Journal of Structural Engineering, 121(3), pp.468-477.
- [9] Lam, L., and Teng, J.G.,” Design-Oriented Stress-Strain Model for FRP-Confined Concrete”, Construction Building Materials, 17(6-7), 2003, pp.471-489.
- [10] Prochazka, J. et al.,”Design of Concrete Structures 1: Elements from Plain and Reinforced Concrete”, 3.edition, Prague: CBS Servis, s.r.o. 2009. ISBN 978-80-903807-5-2.
- [11] N.Chikh, M.Gahmous, R.Benzaid, ”Structural Performance of High Strength Concrete Columns Confined with CFRP Sheets”, Proceedings of the World Congress on Engineering 2012 vol.3, WCE 2012, July 4-6, 2012, London, U.K..
- [12] Seible, F.; Priestley, M. J. N.; Chai, Y. H. (1995). “Earthquake Retrofit of Bridge Columns with Continuous Carbon Fibre Jackets”, Advanced Composites Technology Transfer consortium, Report No. ACTT-95/08, La Jolla, California.
- [13] Fardis MN, Khalili H. “FRP-Encased Concrete as a Structural Material”. Magazine of Concrete Research 1982; 34 (122):191–202.
- [14] Spoelstra M.R., Monti G. “FRP-Confined Concrete Model”. Journal of Composites for Construction 1999; 3(3):143–50.
- [15] Mander J.B., Priestley M.J.N., Park R. “Theoretical Stress–Strain Model for Confined Concrete”. ASCE Journal of Structural Engineering 1988; 114(8):1804–26.
- [16] Walker A.R., Karbhari I M.V. “Durability Based Design of FRP Jackets for Seismic Retrofit”. Composite Structures 80 (2007) 553-568.

- [17] Červenka, V., Červenka, J.: ATENA Program Documentation – ATENA 3D User's manual, Červenka Consulting, Prague, 2011.
- [18] Červenka, V., Jendele, L., Červenka, J.: ATENA Program Documentation – ATENA Theory, Červenka Consulting, Prague, 2012.
- [19] Azadeh Parvin, Wei Wang, "Concrete Columns Confined by Fibre Composite Wraps under Combined Axial and Cyclic Lateral Loads" *Composite Structures* 58 (2002) 539-549.
- [20] T.L.Attard, C.M.Abel, K.Dhiradhamvit, "Seismic FRP Retrofit of Circular Column Bents using a Ductility Wrap Envelope to alter Failure modes", *Engineering Structures* 33 (2011) 1553-1564.
- [21] Ozbakkaloglu, T., and Saatcioglu, M. (2006). "Seismic Behaviour of High-Strength Concrete Columns Confined by Fibre Reinforced Polymers Tubes", *Journal of Composites for Construction*, ASCE, 10(6), 538-549.
- [22] Ozbakkaloglu, T., and Saatcioglu, M. (2007). "Seismic Performance of Square High-Strength Concrete Columns in FRP Stay-in-place Formwork", *Journal of Structural Engineering*, ASCE, 133(1), 44-56.
- [23] Chai, Y.-H., Priestley, M. J. N., and Seible, F., 1991a, "Flexural Retrofit of Circular Reinforced Concrete Bridge Columns by Steel Jacketing- COLRET-A Computer Program for Strength and Ductility Calculation," Report No. SSRP 91-07, Department of Applied Mechanics and engineering Science, University of California at San Diego, La Jolla, CA, USA.
- [24] Chai, Y.-H., Priestley, M. J. N., and Seible, F., 1991b, "Flexural Retrofit of Circular Reinforced Concrete Bridge Columns by Steel Jacketing-Experimental Study," Report No. SSRP 91-06, department of Applied Mechanics and Engineering Science, University of California at San Diego, La Jolla, CA, USA.
- [25] Bart J. Bett, Richard E. Klingner, James O.Jirsa, "Behaviour of Strengthened and Repaired Reinforced Concrete Columns under Reversed Cyclic Deformations", PMFSEL Report no. 85-3, Phil M.Ferguson Structural Engineering Laboratory, The University of Texas at Austin, 1985.
- [26] National Research Council, "Guide for the Design and Construction of EB FRP Systems for Strengthening Existing Structures", CNR-DT 200/2004, Rome-CNR July 13th, 2004.
- [27] Richart, F. E., Brandtzaeg, A., and Brown, R. L., 1928. "A Study of the Failure of Concrete under Combined Compressive Stresses." *University of Illinois Bulletin*, 185.
- [28] M. Shahawy, A. Mirmiran, T. Beitelman, "Tests and Modelling of Carbon-Wrapped Concrete Columns", *Composites Part B: Engineering*, Volume 31, issues 6-7, October 2000, p.p. 471-480
- [29] Cui Ciyan, "Behaviour of Normal and High Strength Concrete Confined with Fibre Reinforce Polymers (FRP)", PhD Thesis, Department of Civil Engineering, University of Toronto, 2009.
- [30] Xiao Y., Whu H., "Compressive Behaviour of Concrete Confined by Various Types of FRP Composite Jackets", *Journal of Reinforced Plastics and Composites*, 22(13), p.p. 1187-1201, 2003b.
- [31] O. Ozcan, B. Binici, G. Ozcebe, "Improving Seismic Performance of Deficient Reinforced Concrete Columns using Carbon Fibre-Reinforced Polymers", *Engineering Structures* 30, 2008, p.p. 1632-1646.

- [32] Sheikh S.A., Yau G., “Seismic Behaviour of Concrete Columns Confined with Steel and Fibres Polymers”, *ACI Structural Journal* 2002, 99(1), p.p. 72-80.
- [33] Miyauchi, K., Inoue, S., Kuroda, T., and Kobayashi, A. (1999). “Strengthening Effects of Concrete Columns with Carbon Fiber Sheet.” *Trans. Japan Concrete Inst.*, 21, 143-150.
- [34] Theriault M., Neale KW, Claude S., “Fibre Reinforced Polymer Confined Circular Concrete Columns: Investigation of Size and Slenderness Effects”, *Journal Composites Construction* 2004; 8; p.p. 313-323.
- [35] T.Jiang, J.G.Teng, “Theoretical Model for Slender FRP-Confined Circular RC Columns”, *Constructions and Building Materials*, volume 32, July 2012, p.p. 66-76.
- [36] Diab H., Wu Z., “Nonlinear Constitutive Model for Time-Dependent Behaviour of FRP-Concrete Interface”, *Composites Science and Technology* 67; 2007; p.p. 2323-2333.
- [37] Al-Salloum YA., “Influence of Edge Sharpness on the Strength of Square Concrete Columns Confined with FRP Composite Laminates”, *Composites Part B: Engineering* 2007;38: p.p. 640-650.
- [38] M. N. Fardis and H. Khalili “Concrete Encased in Fiberglass Reinforced Plastic”, *ACI Journal*, 8:6 (1981), p.p.440–446.
- [39] M. N. Fardis and H. Khalili, “FRP-Encased Concrete as a Structural Material”, *Magazine of Concrete Research*. (34)121 (1982), p.p.191–202.
- [40] Samaan, M., Mirmiran, A., and Shahawy, M. (1998). "Model of Concrete Confined by Fiber Composites." *Journal of Structural Engineering*, 124(9), p.p.1025-1031.
- [41] Toutanji, H.A. (1999). "Stress-strain Characteristics of Concrete Columns Externally Confined with Advanced Fibre Composite Sheets." *ACI Material Journal*, 96(3), 397-404.
- [42] *Design of Reinforced Concrete Structures*, Second Edition 2008, Volume 2, Mashhour Ghoneim and Mahmoud El-Mihilmy.
- [43] *Solution Procedure for Non-Linear Finite Elements Equations*, Project Report, ECI 284, 2003, Ritu Jan, University of California, Davis.
- [44] *Displacement Based Methods, Advanced Earthquake Engineering*, Ecole Polytechnique Federale De Lausanne, 2005.
- [45] L.A.Bisby, ISIS Canada, Educational Module 2 “An Introduction to FRP Composite for Construction”, Department of Civil Engineering, Queen’s University, March 2006.
- [46] *Structural Strengthening Material*, Shanghai Horse Construction, www.horseen.com.
- [47] Zeynep Firat Alemdar, “Plastic Hinging Behavior of Reinforced Concrete Bridge Columns”, PhD thesis, Univeristy of Kansas, April 2010.
- [48] Product Datasheet of SikaWrap-600C/120-Stitched unidirectional carbon fiber fabric, designed for structural strengthening applications as part of the Sika strengthening system.
- [49] Product Datasheet of Sikadur 300, 2-Components Epoxy Impregnation Resin.
- [50] Product Datasheet of Groutex 603, Non-shrinking cement based grouts. PROFIMAT s.r.o..

[51] Method statement of SikaWrap - Manual wet Applications – No. 8504103

[52] Anders Carolin, "Carbon Fibre Reinforced Polymers For Strengthening Of Structural Elements" – Doctoral Thesis 2003:18 – Department Of Civil and Mining Engineering, Lulea University, Sweden

[53] Richart, F. E., Brandtzaeg, A., and Brown, R. L., 1929. "The Failure of plain and spirally reinforced Concrete in Compression." Bulletin No.190, Engineering Experiment Station, University of Illinois.

LIST OF FIGURES

<i>Figure 1 - Stress-strain relationship of fiber, matrix and FRP [26]</i>	19
<i>Figure 2 - Stress-strain diagram for fibers & reinforcement steel [2]</i>	20
<i>Figure 3 - Concrete jacketing of circular & square columns [46]</i>	22
<i>Figure 4 - Steel jacketing of circular & square columns [46]</i>	23
<i>Figure 5 - FRP jacketing of columns [45]</i>	24
<i>Figure 6 - Passive and active confinement of column cross-section</i>	25
<i>Figure 7 - Confining action of FRP</i>	26
<i>Figure 8 - Stress-strain response [28]</i>	28
<i>Figure 9 - Effectively confined core of non-circular section [26]</i>	30
<i>Figure 10 - Concrete confined with FRP strips [26]</i>	30
<i>Figure 11 - Stress-strain response of FRP confined concrete [40]</i>	34
<i>Figure 12 - Stress-strain response of FRP confined concrete [41]</i>	35
<i>Figure 13 - Stress-strain response for FRP confined concrete [9]</i>	38
<i>Figure 14 - Strengthening and confinement ratio</i>	41
<i>Figure 15 - Stress-strain diagram HPC 90/105 [1]</i>	42
<i>Figure 16 - Shear, plastic hinge, and lap splice failure modes of column [7]</i>	44
<i>Figure 17 - Single and double bending retrofit region [12]</i>	46
<i>Figure 18 – a) Envelope of actual and idealized structural response, b) Moment rotation curve, c) Moment curvature curve [44]</i>	48
<i>Figure 19 - Ductility and Confinement Pressure Diagram</i>	50
<i>Figure 20 - Yielding chord rotation [44]</i>	55
<i>Figure 21 - Plastic hinge length [44]</i>	55
<i>Figure 22 - Ultimate chord rotation [44]</i>	56
<i>Figure 23 - Geometry of test specimens [32]</i>	57
<i>Figure 24 - Test setup [32]</i>	58
<i>Figure 25 - Specified displacement history [32]</i>	58
<i>Figure 26 - Geometry of columns [21]</i>	60
<i>Figure 27 - Test setup [21]</i>	61
<i>Figure 28 - Geometry of test specimens [31]</i>	62
<i>Figure 29 - Test setup [31]</i>	64
<i>Figure 30 - Interaction diagram of columns [42]</i>	67
<i>Figure 31 - Cross section of unconfined circular columns</i>	69
<i>Figure 32 - Circular column cross-section</i>	70
<i>Figure 33 - Cross sections of confined circular columns with FRP</i>	71
<i>Figure 34 - N-M diagram of RC circular column wrapped with FRP in hoop direction</i>	74
<i>Figure 35- N-M diagram of RC column wrapped with multi-layers of FRP based on Eurocode</i> ..	74
<i>Figure 36 - Shear and moment diagrams of cantilever columns</i>	75
<i>Figure 37 - Moment Curvature Diagram- Column type C1- Unconfined</i>	78
<i>Figure 38 - Moment Curvature Diagram- Column type C1- Confined by spiral</i>	79
<i>Figure 39 - Moment Curvature Diagram- Column type C1- Confined by spiral & wrap</i>	80
<i>Figure 40 - Moment Curvature Diagram- Column type C1- Unconfined-Fatigue</i>	81

<i>Figure 41 - Moment Curvature Diagram- Column type C1- Confined by spiral-Fatigue</i>	<i>82</i>
<i>Figure 42 - Moment Curvature Diagram-Column type C1-Confined by spiral & wrap-Fatigue...</i>	<i>83</i>
<i>Figure 43 - Comparison of Moment vs. Curvature diagrams for test specimen C1</i>	<i>84</i>
<i>Figure 44 - Interaction between displacement and curvature ductility factors based on equation [52].....</i>	<i>86</i>
<i>Figure 45 - The manufacturing of the circular columns.....</i>	<i>87</i>
<i>Figure 46 - The geometry of circular columns</i>	<i>88</i>
<i>Figure 47- Core Test Specimens of Circular Columns</i>	<i>89</i>
<i>Figure 48 - Preparation of RC columns surface</i>	<i>91</i>
<i>Figure 49 - Preparation of CFRP confined column</i>	<i>92</i>
<i>Figure 50 - Steel pocket footing a) computer model, b) realization.....</i>	<i>93</i>
<i>Figure 51 - RC column encased by steel footing</i>	<i>94</i>
<i>Figure 52 - Arrangement of transverse beam, load cell and hydraulic jack</i>	<i>95</i>
<i>Figure 53 - Connection of tie rod to steel footing</i>	<i>96</i>
<i>Figure 54 - 1st phase: loading history program of high-cycle test, 10⁶ cycles.....</i>	<i>96</i>
<i>Figure 55 - 2nd phase: loading history program of low-cycle test (Displacement vs number of cycles).....</i>	<i>97</i>
<i>Figure 56 - Test set up 2D view</i>	<i>98</i>
<i>Figure 57 - Test set-up.....</i>	<i>99</i>
<i>Figure 58 - Columns Surface a) Number of FRP layers, b) Strain gauges location.....</i>	<i>101</i>
<i>Figure 59 - LVDTs locations, a) high-cycle loading test, b) low-cycle loading test</i>	<i>102</i>
<i>Figure 60 - Static scheme of column with fully fixed support at one end</i>	<i>103</i>
<i>Figure 61 – a) deformation and uplift due to 1st order analysis b) deformation due to 2nd order analysis c) final status.....</i>	<i>104</i>
<i>Figure 62 - Lateral force (Fx) vs. displacement (X) for unstrengthen column C1 (high-cycle loading test)</i>	<i>107</i>
<i>Figure 63 – high-cycle loading test configuration for unstrengthen column C1</i>	<i>109</i>
<i>Figure 64 - Moment diagrams of specimen C1 at 2x10⁵ cycles</i>	<i>111</i>
<i>Figure 65 - Moment diagrams of specimen C1 at 1x10⁶ cycles</i>	<i>111</i>
<i>Figure 66 - Failure of Specimen C1; a) Exposing of reinforcement, b) Cracks and damage</i>	<i>113</i>
<i>Figure 67 – low cycle loading test configuration for unstrengthen column C1</i>	<i>113</i>
<i>Figure 68 - Lateral force (Fx) vs. displacement (V1) Hysteresis curve for unstrengthen specimen C1 (low-cycle loading test).....</i>	<i>114</i>
<i>Figure 69 - Lateral force (Fx) vs. uplift of column base (V3) for unstrengthen specimen C1</i>	<i>114</i>
<i>Figure 70 - Lateral force (Fx) vs. displacement (X) for column type C2 (high-cycle loading test)</i>	<i>116</i>
<i>Figure 71 - Lateral force (Fx) vs. displacement (X) for type C3 (high-cycle loading test).....</i>	<i>117</i>
<i>Figure 72 - Moment diagrams of specimen C2 at 2x10⁵ cycles</i>	<i>120</i>
<i>Figure 73 - Moment diagrams of specimen C2 at 1x10⁶ cycles</i>	<i>120</i>
<i>Figure 74 - Moment diagrams of specimen C3 at 2x10⁵ cycles</i>	<i>121</i>
<i>Figure 75 - Moment diagrams of specimen C3 at 1x10⁶ cycles</i>	<i>121</i>
<i>Figure 76 - Specimen C2 and C3 a) High-cycle loading test, b) Reversed cyclic loading test and corresponding schemes.....</i>	<i>123</i>

<i>Figure 77 - Lateral force (Fx) vs. Displacement (V1) Hysteresis curve for specimen C2</i>	124
<i>Figure 78 - Lateral force (Fx) vs. uplift of column base (V3) for specimen C2</i>	124
<i>Figure 79 - Lateral force (Fx) vs. Displacement (V1) - Hysteresis curve for specimen C3</i>	125
<i>Figure 80 - Lateral force (Fx) vs. uplift of column base (V3) for specimen C3</i>	125
<i>Figure 81 - Failure of specimen C4- Development of cracks</i>	126
<i>Figure 82 - Lateral force vs. Displacement-Hysteresis curve for specimen C4</i>	127
<i>Figure 84 - Newton-Raphson method of nonlinear analysis [43]</i>	130
<i>Figure 85 - Arc length method [43]</i>	131
<i>Figure 86 - Boundary Conditions – Column Type C4</i>	133
<i>Figure 87 - Hysteresis Diagram– Column Type C4 - Atena (Elastic Behavior)</i>	134
<i>Figure 88 - Force-Displacement Envelope Diagrams for all specimens-Experimental</i>	136
<i>Figure 89 - Energy Dissipation in a cycle of Hysteresis diagram</i>	138
<i>Figure 90 - Energy Dissipation-Displacement Envelope Diagrams for all Specimens-Experimental</i>	140
<i>Figure 91 - Lateral Force-Drift Ratio for all Specimens-Experimental</i>	141
<i>Figure 92 – Strengthening ratio vs Confinement ratio comparison of various proposed models</i>	145
<i>Figure 93 - Force-Displacement Envelope Diagrams for all specimens-Atena</i>	146
<i>Figure 94 - Energy Dissipation-Displacement Envelope Diagrams for all Specimens-Atena</i>	147
<i>Figure 95 - Energy Dissipation-Drift Envelope Diagrams for all Specimens-Atena</i>	147
<i>Figure 96 - Envelope line - Experimental vs. Atena</i>	148
<i>Figure 97 - Envelope line for Columns C1 - Experimental vs. Atena</i>	149
<i>Figure 98 - Energy dissipation - deformation for Columns C1- Experimental vs. Atena</i>	149
<i>Figure 99 - Energy dissipation - drift for Columns C1- Experimental vs. Atena</i>	150
<i>Figure 100 - Envelope line for Columns C3 - Experimental vs. Atena</i>	150
<i>Figure 101 - Energy dissipation - deformation for Columns C3- Experimental vs. Atena</i>	151
<i>Figure 102 - Energy dissipation - drift for Columns C3- Experimental vs. Atena</i>	151
<i>Figure 103 - Envelope line for Columns C4 - Experimental vs. Atena</i>	152
<i>Figure 104 – Energy dissipation- deformation for Columns C4 - Experimental vs. Atena</i>	152
<i>Figure 105 - Energy dissipation - drift for Columns C4- Experimental vs. Atena</i>	153
<i>Figure 106 - Specimen type C1</i>	167
<i>Figure 107 - Specimen Type C1- Footing</i>	167
<i>Figure 108 - Specimen Type C1- Test Configurations</i>	168
<i>Figure 109 - Specimen Type C1- Axial and Lateral Loads Application</i>	168
<i>Figure 110 - Strain gauges installation</i>	169
<i>Figure 111 – Steel footing fixed to ground by anchor bolts</i>	169
<i>Figure 112 – Specimen Type C3- Confined with FRP wraps</i>	170
<i>Figure 113 – Specimen Type C2- Confined with FRP wraps</i>	170
<i>Figure 114 – Specimens Type C2 and C3- Test Configurations</i>	171
<i>Figure 115 – Specimens Type C2 and C3- Loads application at lower level</i>	171
<i>Figure 116 – Specimen Type C1- Failure mode</i>	172
<i>Figure 117 – Specimen Type C1- Atena – Cracks Element</i>	173
<i>Figure 118 – Specimen Type C1- Atena – Principal Stresses in Reinforcements</i>	173
<i>Figure 119 – Specimen Type C1- Atena – Principal Stresses in Concrete</i>	174

<i>Figure 120 – Specimen Type C1- Atena – Tensile Strength SIG T (1)</i>	174
<i>Figure 121 – Specimen Type C1- Atena – Tensile Strength SIG T (2)</i>	175
<i>Figure 122 – Specimen Type C1- Atena – Von Mises Stresses in Concrete</i>	175
<i>Figure 123 – Specimen Type C1- Atena – Von Mises Stresses in Reinforcements</i>	176
<i>Figure 124 – Specimen Type C3- Atena – Cracks Element</i>	176
<i>Figure 125 – Specimen Type C3- Atena – Principal Stresses in Reinforcements</i>	177
<i>Figure 126 – Specimen Type C3- Atena – Principal Stresses in Concrete</i>	177
<i>Figure 127 – Specimen Type C3- Atena – Tensile Strength SIG T (1)</i>	178
<i>Figure 128 – Specimen Type C3- Atena – Tensile Strength SIG T (2)</i>	178
<i>Figure 129 – Specimen Type C3- Atena – Von Mises Stresses in Concrete</i>	179
<i>Figure 130 – Specimen Type C3- Atena – Von Mises Stresses in Reinforcements</i>	179
<i>Figure 131 – Specimen Type C4- Atena – Cracks Element</i>	180
<i>Figure 132 – Specimen Type C4- Atena – Principal Stresses in Reinforcements</i>	180
<i>Figure 133 – Specimen Type C4- Atena – Principal Stresses in Concrete</i>	181
<i>Figure 134 – Specimen Type C4- Atena – Tensile Strength SIG T (1)</i>	181
<i>Figure 135 – Specimen Type C4- Atena – Tensile Strength SIG T (2)</i>	182
<i>Figure 136 – Specimen Type C4- Atena – Von Mises Stresses in Concrete</i>	182
<i>Figure 137 – Specimen Type C4- Atena – Von Mises Stresses in Reinforcements</i>	183

LIST OF TABLES

<i>Table 1 - Typical properties of fibers [4]</i>	20
<i>Table 2 - Properties of matrix materials [52]</i>	21
<i>Table 3 - Design-oriented models for confined concrete</i>	39
<i>Table 4 - Analysis-oriented models for confined concrete</i>	40
<i>Table 5 - Detail of test specimens [31]</i>	63
<i>Table 6 - Summary of formulas for confined and unconfined RCC columns</i>	72
<i>Table 7 - Properties of materials – RC columns</i>	73
<i>Table 8 - Unconfined and confined compressive strength of concrete with fatigue [EN1992]</i>	77
<i>Table 9 - Moment curvature Analysis-Column type C1-unconfined</i>	78
<i>Table 10 - Moment curvature Analysis-Column type C1-Confined by Spiral</i>	79
<i>Table 11 - Moment curvature Analysis-Column type C1-Confined by Spiral & wrap</i>	80
<i>Table 12 - Moment curvature Analysis-Column type C1-Unconfined -Fatigue</i>	81
<i>Table 13 - Moment curvature Analysis-Column type C1-Confined by spiral-Fatigue</i>	82
<i>Table 14 - Moment curvature Analysis-Column type C1-Confined by spiral & wrap-Fatigue</i>	83
<i>Table 15 - Summary of Initial yield, ultimate curvature and moment in concrete of column type C1</i>	85
<i>Table 16 - Configuration of test specimens</i>	88
<i>Table 17 - Mix design proportions</i>	89
<i>Table 18 - Properties of Concrete for test specimens (mean values)</i>	90
<i>Table 19 - Summary of steel reinforcement</i>	90
<i>Table 20 - Properties of Sikawrap and Sikadur [48] & [49]</i>	91
<i>Table 21 - Confinement configurations</i>	92
<i>Table 22 - Bending moments- Test specimen C1</i>	110

<i>Table 23 - Bending moments- Test specimen C2</i>	<i>118</i>
<i>Table 24- Bending moments- Test specimen C3</i>	<i>119</i>
<i>Table 25 - Deformation and Uplift due to high-cycle loading test</i>	<i>128</i>
<i>Table 26 – Summary of Experimental Test Configuration</i>	<i>135</i>
<i>Table 27 - Energy Dissipation and Drift of un-strengthened column type C1</i>	<i>138</i>
<i>Table 28 - Energy Dissipation and Drift of strengthened column type C2</i>	<i>138</i>
<i>Table 29 - Energy Dissipation and Drift of strengthened column type C3</i>	<i>139</i>
<i>Table 30 - Energy Dissipation and Drift of un-strengthened column type C4</i>	<i>139</i>
<i>Table 31 - Summary of Maximum Load and Displacement Test Results</i>	<i>142</i>
<i>Table 32 – Compressive strength comparison of the proposed models</i>	<i>144</i>
<i>Table 33 – Comparison of the strengthening ratio of various proposed models</i>	<i>145</i>

BIBLIOGRAPHY

LIST OF PUBLICATIONS

- I. Kostiha, V.; Girgle, F.; Štěpánek, P.; Mansour, M., strengthening of circular reinforced concrete columns using FRP wrap, *Conference Proceedings - 1st CECOM 2012 CONFERENCE*, ISBN 978-83-7283-514-7, Publisher Lodz University of Technology, Lodz, Poland, 2012.
- II. Kostiha, V.; Girgle, F.; Štěpánek, P.; Mansour, M.; Kučerová, A Strengthening of reinforced concrete columns using FRP wrap, *Conference Proceedings - Conference 19. Concrete days 2012*, ISBN 978-80-87158-32-6, Czech Concrete Society, Prague, 2012.
- III. Kostiha, V.; Girgle, F.; Štěpánek, P.; Mansour, M.; Laníková, I., Strengthening of reinforced concrete elements using composite NSM reinforcement, *Conference Proceedings - Conference 19. Concrete days 2012*, ISBN 978-80-87158-32-6, Czech Concrete Society, Prague, 2012.
- IV. Mansour, M., Confinement of high strength concrete circular reinforced concrete columns using CFRP, *Conference Young scientist 2013*, ISBN 978-80-553-1305-4, Technical University of Košice, Faculty of Civil Engineering, Košice, 2013.
- V. Mansour, M., FEM modelling of FRP-confined circular concrete columns, *Conference Young scientist 2013*, ISBN 978-80-553-1305-4, Technical University of Košice, Faculty of Civil Engineering, košice, 2013.
- VI. Kostiha, V.; Girgle, F.; Štěpánek, P.; Mansour, M.; Kučerová, A. Design of the resistant structures reinforced by inner FRP reinforcement. *Conference Proceedings- 20th Czech Concrete days 2013*, ISBN: 978-80-87158-34- 0, Czech Concrete Society, Prague, 2013.
- VII. Girgle, F.; Kostiha, V.; Štěpánek, P.; Laníková, I.; Mansour, M., Vliv zesílení sloupů ovinutím kompozitní tkaninou na jejich únosnost, článek ve sborníku- 8. seminár sanácia betonových konštrukcií, ISBN – 978-80-8076-109-7, Jaga, Bratislava, 2013.
- VIII. Mansour, M., Behavior of FRP-confined RC column under high cycle fatigue loading, *16th International Conference for PhD student Juniorstav 2014*, ISBN 978-80-214-4851-3, Brno University of Technology, Faculty of Civil Engineering, Brno, 2014.
- IX. Ondřej, J; Girgle, F.; Kostiha, V.; Štěpánek, P.; Šulák, P.; Mansour, M., Effect of surface treatment and test configuration on bond behavior of GFRP rebar, *Beton TKS*, 3/2018, MK ČR E – 11157 ISSN 1213-3116.
- X. Girgle, F.; Ondřej, J; Kostiha, V.; Bodnárová, L.; Štěpánek, P.; Zlámal, M.; Čairović, D.; Mansour, M., Dlouhodobé vlastnosti kompozitní výztuže při aplikace v betonových konstrukcích, *Beton TKS*, 2/2019, MK ČR E – 11157 ISSN 1213-3116.

CURRICULUM VITAE

PERSONAL INFORMATION

- Nationality: Lebanese and Czech
- Date of birth: 08 October 1976
- Marital status: Married.
- Number of children: 2

EDUCATION

- 2011-present:
Brno University of Technology - Faculty of Civil Engineering, Brno - Czech Republic
PhD candidate - Institute of Concrete and Masonry Structures
(Strengthening of Circular RC columns subjected to lateral cyclic loading)
- 1998-2003:
Czech Technical University - Faculty of Civil Engineering, Prague - Czech Republic
Master of Science degree in Civil Engineering
Major: Building Construction

WORK EXPERIENCES

- 2014 – present: MZ and Partners – Architectural and Engineering Consultancy, Qatar and Lebanon
Occupation: Senior Structural Design Engineer
Main activities and responsibilities: Design of Concrete and Steel Structures, Value Engineering, Coordination.
- 2010 – 2012: DOKA - The Formwork Experts, Lebanon, United Arab Emirates, and Czech Republic
Occupation or position held: Senior Project Engineer
Main activities and responsibilities: Designing cost effective formwork, shoring or scaffolding solution for various concrete construction projects.
- 2008 – 2010: Harsco Infrastructure, United Arab Emirates
Occupation or position held: Team Leader
Main activities and responsibilities: Leading the staff in all daily operations, monitoring working practices of designers, managing and developing key customer accounts, negotiations and proposals, designing cost effective formwork, shoring solution for various concrete construction projects.
- 2003 – 2008: DOKA - Lebanon, United Arab Emirates, and Czech Republic
Occupation or position held: Project Engineer
Main activities and responsibilities: Designing cost effective formwork, shoring or scaffolding solution for various concrete construction projects.

PROJECTS

Project in Algeria: Hama Sea Water Desalination.

Project in Tunisie : Cite de la Culture.

Project in Lebanon: Waste Water Treatment Tank, the Platinum Tower, Beirut Mall.

Project in Jordan: Carrefour Shopping Mall.

Project in Qatar: Residential Tower, Loft Building – B + G +7 floors, 3 Head Quarter Buildings for Army Forces – G + 2 floors, Simulation Building for Army Forces – G + 2 floors, Al Majid Tower – 2B + G + 25 floors, Theater and Cinema building for Army Forces, 12 Hangars for Army Forces, Doha Sooq – 2B + G + 3 floors, Fox Hills Buildings – 3B + G + 7 floors, Parade Stage for Army Forces.

Project in the Czech Republic: Palace Tešnov Building, Residential Central Park Buildings, Výsočanská Radiala Bridge, So 874 Ramp, Moka Silo – Cement Silos, Srkomost /Corridor, Corso II building, SO 310 Tunnel.

Project in United Arab Emirates: Al Durrah Tower, Prime Tower, RAK Bank-Dubai & Ras Al Khaimah, Al Mazaya Tower.